Technical Report Documentation Page

1. Report No.	2. Government Accession No.	3. Recipient's Catalog No.
FHWA/TX-92+1127-1		

4. Title and Subtitle	5. Report Date
AN INVESTIGATION OF STRUT-AND-TIE MODELS FOR DAPPED BEAM DETAILS	May 1991
	6. Performing Organization Code
7. Author(s)	8. Performing Organization Report No.
D. L. Barton, R. B. Anderson, A. Bouadi, J. O. Jirsa, and J. E. Breen	Research Report 1127-1
9. Performing Organization Name and Address	10. Work Unit No. (TRAIS)
Center for Transportation Research The University of Texas at Austin Austin, Texas 78712-1075	11. Contract or Grant No. Research Study 3-5-87/9-1127
12. Sponsoring Agency Name and Address	13. Type of Report and Period Covered
Texas State Department of Highways and Public Transportation; Transportation Planning Division P. O. Box 5051 Austin, Texas 78763-5051	Interim
	14. Sponsoring Agency Code

15. Supplementary Notes

Study conducted in cooperation with the U. S. Department of Transportation, Federal Highway Administration

Research Study Title: "Reinforcement Detail Design in Structural Concrete"

16. Abstract

The objective of the test program undertaken in this study was to develop experimental data for defining various elements of strut-and-tie models. The data was used extensively in establishing design guidelines for details of structural reinforced concrete (Report 1127-3F).

The experimental program was divided into three phases. The first phase consisted of tests of four dapped beam details. A dapped beam was selected as a typical detail, commonly used in highway structures, and one for which several different design approaches have been proposed. Phases two and three consisted of tests of isolated portions (nodes) of the structure as modeled using the strut-and-tie approach. Nine CTT (compression-tension-tension) and ten CCT (compression-compression-tenson) nodes were tested. At these nodes three forces converge at a point in the strut-and-tie model. Variables included reinforcement arrangement and layout, concrete strength, bearing area of the effective strut, and anchorage details.

The results indicated that the dapped beam detail can be efficiently and effectively designed using a strut-and-tie model. The isolated node tests provide useful information on the performance of the concrete in the compression strut and on the anchorage of reinforcement in the node. The node tests provide an inexpensive way to determine critical data for developing design guidelines.

17. Key Words	18. Distribution Statement
strut-and-tie models, dapped beams, details, structural reinforced concrete, compression, tension, nodes, reinforcement, anchorage, bearing area, strength	No restrictions. This document is available to the public through the National Technical Information Service, Springfield, Virginia 22161.

19 Security Classif. (of this report)	20. Security Classif. (of this page)	21. No. of Pages	22. Price
Unclassified	Unclassified	212	

AN INVESTIGATION OF STRUT-AND-TIE MODELS FOR DAPPED BEAM DETAILS

by

D.L. Barton, R.B. Anderson, A. Bouadi, J.O. Jirsa and J.E. Breen

Research Report Number 1127-1

Research Project 3-5-87/9-1127

"Reinforcement Detail Design in Structural Concrete"

Conducted for

Texas State Department of Highways and Public Transportation

In Cooperation with the

U.S. Department of Transportation

Federal Highway Administration

by

CENTER FOR TRANSPORTATION RESEARCH
BUREAU OF ENGINEERING RESEARCH
THE UNIVERSITY OF TEXAS AT AUSTIN

May 1991

NOT INTENDED FOR CONSTRUCTION, PERMIT, OR BIDDING PURPOSES

James O. Jirsa, P.E. (Texas No. 31360)
John E. Breen, P.E. (Texas No. 18479)

Study Supervisors

PREFACE

The use of strut-and-tie models is an attractive method for detailing reinforced concrete structures. The strut-and-tie model offers the designer a rational procedure for "visualizing" the flow of forces in a structure or a detail. The literature contains many papers dealing with the concepts involved in strut-and-tie modeling. However, very little experimental research has been done to establish the limits needed to ensure that strut-and-tie models are correctly conceived by the designer and that the elements of the model (struts and ties) will develop the strengths needed to transfer forces properly within the structure. The objective of this portion of the program was to provide experimental data which could be used to verify the feasibility of using strut-and-tie models and to determine pertinent compressive stress levels in the concrete struts as well as bond and anchorage requirements for the tension elements or ties.

SUMMARY

The objective of the test program undertaken in this study was to develop experimental data for defining various elements of strut-and-tie models. The data was used extensively in establishing design guidelines for details of structural reinforced concrete (Report 1127-3F).

The experimental program was divided into three phases. The first phase consisted of tests of four dapped beam details. A dapped beam was selected as a typical detail, commonly used in highway structures, and one for which several different design approaches have been proposed. Phases two and three consisted of tests of isolated portions (nodes) of the structure as modeled using the strut-and-tie approach. Nine CTT (compression-tension-tension) and ten CCT (compression-compression-tenson) nodes were tested. At these nodes three forces converge at a point in the strut-and-tie model. Variables included reinforcement arrangement and layout, concrete strength, bearing area of the effective strut, and anchorage details.

The results indicated that the dapped beam detail can be efficiently and effectively designed using a strut-and-tie model. The isolated node tests provide useful information on the performance of the concrete in the compression strut and on the anchorage of reinforcement in the node. The node tests provide an inexpensive way to determine critical data for developing design guidelines.

IMPLEMENTATION

The results of this portion of the study are intended to provide the experimental data needed to develop specific design guidelines for use of the strut-and-tie model in detailing reinforced concrete structures. The design guidelines are presented in Report 1127-3F.

TABLE OF CONTENTS

LIST OF FIGURES

LIST OF TABLES

CHAPTER 1
INTRODUCTION

1.1 Background

In recent years, rapid advancement in the use of structural concrete has occurred. Longer spans, more complex geometries and new construction techniques are being utilized. The term "structural concrete" is used to address the wide spectrum of reinforced and prestressed concrete ranging from elements with only unstressed or "passive" reinforcement to elements with all prestressed or "active" reinforcement. Composite construction with structural steel members is used where economically beneficial. The industry trend is toward higher strength materials, especially higher strength concrete. The diversity of forms and types of reinforcement has added to the complexity of structural design. These new technologies create a need for a better understanding of and approach to detailing practices. Design involves far more than analysis to determine member forces and proportioning the members to obtain safe stresses. It requires a certain amount of "detailing" which affects the overall safety, economy, and constructability of the structure. In concrete structures, detailing would encompass:

1. Preparation of drawings showing the size and location of structural elements and reinforcement.

2. Specification of bar details such as anchorage provisions and location of splices and overlaps.

Detailing should not be confused with the "details" of a structure. Details would include statical or geometrical discontinuities such as point loads or frame corners, corbels, recesses, holes and other openings[15]. Examples of details which may occur in bridge and building construction are shown in Fig. 1.1. The structural engineer must be concerned with the "detailing" of reinforcement whether he is designing the "details" or other parts of the structure. Details and detailing are equally important in monolithic construction and "mixed" structural systems because they are essential to overall structural integrity.

Neither the ACI Building Code[1] nor the generally similar provisions of the AASHTO Bridge Specifications[2] address detailing of reinforcement extensively or uniformly. Provisions governing development length, lap splices, bar spacing, and reinforcement details such as standard hooks and bends are included. Detailing of transverse or confining reinforcement in members subjected to axial or shear forces is described by general guidelines. Even though the codes offer no general method or philosophy, the designer is able to detail reinforcement in standard portions of structures expeditiously.

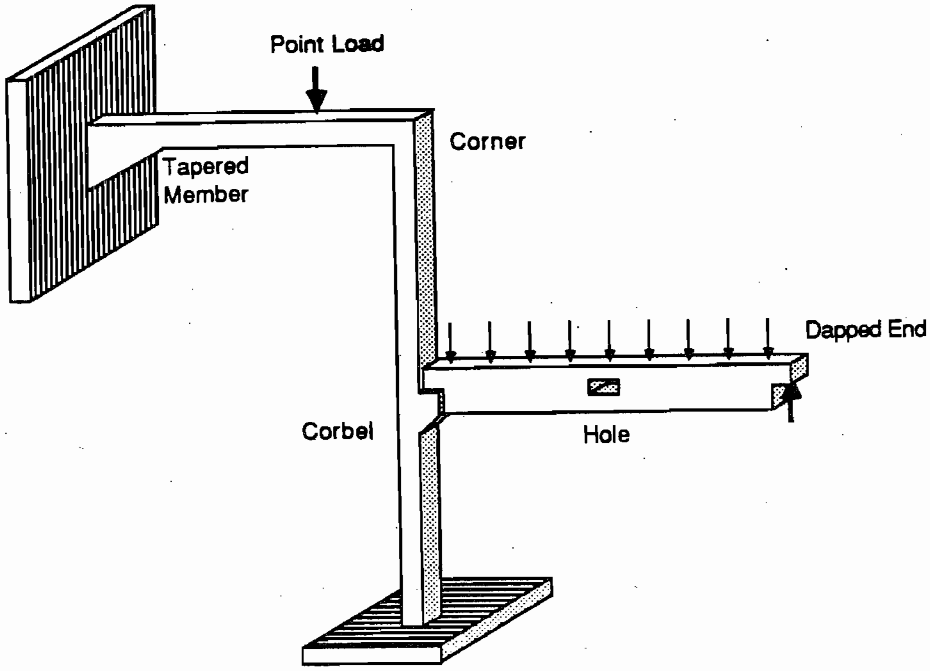

Figure 1.1 "Details" That May Exist in Actual Structures.

To complement design codes, detailing manuals are often utilized. These manuals are collections of drawings of typical details without any consistent philosophical basis. It may be difficult for the designer to adapt "typical details" to new and unusual circumstances. While handbooks of design procedures represent a general approach, each detail may be based on a different design philosophy and may be presented without explanation. In general, it is difficult for the designer to envision the flow of forces and understand the function of the components making up a portion of a structure.

Unusual or complex situations often present the designer with numerous difficulties. There is not a general methodology for "detailing." The ACI Code has some specific provisions for details such as brackets and corbels, anchorage zones, and joints in seismic frames. Additional guidance for design of details may be found in documents published by the Prestressed Concrete Institute[3], the Post-Tensioned Concrete Institute[4], and the Concrete Reinforcing Steel Institute[5]. Various ACI committees have also developed reports and standards covering details and detailing. Most of these manuals and standards tend to be empirical in nature, focused on specific applications and lack a conceptual model to assist the designer. Thus, the recommendations are either extremely vague or extremely rigid and it is difficult to extend them to other applications.

A more fundamental approach to design is the use of strut-and-tie or "truss" models. In this approach, a portion of a structure is modeled as a system of struts and ties. The struts represent compressive forces in the concrete and the ties tension forces in the reinforcement. A statical force path composed of struts and ties is visualized and reinforcement requirements and concrete compressive stresses are determined. This approach promotes a better understanding of force transfer mechanisms and improves the designer's ability to handle unusual circumstances.

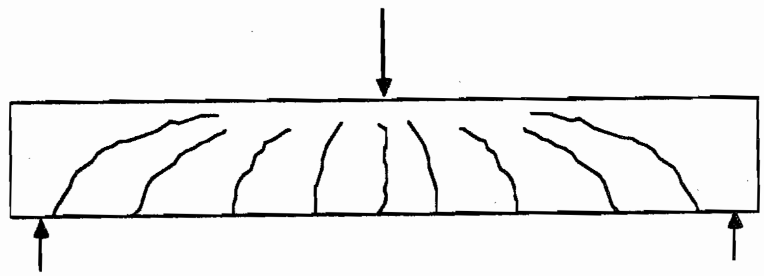

(a) Typical cracks in reinforced concrete beam

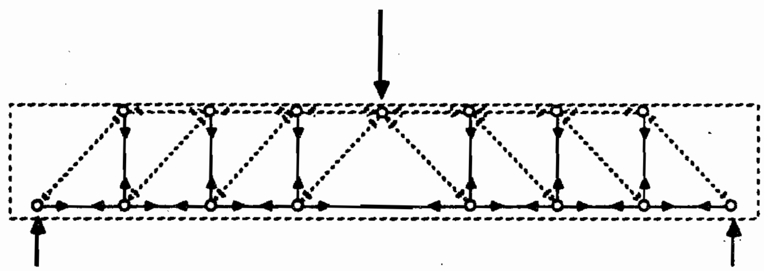

(b) Analogous truss representing flow of forces.

Figure 1.2 Truss Analogy.

Truss models for shear design of reinforced concrete beams were introduced by Ritter[6] near the turn of the century. The procedure was later generalized by Mörsch[7]. In truss models for shear, the reinforced concrete beam is represented by an analogous truss. A typical reinforcement scheme in a cracked reinforced concrete beam will mobilize "truss" action as shown in Fig. 1.2. Fundamental work, incorporating truss models for reinforced concrete detail design, was carried out and presented by Leonhardt[8]. Various researchers, including Neilsen et al.[9], Lampert and Thürliman[10], Mitchell and Collins[11], and Ramirez[12], have worked to refine and expand the method so it is applicable to shear, torsion, and the interaction of these actions, as well as bending. Recently, MacGregor[13], Marti[14], and Schlaich, Schäfer and Jennewein[15] have published refined methods for detailing structures using truss models. In a major contribution for English language readers Schlaich et al.[15] have presented the "strut-and-tie" model as a generalization of previous truss models applicable to the entire structural concrete spectrum. The present study, following the proposal of Schlaich and his co-workers, identifies the strut-and-tie model as a unified design concept applicable to all portions of the structure.

Despite considerable recent progress, the strut-and-tie model is still highly conceptual and has not been subjected to comprehensive verification through tests. Empirical expressions developed for the failure criterion of cracked concrete struts are a necessary part of the model and have been widely discussed[9, 11, 12, 16]. Also, stress checks at the nodes require highly graphical procedures which are cumbersome during design. Some portions of the method have been fully developed. Lack of consistent code provisions can allow the designer to make unreasonable assumptions regarding the flow of forces and subsequent reinforcement detailing. Dimensioning of the strut and tie members and limiting of the strut and nodal concrete stresses must be better quantified before the method can be practically implemented.

1.2 Project Description and Scope

The research described herein is part of a larger study supported by the Texas State Department of Highways and Public Transportation (TSDHPT) to develop general guidelines based on refined strut and tie models for the detailing of structural concrete utilized in U.S. and Texas transportation structures. It is envisioned that the designer will approach the detailing of a concrete member using the strut-and-tie model much as he would the detailing of a steel truss. After selecting a suitable truss to carry the applied loads for the given boundary conditions, the designer would analyze the truss for member forces. The truss members would then be proportioned to carry the indicated forces. Lastly, the designer would detail the connections at the nodes. Simple strut-and-tie models could be applied to numerous design situations. The research reported herein involves the use of specific application of strut-and-tie or truss models to the detailing of dapped end beams.

Dapped end details are used by the TSDHPT in precast bridge construction as part of "drop-in" beams. In this system a precast beam is cantilevered across a support location which corresponds to a hinge. Drop in beams span between hinges. The connection at the hinge is made by notching the upper corner of one beam and lower corner of the other. The notched area is referred to as a dapped end detail (Fig. 1.3).

The investigation consisted of four separate tasks. The first task was a review of literature concerning the strut-and-tie model which is presented in Chapter 2 and is discussed in considerable detail in Report 1127-3F. A summary of the basic elements of the strut-and-tie model is presented. Various approaches presented in the literature are utilized to describe the current state of the strut-and-tie model as a design method.

The second task involved an experimental study of dapped beams. Three methods of designing dapped end details were examined. The strut-and-tie models described in

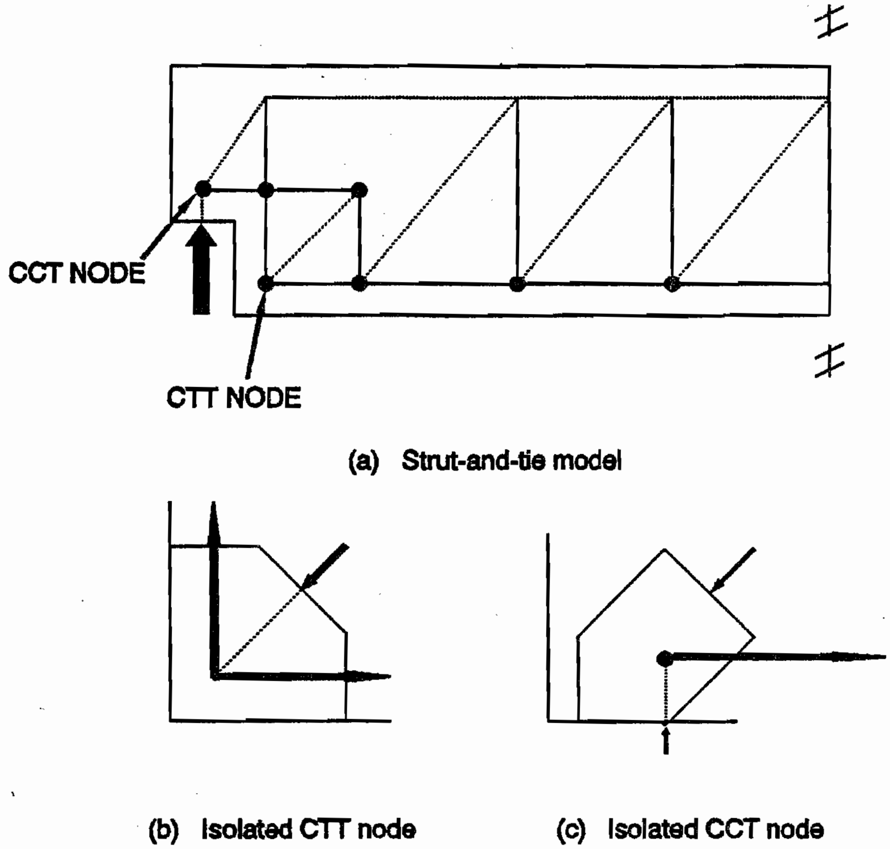

Figure 1.3 Strut and Tie Model of the Prototype Dapped Beam.

Chapter 2 were utilized to develop the dapped end detail. Design procedures recommended by the Prestressed Concrete Institute (PCI) along with the method currently used by the TSDHPT were also reviewed.

After reviewing the strut-and-tie model in current literature and trying to design dapped end members using this approach, it was apparent that the existing state of knowledge was not sufficient for application of the model to complex detailing situations. Particularly troublesome were the nodes. Therefore, the third and fourth stages of the study were focused on developing an in-depth understanding of isolated nodes (See Fig. 1.3). Physical tests were performed to enhance the understanding of the node.

In the third task, behavior of nodes joining two tensile ties and one compression strut [CTT Node, Fig. 1.3(b)] were studied. In the fourth task the reaction area of a dapped beam where two compression forces and a tension tie meet [CCT node, Fig. 1.3(c)] was isolated and tested. These two node cases were chosen because they occur frequently in design and can be studied with relatively simple tests. The node tests complimented the tests of the full-sized, dapped beams studied in Task 2. In the isolated node test specimens, reinforcement patterns similar to those present in the nodes of the full-sized, dapped beams were used.

CHAPTER 2
THE STRUT-AND-TIE MODEL

2.1 Introduction

In the strut-and-tie model, the stress distribution is idealized as a static force system consisting of three basic elements:

Struts
Ties
Nodes

The strut-and-tie model behaves essentially as a truss. Compressive forces are directed along struts representing compressive stress fields within the concrete. Tensile forces are directed along ties which represent reinforcement. Intersections of struts and ties occur at nodes which are idealizations of areas in which internal forces are redirected.

By replacing a complex structural system with a strut-and-tie model, estimates of the internal forces in the system can be obtained by analyzing the truss with the external forces applied to the system. The estimates of internal forces may then be used to determine reinforcement requirements, check concrete stresses and determine anchorage requirements. Some typical examples of strut-and-tie models are illustrated in Fig 2.1.

In this chapter, a brief overview of the strut-and-tie procedure for design of structural concrete is presented. A more comprehensive evaluation of the strut-and-tie model is presented in Report 1127-3F. The following discussion is a summary of the proposals of several researchers regarding application of strut-and-tie models. The focus is on design of details for which no rational design methods currently exist. Therefore, applications such as uniformly loaded simple beams are only briefly mentioned.

2.2 Basic Principles

2.2.1 Background and Assumptions. The strut-and-tie model is a limit analysis approach to the design of structural concrete. More specifically, the strut-and-tie model is a static or lower bound plasticity solution. Marti[14] explains that strut- and-tie models represent a possible equilibrium system of forces within a structure at its ultimate load. While the plasticity theory behind the strut-and-tie model is quite complex, it is primarily used to establish a rational basis for the method. For most practical applications, it is only necessary to understand that a properly chosen and dimensioned strut-and-tie model represents a lower bound estimate of the true capacity of a structural element assuming other brittle failures such as stability, local crushing, or anchorage are precluded.

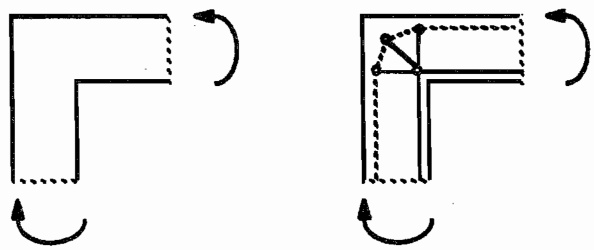

(a) Moment opening corner

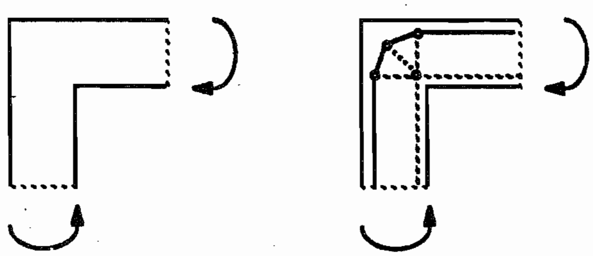

(b) Moment closing corner

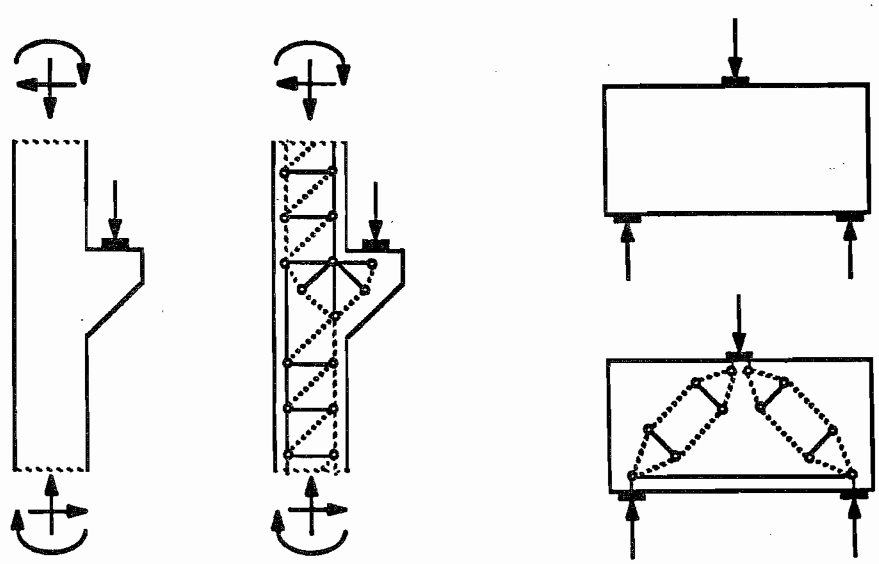

(c) Corbel

(d) Deep beam

Figure 2.1 Examples of Strut-and-Tie Models (From Ref. 1).

Although development of a detailed mathematical verification for the strut-and-tie method is unnecessary to understand its application, awareness of the assumptions is important. The most important assumptions are summarized below:

1) Failure is due to the formation of a "mechanism" resulting from yielding of one or more ties.

2) Crushing of the concrete struts does not occur prior to yielding of the ties. This is prevented by limiting the stress level in the concrete.

3) Only uniaxial forces are present in the struts and ties.

4) All external loads are applied at the nodes of the strut-and-tie model.

5) The reinforcement is properly detailed to prevent local bond failures.

2.2.2 Types of Strut-and-Tie Models. Strut-and-tie models are often divided into two categories based upon the regions of the structure to which they apply[13, 15, 17, 18]. The distinction is based on the elastic stress distribution within the structure. While elastic stresses are not necessarily representative of the stress distribution in an actual concrete structure, they are utilized to characterize different areas of a structure. Division between regions of a structure can be illustrated by considering a simple beam under a central concentrated load as shown in Fig. 2.2a. The elastic state of stress in the beam may be characterized by the use of stress trajectories (contours of principal stress). At the concentrated load, and at the supports, where the stresses are "Disturbed", the areas are defined as D-regions. Between D-regions, the stress distribution is essentially uniform and regular and the linear strain profile assumption of "Bernoulli" is applicable. These areas are identified as B-regions. D-regions may also result from geometrical discontinuities. The subdivision of other types of structures into B and D regions is illustrated in Fig. 2.3.

Design of B-regions is accomplished using a special type of strut-and-tie model which is generally termed the "truss analogy". An example of a truss model is illustrated in Fig. 2.2b. The truss model has been used extensively as a conceptual model for shear design. In the truss model for a simply supported beam the lower horizontal chord represents longitudinal reinforcement while the upper chord represents the concrete compression zone. The stirrups are the truss vertical members. Inclined compression struts are used to represent diagonal compression in the web of the beam. The truss model can be most easily used for the design of beams or B-regions. Its use in D-regions is mainly confined to location where concentrated loads produce compression fields which radiate outward from the load (Fig. 2.4). In the strut-and-tie model, the truss analogy is generalized and extended so that it may be applied to a variety of design situations[15, 17, 18]. The wide range of D-regions which occur in structures can be handled using strut-and-tie models.

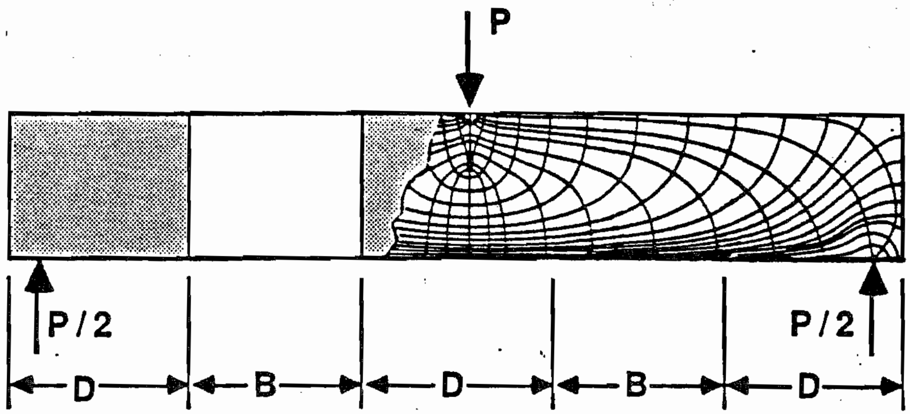

(a) Stress trajectories and B- and D-regions

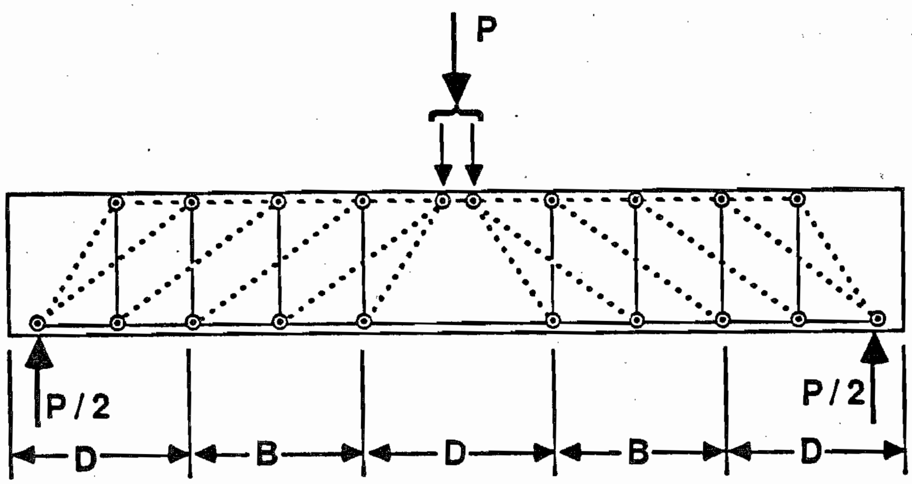

(b) Truss model or strut-and-tie model

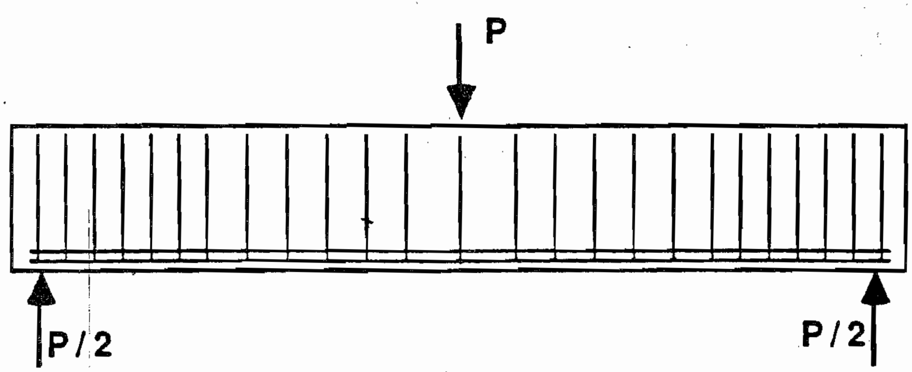

(c) Actual reinforcement layout

Figure 2.2 Application of Strut-and-Tie Model to Simple Beam.

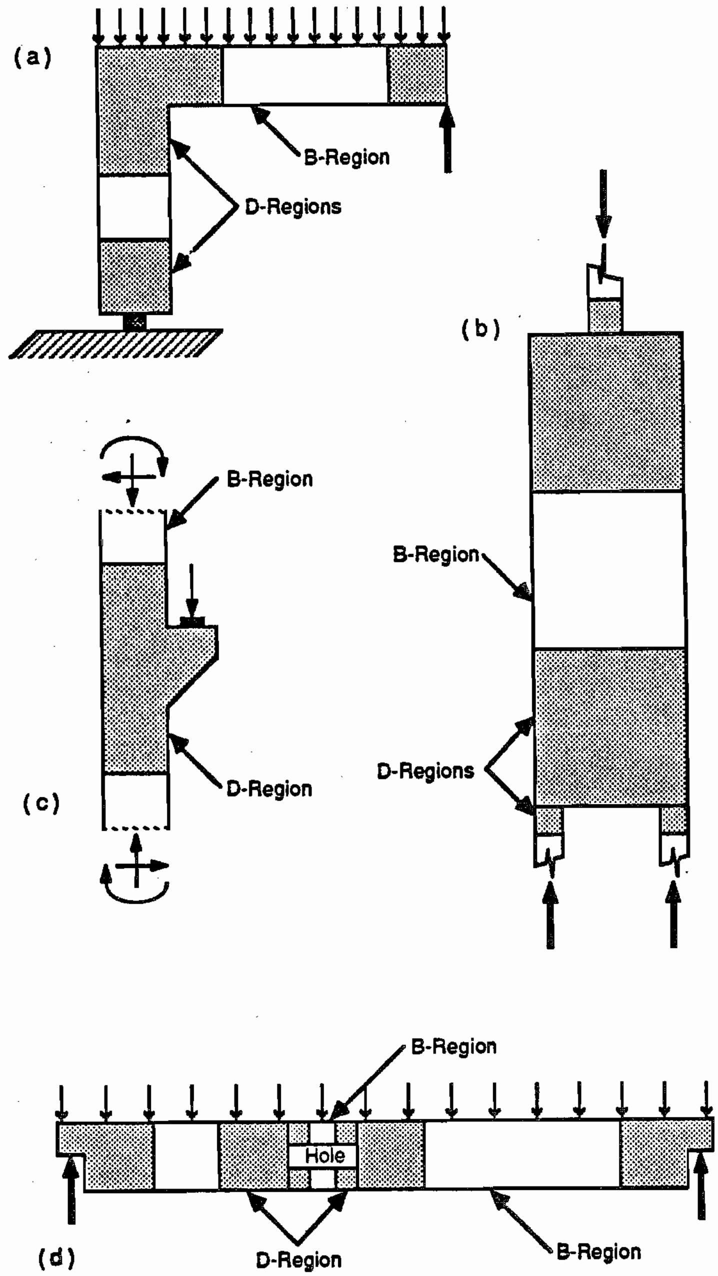

Figure 2.3 Examples of B- and D-Regions (From Refs. 13 and 15).

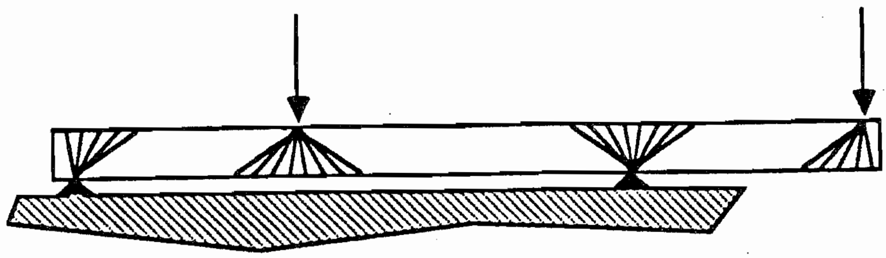

Figure 2.4 Compression Fields Radiating Outward From Concentrated Loads.

2.2.3 Design Procedure. The general procedure in applying the strut-and-tie model is summarized in Fig. 2.5. After the basic structural system is established, loads and member sizes can be estimated and the structure analyzed to determine reactions. To apply the strut-and-tie model, a specific area of the structure which is to be designed (the "detail") can be isolated, dimensions estimated and forces acting on the specific area determined. The detail can be replaced by a strut-and-tie model which satisfies equilibrium and the local boundary conditions. Internal forces in the struts and ties can be determined from equilibrium. The reinforcement can be dimensioned using tie forces and stress levels in the concrete struts checked. Finally, the nodes are evaluated to ensure proper development of reinforcement and transfer of forces.

Design using the strut-and-tie model is often an iterative procedure as many of the steps are interrelated. It is likely that the geometry of the model and the detail will need to be altered as specific reinforcement sizes, anchorage requirements, etc. are developed. A sketch of the detail drawn to scale can help the designer get a "feel" for the force transfer mechanism.

2.3 Elements of the Strut-and-Tie Model

2.3.1 Ties. Ties are the tension members of the strut-and-tie model. Usually, tie forces are resisted by reinforcement placed symmetrically about the line of action of the force. The reinforcement must extend the entire length of the tie and should be properly anchored at the nodes. The amount of reinforcement to be provided is determined from the tie force. Ideally, the tie should be proportioned so that at the ultimate design load it will just reach yield. In order to ensure a ductile failure mode, sufficient yielding must occur to allow the formation of a mechanism prior to crushing of the concrete. Tie reinforcement may consist of single or multiple bars or of prestressing strands. Schlaich[15] indicates reinforcement considered to be part of a given tie should undergo similar strains in order to act as a unit or a single tie.

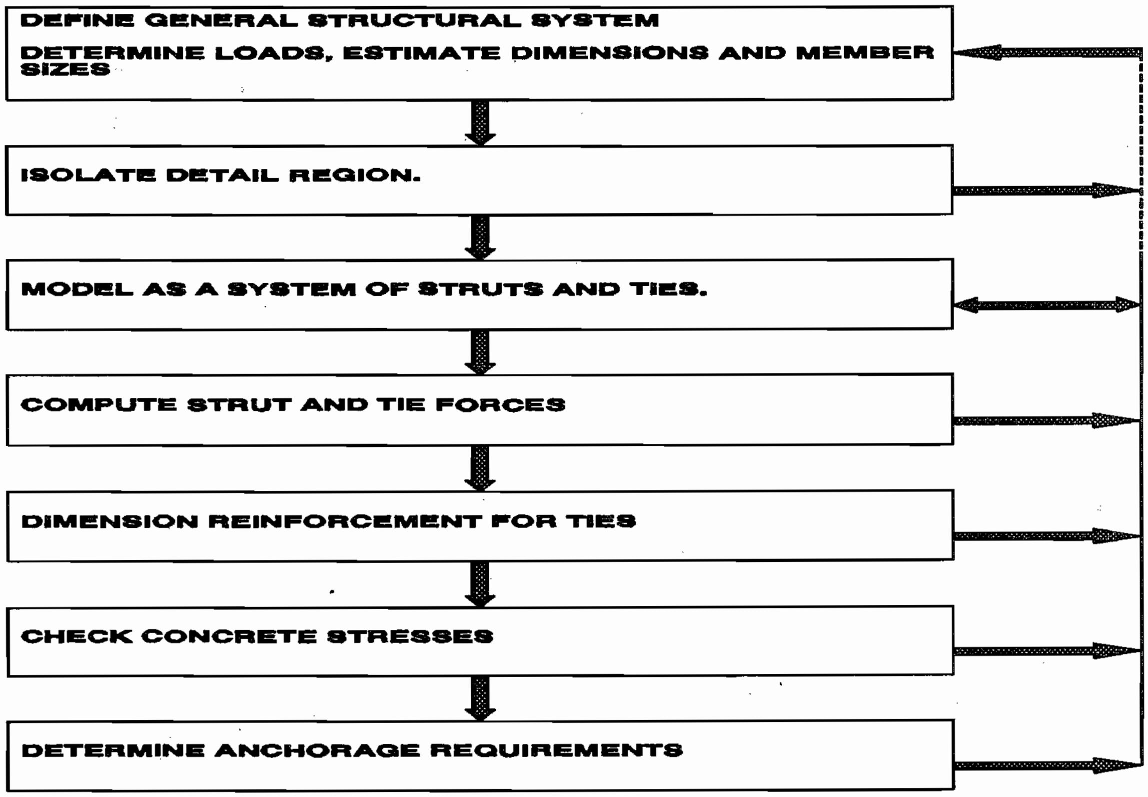

Figure 2.5 Strut-and-Tie Model Design Procedure.

2.3.2 Struts. Compression members of the strut-and-tie model are known as struts. Struts are usually considered to be comprised of concrete. Struts represent stress fields in the concrete. Various types of struts have been developed to characterize different stress fields. Three configurations are sufficient to model most situations (15). These are the prism, fan and bottle struts illustrated in Fig. 2.6. A prismatic strut is the simplest idealization of a compressive stress field. Prisms are generally used to model stress fields having uniform parallel stress trajectories. Fan shaped stress fields are developed at points of concentrated loading or at supports. Figure 2.7 illustrates a fan region such as that which develops at the support in a simple beam. This fan region incorporates a series of trapezoidal struts which act to distribute force from the node at the point of reaction to several stirrups.

In some cases, a stress field which narrows near points of concentrated loads or at supports is modeled using a bottle shaped strut as shown in Fig. 2.8. The inclined struts produce tensile stresses normal to the line of action of the applied forces which must be resisted by transverse reinforcement or by tension in the concrete. Figure 2.8 shows the bottle or bulb strut represented using a simple strut-and-tie model for analysis.

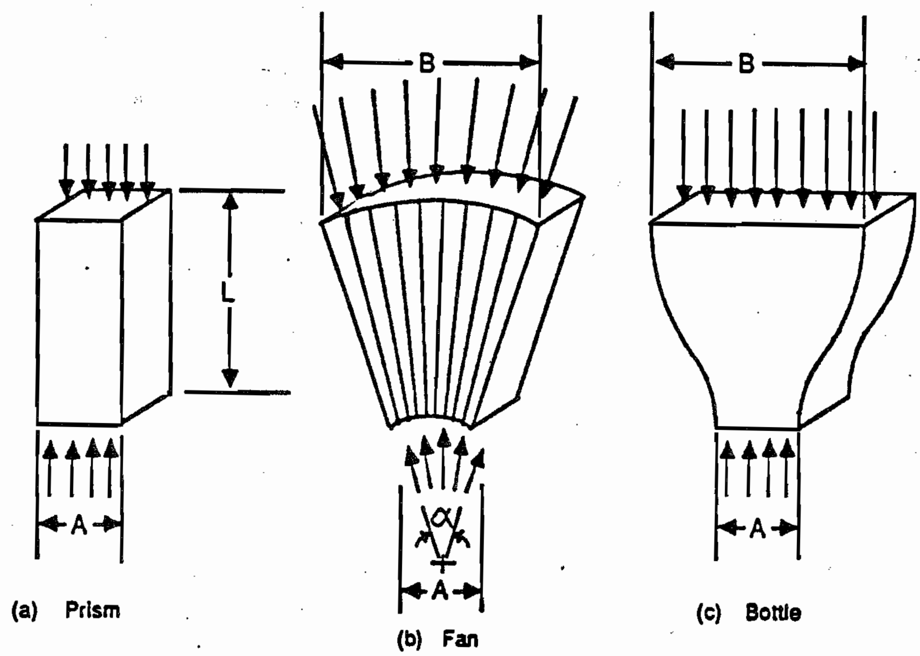

Figure 2.6 Basic Types of Struts (From Ref. 15).

2.3.3 Nodes. Nodal regions connect the elements of the strut-and-tie system. In strut-and-tie models, nodes represent the pinned joints of a truss. Physically, nodes represent regions in which internal forces are redirected. The importance of nodes in the design process is twofold. First, concrete stress levels in nodes must be controlled to allow for the safe transfer of forces. Secondly, dimensioning of nodes is the key to satisfying anchorage requirements for reinforcement.

Figure 2.9 illustrates singular and smeared nodes. The singular node connects strut and tie forces in relatively small areas. Smeared nodes, in contrast, join wide stress fields or ties made up of a number of distributed bars. Of the two types of nodes, the singular node is generally the more critical since the force transfer is more abrupt and creates higher stress concentrations. The following discussion is focused on singular nodes. Nodes may be grouped into subsets relating to the type of elements which they join. For instance, a node joining two compression struts and one tension tie is termed a CCT-node. Examples of various singular nodes are shown in Fig. 2.10.

The "dimensioning" of nodes is largely determined by two constraints. The first constraint is that all the lines of actions of strut and tie as well as any external forces must coincide. Secondly, the widths and relative angles of the struts and ties determine node geometry.

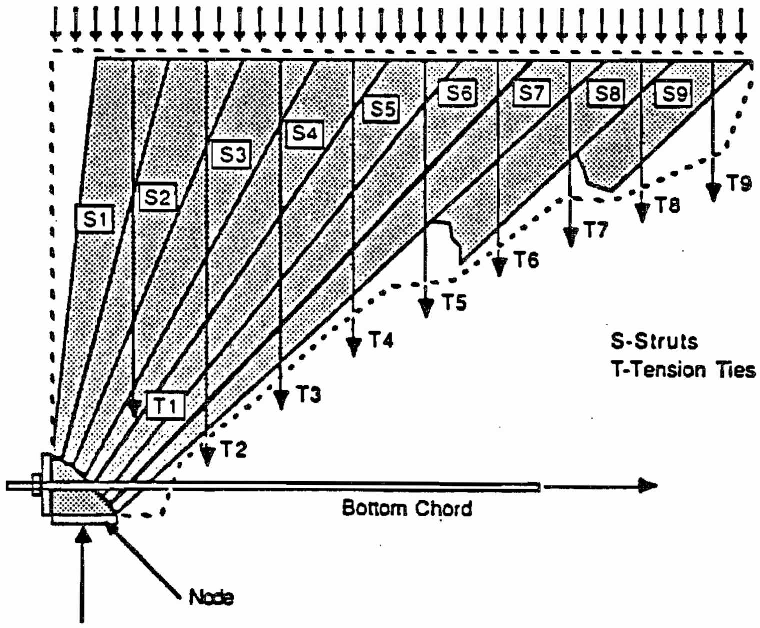

Figure 2.7 Fan Shaped Compressive Stress Region at Beam Support.

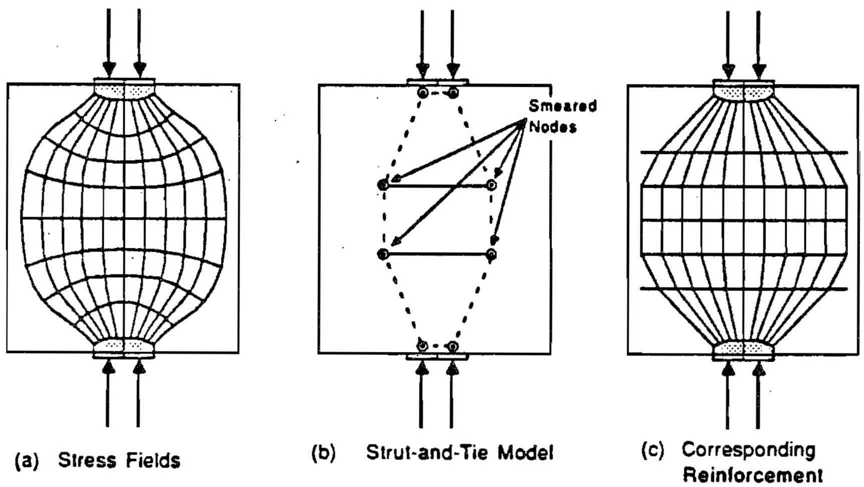

Figure 2.8 Bottle or Bulb Shaped Struts (From Ref. 15).

Dimensioning of the node and checking boundary stresses are interrelated. Node geometry is selected so that stresses along the border of the node do not exceed the limiting value of concrete stress (see Section 2.4 for limiting stresses). Furthermore, Schlaich(15) recommends dimensioning the node so that a state of planar hydrostatic stress within the node results. This state of stress is achieved by choosing the node geometry so that the stresses on all the node's faces are equal. An example of a CCC-node under a hydrostatic stress state is shown in Fig. 2.11. Because the node is hydrostatic, strut forces are proportional to their width and the sides of the node are perpendicular to the axis of each of the struts.

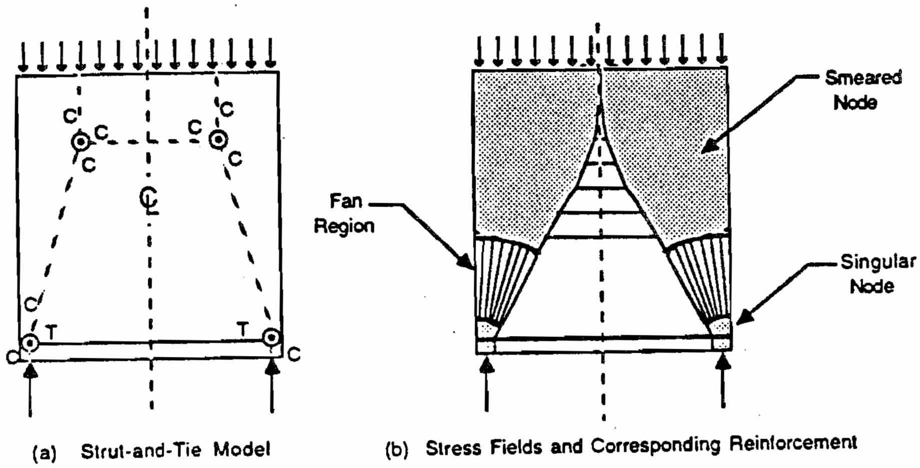

Figure 2.9 Singular and Smeared Nodes (From Ref. 15).

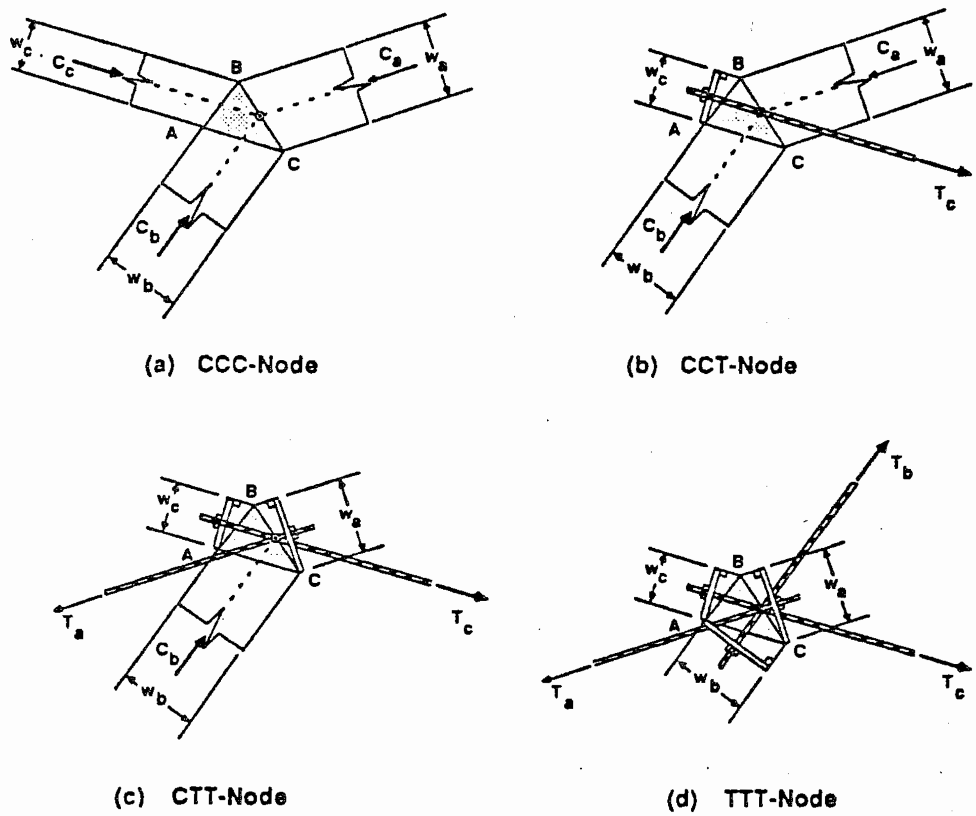

Figure 2.10 Examples of Singular Nodes.

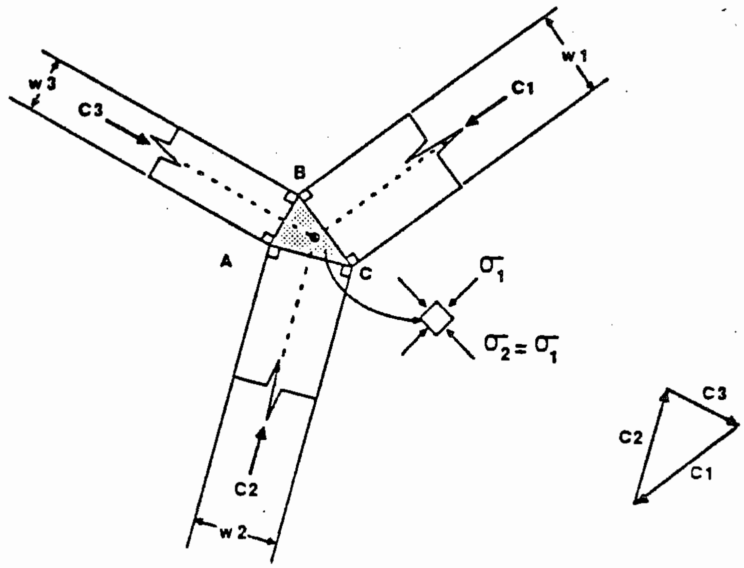

Figure 2.11 CCC-Node Under Hydrostatic Stress State (From Ref. 14).

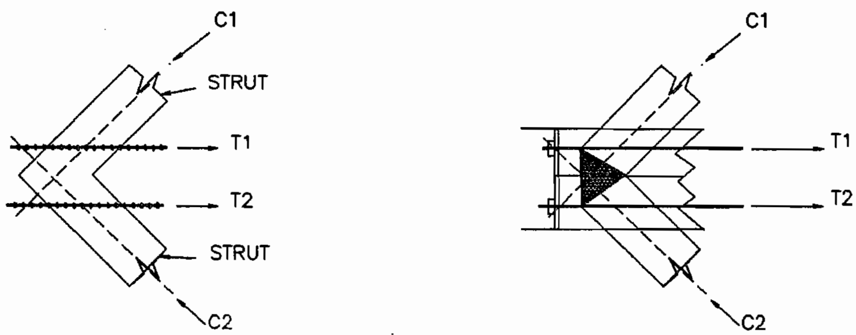

(a) actual reinforcement layout (b) Idealized tie anchors

Figure 2.12 Idealization of Tie Forces Within Nodal Regions.

In some cases the geometries of the struts and ties may not allow for equalization of the boundary stresses. More complex situations are discussed in Report 1127-3F.

Nodes anchoring tension ties are dimensioned in a manner similar to the CCC-node. This is made possible by assuming the tie forces act from behind the node to compress the nodal region[15]. The anchorage of reinforcement is often visualized as a plate even though most reinforcement is anchored by simply providing sufficient development length (see Fig. 2.12). The dimensions of nodes joining ties is often controlled by the width of the tie. Thus, placement of reinforcement can be critical to the design of nodes. The use of multiple layers of reinforcement increases the width of the tie and reduces stress levels in the node (Fig. 2.13).

One of the most commonly occurring nodes is the CCT-node located at the supports of beams (Fig. 2.13). The dimensions of the nodes in Fig. 2.13 are defined by the width of the tension tie. Where the reinforcement is relatively close to the bottom of the beam, the tie width is defined by Schlaich et al.(15) as being twice the distance from the center of gravity of the reinforcement to the bottom of the beam. It is obvious, however, that as the center of gravity of the reinforcement is moved further from the bottom of the beam there must be a limit on the tie width. Marti(14) therefore, defines the tie width w (Fig. 2.14) using the mechanical reinforcement ratio "ω":

$$w = \omega h$$

where:

$$\omega = \frac{A_s f_y}{b h f_{ce}}$$

b	=	width of beam
h	=	height of beam
A_s	=	area of flexuraalreinforcement
f_y	=	yield of strength of flexural reinforcement
f_{ce}	=	effective concrete stress (see Sec. 2.4)

Schlaich(15) suggests that dimensions of the CCT-node are dependent on factors such as the relative magnitude of stress fields and the amount of tie reinforcement. Only a few node configurations have been addressed to a degree that would allow designers to use them with confidence. Fundamental node dimensioning techniques have not been verified experimentally. Figure 2.15 shows CCT-nodes with different strut widths results from where reinforcement anchored using straight bars or hooked bars.

The final step in evaluating a node is checking anchorage of tie reinforcement. Anchorage is achieved by providing proper development length or in special circumstances by attaching the reinforcement to bearing plates or other fixed components. The key to determining anchorage requirements is selecting the point at which the reinforcement must be fully developed. In the case of the CCT-node shown in Fig 2.16, the anchorage is considered to begin at the inside of the support because of the compression stresses from the bearing plates. If sufficient space is not available for hooks or normal development lengths, end plates or continuous reinforcement details such as "U's" may be utilized. Also, confining hoops or spirals may be used to improve development.

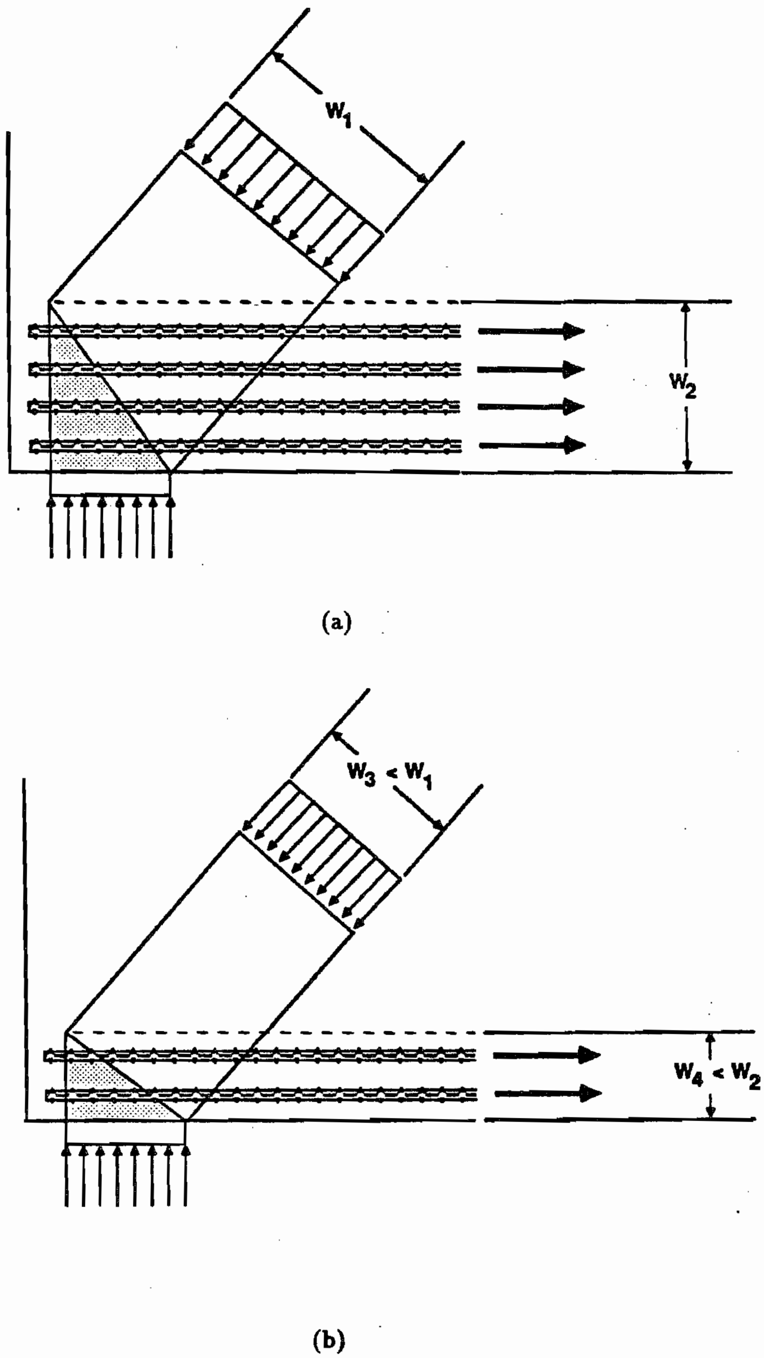

Figure 2.13 Effects of Decreasing Tie Width on Node Geometry (From Ref. 15).

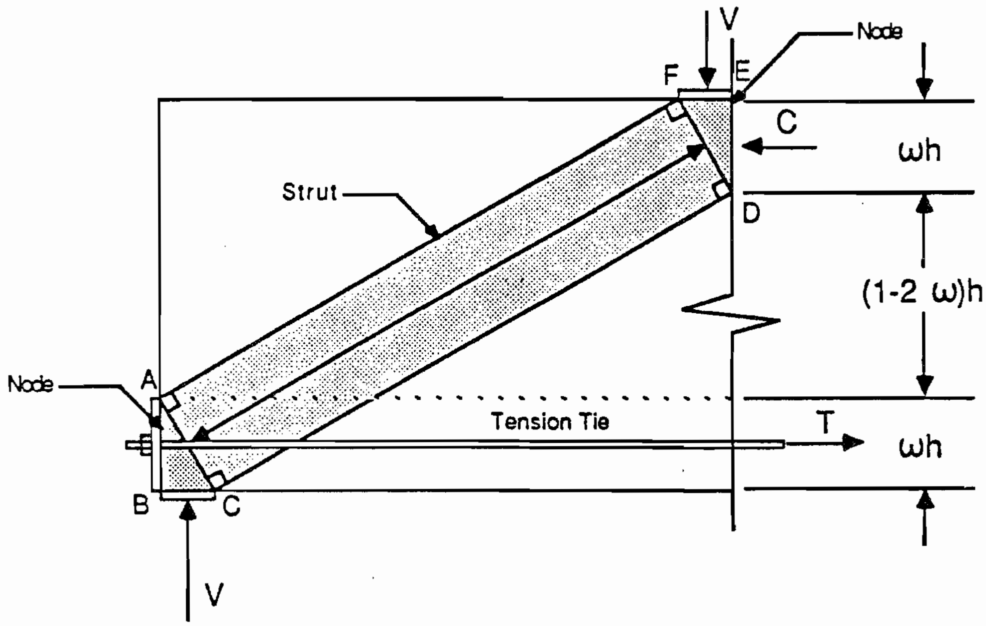

Figure 2.14 Tie Width as Defined by Mechanical Reinforcement Ratio (From Ref. 14).

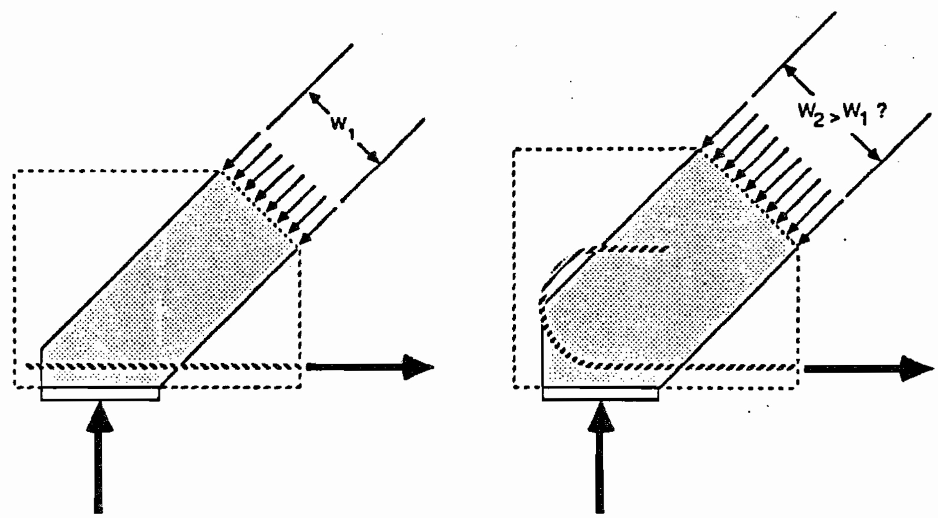

(a) Possible compressive stress field in CCT-node with straight bar anchoring tensile tie

(b) Possible compressive stress field in CCT-node with hooked tensile tie

Figure 2.15 Effect of Anchorage Detail on CCT-Node Geometry.

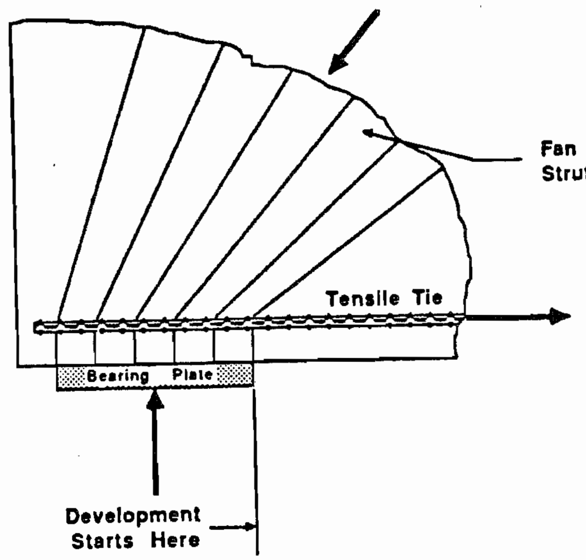

Figure 2.16 Anchorage of Reinforcement in CCT-nodes.

2.4 Effective Concrete Strength Limits

The general goal in structural concrete design is to produce members in which the critical section will exhibit ductile behavior under extreme overload. This is done by ensuring that the reinforcement yields before the concrete fails. To ensure ductile behavior it is necessary to place a limit on stress levels in the concrete.

In general, the effective strength of the compression struts is chosen as some portion of the concrete cylinder compressive strength, f_c'. The effective strength, f_{ce}, is equal to $\nu f_c'$ where ν is an efficiency factor and f_c' is the 28-day compressive strength. Because the strut-and-tie model is associated with the ultimate limit state, substantial cracking may be expected to reduce the concrete compressive strength. Furthermore, in the strut-and-tie model, struts are assumed to be loaded uniaxially. Actually, frictional forces, aggregate interlock and dowel forces are present which may also affect concrete strength. Hence, an efficiency factor, ν, is introduced to reflect this decrease.

Considerable research has been conducted in an effort to determine the limiting concrete compressive stress for struts. Much of this work has focussed on the webs of beams. Empirical relations for the efficiency factor of concrete struts in beam webs as suggested by Neilsen(9), Thurlimann(16), and Ramirez (12) are summarized in Fig. 2.17. Collins and Mitchell(11) present a more detailed method of determining the limiting stress in compression struts which is based on results of tests on shear panels. The compressive strength is related to the principal tensile strain along with the cylinder compressive strength.

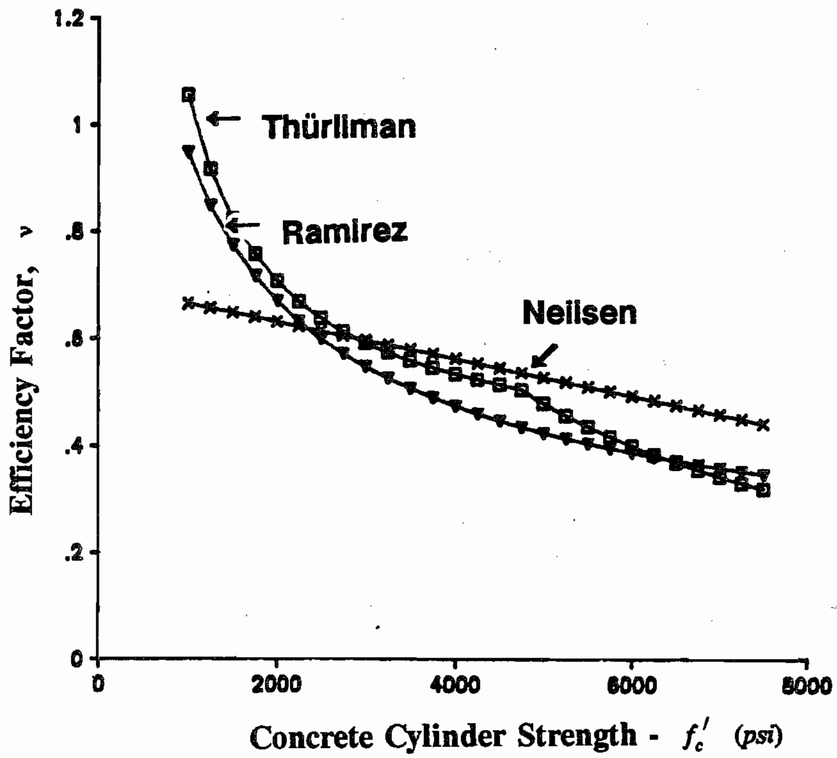

Figure 2.17 Effective Concrete Compressive Strength.

The various proposals for effective concrete stress are based on tests of continuous compression fields either in beams or shear panels. In more general applications, recommendations are required for isolated struts and nodes where the state of stress may be quite different from the continuous compression fields. Proposals for effective concrete strength from References 13 and 15 are summarized in Tables 2.1 and 2.2, respectively. It should be noted that a variety of different terms have been used in the literature to express the effective concrete stress. In this report f_{ce} will be used for consistency.

2.5 Modeling

2.5.1 General Guidelines. One of the key elements in the application of the strut-and-tie model is selection of an appropriate design model for a specific detail. Model development is constrained by the following considerations:

- Ease of Fabrication

TABLE 2.1 Effective Concrete Strength Limits Proposed by Schlaich[15]	
STATE OF STRESS AND/OR REINFORCEMENT LAYOUT FOR STRUT OR NODE	f_{ce}
Undisturbed and uniaxial state of compressive stress that may exist for prismatic struts and CCC-nodes	$0.85\,f_c'$
Tensile strains and/or reinforcement perpendicular to the axis of the strut may cause cracking parallel to the strut with normal crack width; this applies also to nodes where reinforcement is anchored in or crossing the node.	$0.68\,f_c'$
Tensile strains causing skew cracks and/or reinforcement at skew angles to the strut's axis	$0.51\,f_c'$
For skew cracks with extraordinary crack width. Skew cracks would be expected if modeling of the struts departs significantly from the theory of elasticity's flow of internal forces. Considerable redistribution of internal forces would be required to exploit the member's ultimate capacity.	$0.34\,f_c'$

Table 2.2 Effective Concrete Strength Limits Proposed by MacGregor[13]	
Structural Member	f_{ce}
Truss Nodes:	
Joints bounded by compressive struts and bearing areas	$0.85\,f_c'$
Joints anchoring one tension tie	$0.65\,f_c'$
Joints anchoring tension ties in more than one direction	$0.50\,f_c'$
Isolated compression struts in deep beams or D-regions	$0.50\,f_c'$
Severely cracked webs of slender beams:	
Strut angle = 30°	$0.25\,f_c'$
Strut angle = 45°	$0.45\,f_c'$

- Equilibrium
- Ductility
- Serviceability

In many cases practicality and ease of fabrication will have the greatest influence upon the configuration of the design model. Models which result in details that are overly congested or difficult to fabricate should be avoided. The reinforcement pattern selected for the detail should follow the reinforcement scheme used in adjacent portions of the structure.

In order to satisfy the requirements of the theory of plasticity, a model must be in equilibrium under the applied loads. However, if the selected force system or "truss" is to develop fully, the load carrying capacity of the struts and the rotational capacity of the nodes must not be exceeded before the ties yield. To fulfill the latter ductility requirement, it is suggested(15,17) that the model be oriented so as to approximate elastic stress trajectories.

A fundamental consideration in any design process is serviceability. According to Schlaich(15,17), crack control is provided by orienting the strut-and-tie model according to the elastic stress trajectories. In addition, accepted standards for bar spacings, minimum reinforcement, and control of creep and shrinkage should be followed.

In the B-regions of beams, inclined compression strut angles are limited to promote better serviceability behavior. It may be shown that the choice of a strut angle determines the relative amounts of longitudinal and transverse reinforcement. A very low strut angle requires a large amount of longitudinal reinforcement relative to transverse reinforcement while the converse is true for steep angles. In either case extreme strut angles may result in excessive cracking. Although various limits have been proposed, there is some agreement that strut angles should be between 30 and 60 degrees. Limits on strut angles have not been fully addressed for structural components other than beams even though it is apparent that similar problems may be encountered in other detailing situations. In more general details, however, it may be difficult to establish a frame of reference from which to measure strut angles.

2.5.2 Model Development. Some authors, in particular Schlaich(15), emphasize developing a model which conforms to the elastic stress trajectories within the structure. The elastic stress distribution in a structural element may be determined from a finite element analysis. A strut-and-tie model condenses internal forces along a few discrete lines of action of strut-and-tie elements and can only follow the continuous elastic stress distribution in a very general sense.

An example of the orientation of strut-and-tie elements along elastic stress trajectories is illustrated in Fig. 2.2 for the case of a truss model of a simple beam. In the upper portion of the beam principal compressive stresses are nearly parallel to the beam axis and are represented in the truss model by the upper horizontal strut. In the same manner the lower tension tie represents principal tensile stresses in the lower portion of the beam. Rather than selecting the location of the upper and lower chords based on the elastic stress distribution, the distance between the upper and lower chords is chosen to maximize the moment capacity of the section. Inclined compression struts are aligned with the curvature of compression trajectories near mid-depth of the beam but deviate from the compression stress directions at other locations. The same is true of stirrups (vertical ties) which correspond to principal tensile stresses only near the top of the beam and are oriented vertically primarily for ease of fabrication. Thus the truss model for a simple beam represents only an approximation of the elastic stress trajectories.

An alternative method for developing strut-and-tie models based on estimated load paths is presented by Schlaich[15]. Figure 2.18 demonstrates the load path for a typical D-region. After equilibrium of the D- region free body is satisfied, stresses on the boundaries are computed. The boundary stresses are subdivided and resultant force determined. A suitable load path between the resultant forces is then drawn. Load paths should follow the most direct route between forces and should not cross one another. After drawing the load paths a strut-and-tie model may be constructed. Load paths may be used in conjunction with elastic stress trajectories to aid in model development of the strut-and-tie system.

The selection of strut-and-tie elements is often complicated by the fact that, for any given detail, there may be more than one valid configuration. In general, the most suitable configuration is one that provides a path with the fewest deviations. Since the concrete struts are undeformable in comparison to the tension ties, the model should be chosen to minimize the volume of reinforcement[15]. Figure 2.19 illustrates two examples of this concept. In any case, the designer must rely heavily on judgement and practical considerations in the development of a suitable detail.

2.6 Summary

The strut-and-tie approach is a unified design concept that permits consistent treatment of all portions of a structure. It is a generalization of the well known truss analogy which has been used extensively as a conceptual model for concrete beams subjected to shear, bending and torsion. Strut-and-tie models have their basis in the theory of plasticity, but they may be applied by using a consistent set of rules without the need of complex theories.

The method is especially helpful in detailing situations for which no rational design procedure exists. The designer must envision the flow of forces within a detail and provide a viable means of transferring the force. By visualizing the flow of forces, the designer will have a better understanding of behavior.

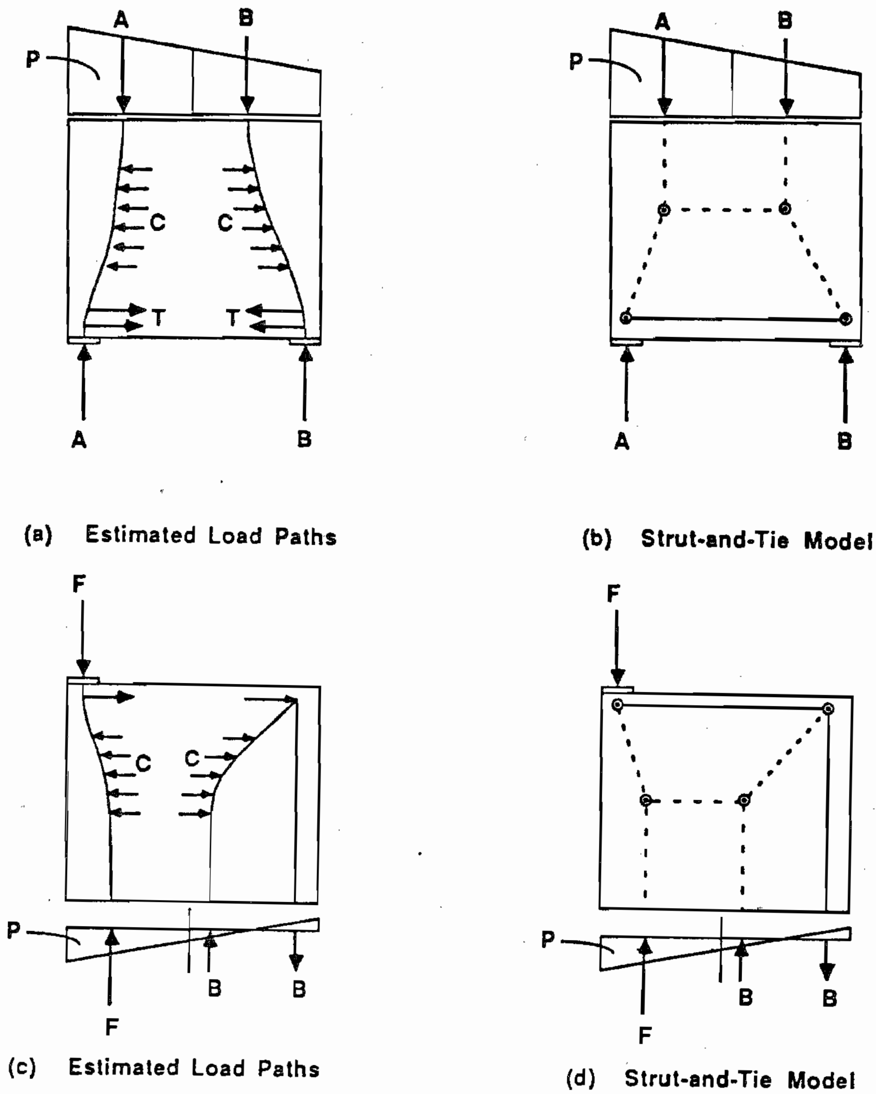

Figure 2.18 Load Path Method for Development of Strut-and-Tie Models (From Ref. 15).

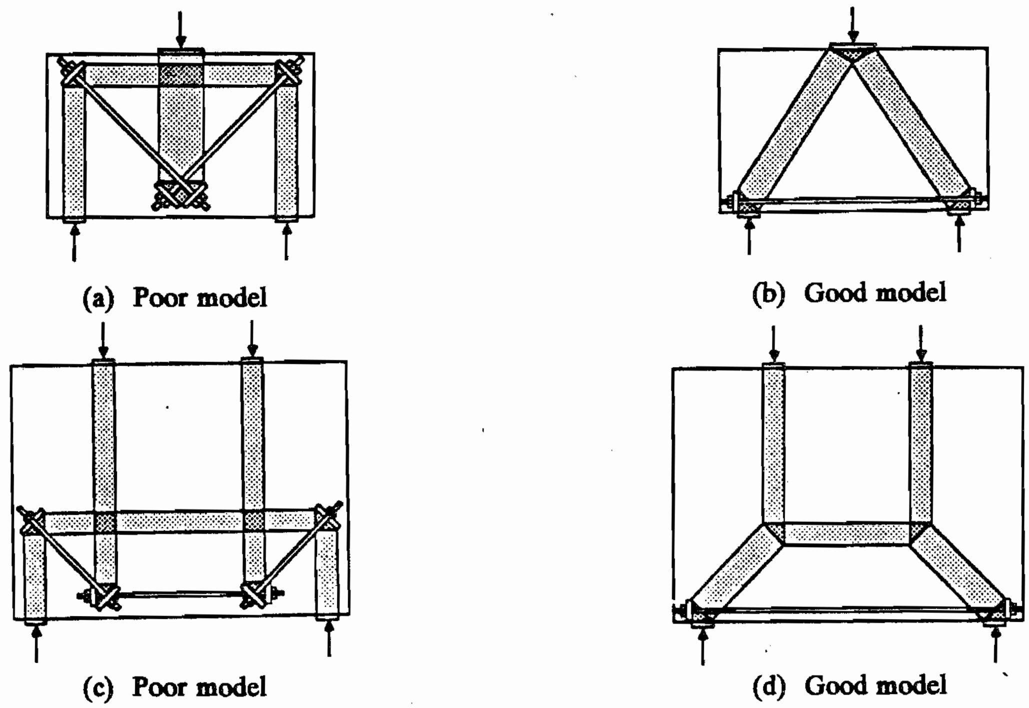

Figure 2.19 Optimization of Strut-and-Tie Models (From Refs. 13 and 15).

Despite the advantages of the strut-and-tie model, portions of it lack adequate definition and have not been extensively verified for use in designs meeting U.S. codes. Further research in the application of strut-and-tie models to various design situations is needed. Specific areas in which further guidance is required include:

- Distribution and spacing of reinforcement in ties
- Allowable concrete stress levels
- Nodes
- Serviceability criteria

The objective of this study was to review existing data and to produce new data addressing the areas identified above.

CHAPTER 3
TESTS OF DAPPED BEAM DETAILS

3.1 Introduction

In order to evaluate the use of the strut-and-tie model as a design tool, a dapped end beam was chosen for testing. The objective was to compare the behavior of specimens designed using strut-and-tie models and those designed using other accepted practices. Since the strut-and-tie model is presumed to represent internal forces within the structure, measured internal force distributions were compared with those assumed in the strut-and-tie model.

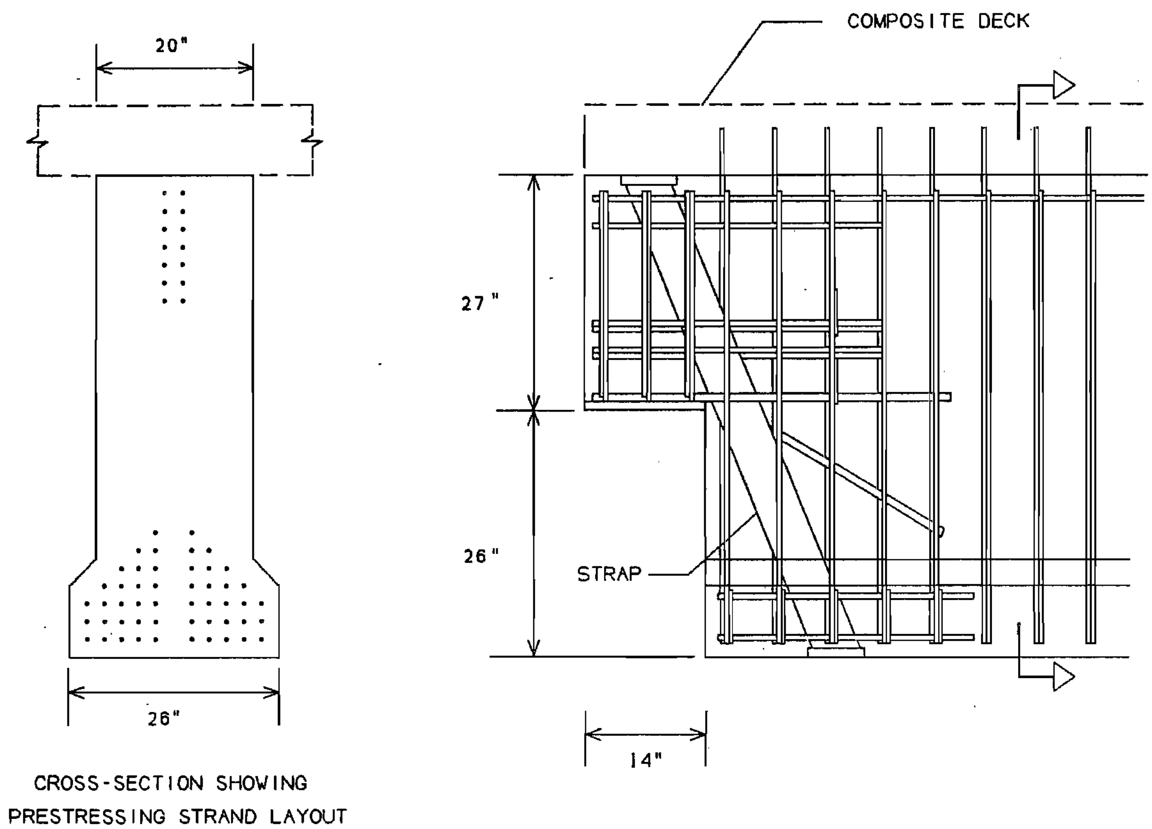

Figure 3.1 Prototype TSDHPT Dapped End Geometry.

3.2 Prototype and Model Selection

A typical TSDHPT dapped end detail is shown in Fig. 3.1. The test specimens were approximately half-scale models of the prototype TSDHPT girder (Fig. 3.2). In most TSDHPT girders with dapped ends, the girders are prestressed. The test specimens contained deformed reinforcement only. The reinforcement details and the beam section

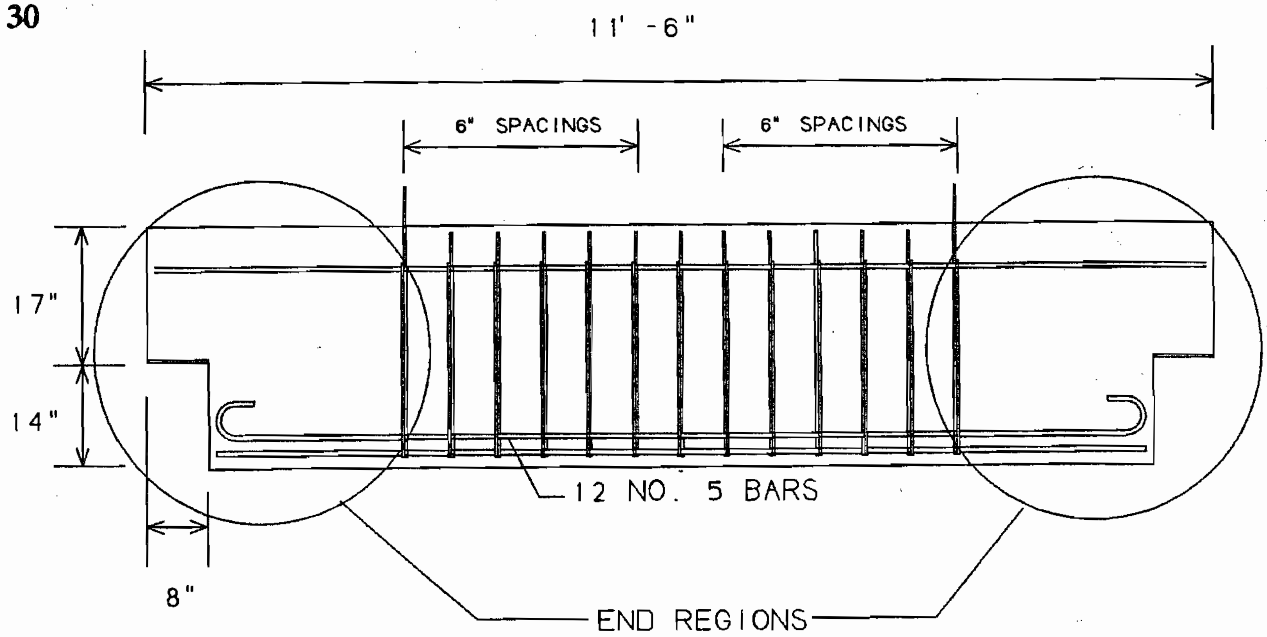

Figure 3.2 Test Specimen Geometry.

reinforcement consisted of 12 #5 bars arranged in two rows. Two #5 bars were placed longitudinally in the top portion of the beam to facilitate fabrication. The top four inches of the specimen were unreinforced to simulate the additional depth of a composite bridge deck. Outside of the dapped end regions #3 stirrups were placed at 6 in. on center. The stirrup details used are similar to TSDHPT practice (see Fig. 3.3). Each stirrup consisted of four legs with the center legs forming a hoop at the top to act as shear connectors for the composite deck. The beam had a rectangular cross-section with a 12 inch width which was selected to preclude any local compression failures and to represent the thickened end region often used in typical girders.

A total of four details were tested using two beams. Each detail was designed for an end load of 100 kips and a concrete compression strength of 5000 psi. No load factors or understrength factors were used. Grade 60 deformed reinforcing bars were utilized in the test specimens were standard deformed bars. All bars of a given size were from the same heat. Results of tensile tests on the bars indicated a yield point of 61 ksi for #3 bars and 67 ksi for #7 bars. Mild steel bar stock utilized for the strap had a yield stress of 48 ksi.

The concrete mix proportions are summarized in Table 3.1. The maximum coarse aggregate size was 3/4 inch. Six by twelve in. cylinder tests were utilized to determine the compressive strength of the concrete. The 28-day strength and the strength at the time of testing is given in Table 3.2 for each of the details.

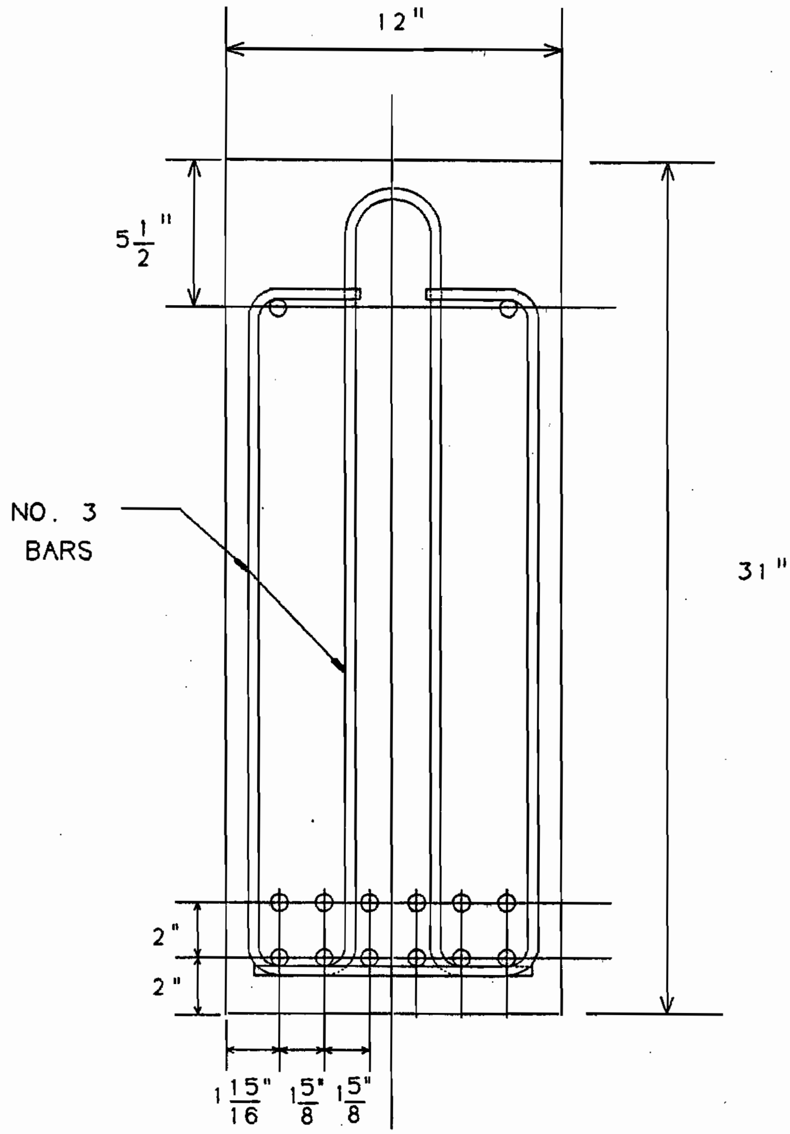

Figure 3.3 Cross-section Through Test Specimen.

3.3 Specimen ST1 - Strut-and-Tie Model

3.3.1 Choice of Model. A number of models have been proposed for dapped members which are based on different load paths. In the first case (Fig. 3.4a), a primary vertical tie placed just beyond the interface of the dap and by a horizontal tie extending from the dap into the full depth section provide the primary tensile ties for transferring forces. In the second case, a diagonal tie extending from near the top of the dapped portion of the beam down to the lower portion of the full depth section (Fig. 3.4b) provides the primary tensile force transfer capacity. The third case represents a case which combines the previous two cases (Fig. 3.4c).

Table 3.1 Concrete Mix Proportions

Cement	434	lb/yd
Coarse Aggregate	1870	lb/yd
Fine Aggregate	1385	lb/yd
Water	250	lb/yd
Retarder	14	oz/yd
Superplasticizer	47	oz/yd

The selection of a particular model represents a compromise between ease of fabrication and fidelity to the elastic principal stress directions shown in Fig. 3.5. The model in Fig. 3.4a results in a reinforcement pattern which is easy to place and is well suited to the overall reinforcement pattern of the beam. However, the model forces the load path to deviate substantially from elastic stress directions. The diagonal reinforcement required by the model in Fig. 3.4b is slightly more difficult to place and anchor properly but follows the principal elastic tensile stress directions closely. More complicated models such as the one shown in Fig. 3.4c result in congestion which complicates fabrication. However, it is obvious that the confinement provided in the crack-prone re-entrant corner region and the distribution of reinforcement should result in better performance.

Table 3.2 Summary of Concrete Strengths

Detail	28-Day Strength (psi)	Test Strength (psi)
ST1	6310	6280
MF	6310	6420
PCI	7470	7470
ST2	7470	7470

For test ST1 the strut-and-tie model shown in Fig. 3.6a was selected. It is assumed that a vertical load acts on the span away from the dap. Dead load is neglected to simplify the discussion.

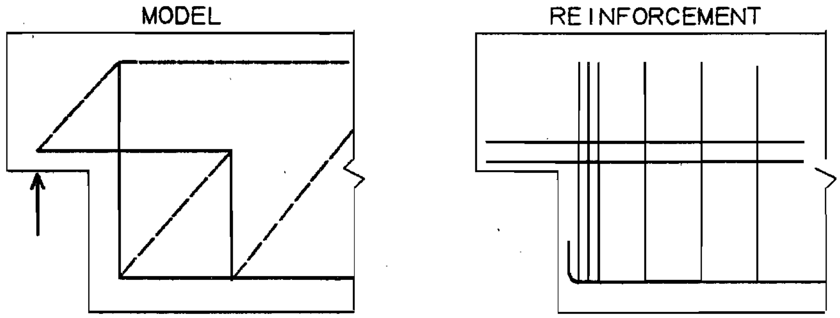

(a) Strut-and-tie model w/orthogonal ties (Ref. 15)

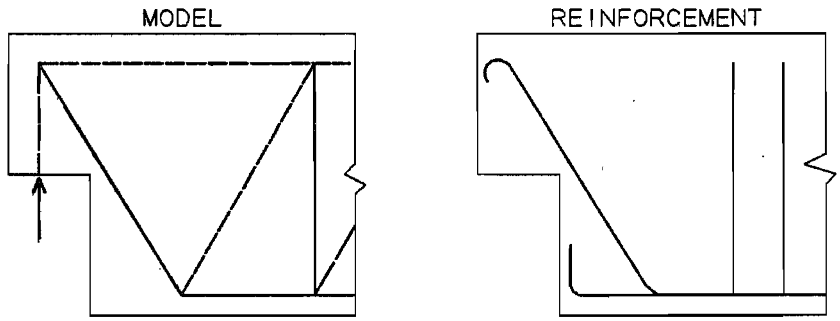

(b) Strut-and-tie model w/skewed ties (Ref. 17)

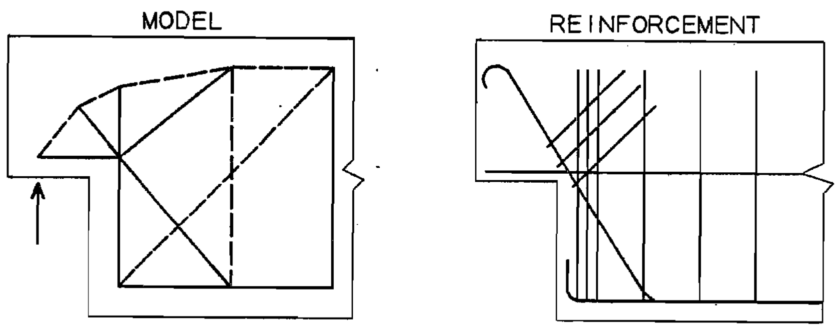

(c) Combined strut-and-tie model (Ref. 19)

——— TENSION MEMBER
— — COMPRESSION MEMBER

Figure 3.4 Strut-and-Tie Models for Dapped Beams.

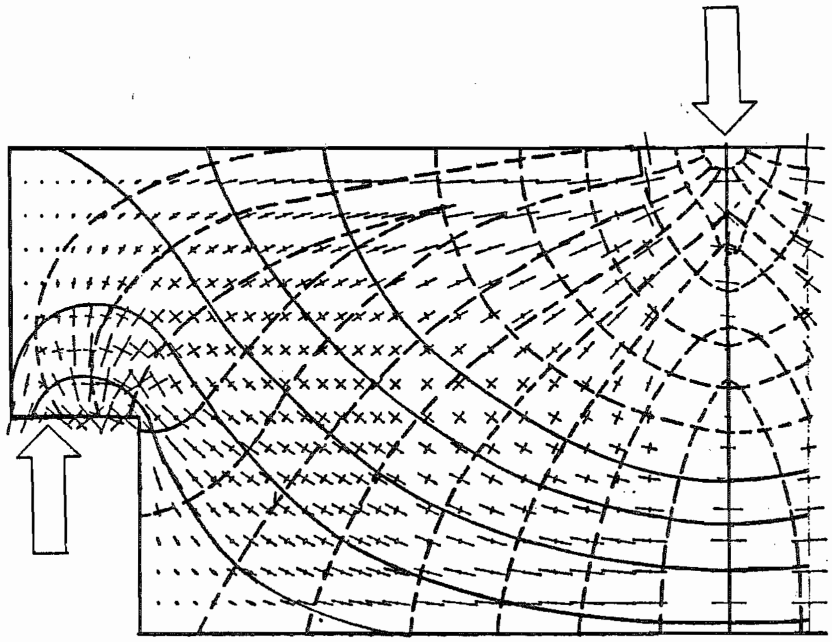

Figure 3.5 Elastic Stress Trajectories in a Dapped End (From Refs. 21, 24).

3.3.2 Design of ST1. The inclined compression strut angle, $\alpha = 50°$ was selected. The angle determines the magnitude of the forces in the members of the strut-and-tie model. Examination of tie forces in Fig. 3.6b shows that selecting a relatively steep angle is advantageous as a smaller area of reinforcement is required for the horizontal ties. A further consideration on selection of the strut angle, α is placement of reinforcement. Adequate space must be allowed for placement of reinforcement for ties 1 and 2. After selecting the strut angle, forces in the ties were determined and reinforcement for the ties was selected. It is logical to select reinforcement for vertical ties first. The force in the vertical ties is independent of model geometry and equals the beam reaction. Reinforcement should be placed within the boundary region where the ties are considered to act as shown in Fig. 3.7. For the vertical ties, the use of stirrups similar to the main shear reinforcement in the beam is most practical.

After selecting vertical reinforcement, horizontal reinforcement in the dapped end was determined (element 1 in Fig. 3.4a) from the tie force given in Fig. 3.6b. The location of vertical and horizontal tie reinforcement (elements 1,2 and 3 in Fig. 3.6a) should be checked to ensure consistency with the strut angle previously assumed. It may be necessary to revise the model geometry and repeat the design process at this stage.

After reinforcement for ties 1, 2 and 3 (Fig. 3.6a) was determined and located according to the strut angle selected, reinforcement for the lower longitudinal tie (member 7 in Fig. 3.6) was calculated. In most cases flexural reinforcement provided in the beam would be utilized for this tie element. After determining the size and placement of

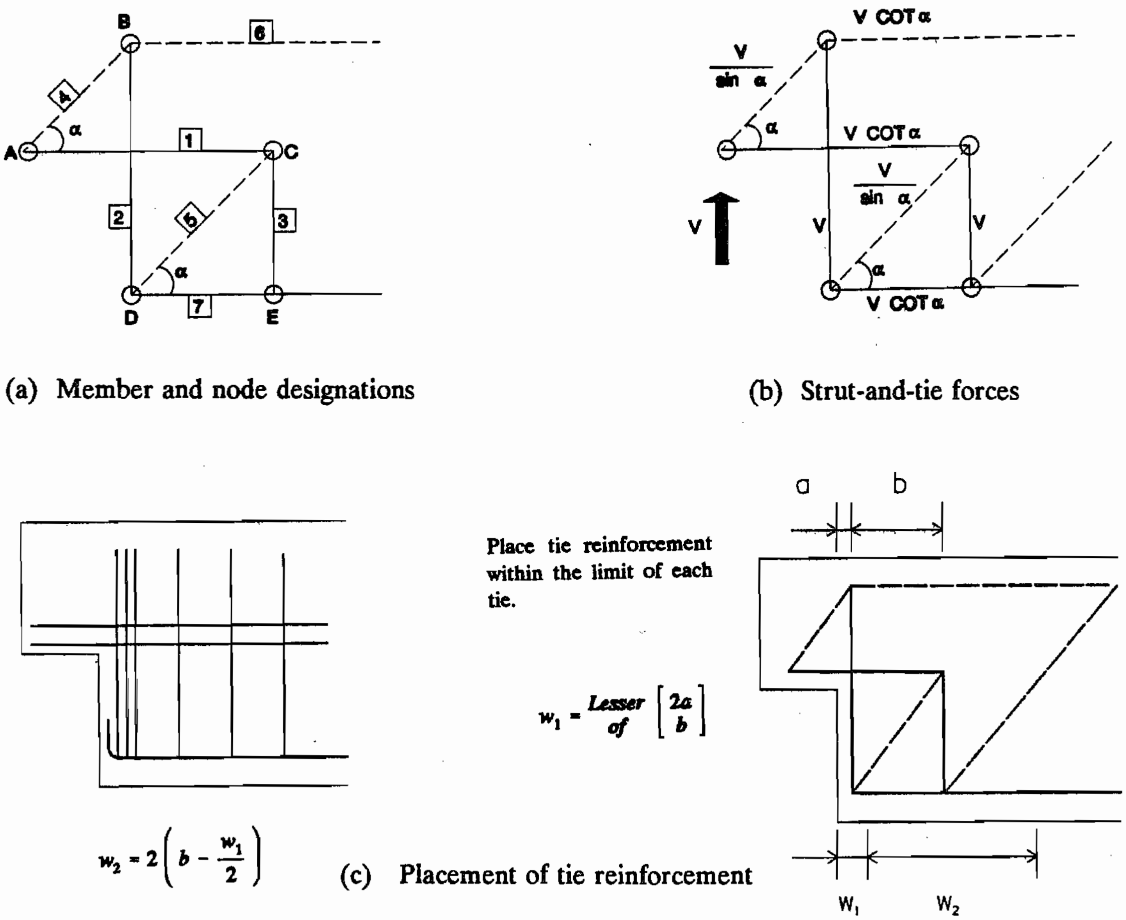

(a) Member and node designations

(b) Strut-and-tie forces

(c) Placement of tie reinforcement

Figure 3.6 Dapped Beam Model and Member Forces.

reinforcement within the dapped end, stresses in the concrete within the compression struts and at the boundaries of the nodes should be checked. If the dapped end is rectangular in cross- section, the critical areas for concrete compression stresses are at nodes A, B and D. Nodes A and B are CCT nodes. Methods of analyzing CCT-nodes were discussed in Section 2.3.3 and tests of such nodes are discussed in Chapter 6. The second area of concern with respect to concrete stress is the nodes at the lower corner of the full depth section (node D in Fig. 3.6a). The region joins two tension ties and a compression strut. Studies of the CTT node are presented in Chapter 7. Since the initial dapped beam tests were conducted prior to the tests on CCT and CTT-nodes, the geometry of the node for initial design purposes was defined by the width of the two ties and the angle of the compression strut. The resulting geometry was used to determine the stresses along the boundary of the CTT node.

Limitations on concrete stresses were discussed in Section 2.4. For initial design of the dapped beam a conservative lower bound on the allowable stresses in both the struts

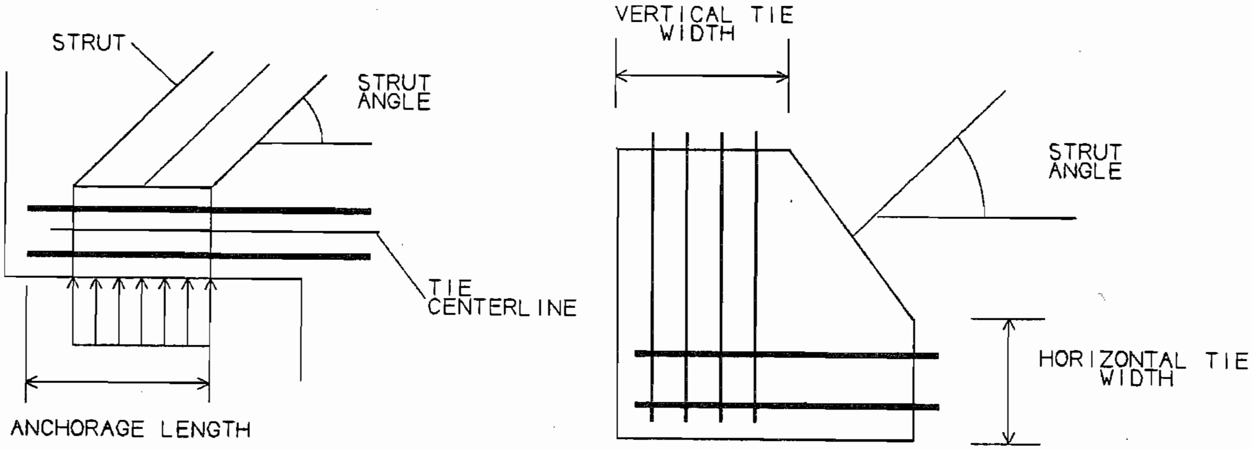

(a) CCT-node at support (b) CTT-node at bottom corner

Figure 3.7 Dapped Beam Nodes.

and node boundaries of dapped ends was selected. The allowable stress (see Table 2.2 and Ref. 12) was taken as 50% of the concrete compressive strength.

In the final step in the design process, anchorage of all ties must be examined. Of primary concern was the anchorage of the horizontal ties (elements 1 and 7 in Fig. 3.6) at Nodes A and D. In the case of tie 1, anchorage near the reaction may be assumed to start at the edge of the bearing area shown in Fig. 3.7. In most cases, however, adequate anchorage length will not be available even if hooks are employed. Possible solutions include welding the tie to an external bearing plate or using continuous bars bent with an end loop in the horizontal plane. The opposite end of the horizontal tie 1 must also be anchored by providing adequate development length. The point at which the tie must be fully developed cannot be precisely determined. A similar situation exists for the lower horizontal tie except that no bearing plate is available at that location. It can be seen that closed hoop vertical ties will help confine the concrete around the horizontal tie elements and improve anchorage characteristics. Obviously, anchorage of the vertical ties is equally important. In most cases stirrups will be used to provide the reinforcement for the vertical ties. The stirrups should be anchored around longitudinal reinforcement at both ends.

Following the procedures outlined above, the arrangement of reinforcement is summarized in Fig. 3.8. A sketch of the reinforcement is shown in Fig. 3.9. The vertical ties were arranged as shown in Fig. 3.3. The horizontal tie at the bottom of the dap was reinforced with three #4 bars and four #3 hoops. In keeping with TSDHPT detailing practices, the #4 bars were welded to a steel bearing plate at the base of the dap. A series of vertical bars were also welded to the bearing plate as typical of TSDHPT practice. The bearing plate assembly is shown in Fig. 3.9. Anchorage of the horizontal tie within the full depth section was provided by extending the reinforcement 14.5 in. beyond the center of node C (Fig. 3.6), a distance approximately 25 percent greater than the ACI or AASHTO

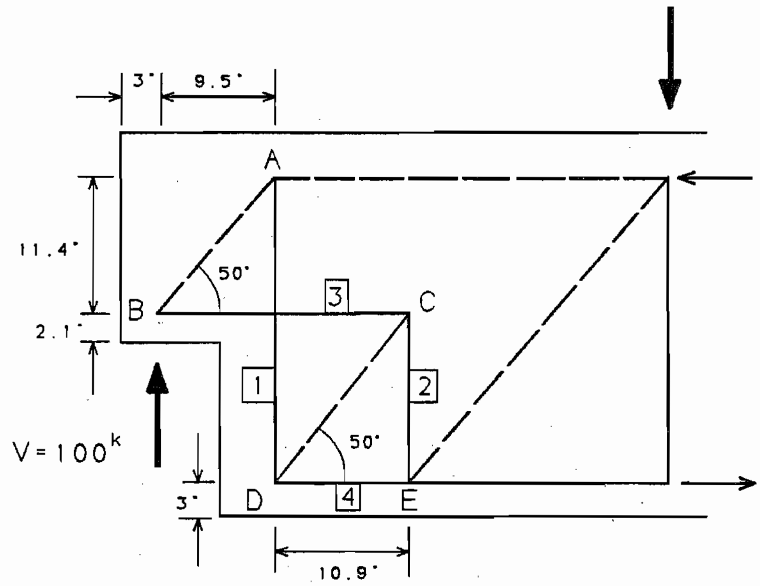

TIE	FORCE (kips)	AREA REQUIRED (in^2)	AREA PROVIDED (in^2)	DESCRIPTION OF REINFORCEMENT
1	100	1.67	1.76	4 sets of #3 stirrups
2	100	1.67	1.76	4 sets of #3 stirrups
3	83.3	1.39	1.48	Three #4 bars and four #3 hoops
4	83.3	1.39	3.68	Twelve #5 bars

Figure 3.8 ST1 - Reinforcement Summary.

development length[1,2]. The beam flexural reinforcement provided tie number 4. At the end of the full depth section, the #5 bars cannot be anchored using straight development lengths. Thus, the top row of the flexural reinforcement was terminated with 180 degree hooks. This ensures that enough reinforcement is anchored to resist the force predicted by the strut-and-tie model. Because of the relatively large width of the test specimens, it was felt that the compression stresses in the concrete would not control the behavior of the specimen. Thus, a detailed examination of the struts and nodal regions was not conducted as part of the specimen design. In addition to reinforcement provided specifically to satisfy the requirements of the strut-and-tie model, some additional reinforcement was used. Three #3 hoops were placed vertically within the nib. This reinforcement along with the vertical bars welded to the bearing plate served to provide local shear reinforcement for the nib. The nib reinforcement used in the specimen is typical of TSDHPT detailing practices. A series of #3 ties were used to support the stirrups making up the vertical ties. Beyond the vertical tie reinforcement, stirrups were placed on 6 in. centers.

More reinforcement was provided than was required as bar areas were rounded and minimum bar size used (Fig. 3.8). In order to have a basis for comparing different specimens, it is helpful to assess the theoretical capacity of the final design. Using strut-

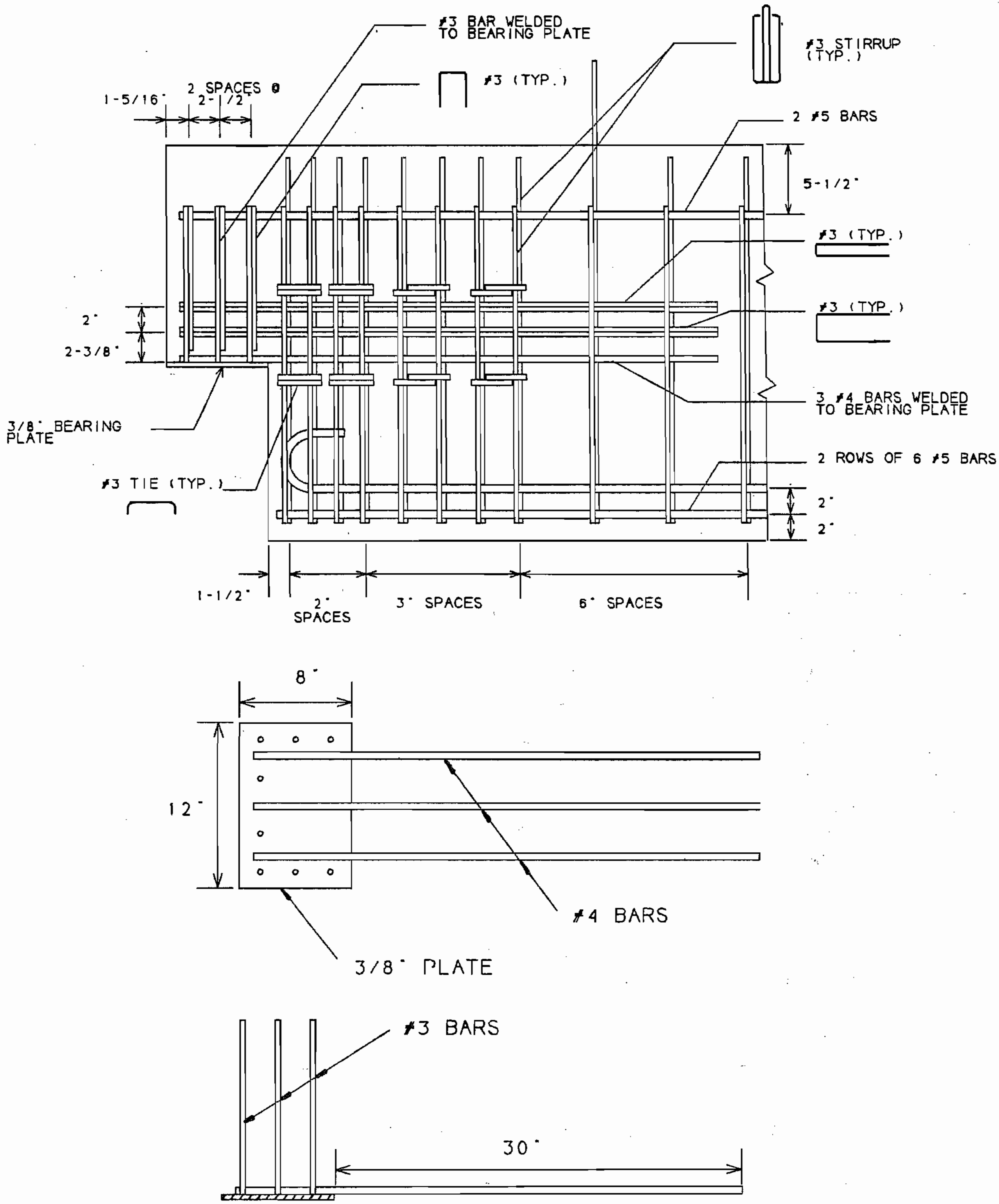

Figure 3.9 ST1 - Reinforcement Layout.

and-tie model principlaes, it is assumed that failure will be due to yielding of reinforcement and the ultimate load will not be affected by concrete strength. The predicted strength of ST1 was 106 kips and was controlled by the capacity of the vertical ties.

3.4 Specimen PCI - Prestressed Concrete Institute Design Method

3.4.1 General Description. The design method presented in the *Prestressed Concrete Institute Design Handbook*[3] is primarily based on research performed at the University of Washington[20, 22] and sponsored by the Prestressed Concrete Institute (PCI). The general design procedure presented in Ref. 3 pertains to reinforced members with short "daps" and relatively thick webs. The PCI design method combines aspects of the strut-and-tie approach with shear friction theory. Two basic reinforcement patterns are defined by the PCI procedure. The first consists of an orthogonal system of reinforcement (Fig. 3.10a). A skewed system of reinforcement is also possible (Fig. 3.10b).

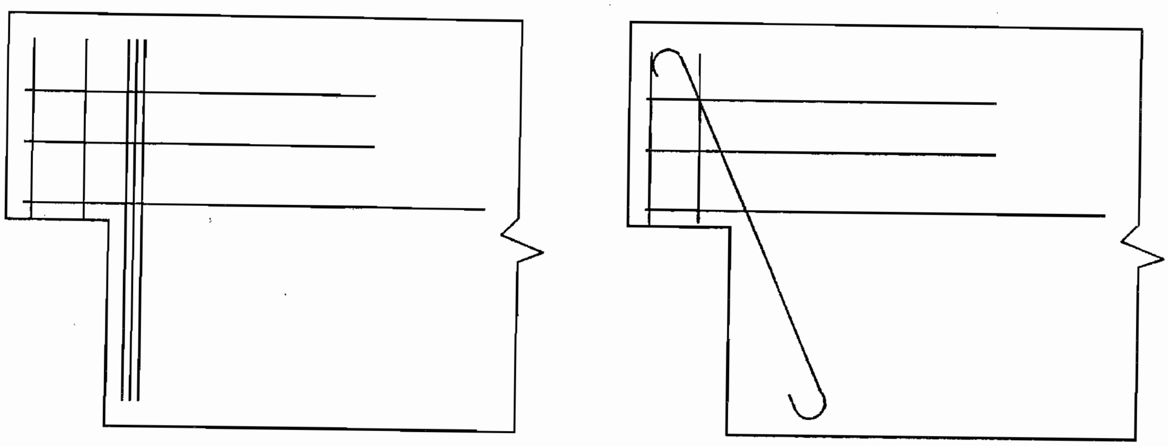

(a) Orthogonal reinforcement (b) Skewed reinforcement

Figure 3.10 PCI Design Methods - Reinforcement Patterns (From Ref. 1).

3.4.2 Reinforcement Requirements. The PCI design procedure is illustrated in Fig. 3.11 for the orthogonal reinforcement pattern. Primary reinforcement is placed vertically near the dap interface and horizontally near the bottom of the dap. The required area of primary reinforcement (A_{sh} and A_s) may be derived by considering a simple strut-and-tie model (Fig. 3.11b). The primary vertical reinforcement (A_{sh}) consists of a group of closely spaced stirrups placed as close as possible to the interface of the dapped beam. Primary horizontal reinforcement (A_s) consists of a series of bars placed near the bottom of the extended end. For the test specimen primary vertical and horizontal reinforcement was sized using the strut-and-tie model shown in Fig. 3.12. Four groups of #3 stirrups were

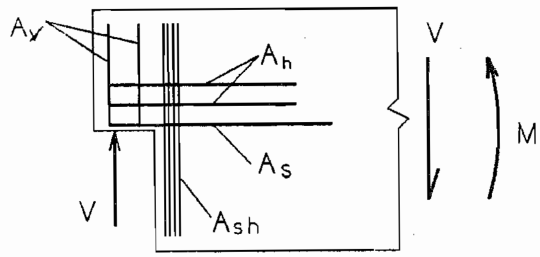

(a) Reinforcement pattern and loading

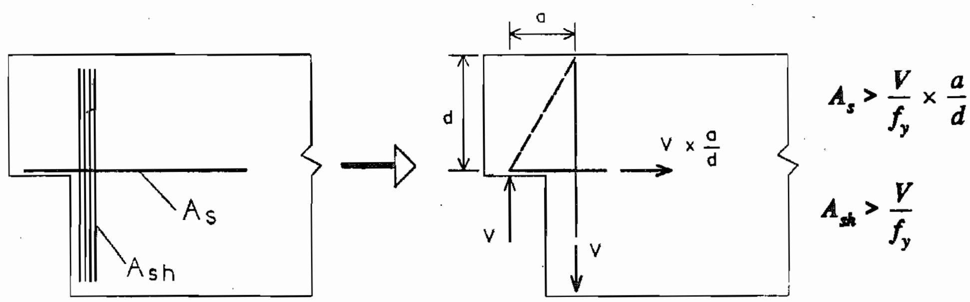

(b) Step 1 - Primary reinforcement

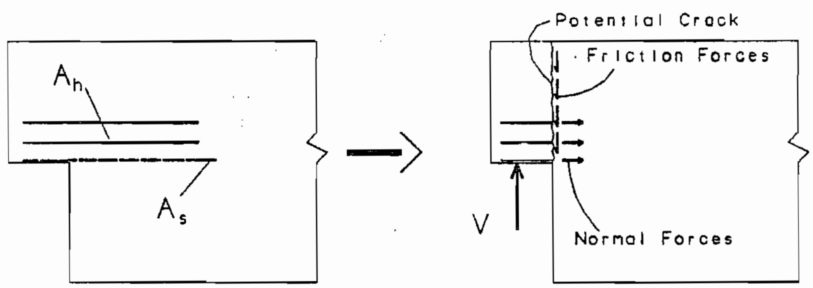

FICTIONAL RESISTANCE > SLIDING FORCE, V

$$\mu_e \,(A_s + A_h)\, f_y > V$$

where: $\mu_e = \dfrac{(1000 \text{ psi})\, \mu\, b\, h}{V}$, the effective coefficient of friction

and b = width of beam

h = height of dap

μ = coefficient of friction (1.4)

Minimum distributed reinforcement: $A_h > 0.5\, A_s$

(c) Step 2 - Shear friction reinforcement

Figure 3.11 Summary of PCI Design Method.

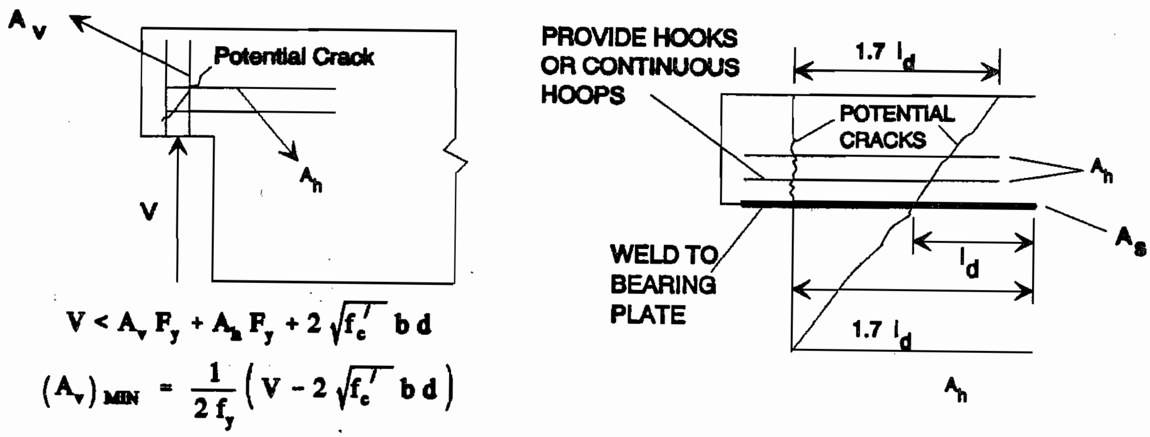

(d) Step 3 - Local (vertical) shear reinforcement (e) Anchorage requirements

Figure 3.11 Summary of PCI Design Method (continued).

placed adjacent to one another providing the primary vertical reinforcement. The #5 bars were provided as primary horizontal reinforcement. The primary horizontal reinforcement was welded to a bearing plate similar to that used in specimen ST1.

The next step in the PCI design procedure is to determine an additional area of distributed horizontal reinforcement (A_h) based on shear friction developed across a potential vertical crack beginning at the re- entrant corner (Fig. 3.11c). The total area of horizontal reinforcement must be large enough to produce a frictional force along the crack which equals the reaction. The frictional resistance is determined using the coefficient of friction μ = 1.4 but not exceeding a value of 1000 psi on the critical concrete section. A minimum area of shear friction reinforcement (A_h) equal to one-half the primary horizontal reinforcement (A_s) must be provided. The shear friction reinforcement (A_h) is distributed over the lower two-thirds of the dap. Three #3 bars bent in continuous hoops were provided to meet the distribution requirement on the lower 2/3 of the dap but only two #3 hoops were required for shear friction reinforcement (Fig. 3.12).

The final step in the PCI design procedure is to provide local shear reinforcement (A_v) for the extended end. The local shear reinforcement serves to resist the formation of a diagonal tension crack in the dap (Fig. 3.11d). Required shear reinforcement (A_v) is determined in a manner similar to the design of shear reinforcement in deep beams. The shear reinforcement in the nib was identical to that used in ST1.

3.4.3 Anchorage Requirements. In addition to providing the proper amount of reinforcement, the PCI design procedure gives detailing requirements which ensure that the necessary forces may be developed in the reinforcement. Some of these detailing considerations are illustrated in Fig. 3.11e. To positively anchor the primary horizontal reinforcement in the extended end welding bars to bearing plate or to crossbars is suggested. The primary horizontal reinforcement should be extended at least one development length past a potential diagonal crack beginning at the bottom corner of the

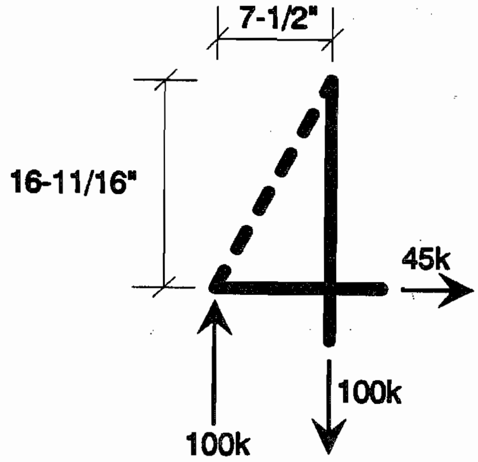

VERTICAL REINFORCEMENT (A_{sh})

Required: 1.67 sq. in.

Provided: 4 sets of #3 stirrups
(1.76 sq. in.)

HORIZONTAL REINFORCEMENT (A_s)

Required: 0.75 sq. in.

Provided: 3 - #5 bars
(0.92 sq. in.)

(a) Primary reinforcement

SHEAR FRICTION

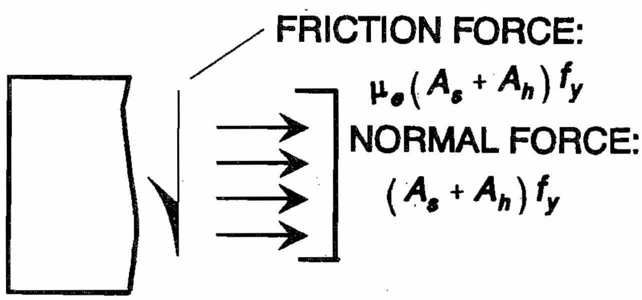

$$100 = \mu_e(A_s + A_h)f_y$$

$$(A_s + A_h) > 0.59 \text{ sq. in.}$$

MINIMUM DISTRIBUTED REINFORCEMENT: (A_h)

Required: 0.38 sq. in.

Provided: 3 - #3 hoops
(0.66 sq. in.)

(b) Distributed reinforcement

Figure 3.12 Specimen PCI Design Summary.

beam (see Fig. 3.11e). All horizontal reinforcement should extend a distance of 1.7 times the development length past the end of dapped portion of the beam. The bottom layer of horizontal reinforcement (A_s) will typically consist of larger bar sizes than that used for the shear friction reinforcement (A_h). Thus, required development lengths may differ. Primary horizontal reinforcement in the test specimen was extended 35 in. beyond the interface of the dap. The required extension is 32.5 in. based AASHTO/ACI development length requirements. Final reinforcement details are shown in Fig. 3.13.

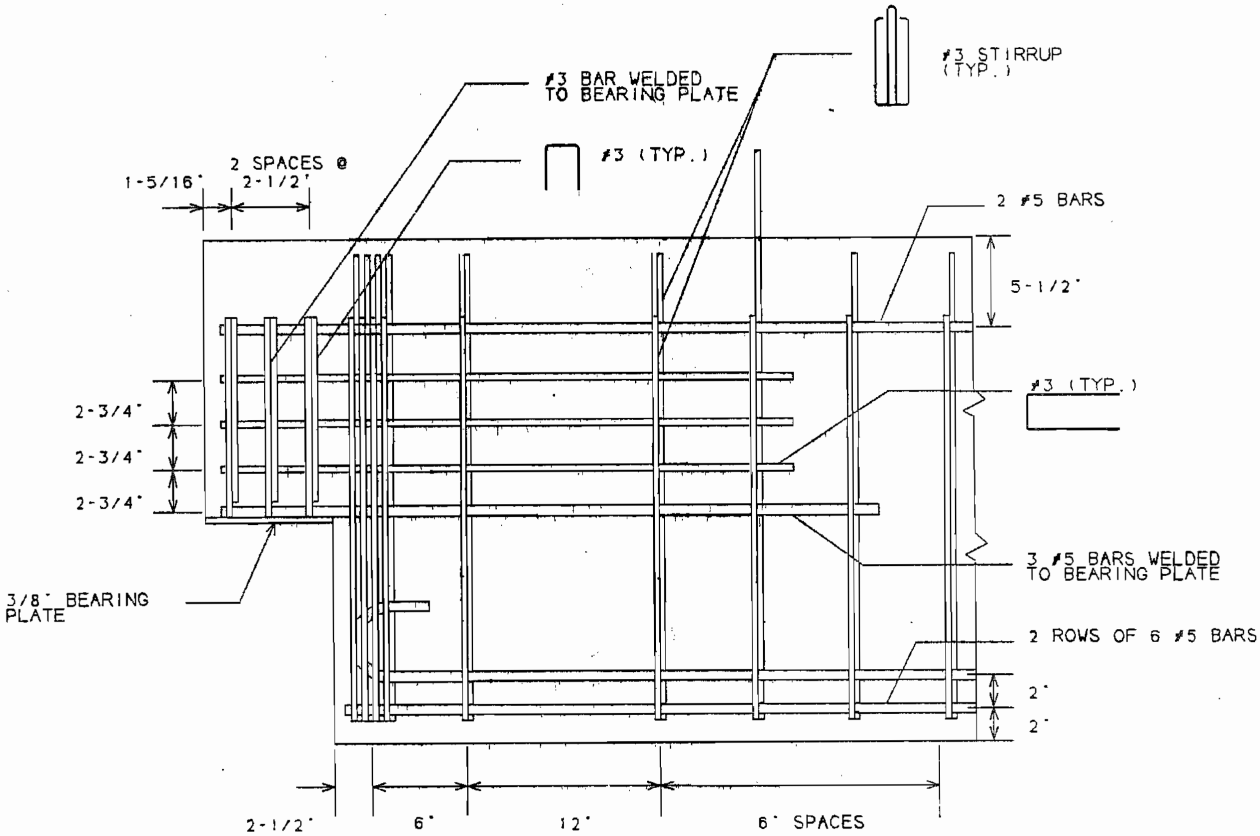

Figure 3.13 Specimen PCI - Reinforcement Layout.

3.4.4 Concrete Strength. The PCI limit on the shear capacity of the dapped end is based on the compressive strength of the concrete and the proportions of the dap. The limit is given by the following equation:

$$V_u \leq 0.2 f_c' \leq 800\, bd$$

where V_u = Shear strength of the nib; f_c' = 28 day cylinder compressive strength; b = width of the nib; d = distance from top of beam to center of dap reinforcement, A_s (see Fig. 3.11b).

To predict the capacity of Specimen PCI, it was assumed that its capacity would be controlled by the component of reinforcement with the smallest capacity relative to its required capacity. In this case, the primary vertical reinforcement controls and the predicted capacity is 105.6k.

3.5 Specimen MF -- Menon/Furlong Design Procedure

3.5.1 General Description. This design method is based upon a research study conducted by the Center for Transportation Research at the University of Texas at Austin. The study, co-sponsored by the TSDHPT and the Federal Highway Administration was conducted by Menon and Furlong[23] and is currently used by the TSDHPT for dapped beams.

The Menon/Furlong design method utilizes a "strap" placed diagonally from the top of the dap to the bottom corner of the full depth section. The strap consists of a series of mild steel flat bars welded to anchor plates at each end. In addition to the strap, horizontal shear friction reinforcement is also provided. The arrangement of reinforcement is illustrated in Fig. 3.14a. The detail was developed specifically for the design of prestressed bridge girders. A sketch of the reinforcement is showin in Fig. 3.16.

3.5.2 Reinforcement Requirements. The first step in the design procedure is to determine the required area of horizontal reinforcement using shear-friction principles (Fig. 3.14b). A crack parallel to the strap is assumed. An area of reinforcement must be provided across the crack so that the frictional resistance along the crack will be greater than the sliding force. The sliding force is the component of the reaction (V) which acts parallel to the strap. Sliding is resisted when normal forces are developed across the crack. Normal forces are produced by the horizontal shear friction reinforcement (A_s) and by the component of the reaction (V) acting normal to the axis of the strap. Frictional resistance is the product of the normal forces and the modified coefficient of friction (μ'). The assumed crack surface contains areas with steel-to-concrete contact along with areas of concrete-to-concrete contact. Each of the situations is characterized by a different coefficient of friction (Fig. 3.14b). Thus, a weighted coefficient of friction is determined for the entire crack surface based on the area of the steel strap relative to the area of concrete. The weighted coefficient of friction is then used to determine the modified coefficient of friction using the formula shown in Fig. 3.14b. The shear friction reinforcement in Specimen MF was designed as shown in Fig. 3.15a. Three #4 bars and a #3 bar bent into a hoop were provided as shear friction reinforcement. The #4 bars were welded to a bearing plate as in Specimens ST1 and PCI.

The next step in the Menon/Furlong procedure is to design the strap. A trapezoidal section is defined by an assumed diagonal crack beginning at the re-entrant corner (Fig. 3.14c). Required strap force is determined by summing moments about point B. The free body is assumed to extend horizontally past the re-entrant corner a distance equal to twice the height of the dap. Point B is located at half the distance from the top of the beam to the neutral axis (c). The neutral axis position may be determined by taking the static moment of areas on a section through the beam about the neutral axis using transformed steel areas. Forces which act on the section include the reaction, strap force, forces in the horizontal reinforcement and stirrup forces. The stirrups indicated in Fig. 3.14c are provided as normal beam shear reinforcement and are designed as if the dap were not present. Stirrups placed at 3, 12, and 10-inch spacing beginning at the start of the full depth section were provided to represent normal beam shear reinforcement. The stirrup at the extreme end of the section was neglected in the strap design as it is positioned very close to the boundary of the section. The strap area was determined by summing moments about point B on the section in Fig. 3.15. A drawing of the strap assembly used in the test specimen is shown in Fig. 3.16. A portion of the horizontal shear friction reinforcement was welded to a bearing plate assembly similar to that in ST1 and PCI. Local shear

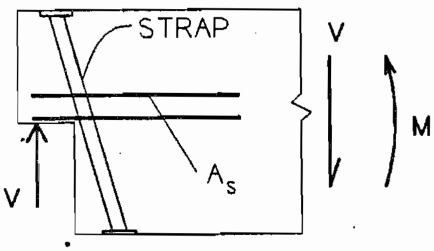

(a) Reinforcement pattern and loading

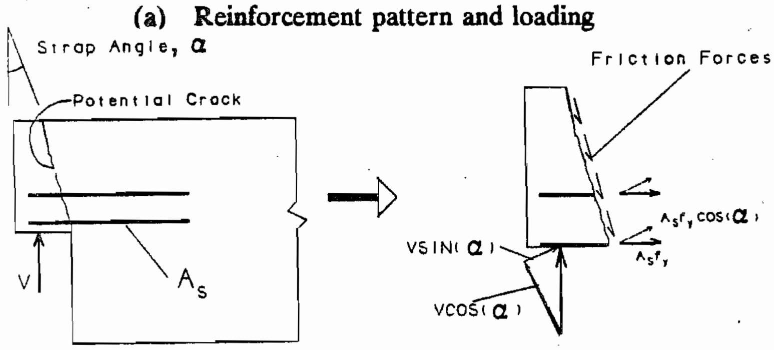

FRICTIONAL RESISTANCE > SLIDING FORCE

$$\mu'(V\,SIN\,\alpha + A_s f_y\,COS\,\alpha) > V\,COS\,\alpha$$

$$\mu' = \left(\frac{300\mu_w}{v} + 0.5\right) = \textit{Modified coeff. of friction}$$

μ_w = Weighted coefficient of friction determined based on relative areas of steel and concrete along crack surface

μ = 0.7; steel to concrete

μ = 1.4; concrete to concrete

$v = V / A_{cr}$, where A_{cr} = Area of Crack Surface

(b) Step 1 - Shear friction reinforcement

Figure 3.14 Summary of Menon/Furlong Design Method.

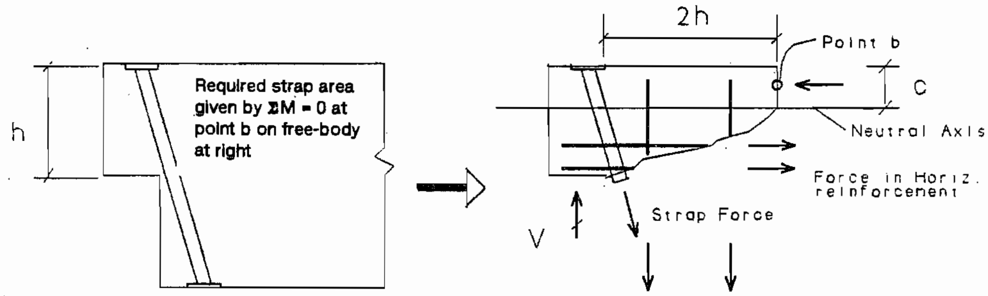

(c) Step 2 - Strap

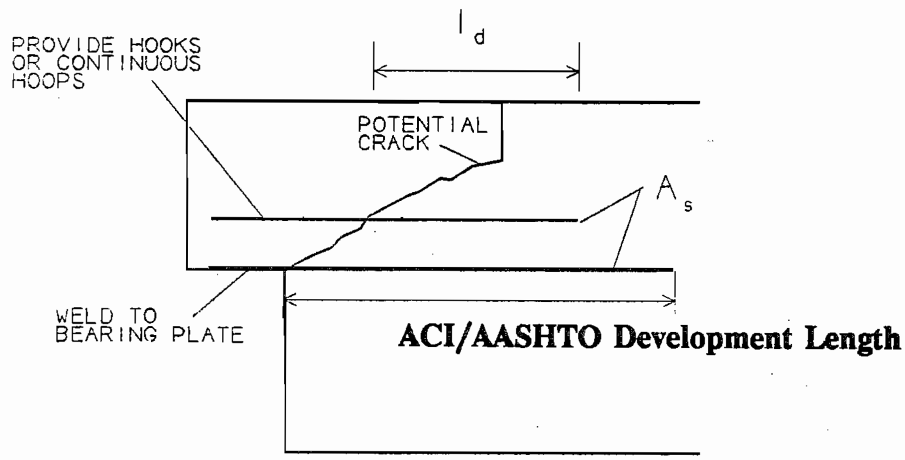

(d) Anchorage requirements

Figure 3.14 Summary of Menon/Furlong Design Method (continued).

welded to a bearing plate assembly similar to that in ST1 and PCI. Local shear reinforcement for the nib was identical to the previous two specimens. A sketch of the reinforcement is shown in Figure 3.16.

To anchor bars within the dap, it is recommended that the bottom layer of reinforcement be welded to a bearing plate placed beneath the dap. At the opposite end the reinforcement must extend at least one development length past the diagonal crack assumed in determining the strap area (Fig. 3.14d).

The predicted capacity of Specimen MF was determined from the failure modes possible: shear friction failure or failure due to yielding of the strap. Failure due to yielding of the strap was found to be critical. Calculating the strap force acting on the section in Fig. 3.15c by using the area of the strap actually used, it was estimated that a reaction (shear capacity) of 112k can be resisted by Specimen MF.

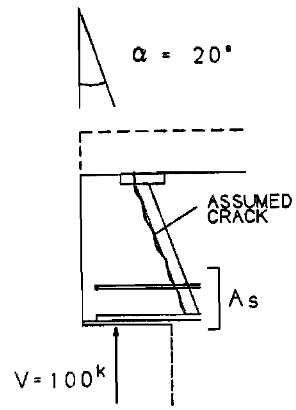

$$SLIDING\ FORCE = V\ COS(\alpha)$$
$$NORMAL\ FORCE = A_s F_y\ COS(\alpha) + V\ SIN(\alpha)$$
$$COEFFICIENT\ OF\ FRICTION = 1.3$$
$$FRICTION\ FORCE = 1.3\,(56A_s + 34)$$
$$\frac{SLIDING}{FORCE} = \frac{FRICTION}{FORCE}$$

<u>Required:</u> 0.68 sq. in.

<u>Provided:</u> 3 - #4 bars and 1 = #3 hoop (0.82 sq. in.)

(a) Shear friction reinforcement (A_s)

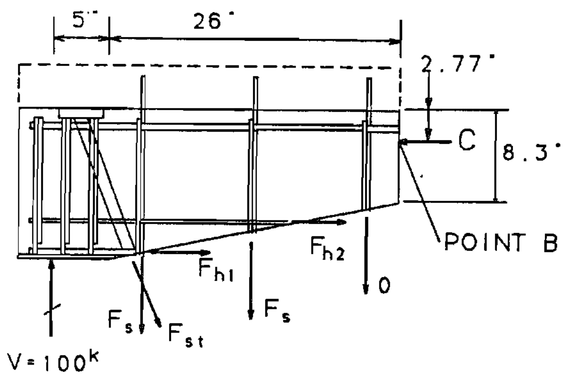

STRAP AREA

$$\sum M_B = 0$$

<u>Required:</u> 1.0 sq. in.

<u>Provided:</u> 4 - 1¼ x ¼″ flatbars
(1.25 sq. in.: f_y = 50 ksi)

F_s = Stirrup Force = 26.4^k
F_{hl} = Force in lower horizontal = 36^k
F_{hs} = Force in upper horizontal = 13.2^k
C = Concrete compressive force
F_{st} = Strap force

(b) Strap design

Figure 3.15 Speciment MF, Design Summary.

3.6 Specimen ST2 -- Modified Strut and Tie

Specimen ST2 was designed using the modified strut-and-tie model shown in Fig. 3.17. In the design the truss geometry was varied to determine if internal forces could be distributed as desired. In contrast to the model used in the design of specimen ST1, the location of node A was lowered. The change in node A significantly affects the force distribution within the truss. The force level in the first vertical tie is reduced by 50 percent compared to ST1. Correspondingly, the force level in horizontal tie 4 is increased by 50 percent and the tie extends further into the beam to node E. Also, equilibrium requirements at node E result in struts that are not collinear. The reinforcement requirements are summarized in Fig. 3.17. Figure 3.18 shows the overall detail.

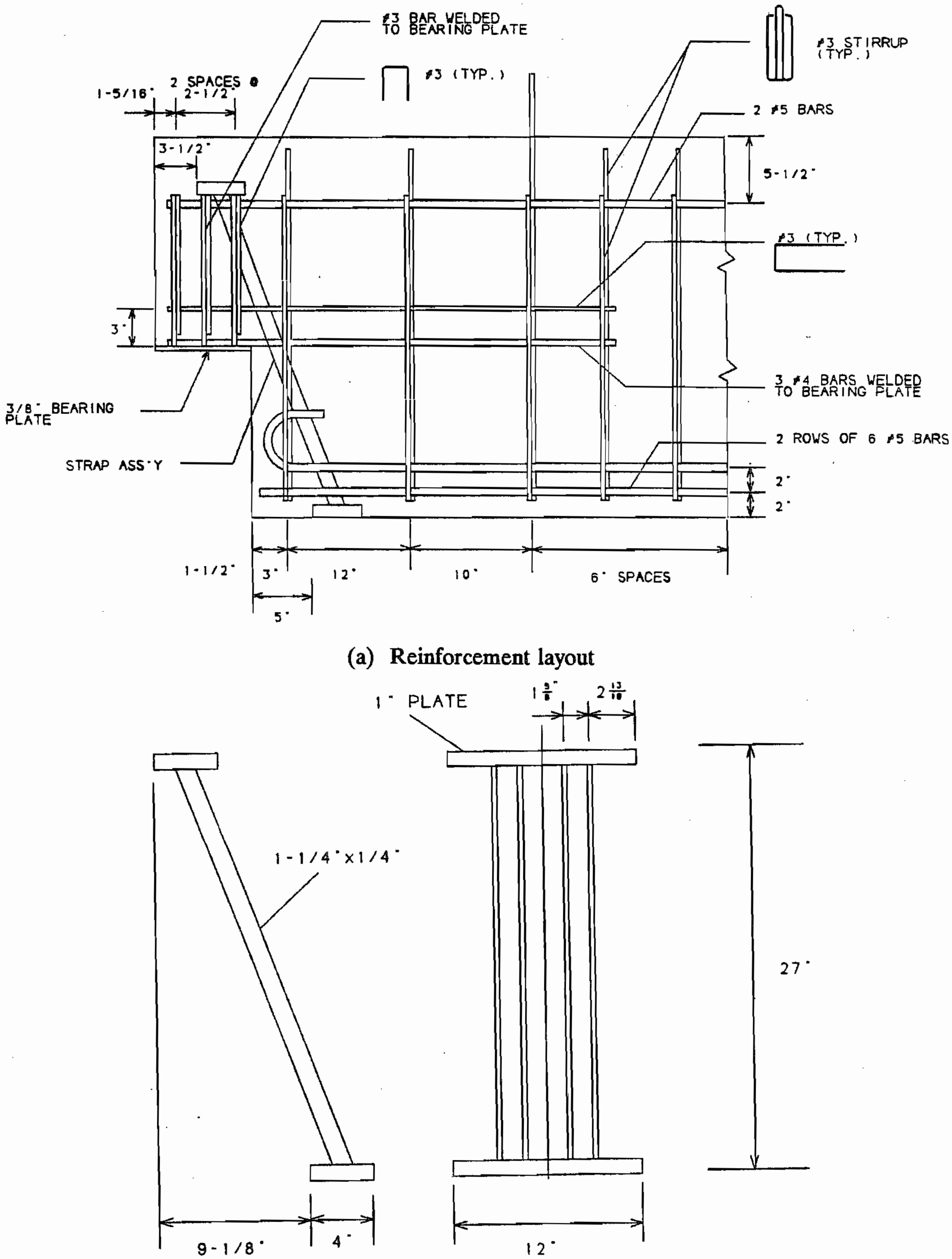

(a) Reinforcement layout

(b) Strap assembly

Figure 3.16 Specimen MF

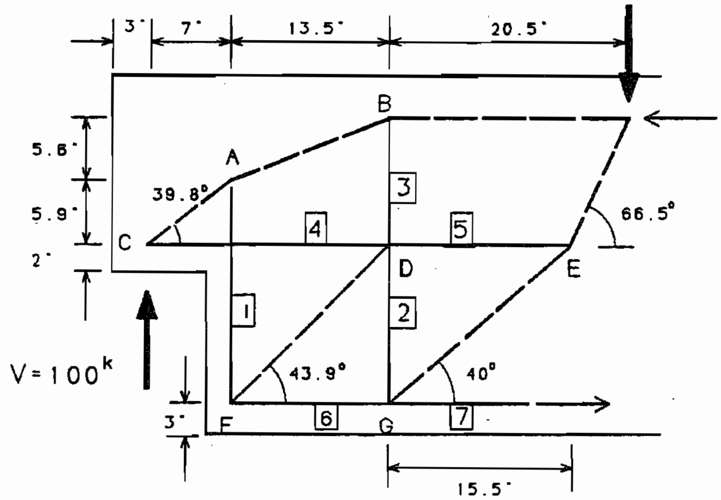

TIE	FORCE (kips)	AREA REQUIRED (in^2)	AREA PROVIDED (in^2)	DESCRIPTION
1	50	0.83	0.88	Two sets of #3 stirrups
2	100	1.67	1.76	Four sets of #3 stirrups
3	50	0.83	1.76	Four sets of #3 stirrups
4	120	2.0	2.04	Four #5 bars and two #4 hoops
5	71.9	1.20	2.04	Four #5 bars and two #4 hoops
6	48	0.50	3.68	Twelve #5 bars
7	167	2.78	3.68	Twelve #5 bars

Figure 3.17 Specimen ST2 - Design Model and Reinforcement Summary.

The first vertical (tie 1) was provided with two sets of #3 stirrups and the second vertical tie (tie 2) with four sets of #3 stirrups. The reinforcement for vertical tie 2 was continued to provide reinforcement for tie 3. Thus, tie 3 had more than double the reinforcement it actually required (Fig. 3.17). This was done because it seemed impractical to terminate a portion of the stirrups used for tie 2. Four #5 bars and two sets of #4 bars bent in continuous hoops were used to reinforce the upper horizontal ties. The #5 bars were welded to a bearing plate assembly similar to other details. The horizontal reinforcement was continued through to node E to reinforce tie 5. The #4 hoops were extended approximately 14 in. past the center of node E to anchor the force developed there. As in ST1, the beam flexural reinforcement provided horizontal ties 6 and 7 as in ST1. Local shear reinforcement for the nib was identical to that used in the other details. The predicted capacity of ST2 was 102k.

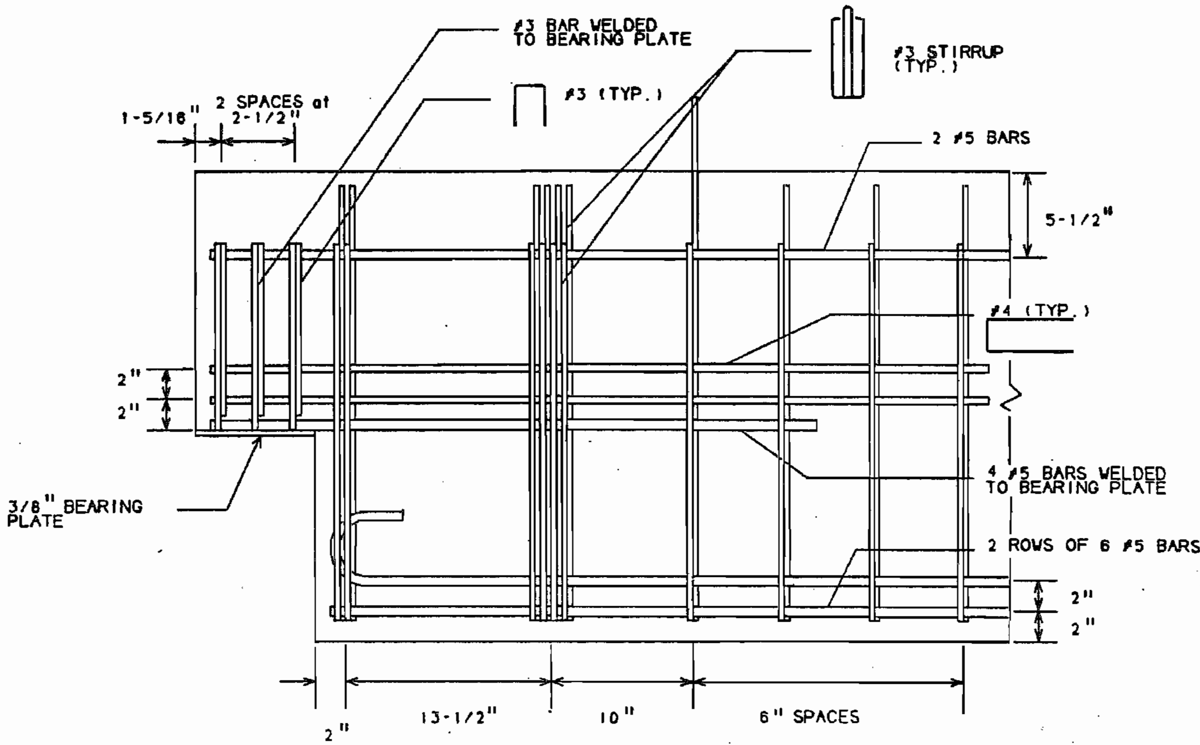

Figure 3.18 Specimen ST2 - Reinforcement Layout.

3.7 Summary of Dapped Beam Design Procedure

The dapped beam example highlights both the strengths and weaknesses of the strut-and-tie model as a design method. The primary advantage of the strut-and-tie model is that it requires only the application of a few basic principles and the designer does not have to be as concerned with the limitations typical of empirically based methods. Required areas of reinforcement are easily determined and the model is easily adapted to differing reinforcement patterns. In addition, other types of loads such as axial tension are easily included into the procedure. In theory, the strut-and-tie model may also be adapted to include the use of prestressed reinforcement. However, the method has the shortcomings of not adequately defining required effective concrete strengths, node dimensions, anchorage lengths and reinforcement placement.

The PCI and Menon/Furlong design procedures are based, in part, on principles similar to those of the strut-and-tie model. The PCI method, for instance, is partially based on a simple strut-and-tie model. In the Menon/Furlong method an equilibrium system of forces is assumed which is, in principle, similar to the internal equilibrium of strut-and-tie models. Each of the empirical design procedures differs from strut-and-tie model principles by incorporating shear friction reinforcement and by other detailing considerations derived from test data.

The PCI design method is easy to use and is based on a great deal of experimental results. It offers some flexibility as two reinforcement options are available. Both vertical and axial loadings are considered. Additionally, limitations on concrete strength pertain only to the nib, neglecting other portions of the dapped end detail.

The Menon/Furlong design procedure is easy to use but offers only one choice in reinforcement pattern. It addresses the use of prestressed reinforcement and is primarily intended for use with bridge structures. This design procedure lacks specific requirements for limiting concrete stresses.

3.8 Test Procedure

Each detail was tested to failure. The test setup is shown in Fig. 3.19. Load was applied at the dapped end using a hydraulic ram and monitored using a pressure transducer. In order to determine the internal force distribution as accurately as possible, each detail was instrumented with a large number of strain gages. In addition to strain gages on the reinforcement, embedment strain gages were placed in key locations in the concrete to determine concrete strains. A linear potentiometer was utilized to measure vertical end displacement as indicated in Fig. 3.19. Strain and displacement readings were taken using a personal computer based data acquisition system. The basic procedure was quite simple and is summarized below:

1) Apply load increment.
2) Record initial strain gage and displacement readings.
3) Mark cracks and record observations.
4) Record strain gage and displacement readings just before next load increment is applied.

The test procedure required the imposition of a reaction on the top surface of the beam not far from the dapped end. In an actual structure it is likely that such a large concentration of load would not be present. The concentrated load influenced some of the crack patterns and may have influenced strain gage readings also. However, it was necessary to use this loading arrangement to keep the test specimens to a reasonable size and to permit a single loading setup.

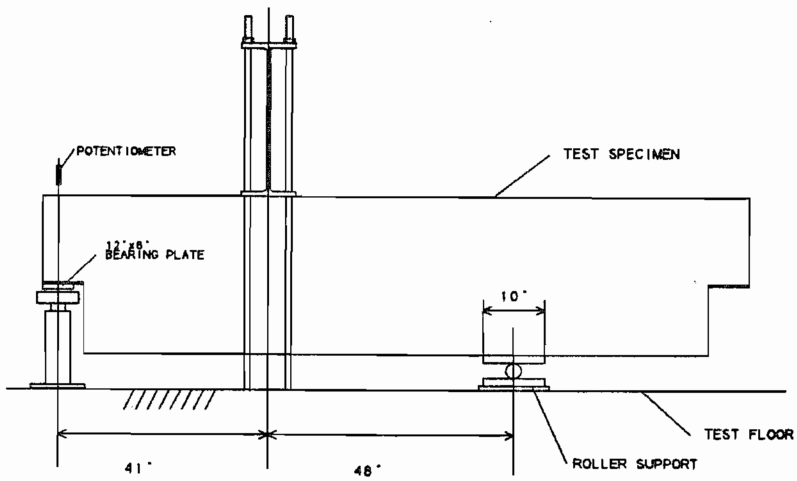

A) SIDE VIEW

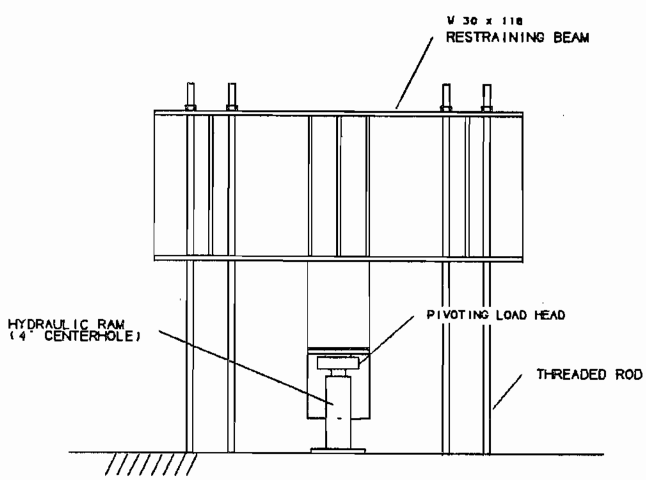

B) END VIEW

Figure 3.19 Dapped Beam Test Setup.

CHAPTER 4
TEST RESULTS -- DAPPED BEAMS

4.1 Behavior of Specimens

In this section, a brief summary of the behavior of each of the test specimens is presented in terms of load vs. deflection curves and crack patterns. More details of the results are given in Ref. 24.

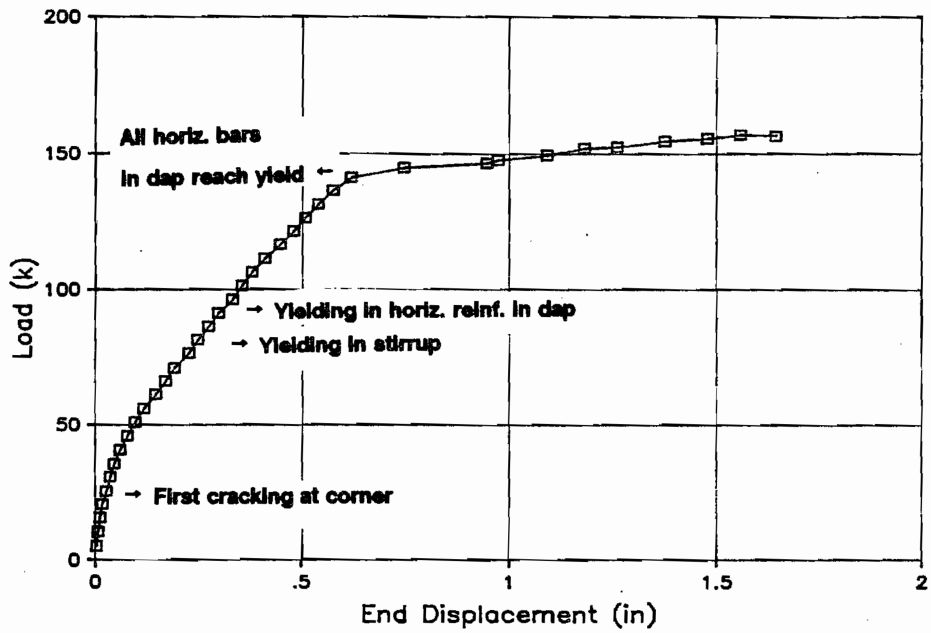

Figure 4.1 Specimen ST1, Load/Deflection Plot.

4.1.1 Specimen ST1. The load-deflection plot for ST1 is shown in Fig. 4.1. At a load of approximately 20k, a small crack began at the re-entrant corner. As load was increased, this crack became more pronounced and a second crack formed just below the re-entrant corner (35k). At 70k a large, diagonal crack formed near the bottom corner of the full depth section and extended upward at approximately 45 degrees. Yielding in the first stirrup beyond the re-entrant corner occurred at a load of approximately 85k. The first layer of horizontal reinforcement at the bottom of the dap reached yield at approximately 90k. At 100k (design load), the first three sets of stirrups had reached yield or were very close and a second diagonal crack had formed in the full depth section. Cracking at 110k may be seen in Fig. 4.2a. At this load, yielding was measured in the first four sets of stirrups and in all three layers of horizontal reinforcement located at the bottom of the dap. Beyond this load the specimen deflection increased rapidly. At ultimate (155k) stirrups in

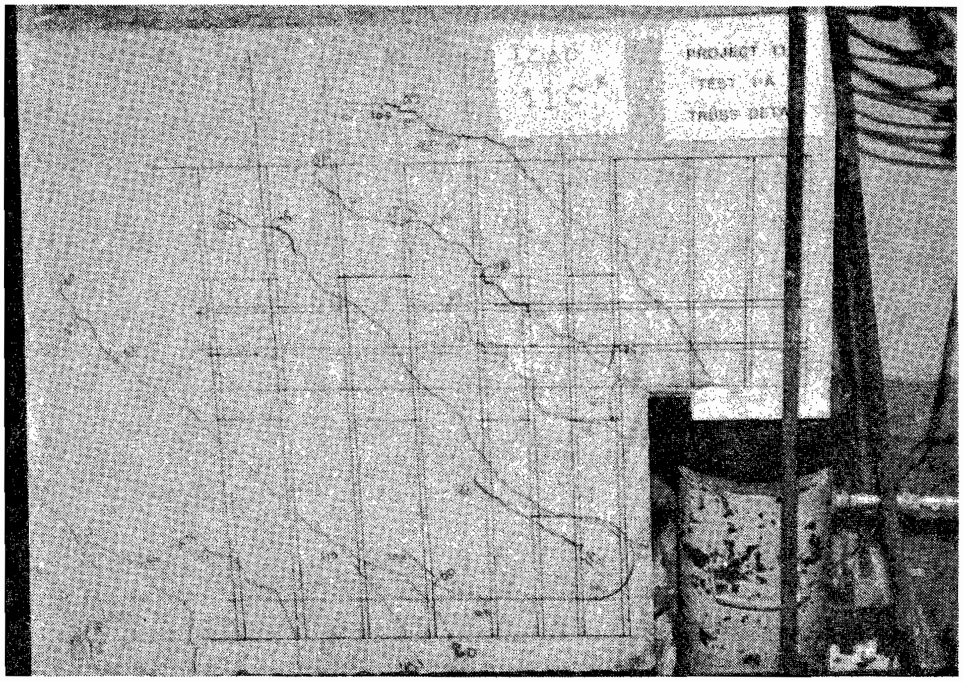

(a) 110k load

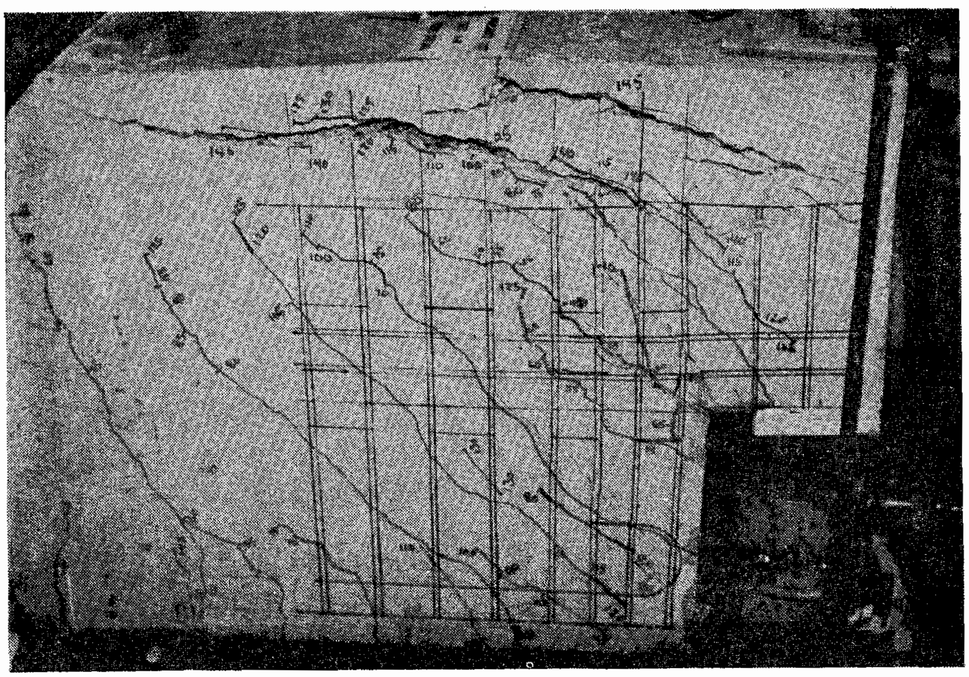

(b) Final crack patterns

Figure 4.2 Specimen ST1, Crack Patterns.

the upper portion of the beam lost anchorage and the concrete compression zone began to spall (Fig. 4.2b).

4.1.2 Specimen PCI. Initially, the specimen was loaded to approximately 110k when a leak developed in the hydraulic loading system. The specimen was unloaded, the problem was corrected, and the specimen was loaded to failure. Load-deflection plots for both loadings are shown in Fig. 4.3. Difference in the load-deflection diagrams may have been influenced by a problem with deflection instrumentation in the second loading.

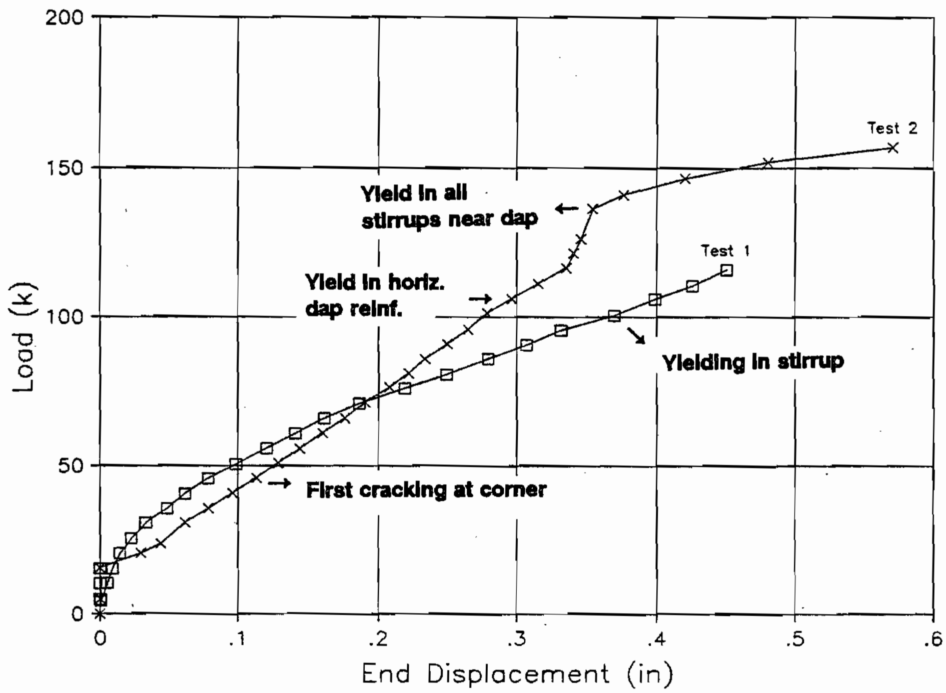

Figure 4.3 Specimen PCI, Load-Deflection Plots.

During the first loading on PCI, a re-entrant corner crack formed at a load of 30k. At 60k flexural cracking was observed and the corner crack extended well into the beam. During the second loading, a large diagonal crack located in the lower portion of the full depth section formed suddenly at a load of 100k (Fig. 4.4a). Yielding in the first stirrup beyond the re-entrant corner also occurred at 100k of load. The horizontal reinforcement within the dap began to yield at a load of 105k. As load was increased to 140k, yielding of the entire group of stirrups beyond the re-entrant corner was noted. At ultimate (160k), the upper portion of the beam began to separate in a manner similar that of Specimen ST1 (Fig. 4.4b). Deformation increased rapidly and crushing in the beam compression region was noted.

4.1.3 Specimen MF. The load-deflection plot for this specimen is shown in Fig. 4.5. The specimen remained uncracked until a load of approximately 25k at which a diagonal crack at the re-entrant corner formed. Yielding in the strap began at a load of

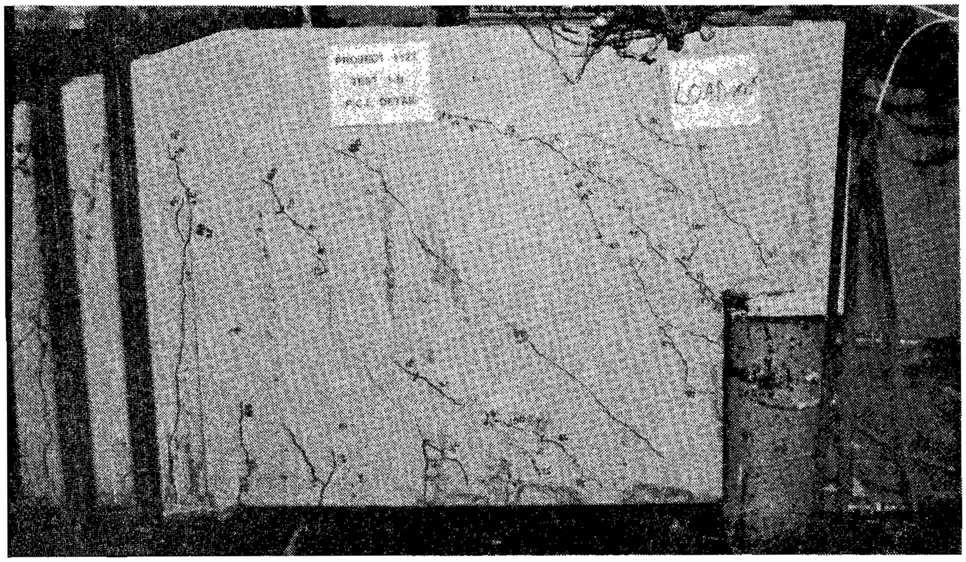

(a) At load of 100k

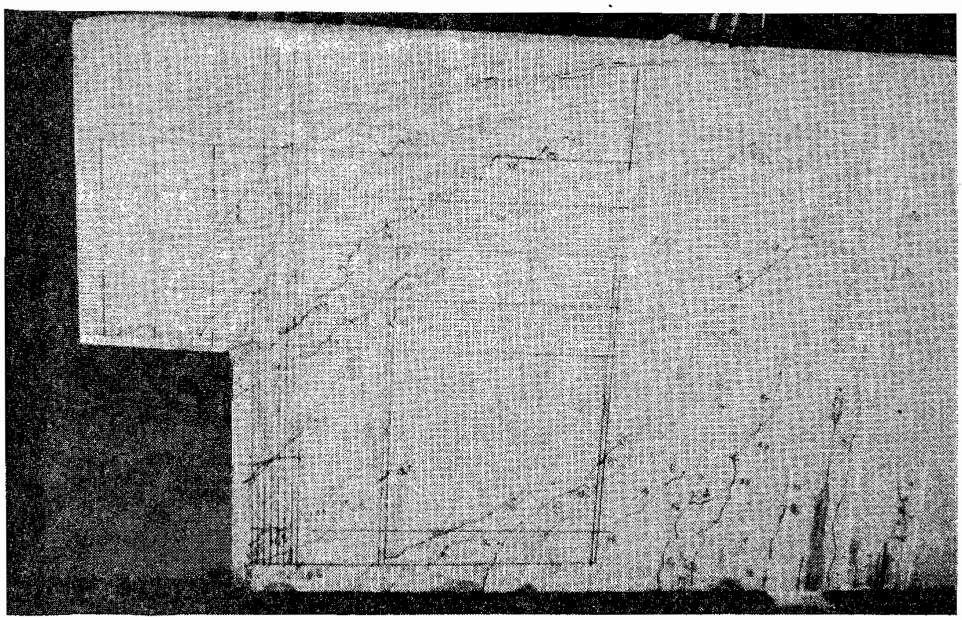

(b) Final crack patterns

Figure 4.4 Specimen PCI, Crack Patterns.

85k. After yield was reached, cracking in the re-entrant corner increased. At 100k (design load) very wide cracks were seen in the re-entrant corner region (Fig. 4.6a). Increasing the load to 105k resulted in yielding of the horizontal reinforcement in the dapped end and the vertical stirrup closest to the dapped end. At this load the load-deflection curve began to flatten rapidly. Diagonal cracking in the lower portion of the full-depth section developed. Failure occurred at about 135k due to crushing of the beam compression zone (Fig. 4.6b).

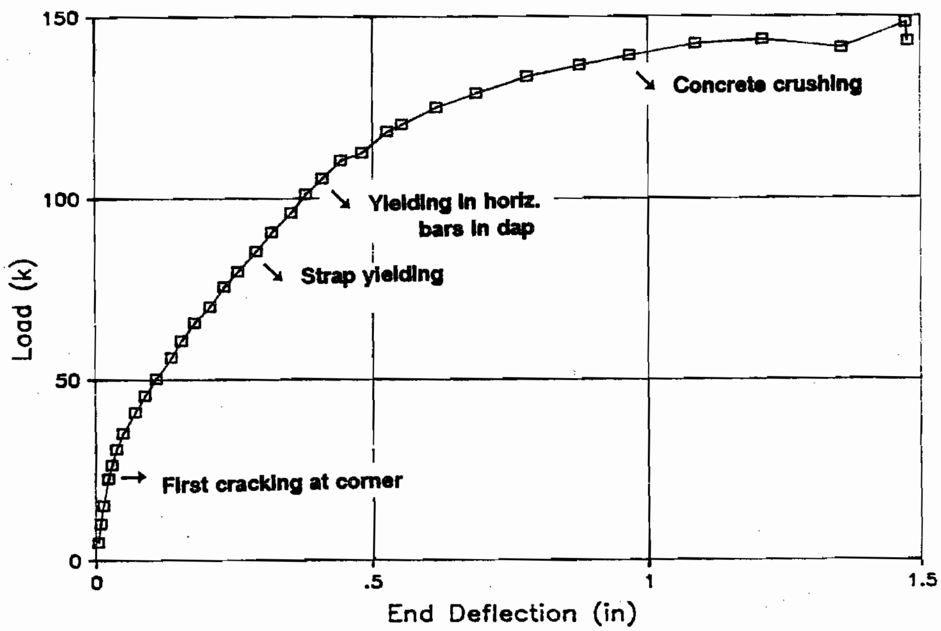

Figure 4.5 Specimen MF, Load-Deflection Plot.

4.1.4 Specimen ST2 -- Modified Strut-and-Tie. The load-deflection plot for this detail is shown in Fig. 4.7. Cracking first occurred at 30k. The first set of stirrups beyond the dap yielded at a load of 80k. Yield was reached in the horizontal reinforcement in the dap at 110k (Fig. 4.8a). Further increases in load resulted in the re-entrant corner crack becoming very large due to a loss of anchorage between the upper portion of the beam and the group stirrups located about 15 in. from the dapped end (Fig. 4.8b). Failure occurred at a load of 130k due to crushing of the compression zone of the beam.

4.2 Comparison of Strength

The capacity of the details is compared in Fig. 4.9. The figure indicates both calculated and measured capacities. Computed capacities (discussed in Chapter 3) were based on the actual amount of reinforcement used in the specimens. All of the specimens carried loads well in excess of computed capacities. The PCI detail developed an ultimate

(a) At load of 100k

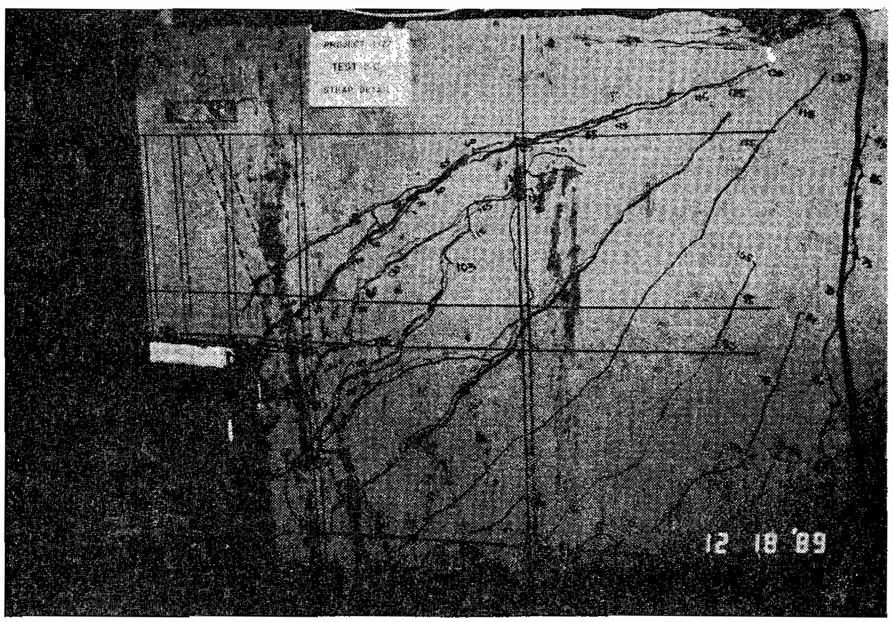

(b) Final crack patterns

Figure 4.6 Specimen MF - Crack Pattern.

shear capacity 52 percent larger than predicted. Specimen ST1 (strut-and-tie) reached a load 42 percent larger than computed. Specimens MF and ST2 (modified strut-and-tie) developed loads 21 and 27 percent higher than computed. It should be noted that in the PCI detail, additional stirrups were provided in the vicinity of the dap to prevent a diagonal tension failure in the full depth section. In computing the predicted failure load, it was assumed the additional stirrups would not contribute to the ultimate capacity of the dapped end. If only one of the additional stirrups was assumed to contribute to the vertical reinforcement provided for the dap, overload capacity would be only 21 percent.

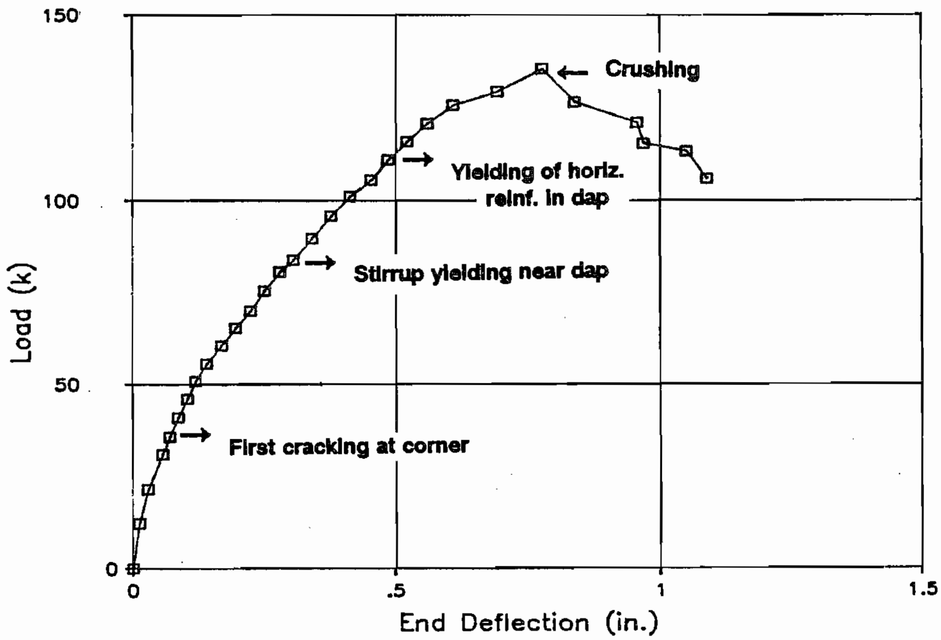

Figure 4.7 Specimen ST2, Load-Deflection Plot

The reinforcement for each detail is compared in Fig. 4.10. A direct comparison of reinforcement presents problems because of differences in design procedures. It was assumed that two sets of # 3 stirrups (Fig. 3.3) are required for shear in the full depth section within the area in which vertical reinforcement is compared. For the strap in Specimen MF an adjustment was made to account for the skewed orientation of the strap and for the difference in yield stress. The strap area in the Menon/Furlong detail was converted into horizontal and vertical areas of reinforcement based on the sine and cosine of the strap angle. In addition, strap areas were decreased according to the ratio of strap yield stress to the yield stress of the deformed bar reinforcement. Thus, the comparison is based on all material having a yield stress of 60ksi.

Comparing the horizontal reinforcement (Fig. 4.10a) indicates a substantial variation in required reinforcement areas between the details. PCI and MF required approximately

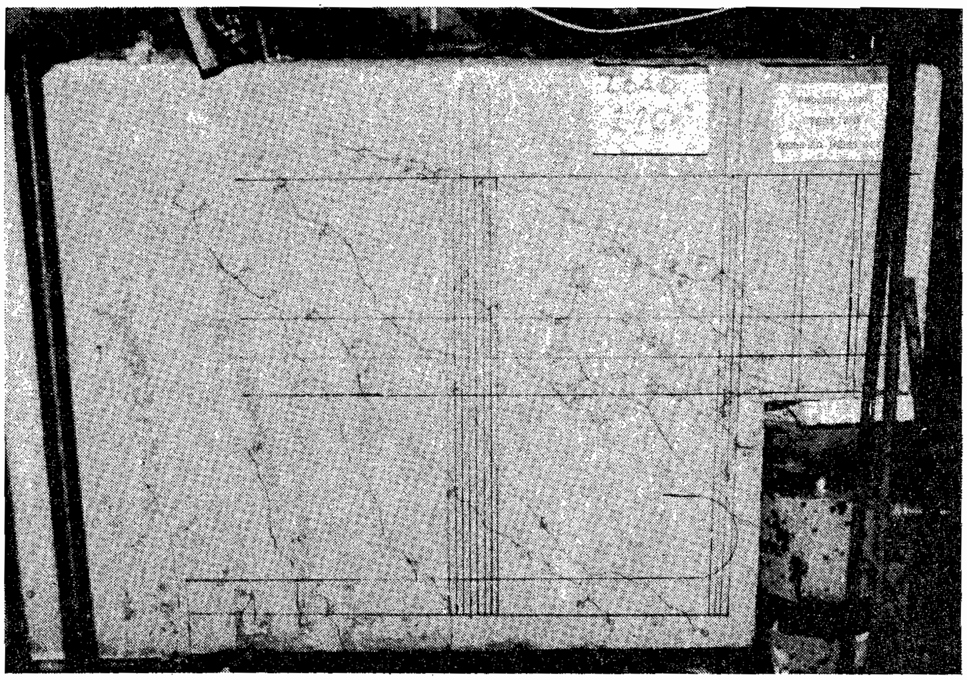

(a) At load of 110k

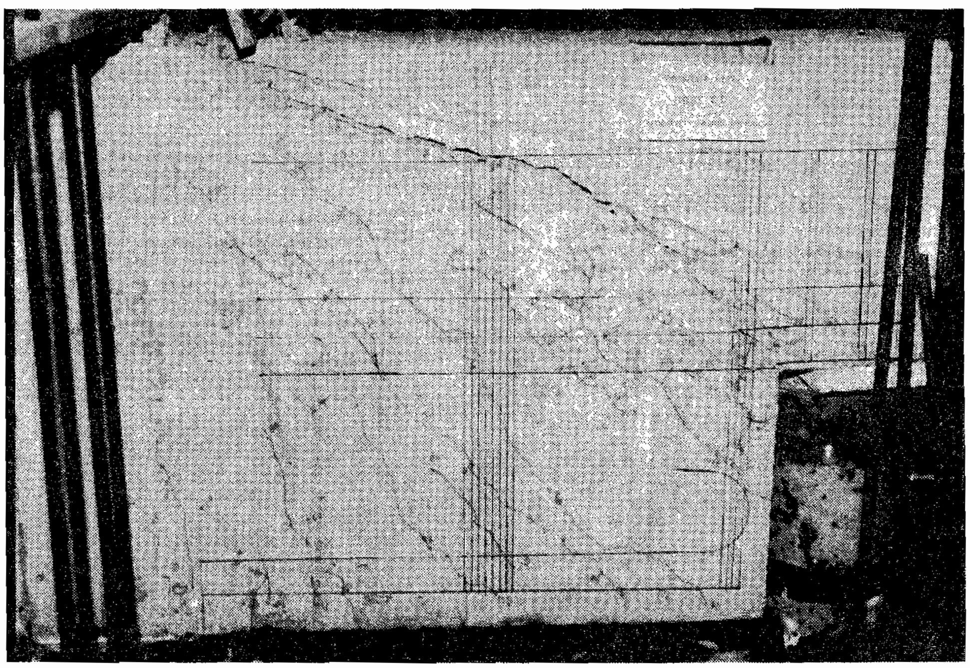

(b) Final crack patterns

Figure 4.8 Specimen ST2 - Crack Pattern.

the same amount of horizontal reinforcement. However, a great deal more excess horizontal reinforcement was actually provided in PCI which may partially account for the greater capacity exhibited by this detail. ST1 required approximately 25% more horizontal reinforcement than PCI and 40% more than MF. ST2 required double the area of horizontal reinforcement compared with MF.

The vertical reinforcement (Fig. 4.10b) required in MF is considerably smaller than the others. PCI and ST2 (modified strut-and-tie) required approximately 50% more reinforcement then MF. ST1 (strut-and-Tie) required a substantially larger area of vertical reinforcement. The area of reinforcement and shear capacity is not directly related as can be seen by the results in Fig. 4.9.

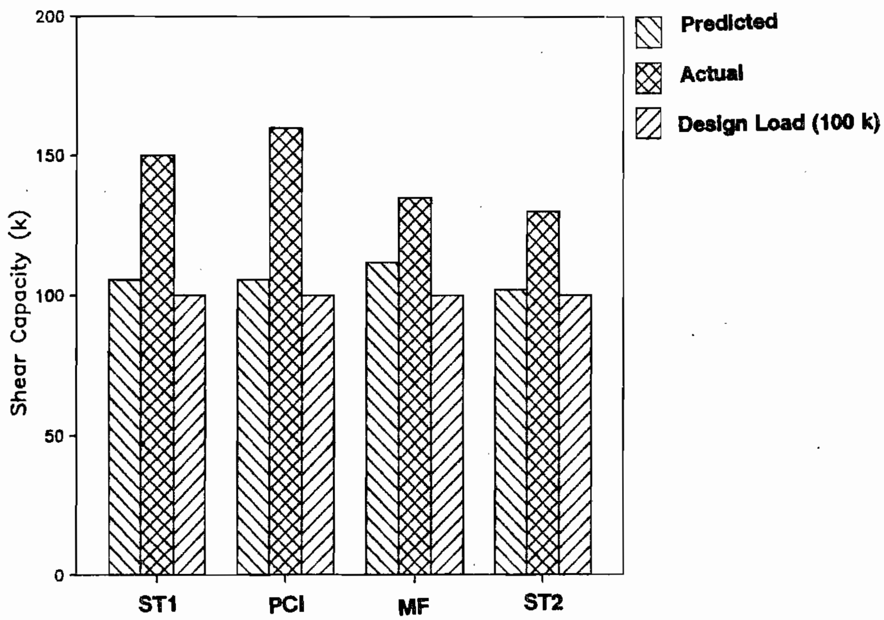

Figure 4.9 Comparison of Specimen Shear Capacities.

4.3 Cracking

In Fig. 4.11, the cracking load and the load at first yield are shown. Cracking loads are in the range of 20 to 30k for all specimens. First yield in the reinforcing bars in PCI and MF occurred at higher loads (around 100k) than the other two specimens (about 80k). In MF the strap yielded earlier but f_y was low compared with the reinforcing bars. In both PCI and MF the vertical reinforcing bars were concentrated near the re-entrant corner. Concentrating the reinforcing seemed to distribute forces better and delayed yielding.

The test results indicated that control of the diagonal crack at the re-entrant corner is a primary concern for serviceability. Placing a large amount of vertical reinforcement close to the re-entrant corner seemed to arrest cracking somewhat more effectively than

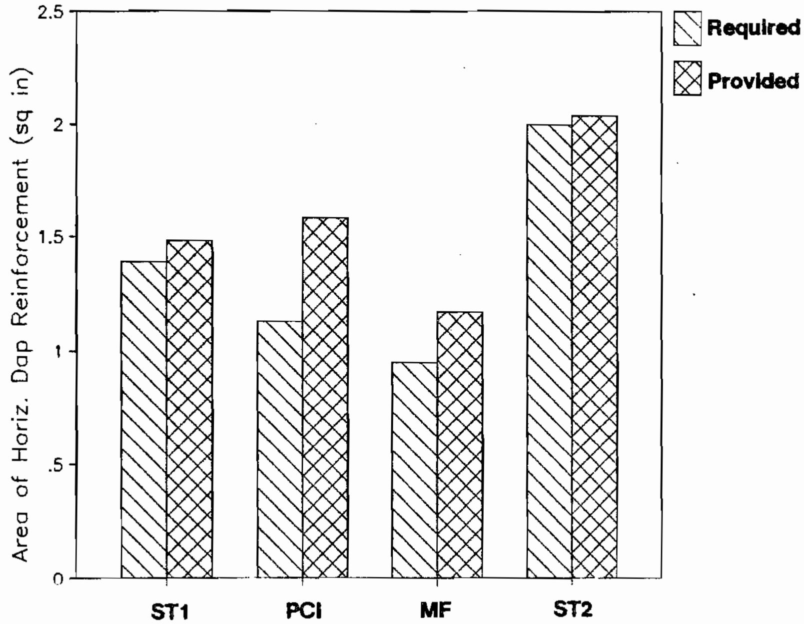

(a) Horizontal reinforcement (excluding top bars)

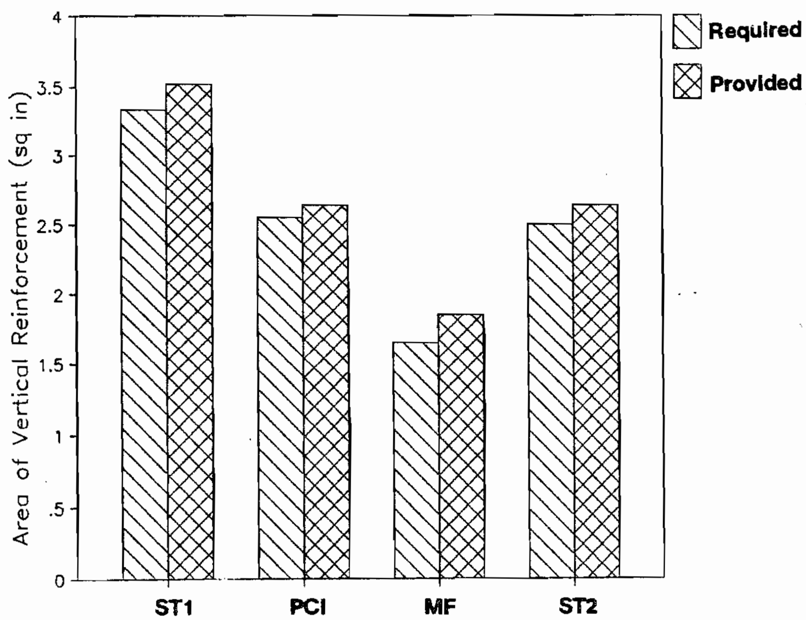

(b) Vertical reinforcement (within a distance h from corner)

Figure 4.10 Comparison of Reinforcement Areas.

distributed reinforcement. Cracking was controlled slightly better in Specimen PCI than in the others.

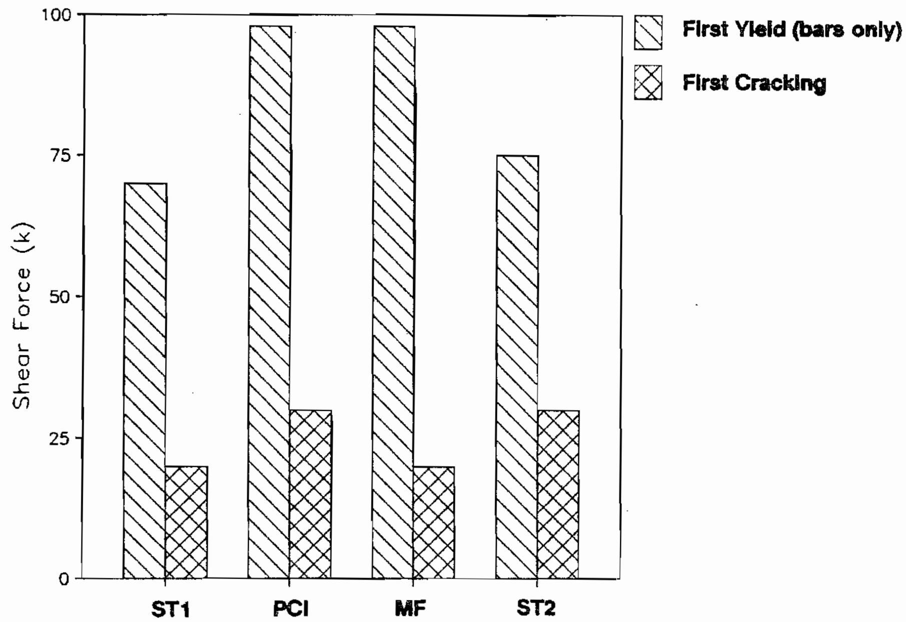

Figure 4.11 Comparison of Loads at Cracking and at Yield of Reinforcing Bars.

4.4 Construction

Another consideration in evaluating the details is ease of fabrication. Specimen MF was slightly more difficult to fabricate because of the effort involved in making the strap assembly and insuring its proper placement. The strap also created congestion in the dapped end region. The congestion could increase the effort involved in fabrication, particularly if prestressed reinforcement was utilized. The remaining details required approximately the same level of effort to fabricate. Specimen PCI was slightly easier to construct because the vertical reinforcement was concentrated in one area and allowed for easier access to other reinforcement.

4.5 Evaluation of the Test Results

4.5.1 Strut-and-Tie Models. The strut-and-tie model represents the internal force distribution as a system of struts and ties. A reasonable correlation between assumed and actual internal forces should exist. It is acknowledged that a design strut-and-tie model is chosen somewhat arbitrarily and that other viable force transfer mechanisms may actually develop. The test specimens developed ultimate loads substantially larger than predicted by the design models. Since the strut and tie represents a plastic mechanism, it is assumed that the forces are distributed in a well- defined manner. In the real structure the mechanism develops gradually. Only after sufficient deformation has occurred will the internal forces reflect the assumed distribution. In this section, results from the experimental program are compared with the behavior of the strut-and-tie models. The ability of strut-and-tie models to be adapted to observed behavior is explored.

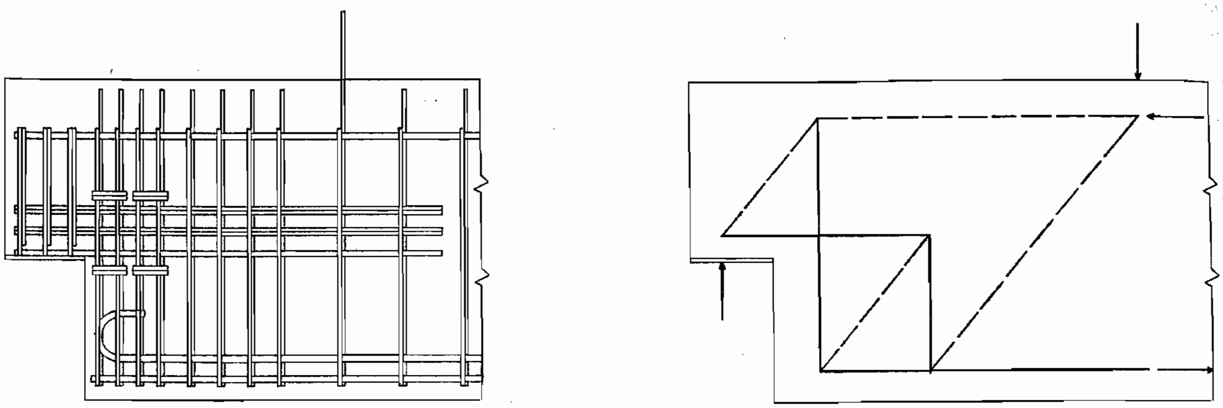

Figure 4.12 Specimen ST1, Design Model and Reinforcement.

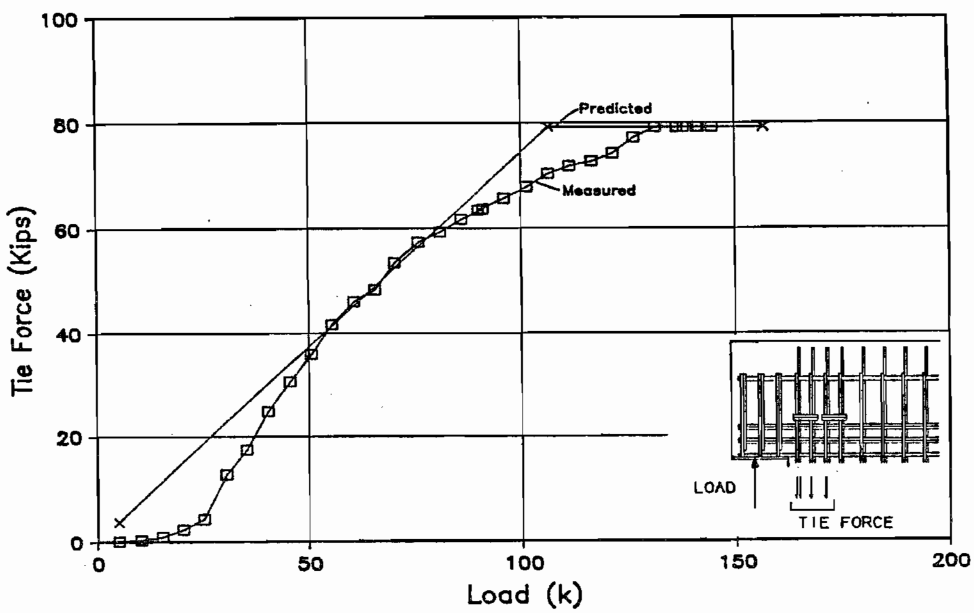

Figure 4.13 Comparison of Measured and Calculated Vertical Tie Force for ST1.

4.5.2 Specimen ST1. This detail was designed using the strut-and-tie model shown in Fig. 4.12. Details of the design were described in Section 3.2.2. In Fig. 4.13 the predicted and measured forces in the vertical tie adjacent to the dap are compared. Measured forces are determined from the strain gages applied to the outer legs of the first three stirrup groups. To determine the stirrup forces it is assumed that the strains measured on the outer leg are the same as the strains on the inner legs. The predicted forces are scaled down to reflect the percentage of reinforcement for which strain measurements were available. The predicted force is indicated by the straight line and corresponds to 75 percent of the total force indicated by the strut-and-tie model in the group of bars which make up the tie. The plot shows measured forces are significantly smaller than predicted forces at low loads when the specimen is largely uncracked. The forces correlate more closely after the formation of the diagonal crack at the re-entrant corner (30k load) and up to the design load (100k).

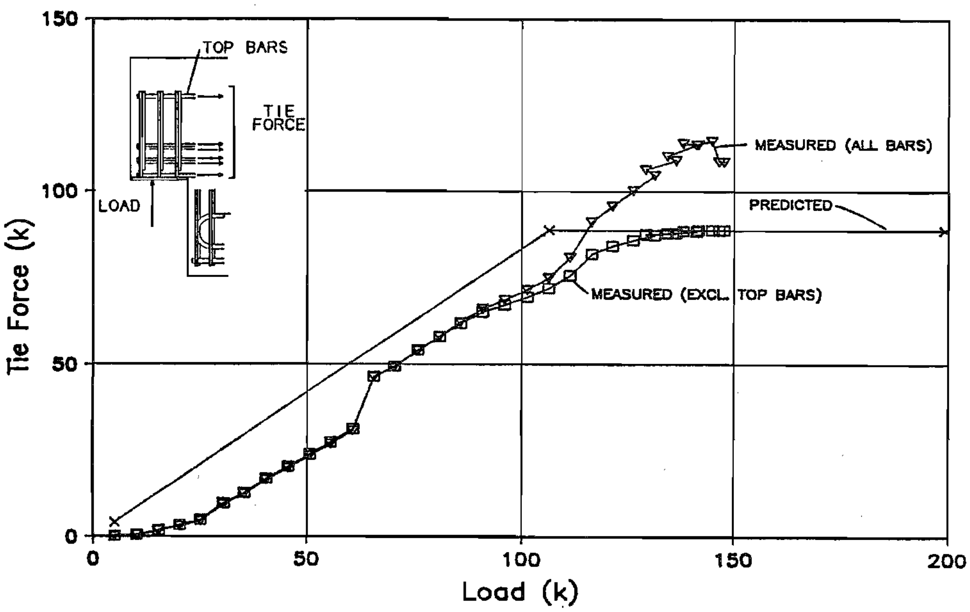

Figure 4.14 Comparison of Measured and Calculated Upper Horizontal Tie Force, ST1.

Horizontal tie forces from the dapped end are compared in Fig. 4.14. The measured tie forces are shown both including and excluding the upper longitudinal reinforcement (top bars). After cracking occurs, measured values increase and follow predicted forces reasonably well. As the load increases beyond the 100k design load, the lower layers of horizontal reinforcement reach yield. The upper layer of reinforcement (top bars) then begins to develop force. Below the 100k load level the top reinforcement develops very little force. Above 100k the top reinforcement develops substantial force and seems to participate in the mechanism of load transfer.

A comparison of lower horizontal tie forces is shown in Fig. 4.15. Except at low load levels, the predicted forces compare well with the measured values. The reinforcement did not yield and thus force continued to increase after the design load of 100k was reached.

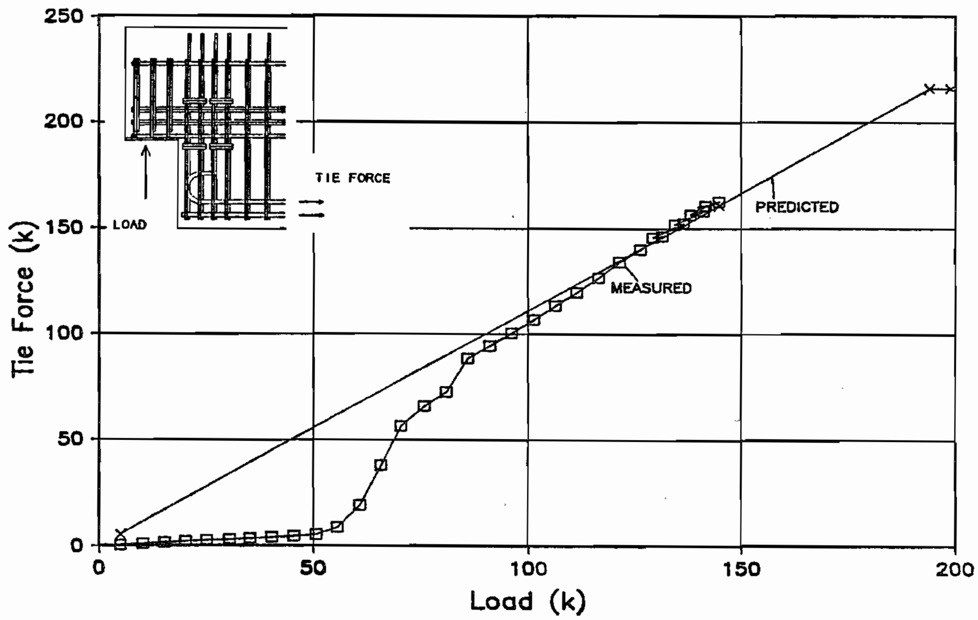

Figure 4.15 Comparison of Measured and Calculated Lower Horizontal Tie Force, ST1.

The design model indicates that a second vertical tie will develop in the lower portion of the beam (see Fig. 4.12). The force in this tie should be equal to the reaction. As an indication of the forces developed in this region, a comparison of the force developed in the fifth stirrup group is shown in Fig. 4.16. As the figure shows, the force developed in the stirrup is quite small compared to the predicted values. It is likely that tension in the concrete carried much of the force and relieved the tie.

While the forces in the elements of the design model compare relatively well in most locations to measured forces at the design load of 100k, the excess capacity exhibited by the specimen is not accounted for directly. In attempting to reconcile this difference it is helpful to isolate portions of the structure by using the crack patterns. Figure 4.17 shows a trapezoidal free-body section taken along the boundary of the diagonal crack beginning at the re-entrant corner. Forces estimated from test results at the 100k load (shown on Fig. 4.17) were determined from strain gage readings if possible. If no strain gage readings were available for a particular bar, the strain levels were estimated from nearby gages. In the strut-and-tie mechanism, the first four stirrup groups should each resist a load of 25k at a 100k applied load. Measured stirrup forces were highest in the stirrups closest to the re-entrant corner and were less away from the dap. Since the first four stirrup groups balanced only about 80 percent of the reaction, it is possible that (1) secondary force transfer mechanisms such as friction, aggregate interlock, concrete tensile strength and dowel action account for the additional force or (2) the "tie" could encompass more than four stirrups. This is plausible in that no clear division exists between ties and the definition of a tie boundary is somewhat arbitrary. The model in Fig. 4.17 is similar to the design

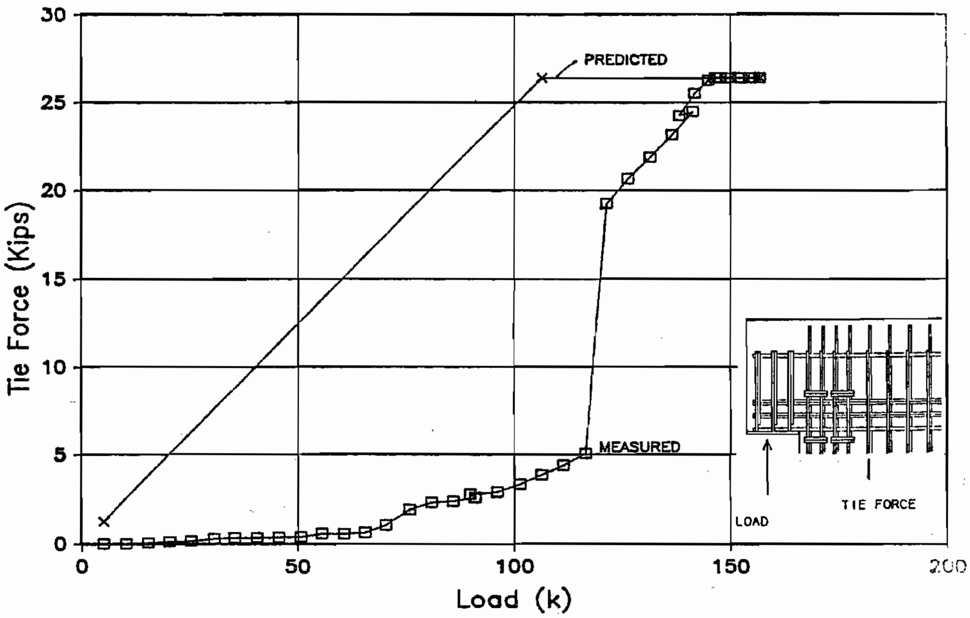

Figure 4.16 Comparison of Measured and Calculated Forces in Second Vertical Tie, ST1.

model. However, test results show the centroid of the stirrup forces to be further from the reaction and the horizontal force slightly less than predicted. Thus, the node (intersection of force resultants) formed by the vertical tie, diagonal strut and the horizontal strut is located higher in the beam than was assumed in the design model.

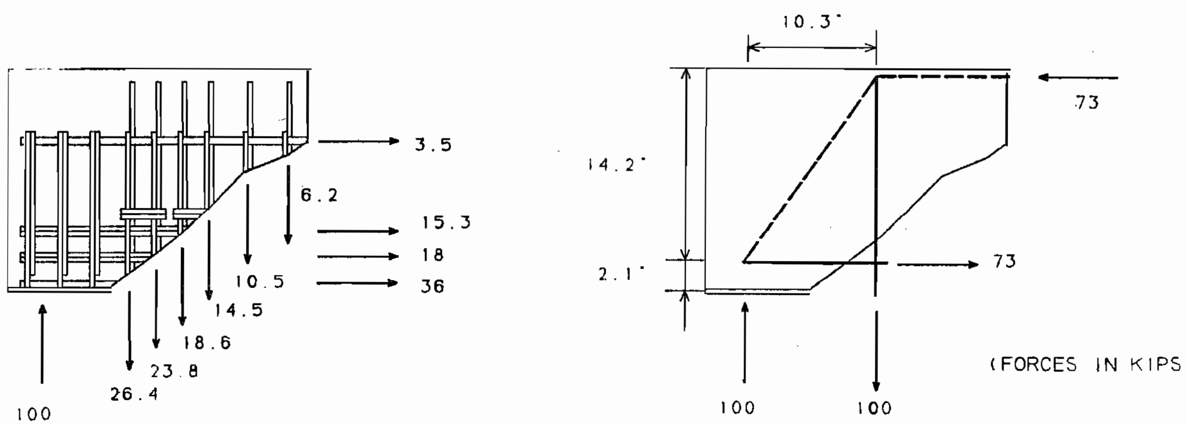

Figure 4.17 Analysis of Upper Portion of Dap at 100k, ST1.

It should be noted that the calculated force in the fifth stirrup group shown in Fig. 4.17 is 10.5k, which is much larger than the value in Fig. 4.16 at 100k. The difference between forces in the lower end of the stirrup (Fig. 4.16) and the upper end (Fig. 4.17) can be attributed to the proximity of gages to cracks. Also, the other large difference in strains in the same bar over the depth of the beam is an indication of the role of bond and anchorage in determining node behavior.

As the load was increased above the 100k level, redistribution of forces was evident. The stirrups near the re-entrant corner yielded and progressively more load was shifted away from the dap. Horizontal reinforcement in the lower portion of the dap yielded and the force in the top reinforcement increased. The increase in force in the upper horizontal reinforcement caused the centroid of the horizontal forces to shift upward. As the forces shifted upward, the intersection of diagonal compression and stirrup forces (the "node" region) moved past the point where the stirrups (vertical ties) were anchored and large horizontal cracks opened in this area (Fig. 4.2).

To model the force mechanism away from the dap toward the applied load, the crack pattern shown in Fig. 4.18a can be considered. Considering the vertical forces alone, the most plausible strut-and-tie system is shown in Fig. 4.18b. It is likely that the crack pattern and truss mechanism away from the load point at the dapped end were influenced substantially by the reaction (load) on the beam at the top surface. Therefore, the idealized strut-and-tie model based only on forces at the dapped end is too simplistic. Also, if the horizontal forces from the dapped end are isolated, the strut-and-tie model shown in Fig. 4.18c offers an alternative horizontal force system. The required force in the tie will be a function of the strut angle. While the models are reasonable, there is not enough information available to fully evaluate the elements in the model and to make direct comparison between the values shown in Fig. 4.15 and the "possible" forces given in Fig. 4.18b for a slightly different truss arrangement than was used to predict the values given in Fig. 4.15.

4.5.3 Specimen ST2. Design of this detail was based upon the strut-and-tie model shown in Fig. 4.19. Details of the design were given in Section 3.6. In Fig. 4.20, forces developed in the first vertical tie are compared to predicted forces. As strain measurements were available for 6 of the 8 bars in this tie, the comparison is based upon 75 percent of the total predicted tie force. At low loads the measured forces follow the predicted loads fairly closely. As the load exceeds 50k, the measured forces become much greater than the predicted forces. The elements of this tie reach yield at a load of about 80k. The forces in the second vertical tie are compared in Fig. 4.21. The measured forces in the upper portion of the tie remain very low up to a load of about 100k after which they increase rapidly to reach yield at a load of about 130k.

Forces developed near the dap in the upper horizontal tie are compared in Fig. 4.22. Comparison is made both including and excluding the top reinforcement as part of the horizontal tie. Throughout most of the load range, measured values were about 20k below predicted values. The top bars remained in compression until the load approached 130k where the bars force began to increase may have acted as part of the tie. Upper horizontal tie forces developed further from the dap are compared in Fig. 4.23. In this region very

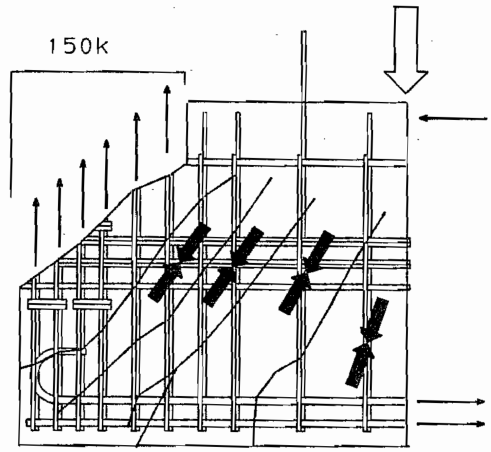

(a) Observed crack pattern

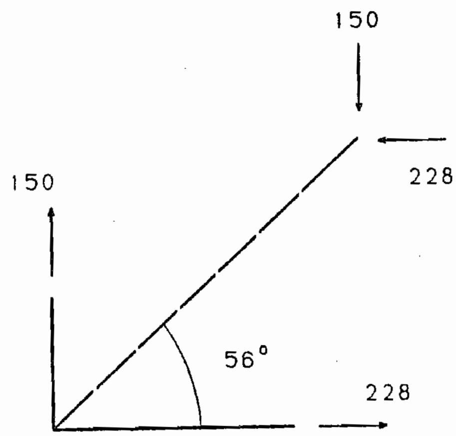

(b) Possible force transfer mechanism considering vertical forces only, ST1

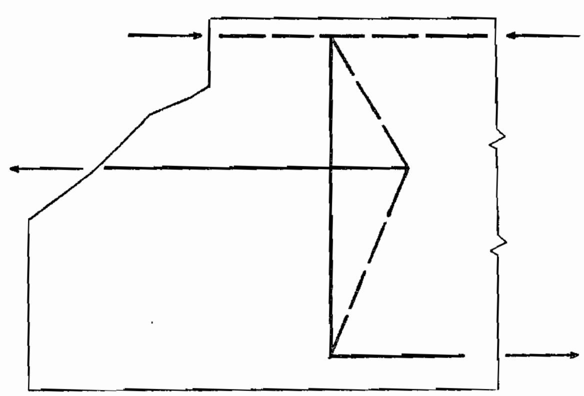

(c) Possible force transfer system considering horizontal forces only, ST1

Figure 4.18 Force Mechanism Away from Dapped End, ST1.

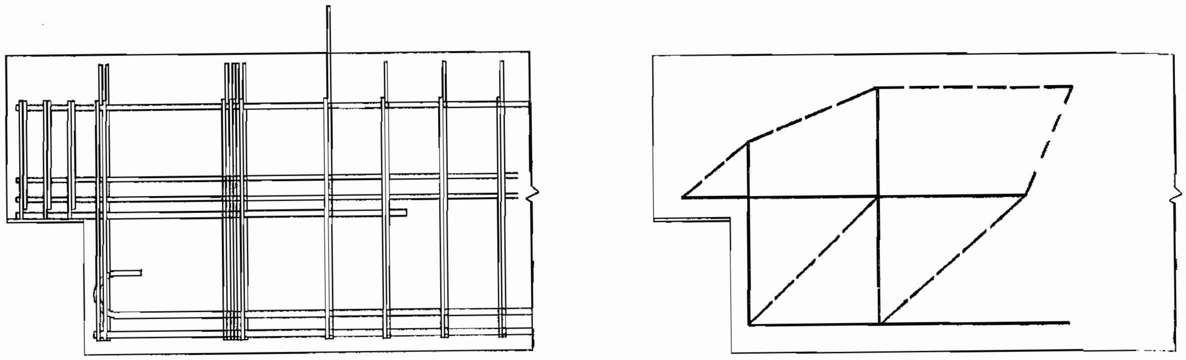

Figure 4.19 Design Model and Reinforcement, ST2.

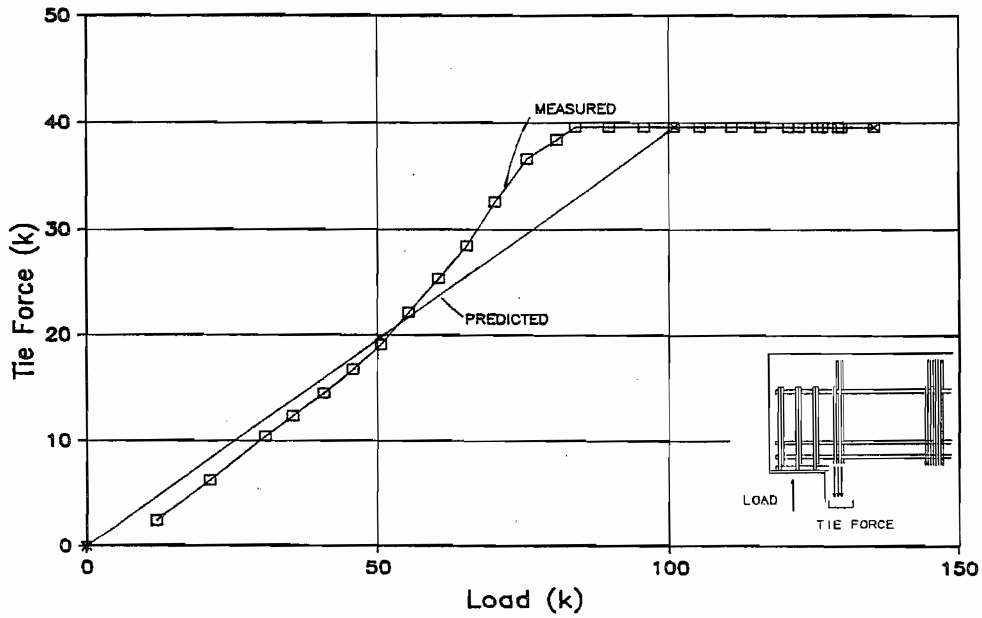

Figure 4.20 Comparison of Measured and Calculated Force in First Vertical Tie, ST2.

little force was developed in the reinforcement until a load of 80k was reached. At 80k, a diagonal crack formed beginning at the bottom corner of the beam and extended upward. Near the design load of 100k, measured forces compared reasonably well with predicted values.

Comparison of lower horizontal tie forces are presented in Fig. 4.24 and 4.25. Forces near the bottom corner of the beam were low when this region was uncracked. At a load of 80k, a diagonal crack formed in this region, and the forces increased dramatically to values reasonably close to those predicted by the design model. The same general trend is indicated in Fig. 4.25 for measurements further from the dap.

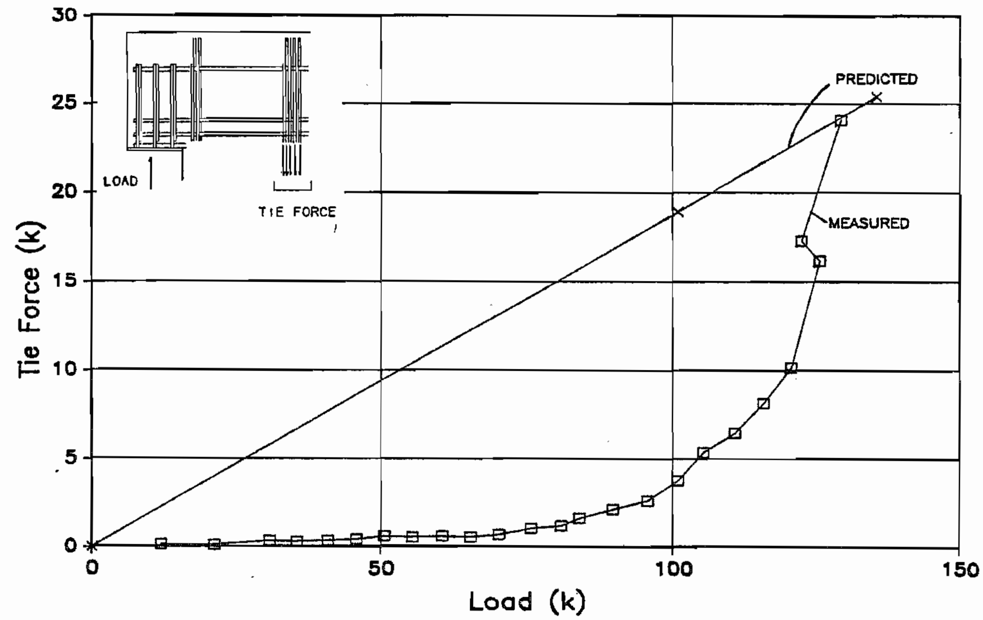

Figure 4.21 Comparison of Measured and Calculated Force in Second Vertical Tie (Upper Portion), ST2.

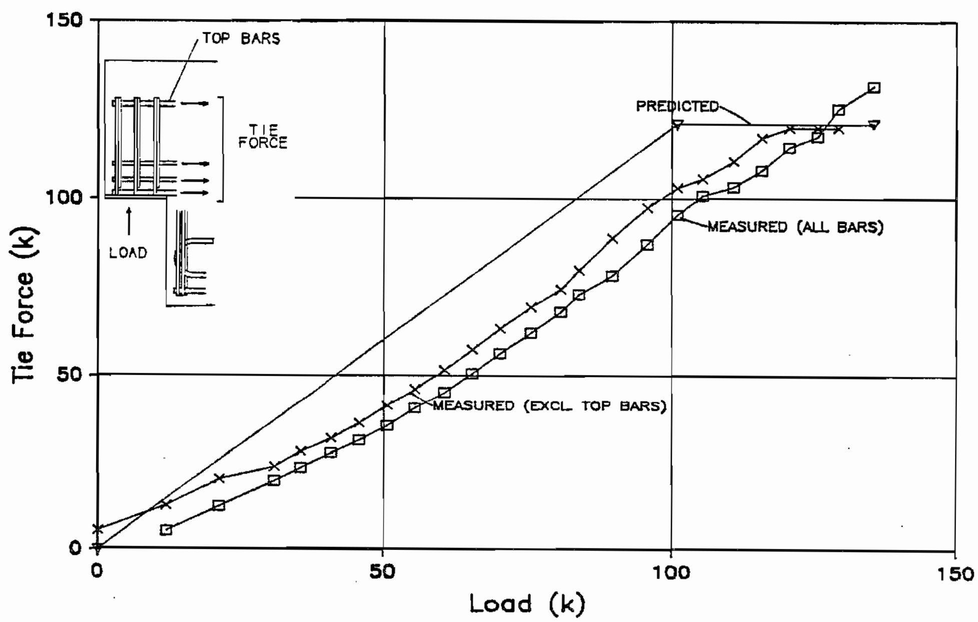

Figure 4.22 Comparison of Measured and Calculated Upper Horizontal Tie Force (Near Dap), ST2.

Analyzing the upper portion of the dap by isolating a section along the diagonal re-entrant corner crack produces the free body diagram shown in Fig. 4.26. Estimates of the forces acting on this section at the 100k load level are shown in Fig. 4.26a. Measured stirrup forces account for only 90 percent of the applied load. If the remaining vertical force is assigned to the second tie, the force system may be characterized by the strut-and-tie model shown in Fig. 4.26b. This model is quite similar to the design model except that the angle of the diagonal compression strut is slightly steeper. This is consistent with values in Fig. 4.22 in which the measured force in the horizontal tie is consistently lower than that based on a 40 degree strut angle. Once again the values shown in Fig. 4.26b do not compar directly with the measured forces shown in Fig. 4.21 because the sections at which the values are considered are not the same. As cracking progresses, the force along any bar will be more uniform, but before that is the case the concrete will carry considerable tension.

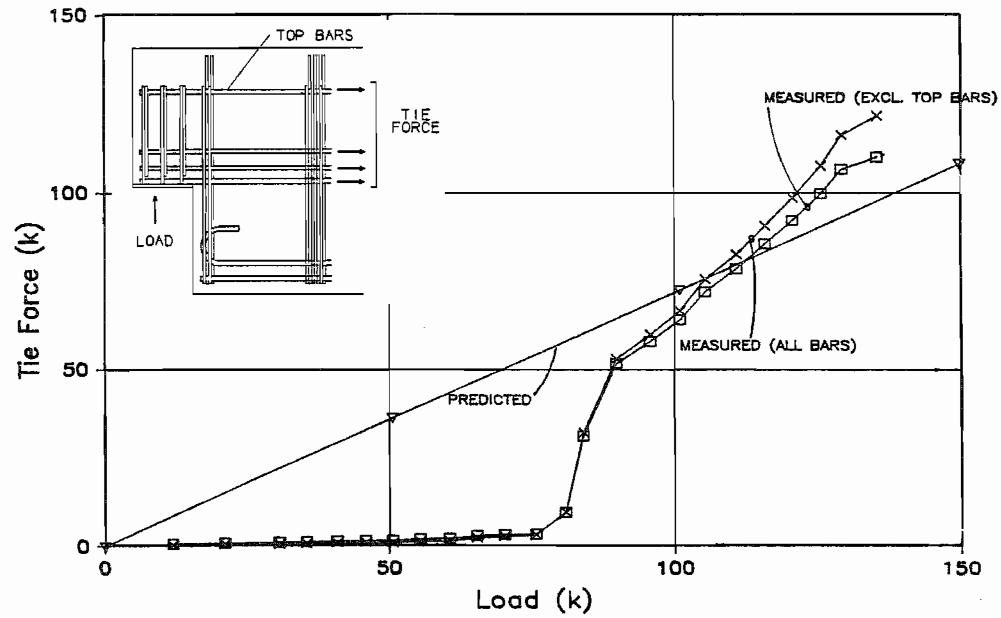

Figure 4.23 Comparison of Measured and Calculated Upper Horizontal Tie Force, ST2.

Figure 4.27 shows a strut-and-tie model of the upper portion of the dap in which the reaction is shifted to move the centroid of the horizontal compression force to a reasonable location. The error in representing the upper portion of Specimen ST2 as a strut-and-tie system is relatively small. A shift in the actual center of load application, normal fabrication tolerances and the existence of other possible force transfer mechanisms could easily account for the changes needed to apply the model shown in Fig. 4.27b.

4.5.4 Specimen PCI. As discussed in Section 3.4, the design was based in part on strut-and-tie procedures. Specifically, the horizontal reinforcement in the dap and the stirrup group just beyond the interface were determined using a simple strut-and-tie model (see Fig. 3.12). A comparison of the forces developed in the stirrup group or vertical tie to forces predicted by the design model is shown in Fig. 4.28. The predicted force is scaled down to reflect the portion of stirrups (2/3) for which strain measurements were available. The measured forces follow the predicted values fairly closely up to the design load of 100k. After this load, the stirrups yield and the measured force levels off.

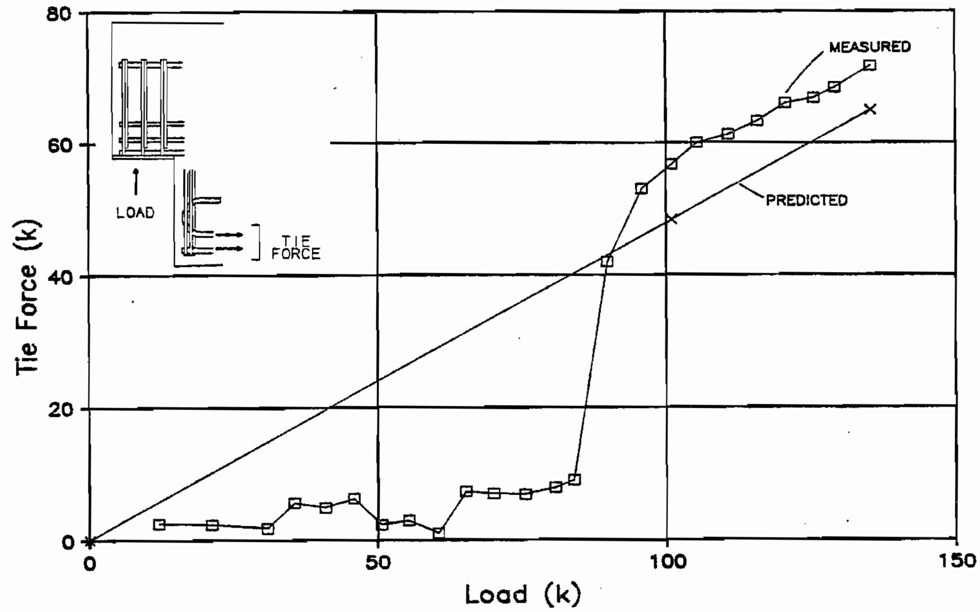

Figure 4.24 Comparison of Measured and Calculated Lower Horizontal Tie Force, ST2.

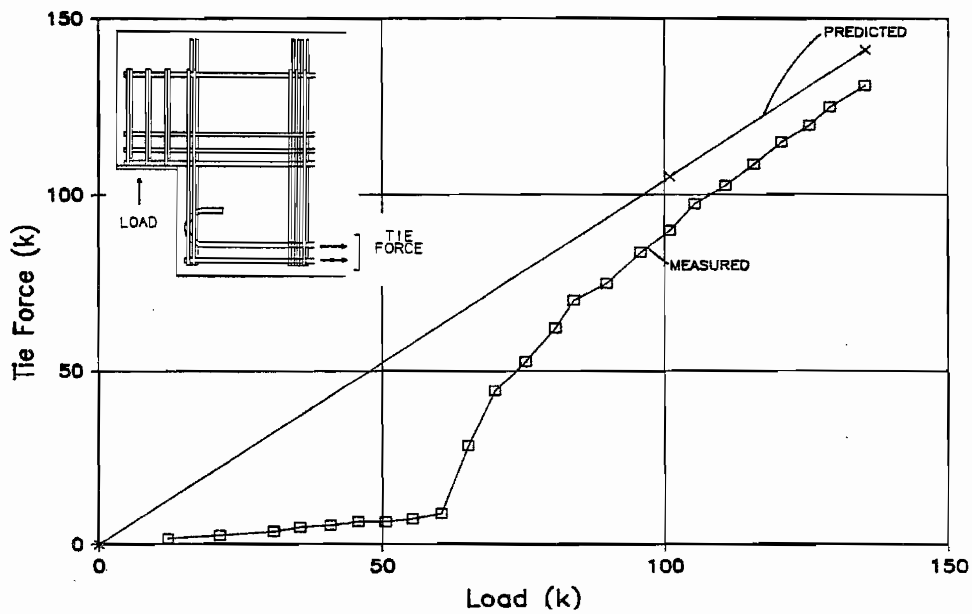

Figure 4.25 Comparison of Measured and Calculated Lower Horizontal Tie Force, ST2.

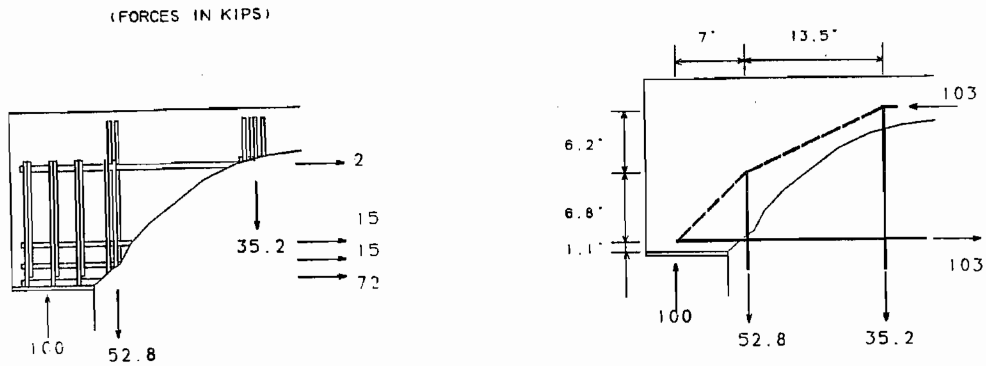

(a) **Estimated forces from test** (b) **Strut-and-tie model**

Figure 4.26 Analysis of Upper Portion of Dap at 100k, ST2.

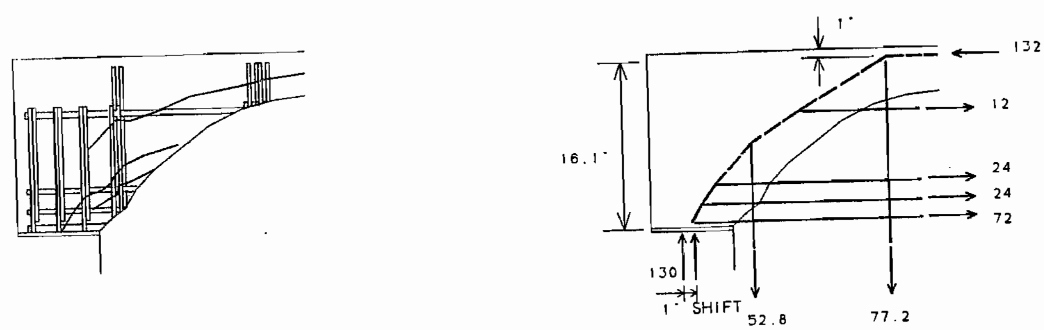

(a) **Crack pattern** (b) **Shifted strut-and-tie model**

Figure 4.27 "Shifted" Strut-and-Tie Model of Upper Portion of Dap, ST2.

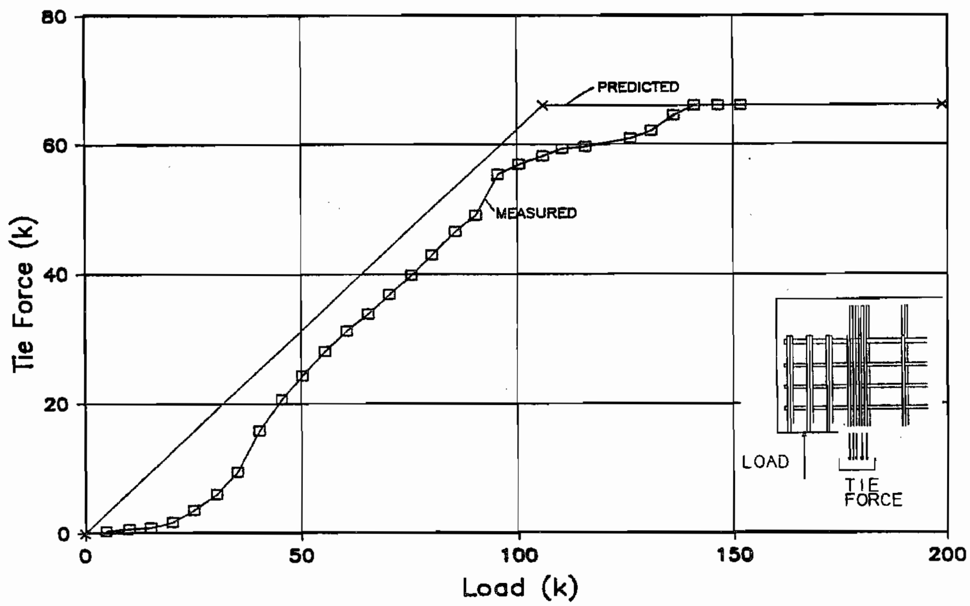

Figure 4.28 Comparison of Measured and Calculated Vertical Tie Force, PCI.

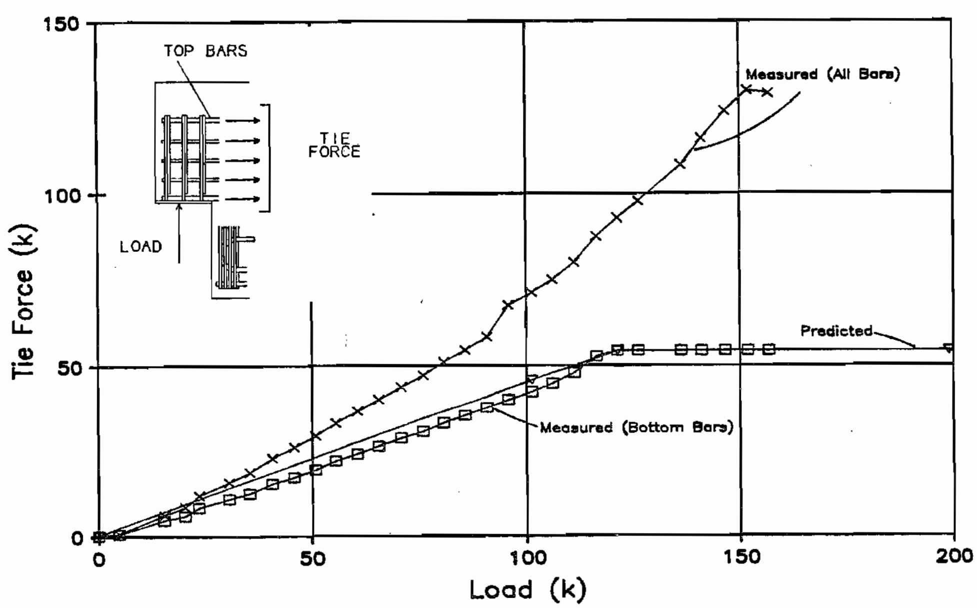

Figure 4.29 Comparison of Measured and Calculated Horizontal Tie Force, PCI.

A portion of the horizontal reinforcement within the dap is also analyzed based on strut-and-tie action. It is assumed that the bottom row of horizontal reinforcement acts as a horizontal tie. Shown in Fig. 4.29 is a comparison of predicted and measured horizontal forces. Measured forces in the bottom layer of reinforcement alone and in all horizontal reinforcement from the dap are shown. The plot indicates that the force in the bottom row of reinforcement follows the forces predicted by the design model quite accurately up to yield. However, significant forces are also present in the horizontal "shear friction reinforcement" from the dapped end.

Figure 4.30 shows forces in the free body diagram formed by isolating the upper portion of the dap along the diagonal re-entrant corner crack. A possible strut-and-tie representation of the internal forces shows that the majority of the vertical load is resisted by the main stirrup group as assumed in design. However, a small portion is also resisted by the adjacent stirrup.

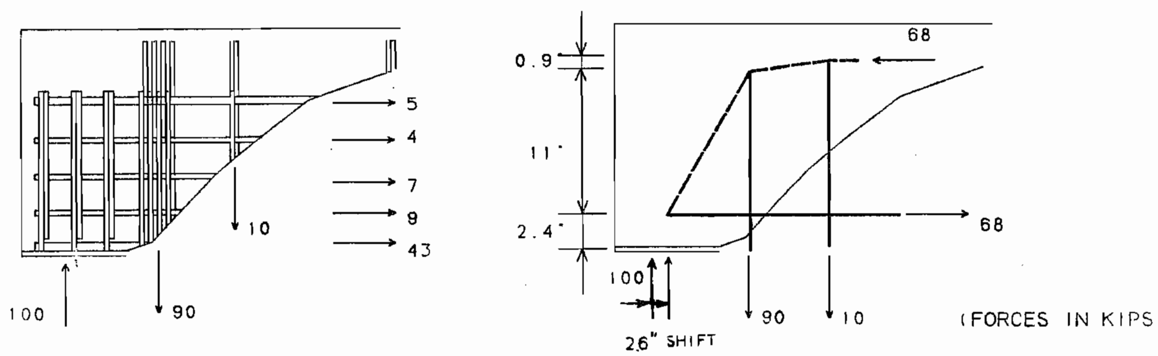

(a) Estimated forces from test **(b) Strut-and-tie model**

Figure 4.30 Analysis of Upper Portion of Dap at 100k, PCI.

A strut-and-tie model of the upper portion of Specimen PCI at 100k is shown in Fig. 4.30. The reaction was shifted 2.6 inches in order to force the center of the horizontal compression force to a reasonable location below the top surface of the beam. Because Specimen PCI was tested without the pivoting load head used in the tests of the other details, the center of load application shifted 1 to 1-1/2 inches during the course of the test as the specimen deformed. The additional shift in reaction to produce a rational strut-and-tie model, was attributed to the presence of additional forces due to friction, aggregate interlock and dowel action acting along the crack surface. The horizontal force in the upper horizontal tie is transferred through a diagonal compression strut and a second vertical tie in the lower corner of the full depth section (see Fig. 4.19). Given the reinforcement pattern used in Specimen PCI (Fig. 3.13), it seems unlikely that the force transfer system shown in Fig. 4.12 could develop. The first vertical tie would need to include the main group of stirrups plus two additional stirrup groups. This would leave only two remaining stirrup groups which intersect the horizontal reinforcement extending from the dap. If these stirrups were assumed to constitute the "second" tie, this quantity of reinforcement could provide only 1/3 of the required capacity. It is interesting to note that, of the details discussed, the PCI Detail has the fewest stirrups. Yet, this detail developed the highest shear capacity. In addition, the force transferred in the horizontal dap reinforcement is greatest for this detail. This seems to indicate that the means of transfer of horizontal force from the dap reinforcement does not require a large number of stirrups beyond those needed to balance the vertical reaction.

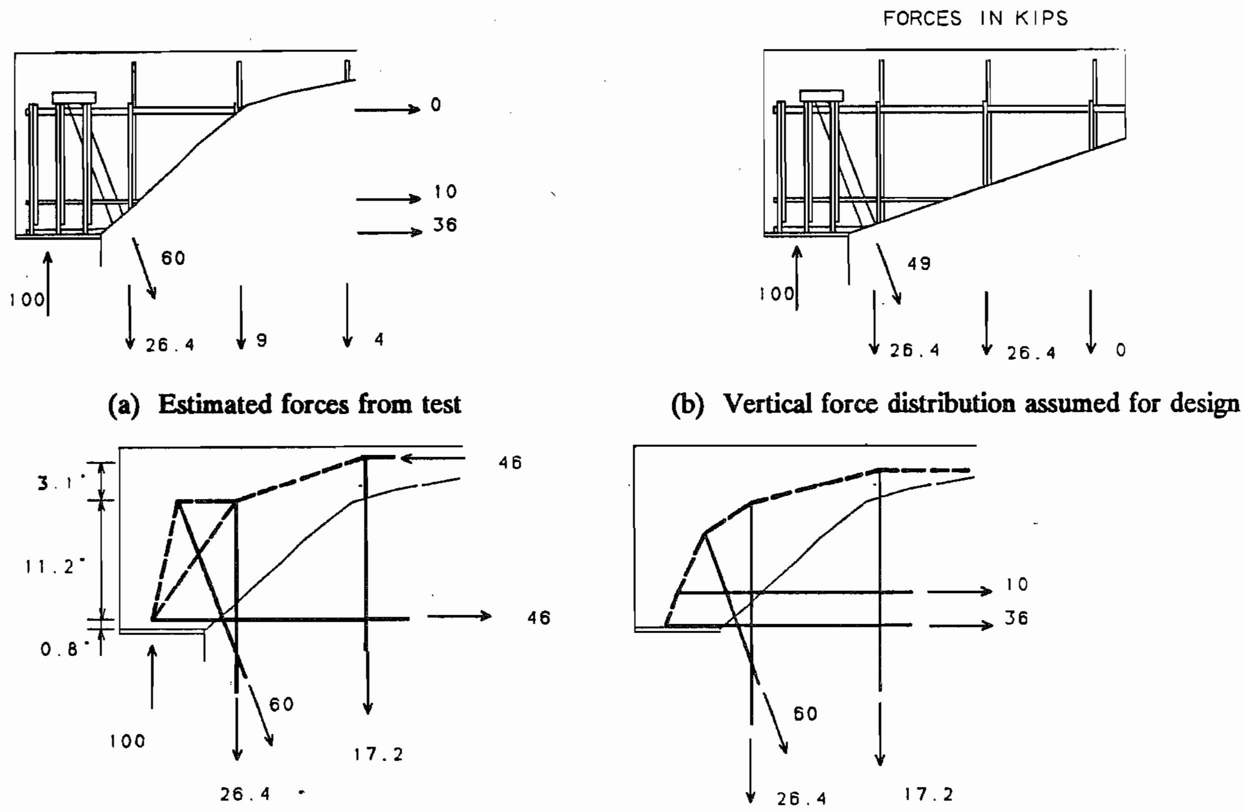

(c) Possible strut-and-tie models

Figure 4.31 Analysis of Upper Portion of Dap at 100k, MF.

4.5.5 Specimen MF. The design procedure is described in Sec. 3.5. In Fig. 4.31a and b, the free body diagram of the upper section of the dap used for design of the detail is compared to a similar diagram based on test results. At the design load of 100k, these sections show reasonably good agreement between predicted and measured internal forces. The only major difference is that the stirrup forces away from the dap are much smaller than predicted. The strap is closer to the re-entrant corner and develops force at a faster rate than the stirrups further away. This area can also be represented as a strut-and-tie model. In Fig. 4.31c two approaches to developing a strut-and-tie model are shown. In the first model it is assumed that forces transferred to the strap at the bearing plate. One compression strut transfers force directly to the strap while the other transfers force to the stirrups. A second method involves treating the strap in the same manner as the other reinforcement. Treating the strap as normal reinforcement is valid as long as the node which occurs on the strap is reasonably close to the bearing plate. In this case both approaches produce similar models. However, the model in which the strap is treated as normal reinforcement seems more rational as it is hard to accept two distinct diagonal compression struts in the relatively small dap.

At the ultimate load of 135k, the measured internal force system is shown in Fig. 4.32a and is represented by a strut-and-tie model in Fig. 4.32b. In this case the strap is treated as normal reinforcement as the node at the strap lies very close to the bearing plate on the strap. At the ultimate load the strut-and-tie representation moves so far beyond the physical dimensions of the beam that it cannot be modified easily by moving the reaction. It is likely that significant forces developed in the concrete to modify the horizontal forces needed for equilibrium of the compression struts.

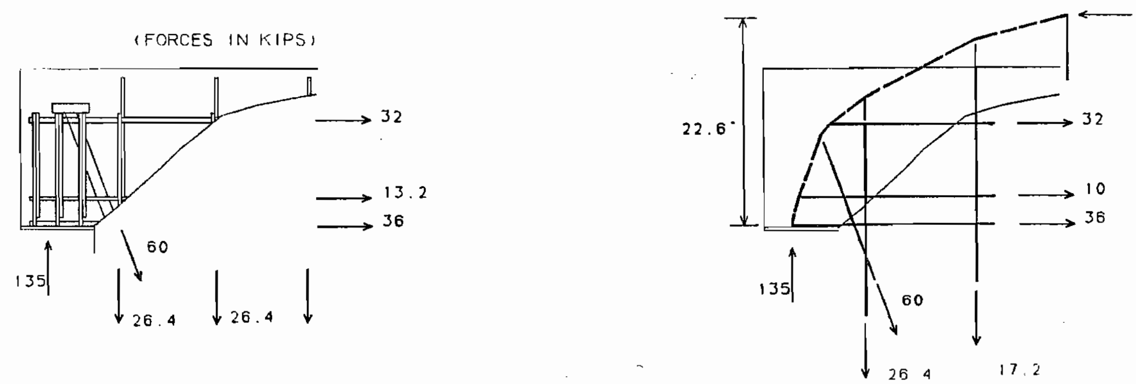

(a) **Estimated forces from test**

(b) **Possible strut-and-tie model**

Figure 4.32 Analysis of Upper Portion of Dap at Ultimate, MF.

4.6 Behavior of Stirrups

Comparison of the strain levels near the center of the stirrups is presented for each of the details in Fig. 4.33 to 4.36. The strain in the stirrups nearest to the re-entrant corner of the beam were higher than those some distance away. For PCI (Fig. 4.35) in which a group of stirrups was placed near the dap, the strain is more uniform than in ST1 (Fig. 4.33) which stirrups were distributed over a larger distance. The strain variation across the

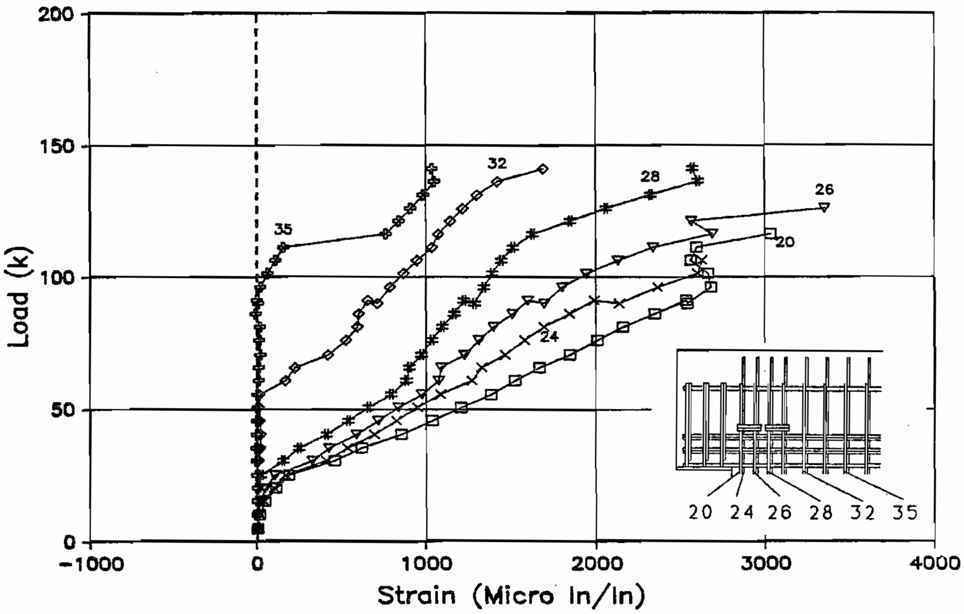

Figure 4.33 Strain in Stirrups, ST1.

stirrup groups also provides some insight as to the definition of ties. For instance in Specimen PCI and ST2 (Fig. 4.34 and 4.35), groups of stirrups which have very nearly the same strain level and function like a single unit can be identified. In such cases, the stirrup groups behave like distinct ties. In the case of ST1 (Fig. 4.33), the stirrup strains vary widely which makes it difficult to characterize any group of stirrups as a distinct tie.

Strain levels in the stirrups adjacent to the dap are compared in Fig. 4.37. The stirrups in Specimens PCI and MF developed significantly smaller strains than in the other specimens. Reinforcement concentrated close to the dap appears to be more efficient in developing forces.

4.7 Behavior of Horizontal Reinforcement at Corner of Dap

Comparison of the strain in the bottom of reinforcement (just above the bottom of the dapped end) for all the details is presented in Fig. 4.38. Concentrating the horizontal reinforcement near the re-entrant corner seemed to have no effect on the relative strain levels in the horizontal reinforcement. In fact, the PCI detail in which horizontal reinforcement was most widely distributed showed the lowest strain levels in the bottom layer of reinforcement.

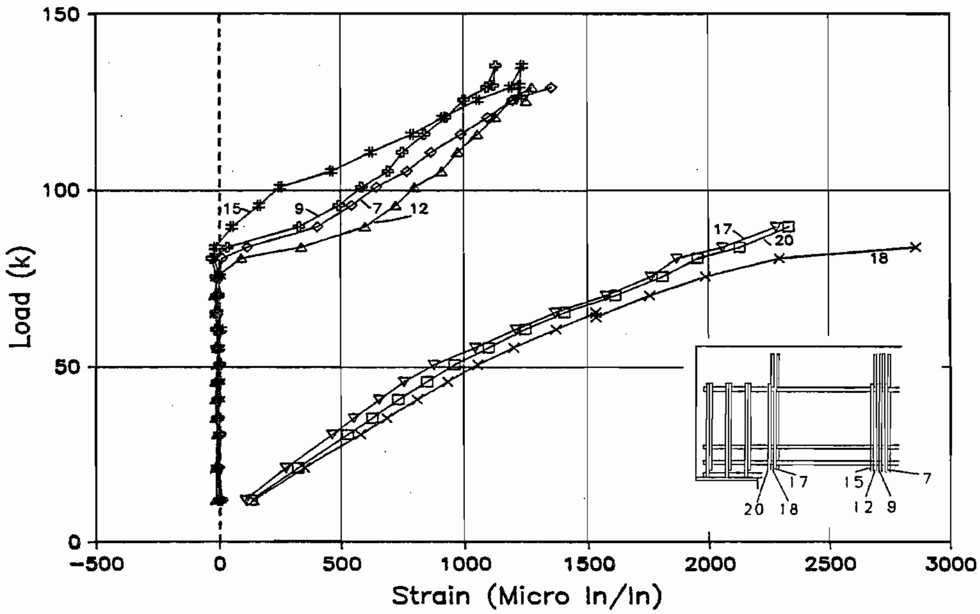

Figure 4.34 Strain in Stirrups, ST2.

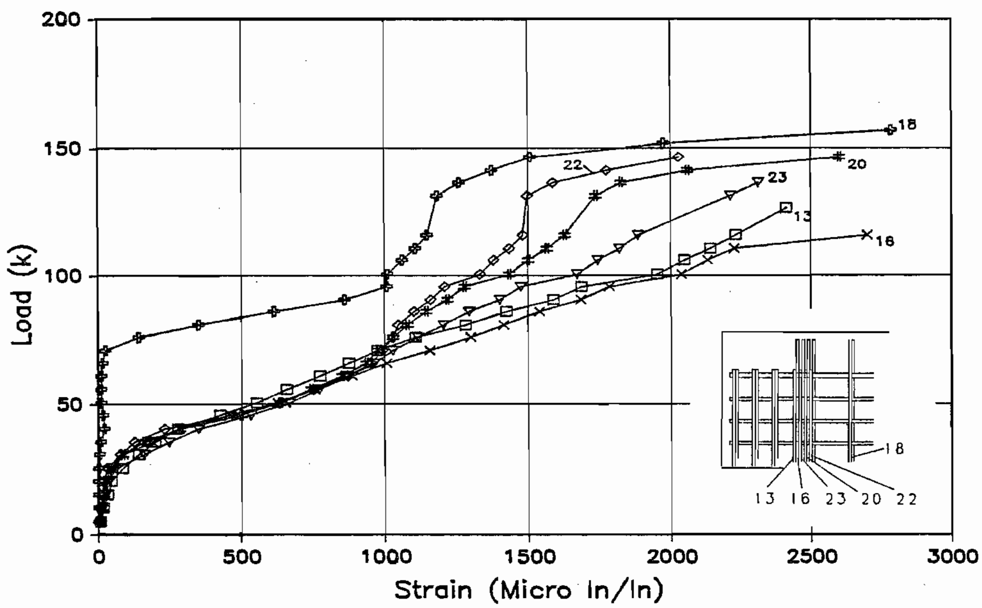

Figure 4.35 Strain in Stirrups, PCI.

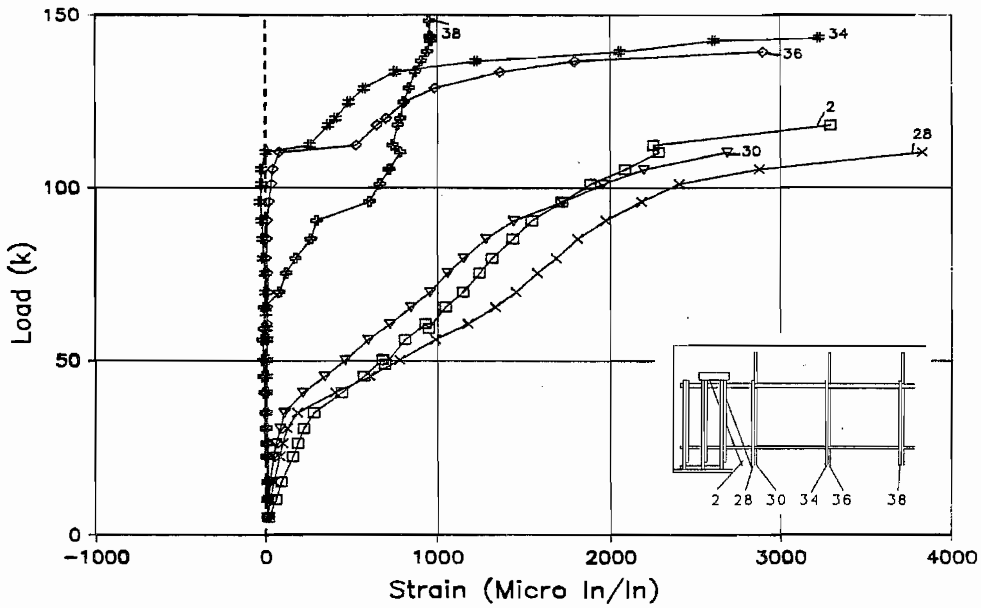

Figure 4.36 Strain in Stirrups, MF.

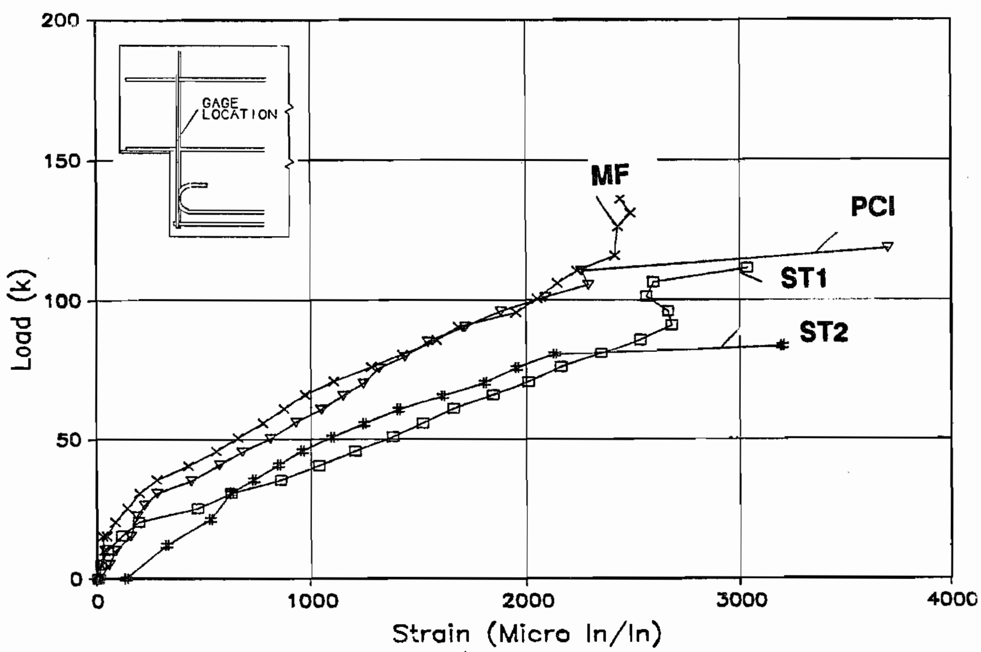

Figure 4.37 Comparison of Stirrup Strains Near Dapped End.

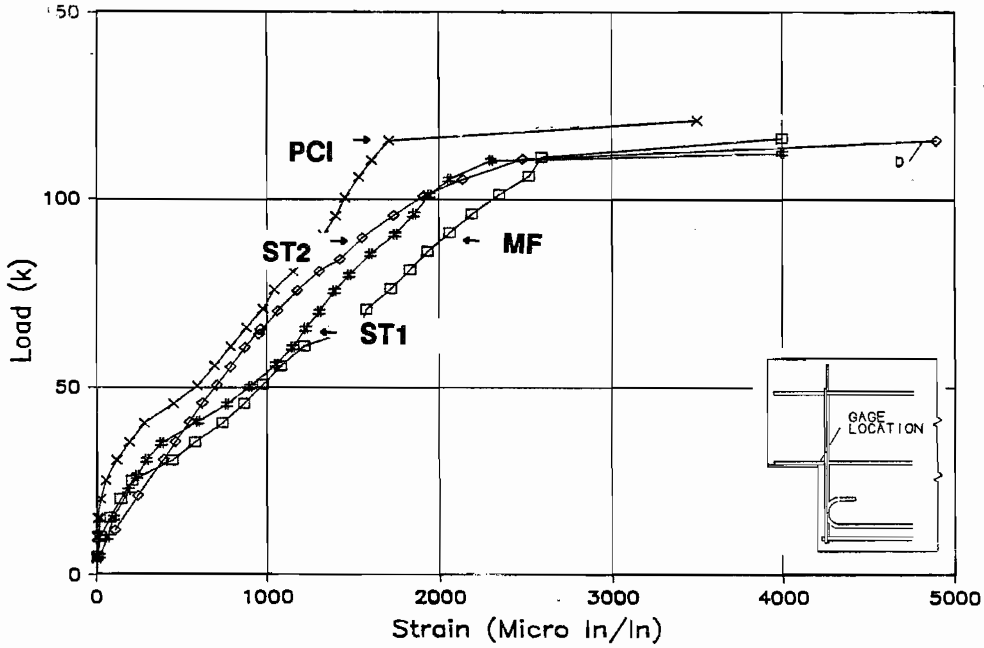

Figure 4.38 Comparison of Strains in Horizontal Dap Reinforcement.

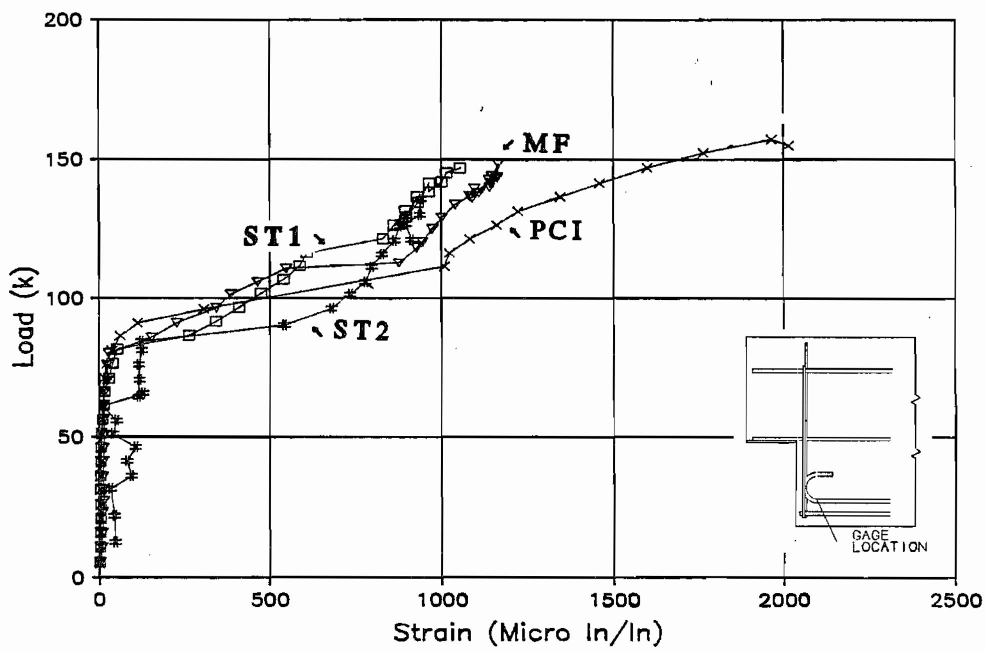

Figure 4.39 Comparison of Strains in Beam Flexural Reinforcement.

4.8 Strains in Beam Reinforcement at Bottom of Beam.

Strains developed in the lower horizontal reinforcement near the start of the hook are compared in Fig. 4.39. Strains were on the order of 25 to 35 percent of yield when the design load was reached. This is consistent with the force predicted by the design strut-and-tie model (Fig. 3.8) if it is assumed that both layers of reinforcement have equal strain levels. The strain level increased significantly as the load was increased past 100k. It is possible that as the load was increased, the top layer which has a hooked anchorage resisted a larger portion of the load.

The variation in strains along the lower longitudinal reinforcement in Specimen MF is shown in Fig. 4.40. Above an applied load of 100k, there is a greater change in strain over the short distance between gages 10 and 11 over the longer distance between gages 11 ad 12. This may be due to the influence of the strap which was located between gages 10 and 11. The strains are consistent with strut-and-tie model principles which would indicate a jump in tension force in this region.

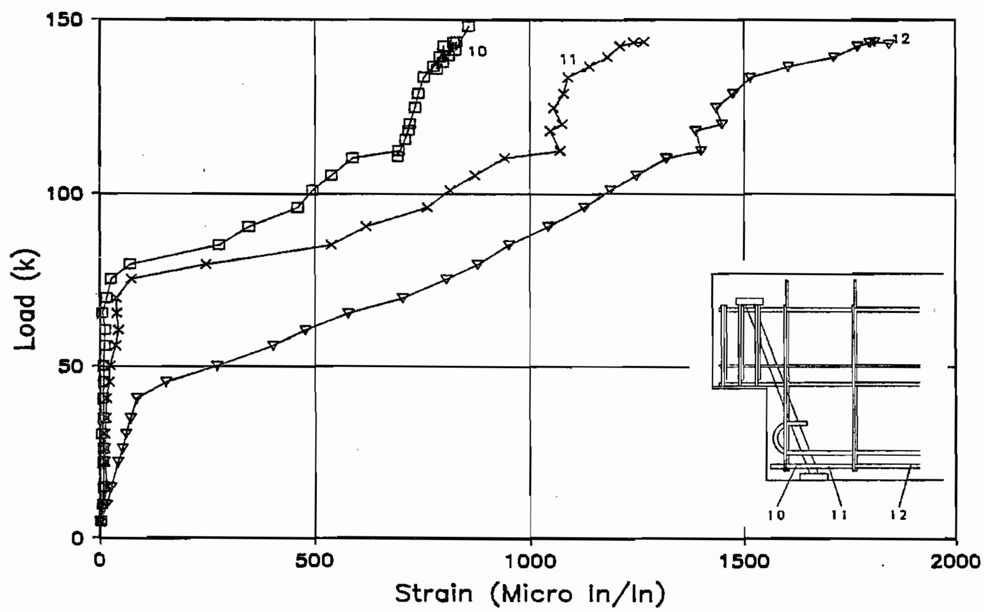

Figure 4.40 Strain Variation Along Beam Flexural Reinforcement, MF.

4.9 Concrete Strains

Embedment gages were utilized in an attempt to measure concrete strains. In general, the results from the gages were difficult to interpret because of the disturbed nature of the concrete. It appears that localized stress concentrations due to the presence of cracks near the gages produced widely varying strain measurements. Some qualitative results can be seen, however. For instance, Fig. 4.41 shows horizontal strain measurements

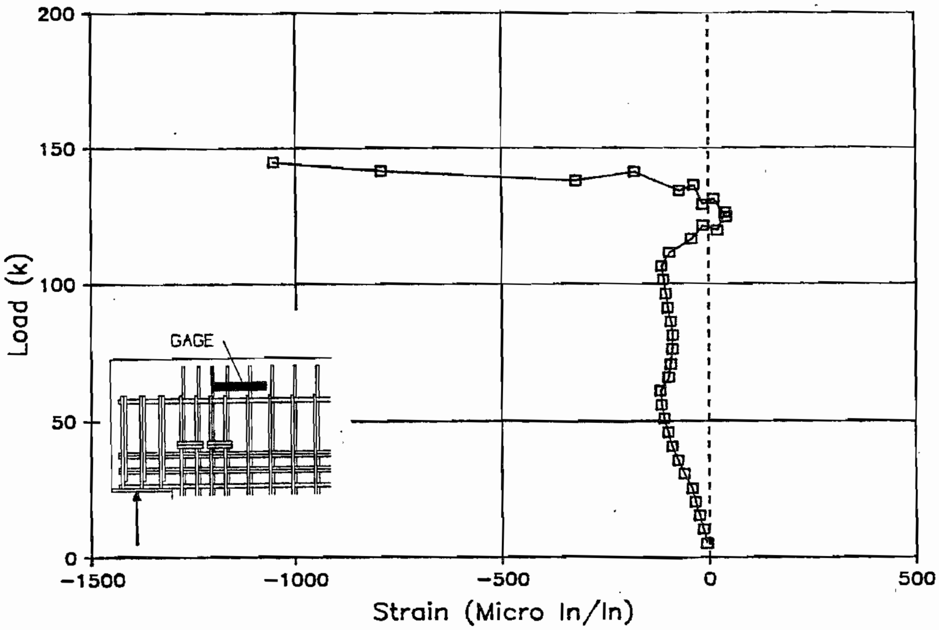

Figure 4.41 Concrete Strain Measurements, ST1.

taken in the upper portion of ST1. The plot indicates that the gage is in compression up to a load of 120k when the neutral axis presumably crossed the gage. The gage remained in tension up to a load of 135k and then went into compression. This is consistent with the discussion presented in Section 4.1.1. At 140k, the upper portion of the beam developed very large cracks which may have reduced its ability to carry compression force. The neutral axis may then have shifted down below the gage location and would explain compression readings at high loads.

4.10 Suggestions for Implementing the Strut-and-Tie Model in a Dapped Beam.

A design procedure for dapped beams based on the principles of the strut-and-tie model and was utilized in the design of ST1. In general the performance of ST1 was found to be comparable to details designed using currently accepted procedures for dapped beams. However, the results of the experimental program provides insight into the selection of primary horizontal and vertical dap reinforcement (Fig. 4.42). Based on the performance of the PCI Detail the most efficient location for the vertical tie reinforcement is as close as possible to the interface between the dap and the full depth section. In addition, the vertical tie reinforcement should be placed in a closely spaced group.

The primary horizontal reinforcement is based on the angle of the inclined compression strut, α . Obviously, selecting a steep angle reduces the required amount of horizontal reinforcement. Based on force measurements at the design load (100k), the compression strut angles which developed in the specimens ranged between 45 and 55 degrees and tended to increase as load was increased beyond 100k. Earlier it was suggested that the compression strut angle be limited to 60 degrees. Strut angles up to 60 degrees seem reasonable based on test results. Using strut angles beyond 60 degrees is probably not advisable as the ratio of horizontal to vertical reinforcement areas becomes quite small. Also, in most cases, geometrical constraints would prevent the use of extremely steep strut angles.

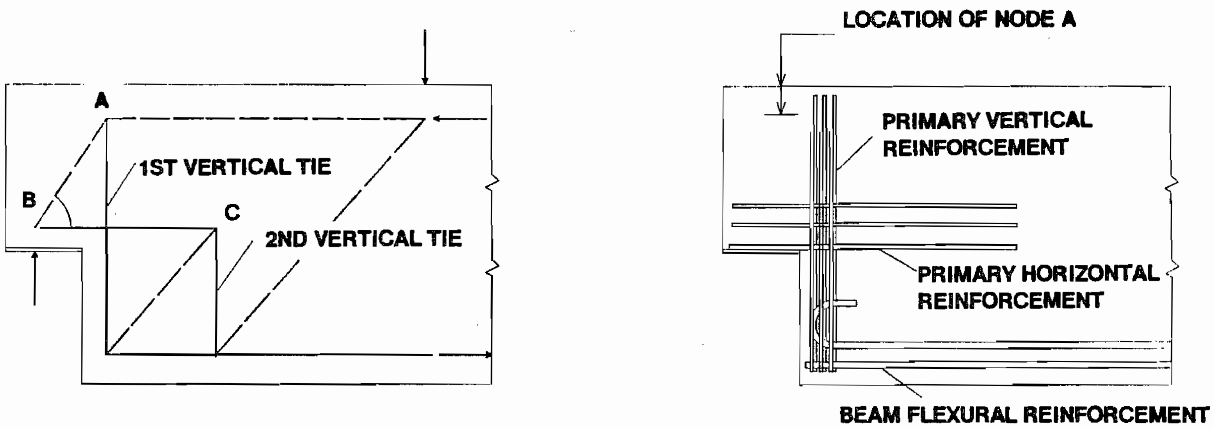

Figure 4.42 Dapped End Design Model and Suggested Reinforcement Detailing.

Another consideration in the selection of a strut angle is the location of node A shown in Fig. 4.42. In design of ST1 it was assumed that the compression strut intersected the centroid of the vertical tie midway between the top of the outer and inner stirrup legs (Fig. 3.9). This produced acceptable behavior well beyond the design load. However, near ultimate, the concrete compression zone near the top of the beam became unstable, presumably due to a loss of anchorage in the ties (stirrups). Selection of a strut angle which places node. A lower in the beam could be beneficial in the event of large overloads. The location of the node can be lowered by providing a larger area of horizontal dap reinforcement.

The distribution of the horizontal dap reinforcement in the test specimens ranged from the relatively wide distribution in the PCI Detail to being concentrated in the bottom of the dap ST2. Based upon the test results, it is difficult to determine whether any specific distribution of horizontal dap reinforcement is better. The PCI design procedure recommends distributing a portion of the horizontal reinforcement over the lower two-thirds of the dap based on test results[3, 20].

Anchorage of horizontal reinforcement within the dap was provided by welding a portion of the reinforcement to a bearing plate at the bottom of the dap and through the use of continuous "hoops". This was found to be necessary as the horizontal reinforcement reached yield within the dap. In ST1, anchorage was provided within the full-depth section, by extending the reinforcement past node C at the top of the second vertical tie (Fig. 4.42). The extension was equal to one development length past the center of the node. Test results indicate reinforcement beyond the center of node C (Fig. 4.42) developed significant force only when loads exceeded design loads. While less anchorage may have been sufficient, the anchorage of the horizontal reinforcement in ST1 appeared to provide some of the excess capacity exhibited in the test.

The beam flexural reinforcement used in the test specimens developed significant forces near its intersection with the primary vertical reinforcement. The magnitude of the forces was consistent with that predicted by the strut-and-tie model. Using hooks on some of the horizontal reinforcement in this region will help to provide sufficient anchorage for the flexural reinforcement.

The only inconsistency exhibited by the strut-and-tie models used in the design of ST1 and ST2 was the means of anchoring the upper horizontal tie into the full depth section. In the design model, the primary horizontal reinforcement in the dap was anchored by the formation of a diagonal compression strut to the lower corner of the beam. This assumed force system required that a second vertical tie be placed as shown in Fig. 4.42. The test results indicated that the primary vertical reinforcement alone was sufficient to transfer forces from the dap to the full section. No additional vertical reinforcement other than standard shear reinforcement appeared necessary. This behavior is consistent with that assumed in the PCI and Menon/Furlong design procedure.

CHAPTER 5
TESTS OF ISOLATED NODES

5.1 Introduction

The purpose of this portion of the test program was to document the behavior of nodes in the strut-and-tie mode. Difficulties in applying the strut-and-tie model to the dapped beam details raised questions about implementation of the model. There was difficulty in determining the size of the nodes so that concrete stress could be checked. Further problems involved assessing the configuration of the compression field. Lastly, little information was available in determining the effect of differing compression strut angles on the various nodes. Compression - Tension - Tension (CTT) and Compression - Compression - Tension (CCT) nodes were selected because they represent critical node types appearing often in structural members and are described in detail by Schlaich, Schäfer, and Jennewein[15].

5.2 CTT Node - Test Program

5.2.1 Description of Tests. Nine isolated CTT-node tests were conducted on two series of specimens. In one series, high strength concrete specimens were used while in the other series low strength concrete specimens were used. The design concrete strength for the specimens in the high strength series was 6000 psi -- the same strength as in the full-sized, dapped beam used for Specimen ST1. Half of this strength, or 3000 psi, was chosen as the design concrete strength for the low strength series. It was thought that this would give a suitable range for investigating the influence of concrete strength on CTT-node behavior. One specimen in each series incorporated a reduced compression strut width for determining the allowable concrete stress at the node boundary and the configuration of the compression stress fields. To study the effect of lateral confinement, each series contained specimens with differing confining reinforcement details. Other specimen variations included: (1) changing the anchorage detail for a high strength specimen; and (2) changing the angle of inclination of the compression strut for a low strength specimen. A replicate specimen was also tested to provide information about the repeatability of the testing procedure. The specimen size, location and type of instrumentation, method of fabrication, and testing procedure were similar for all the specimens.

5.2.2 Specimen Design. The specimens were designed to duplicate as closely as possible the boundary conditions that existed in Specimen ST1 in the dapped beam test series. The placement and amount of steel were identical although differing anchorage details were used in some of the node specimens. The prototype and node specimens also had the same width. Proposals presented by Schlaich et al.[15], Schlaich and Schäfer[18], and Marti[14] give some insight as to the dimensioning of nodes and were used in choosing the specimen size.

The dimensions of the node were governed by the layout of the original strut-and-tie model developed for Specimen ST1 [shown in Fig. 5.1(a)]. The corresponding placement of reinforcement is shown in Fig. 5.1(b). The isolated CTT-node is shown in Fig. 5.1(c). Tensile ties 1 and 2 are identified by their purpose in the full-sized, dapped beam and are designated as transverse and longitudinal ties, respectively. The requirement of applying tension to each tie demanded that the reinforcing steel protrude an appropriate amount so that it could be anchored to the loading system. Holes in the steel members for loading the specimens were drilled in a pattern corresponding to the pattern of the reinforcement. Identical reinforcement patterns were used for all CTT specimens.

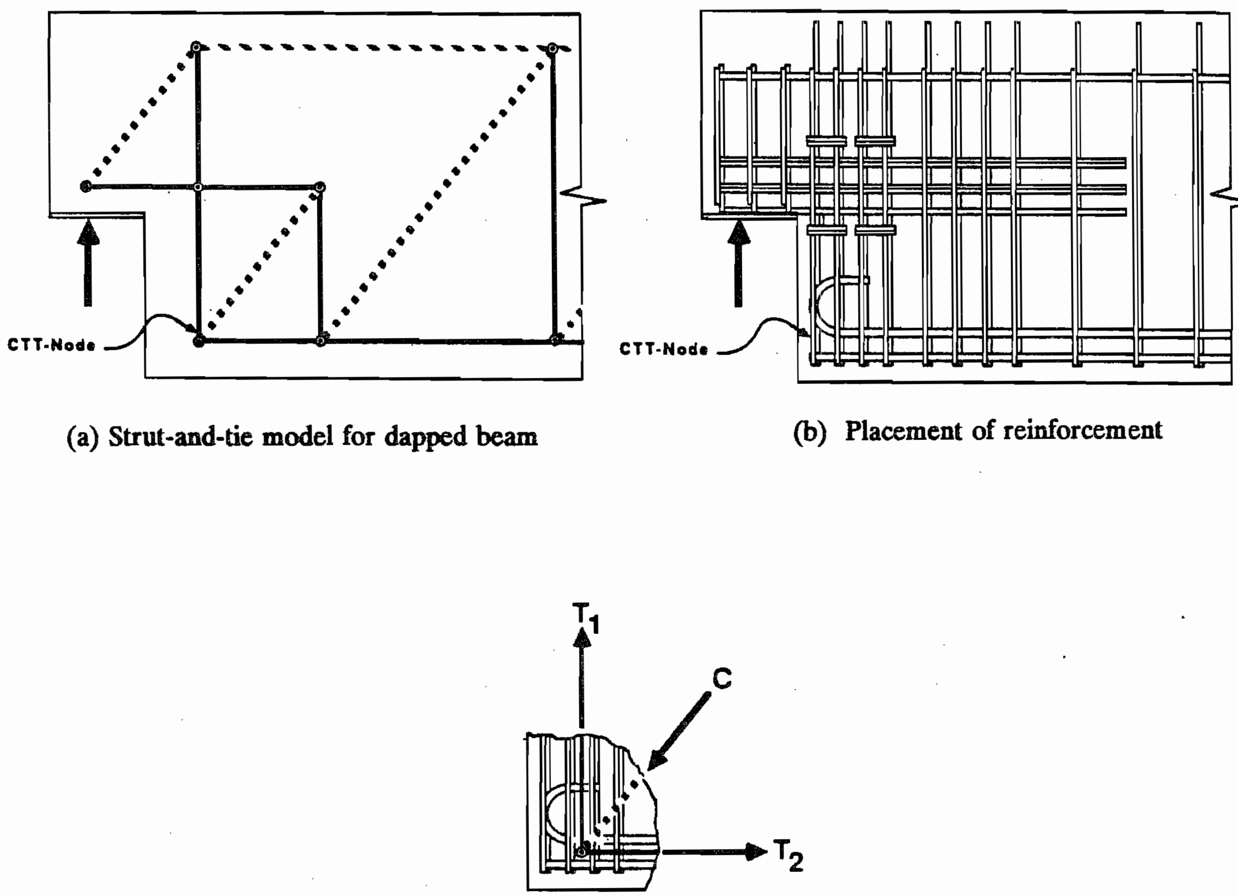

(c) Isolated CTT-node

Figure 5.1 CTT Nodes.

The dimension of the node was governed by the stress field produced by tensile tie 1. The boundaries of the stress field produced by the longitudinal steel in tensile tie 2 were chosen to extend from the bottom of the beam an equal distance away from the center of gravity of the longitudinal steel. The points of intersection of the two stress fields are

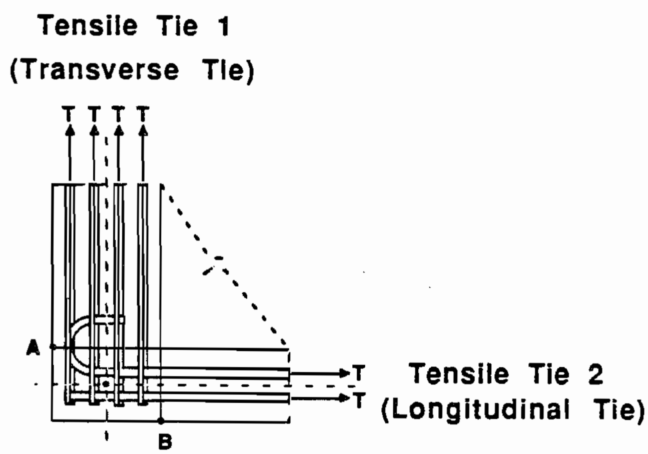

(a) Points of intersection of tensile stress fields

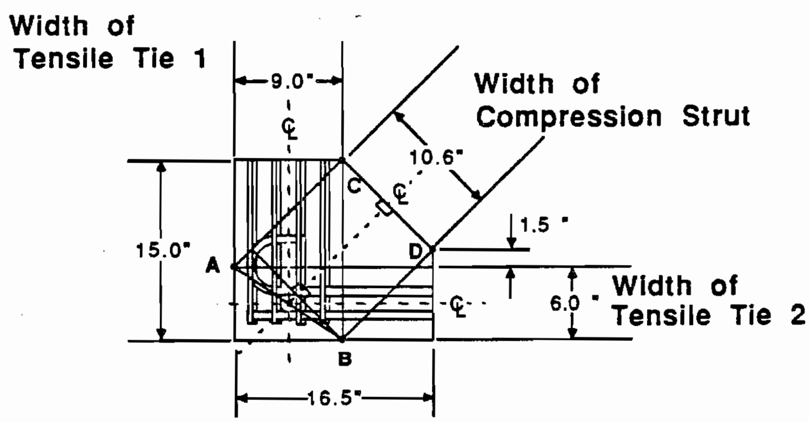

(b) Geometry of CTT-node

Figure 5.2 Determination of Node Boundaries.

labeled A and B as shown in Fig. 5.2a. The geometrical center of the CTT-node was considered to be the centroid of the two tension fields. A 45° dashed line corresponding to the inclination of the compression strut was drawn through the node's centroid. Equidistant lines parallel to the 45° inclined line were extended from A and B until the transverse tie boundary, marked by point C was reached. Thus, the width of the compression strut was determined and extended between the points C and D shown in Fig. 5.2b.

5.2.3 CTT -- Specimen Identification. Each CTT specimen was designated as follows:

First letter: Concrete Strength

H - High
L - Low

Second letter: Strut Width (Bearing Plate)

F - Full (10.6 in.) width
H - Approximately Half (4.0 in.) width

Third and Fourth letters: Reinforcement and Strut Angle

SR - Standard Reinforcing Detail-Confining transverse reinforcement hooked longitudinal steel, and 45° angle.

NC - Non-Confining transverse reinforcement with 45° strut angle.

AC - Angle Change 45° to 30° and standard reinforcing detail

SB - Straight Bar anchorage on the longitudinal steel with confining transverse reinforcement and 45° strut angle.

Suffix:

A, B - Companion specimens (HFSR only)

5.2.4 Specimen Details. Specimens HFSR-A and HFSR-B had reinforcement identical to Specimen ST1 and had similar concrete strengths. Specimen LFSR had the same reinforcement pattern as HFSR-A and HFSR-B but had a reduced concrete strength. Figure 5.3 shows the geometries for Specimens HFSR-A, HFSR-B, and LFSR.

In two specimens, one with high strength concrete (HHSR) and one with low strength concrete (LHSR), reduced compressive strut widths were produced by decreasing the bearing area at the compression face of the specimen. The strut width was chosen so that the average compressive stress over the bearing area was equivalent to f_c' in LHSR. The same strut width was used in Specimen HHSR for comparison. All other dimensions and steel placement were the same as HFSR-A, HFSR-B, and LFSR. Figure 5.4 shows the difference between the two bearing areas.

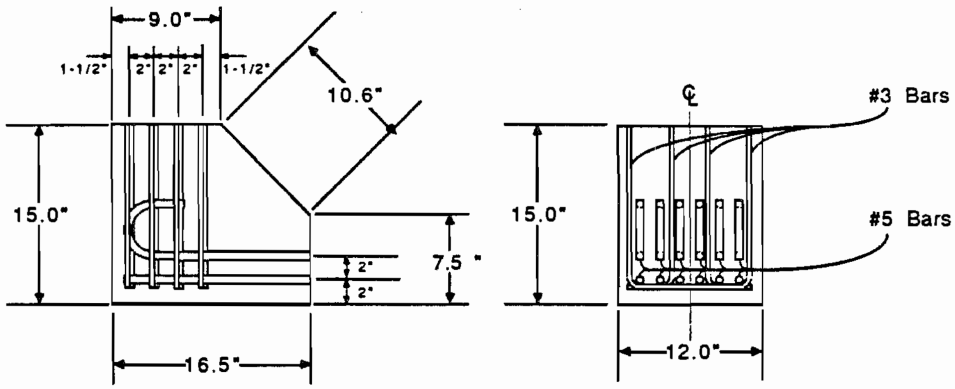

(a) **Side View** (b) **End View**

Figure 5.3 Geometry and Placement of Steel for Specimens HFSR-A, HFSR-B, and LFSR.

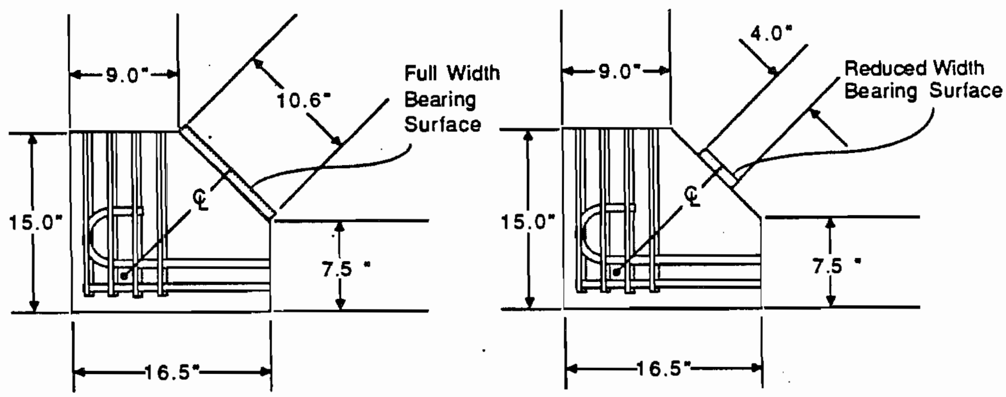

(a) **Typical Full Width Bearing Surface** (b) **Reduced Bearing Surface for Specimens HHSR and LHSR**

Figure 5.4 Bearing Surfaces Used for Isolated Tests.

Each series contained specimens that were detailed with and without confining reinforcement to study the effect of lateral confining pressure on node behavior. Figure 5.5(a) shows the confinement of the CTT-node which was provided by U-shaped hoops and 90° hooks perpendicular to the longitudinal bars. In specimens LFNC and HFNC, the effect of lateral confinement was minimized by turning the transverse 90° hooks nearly parallel to the longitudinal bars as shown in Fig. 5.5(b). Specimen HFSB was tested to determine the behavior of a CTT-node with a different anchorage detail for the longitudinal steel. Specimen HFSB is identical to HFSR except the 180° hook was removed from the top longitudinal steel as shown in Fig. 5.6

Specimen LFAC was the only specimen in this study that was subjected to unequal forces in the tension ties. The purpose of the unequal force was to produce a different

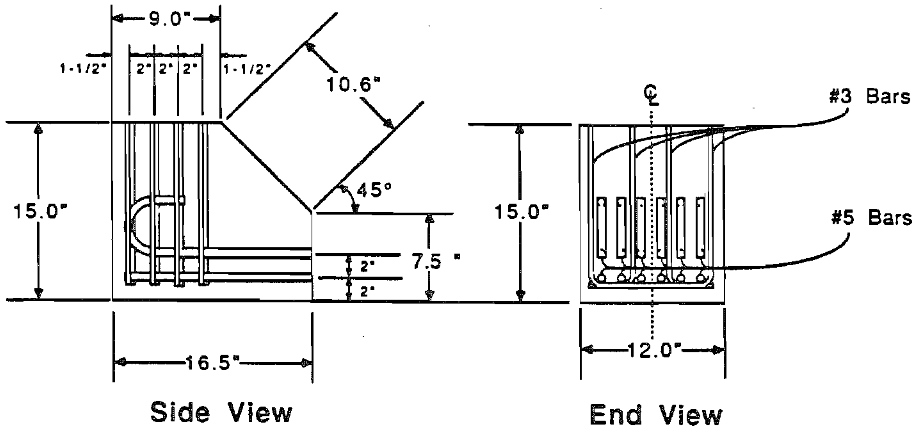

(a) Typical confining reinforcement detail

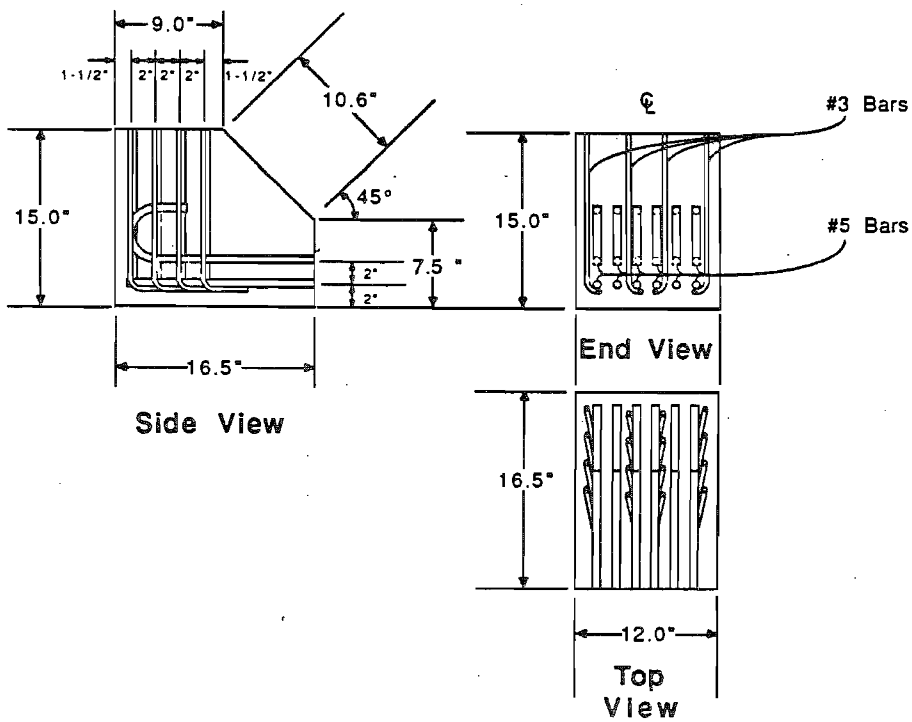

(b) Unconfined specimens HFNC and LFNC

Figure 5.5 Details for Maximum and Minimum Confinement of Node.

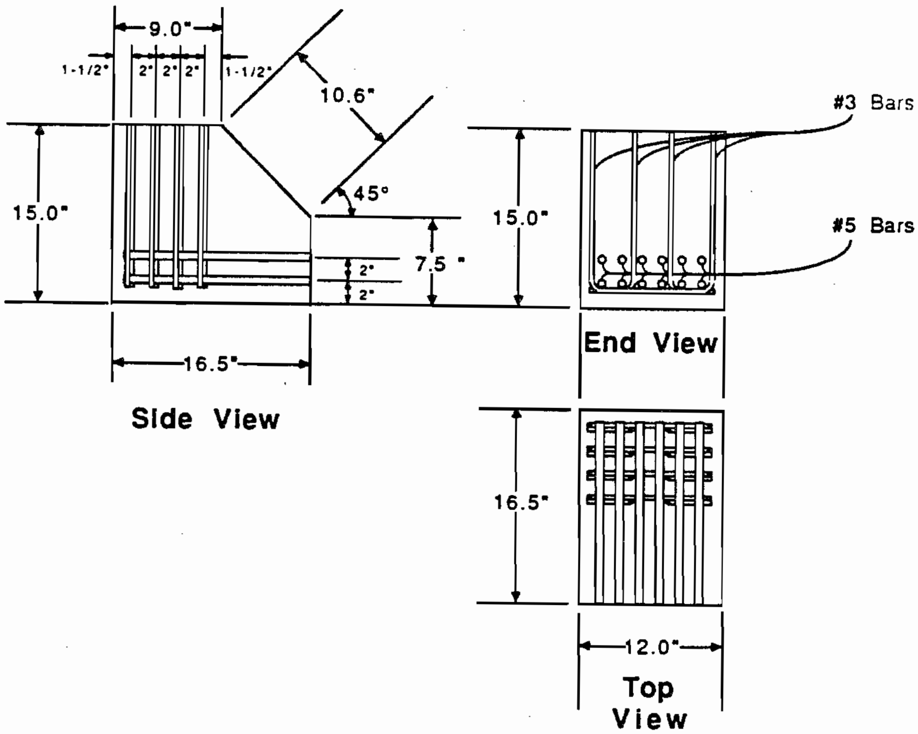

Figure 5.6 Geometry and Placement of Steel for Specimen HFSB.

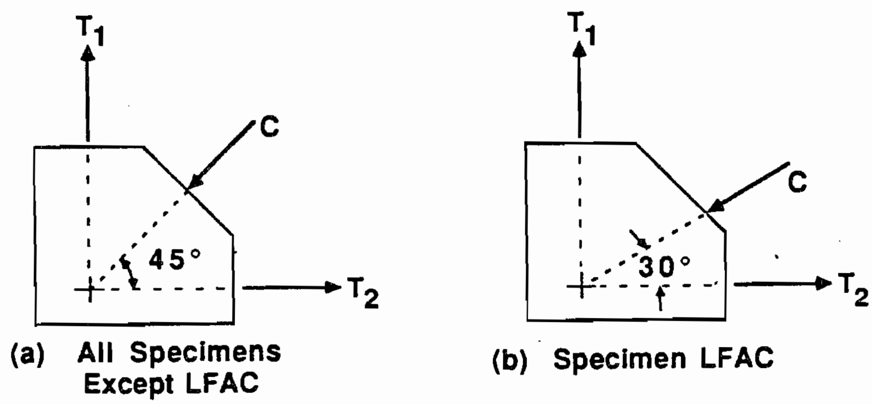

Figure 5.7 Comparison of Specimen Strut Angles.

compression strut angle. A 30° angle from the horizontal was chosen so the force in the longitudinal steel would be approximately 1.7 times the force in the transverse reinforcement. This angle would assure that the transverse steel would not reach its limiting capacity and the longitudinal steel would be highly stressed so that anchorage conditions would be more severe. Figure 5.7 shows the line of action of the compression strut force used in Specimen LFAC and all other node specimens. Specimen LFAC was identical in construction to Specimen LFSR (see Fig. 5.3).

Details for the test specimens and Specimen ST1 are summarized in Table 5.1.

5.2.5 *Materials.*

Concrete. All test specimens were cast with concrete mixes complying with Texas Highway Department Standard Specifications. This standard specifies a maximum 5-in. slump although actual slumps for different batches ranged from 3 to 6 inches. Concrete for Specimen HFSR-A and Specimen LFAC were mixed at the laboratory using a 6 cu. ft. drum type mixer. In both mixes Type 1 Portland cement with washed Colorado River sand as the fine aggregate was used. Coarse aggregate for specimen HFSR-A consisted of crushed limestone with 1/2-in. maximum aggregate size. Coarse aggregate for Specimen LFAC was crushed dolomitic limestone with a 5/8-in. maximum aggregate size. All other specimens were cast using commercially available ready mix concrete with Type 1 Portland cement, washed Colorado River sand and gravel with a maximum aggregate size of 3/4-in. Compression tests were also performed at time of testing and are given in Table 5.1. Split cylinder tests were conducted in order to determine the tensile strength of the concrete. Tests were conducted according to ASTM C496 with 1 in. wide x 1/8 in. thick birch plywood pads and a loading rate of 15,000 pounds per minute. Results of these tests are shown in Table 5.1.

Reinforcing Steel. All node specimens used standard deformed reinforcement conforming to ASTM-A615. Grade 60 #3 bars used as transverse reinforcement in all the isolated CTT-nodes were produced in the same heat (fy = 68 ksi). Grade 60 # 5 bars used as longitudinal reinforcement in Specimen HFSR-A did not have a definite yield plateau and were not used in further tests. In subsequent tests #5 bars having a well-defined yield (fy = 60 ksi).

Mechanical Connectors. To allow easy removal of the isolated CTT-node from the test setup and to equalize the stresses in the bars before testing, each reinforcing bar protruding from the specimen was fitted with a mechanical connector with a integral adjusting nut. An Erico LENTON© connector was used for this purpose. All bar ends were threaded with tapered threads at the Erico Products Inc., Cleveland, Ohio facility. The mechanical connector with adjusting nut was reused after each test. The mechanical connector could develop a bar stress of 85 ksi before the threads stripped. The limiting capacity of the threaded anchor was arbitrarily set at a bar stress of 75 ksi which assured the reinforcement would be well past yield when the test was concluded. Adjusting threads on the exterior of the mechanical connector were cut to a close tolerance and with suitable length to prevent stripping of the adjusting nut.

5.2.6 *Instrumentation.* The specimens were instrumented with electrical resistance strain gages mounted to the longitudinal and transverse steel. Locations were chosen to give information about the behavior and the transfer of forces within the node. Gages in ST1 and CTT node specimens were placed in identical locations although more bars in the node

Table 5.1 Summary of Test Specimens

Specimen	f'_c* (ksi)	Strut Width (in.)	Conf. Trans. Reinf.	Angle of Loading	#3 Bars fy (ksi)	#5 Bars fy (ksi)	#5 Bar Anchorage Detail	Splitting Tensile Strength (psi)
Specimen ST1	6.3	N/A	Yes	50° Design	66.8	60.5	180° Hook	Not Tested
HFSR-A	7.0	10.6	Yes	45°	66.8	59.6	180° Hook	440
HFSR-B	5.8	10.6	Yes	45°	66.8	59.6	180° Hook	490
HHSR	5.8	4.0	Yes	45°	66.8	59.6	180° Hook	490
HFSB	5.8	10.6	Yes	45°	66.8	59.6	Straight Bar	490
HFNC	5.8	10.6	No	45°	66.8	59.6	180° Hook	490
LFSR	3.7	10.6	Yes	45°	66.8	59.6	180° Hook	410
LHSR	3.7	4.0	Yes	45°	66.8	59.6	180° Hook	410
LFNC	3.7	4.0	No	45°	66.8	59.6	180° Hook	410
LFAC	3.9	10.6	Yes	30°	66.8	59.6	180° Hook	390

* At time of testing

specimen were instrumented. Gages mounted on protruding bars were used to obtain a uniform stress level prior to testing and to monitor bar stress levels during testing.

Measurements. The specimen was loaded using double acting center hole rams with hand operated pumps. Hydraulic pressure was used to monitor the applied force. Potentiometers monitored deflections during testing. A computerized data acquisition system was used to collect and record all test data.

5.2.7 *Specimen Fabrication*. Formwork for all specimens was constructed of 3/4-in. plywood reinforced with 2 in. x 4 in. studs at the corners. The protruding reinforcement passed through holes predrilled in two sides of the formwork. These sides were bolted together first to serve as a guide for placing the reinforcing steel. Figure 5.8 shows the assembled formwork and reinforcing cage for one specimen.

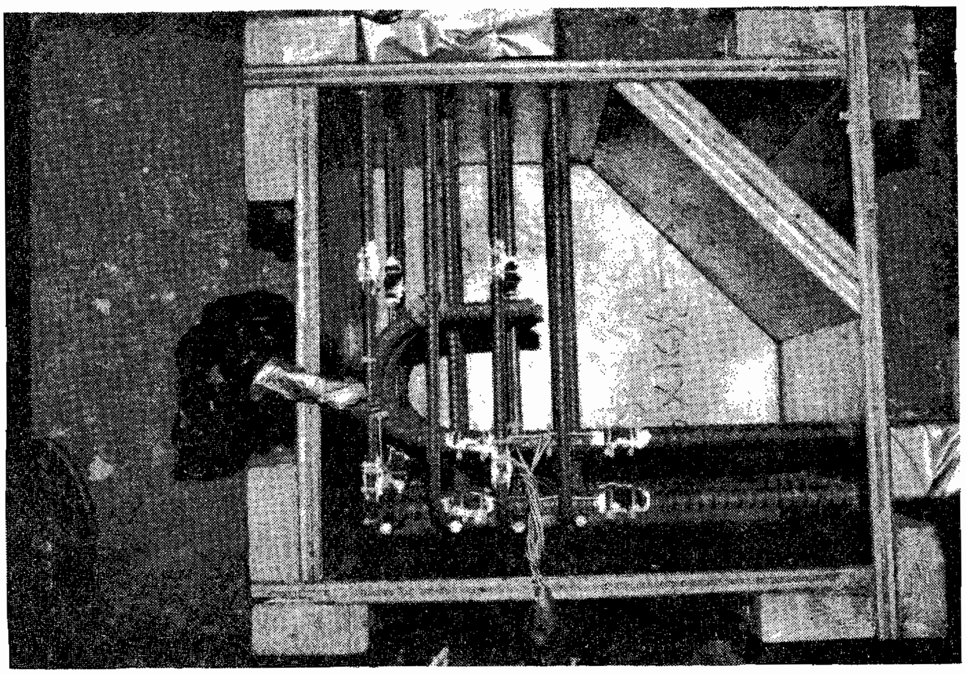

Figure 5.8 Assembled Formwork and Reinforcing Cage.

After casting the specimen and finishing the surface, the specimens were covered with wet burlap. The burlap was covered with a polypropylene plastic sheet to prevent evaporation.

5.2.8 *Test Setup*. A concrete reaction block was constructed for the purpose of transferring the load from the compression face of the test specimen to the reaction floor and wall. The extension block was designed to be removable so different angles of inclination of the compression strut could be investigated. An elevation view of the concrete reaction block is presented in Fig. 5.9.

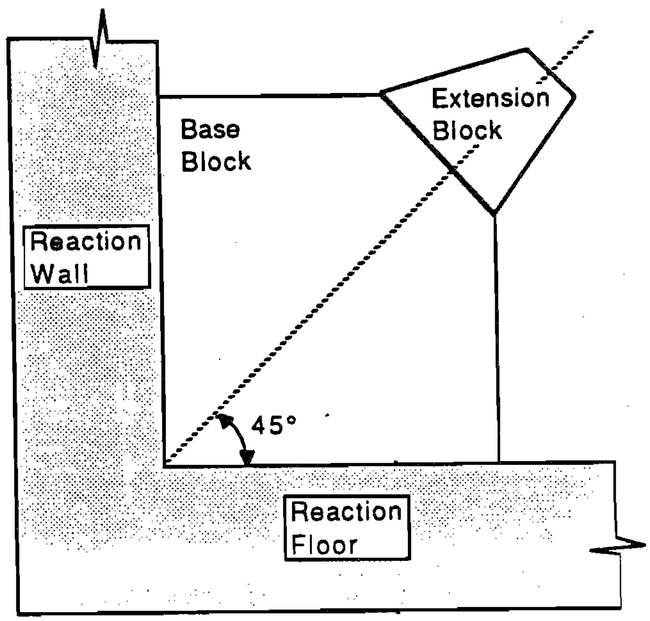

Figure 5.9 Elevation View of Concrete Reaction Block.

The reaction block was bolted to the strong wall to resist the compressive forces developed during the tests. The test setup allowed direct tension loading of the protruding reinforcement in the horizontal and vertical directions. The tensile loading produced an equilibrating compression reaction on the bearing face. Space requirements and magnitude of loading did not permit insertion of tensile rams between the specimen and the strong wall and floor. Therefore, a loading system consisting of fabricated steel members and connecting rods was assembled to allow tensile loading of the specimen by compressive rams. Elevation and plan views of the complete loading system are shown in Fig. 5.10.

The horizontal bearing beam and ram rested on a wooden carriage fitted with ball bearing rollers. The carriage rolled atop the concrete base block. The roller support allowed the bearing beam and ram to move horizontally without friction. A thin layer of hydrostone provided a uniform bearing surface between the specimen and test setup. With the specimen held firmly in place by clamps, all connecting rods and adjustable couplings were retightened by hand. Small adjustments were made at low stress levels by tightening or loosening the adjusting nuts on the mechanical connectors. Loads were applied in approximately 5 kip stages. Deflection vs. load and stress vs. load in both the vertical and horizontal directions were monitored. The plots gave a graphical representation of the behavior of the specimen and were used to detect a malfunction or instability in the setup. Cracks were marked at each load stage. Photographs were taken at varying load levels. Generally, the time interval between load stages was less than 10 minutes. All tests were concluded on the day they were started. The testing process usually took about 6 hours.

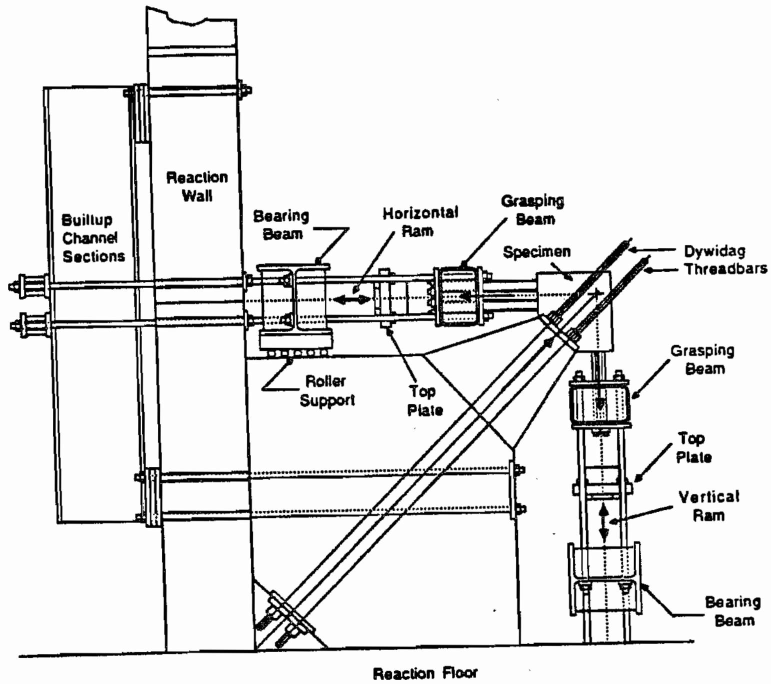

(a) Elevation view

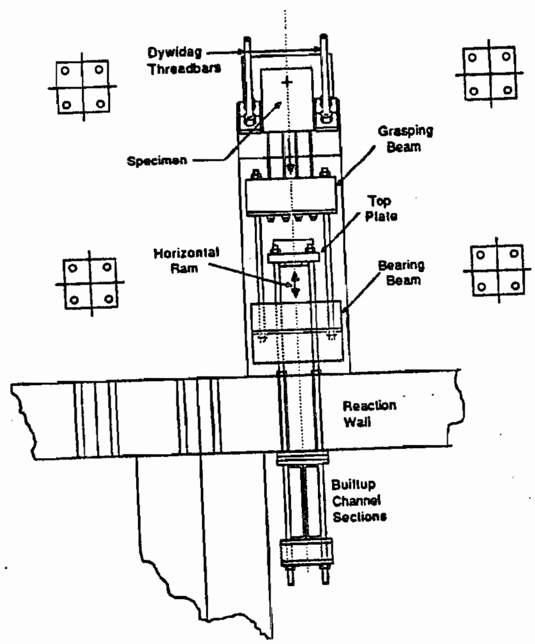

(b) Plan View

Figure 5.10 Test Setup, CTT - Nodes.

Complete details of the design, construction and test procedures for the CTT node tests are included in Ref. 21.

5.3 CCT Node - Test Program

5.3.1 Description of Tests. Ten specimens representing CCT nodes located at the support of the prototype dapped beam (Fig. 5.11) were tested. The dimensions and the shape of all the specimens were the same. The reinforcement layout was based on the dapped beam test specimen. However, a larger reinforcement area and angle of inclination of the compresion strut (60°) was used so that concrete crushing would control the mode of failure. The details of the test specimens is given in Table 5.2. The specimen notation used is as follows:

First letter: Concrete Strength

L - Low
H - High

Second letter: Bearing plate width

F - Full, 12 in.
H - Half, 6 in.

Third letter: Confining reinforcement around tension tie

T - Yes, #3 at 4 in.
O - No

Suffix: Tension tie reinforcement

First letter:

R - Replicate
S - Straight
H - Hooked

Second letter: Distance to center of bottom layer of tension tie reinforcement (cover)

S - Small, 1-¼ in.
L - Large, 3-13/16 in.

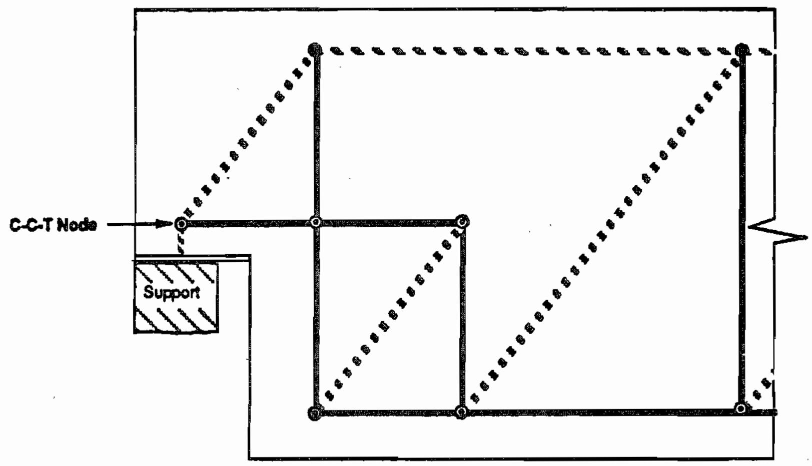

(a) Strut-and-tie model for dapped beam

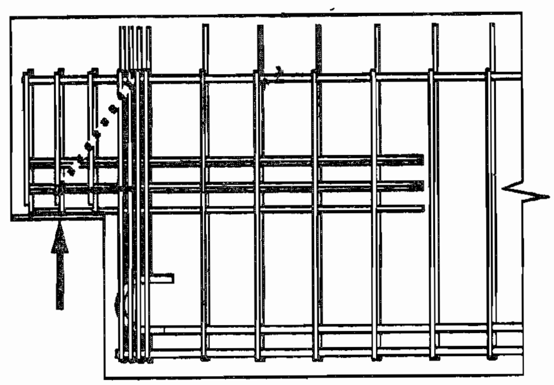

(b) Placement of reinforcement

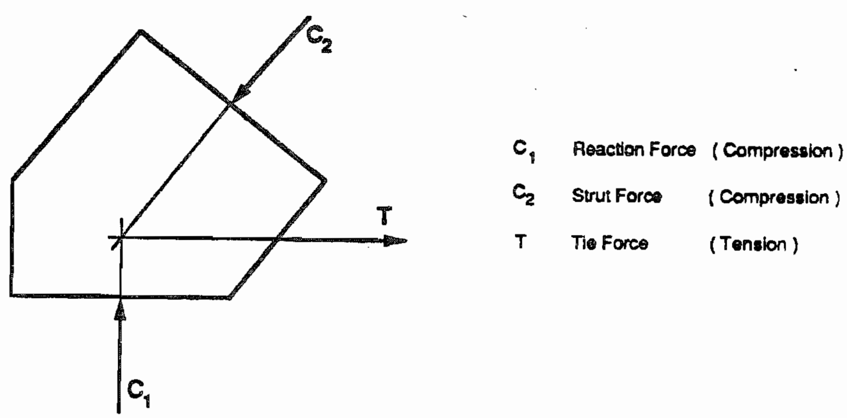

(c) Isolated CCT Node

Figure 5.11 CCT Nodes.

Table 5.2 Summary of Test Details, CCT-Nodes.

			Tension Tie	
Specimen	f'c (psi)	Bearing Plate	Bars	Layout
LFT	2340	Full	3-#5, 8-#6	
LFO	2470	Full	3-#5, 8-#6	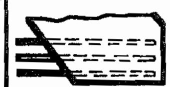
LHT	2490	Half	3-#5, 8-#6	
LHO	2600	Half	3-#5, 8-#6	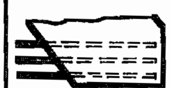
LFT-R	2610	Full	3-#5, 8-#6	

Specimen	f'c (psi)	Bearing Plate	Bars	Layout
HFT	4860	Full	3-#5,8-#6	
HFO-SS	5005	Full	6-#7	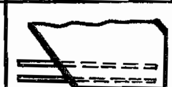
HFO-HS	5015	Full	6-#7	
HFO-SL	5025	Full	6-#7	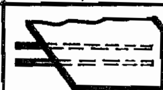
HFO-HL	5025	Full	6 #7	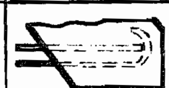

Five tests (LFT, HFT, LFO, LHT, LHO, LFT-R) were performed in order to evaluate the effect of the support size and the confinement condition on the compressive strength of the concrete. Specimens LFT, HFT, LFT-R were confined with #3 ties at 4" (Fig. 5.12b), while LFO and LHO (Fig. 5.12a) were not confined. In order to evaluate the effect of the support bearing size on the performance of the node, two loading plate widths were used. In LFT and LFO a full width support bearing (12 in.) was used (Fig. 5.12c) and in LHT and LHO, a half width support bearing plate (6 in.) was used. Specimens LFT and HFT were identical except for concrete strength.

The effect of the tension tie reinforcement layout on node resistance was examined using HFO-SS, HFO-HS, HFO-SL, HFO-HL (Figs. 5.12d and e). In each case the total steel area was kept constant but the location of the reinforcement and the use of 180° hooks on the lower layer of bars provided a means of studying the anchorage conditions. In addition, two different values of cover from the bottom edge (bearing surface) of the specimen were considered.

5.3.2 Materials.

Concrete. The specimens were cast using ready mix concrete with Type I Portland cement, washed Colorado River sand and 3/8-in. coarse aggregate for specimens with low strength concrete, and 3/4-in. for those with high strength concrete. Cylinders were tested at 7 days, 14 days and 28 days to obtain the strength versus time curve. Three cylinders were tested at each age. The concrete strength determined for the age at time of testing is shown in Table 5.2.

Reinforcing Steel. ASTM-A615 Grade 60 deformed bars were used for all specimens. ACI 318 standard 180° bends were used for the hooked bars. Tensile tests were performed on each group of bars to obtain the yield strength of the bars as follows: #3 - 71.3 ksi; #5 - 72.7 ksi; #6 - 64.8ksi; and, #7 - 71.7 ksi.

5.3.3 Instrumentation.

Strain Gages. The strains were monitored with strain gages mounted on the longitudinal bars and on transverse hoops. Gages were also mounted on the protruding longitudinal reinforcement 2.5 in. from the concrete face.

Demec Gage Readings. Demec points were used to measure the surface strain. The points were placed in a pattern to provide a 2 in. gage length. The arrangement of points is shown in Fig. 5.13. The data for LFO and LHT indicated that the arrangement selected did not give principal strains. An arrangement providing strain rosettes was used for the remaining specimens to permit computing the principal strains.

5.3.4 Specimen Fabrication. Because the small size of the specimen reduced the tolerances, special care was taken to maintain the angles and dimensions of the forms. A

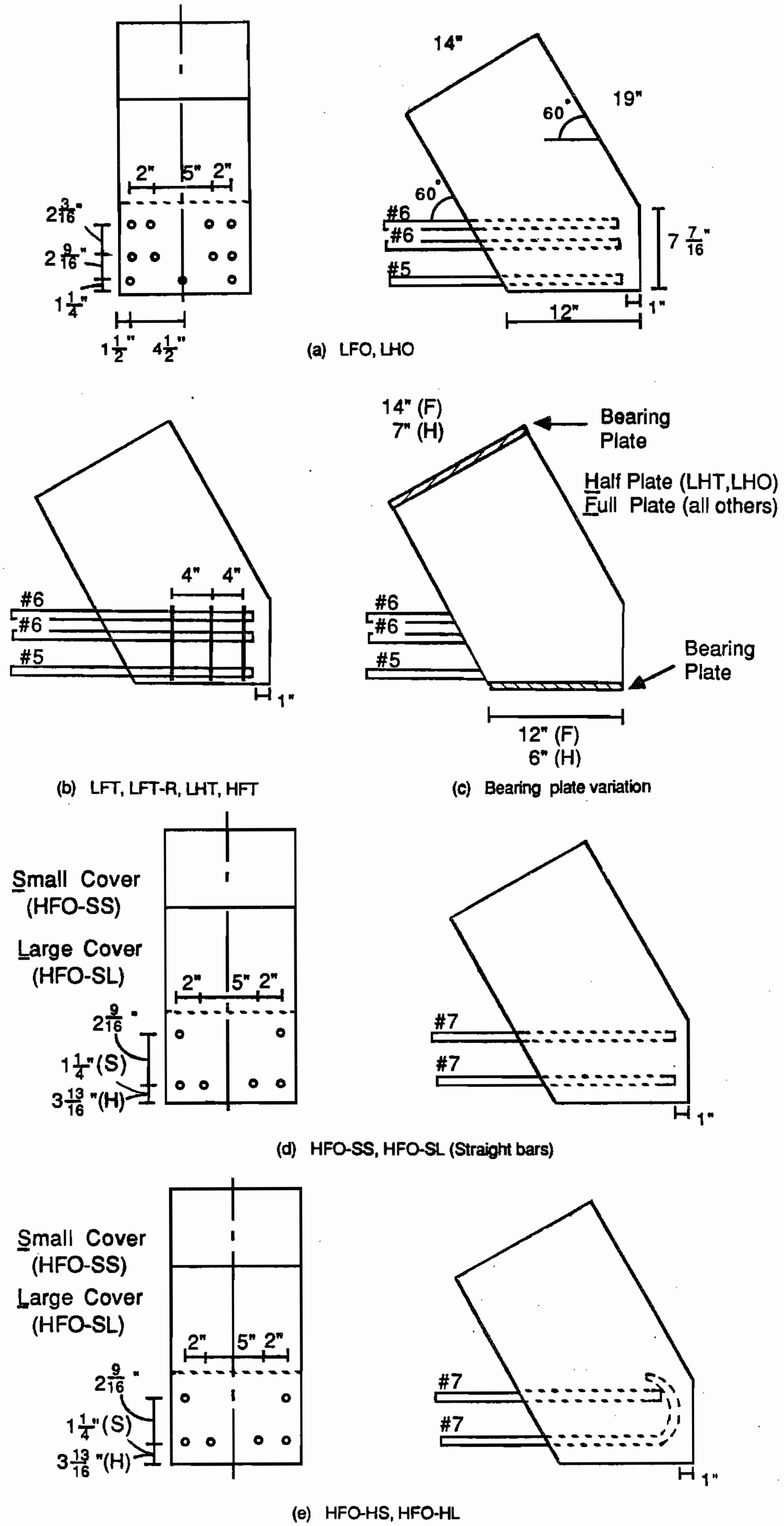

Figure 5.12 Reinforcement Details and Specimen Geometry - CCT Nodes

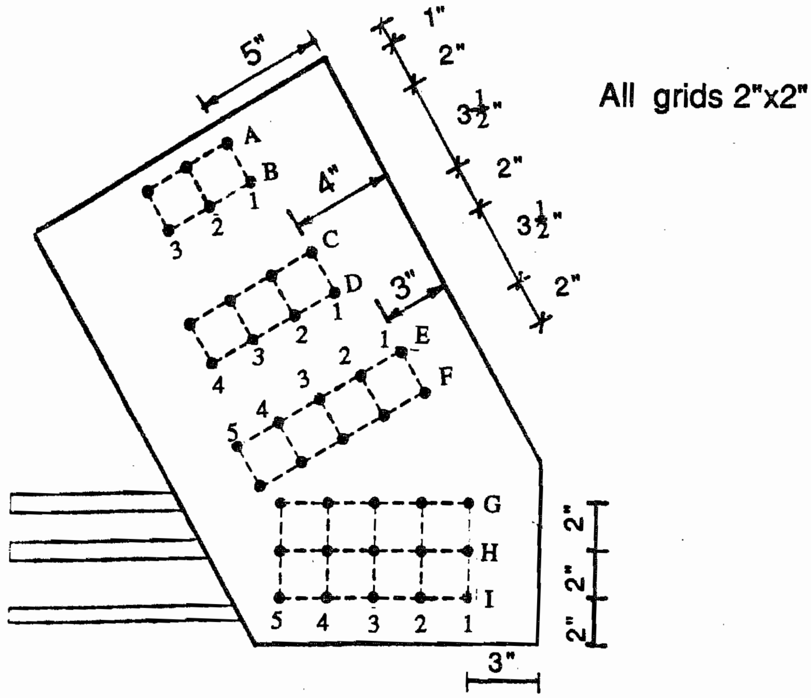

(a) LHT and LFO

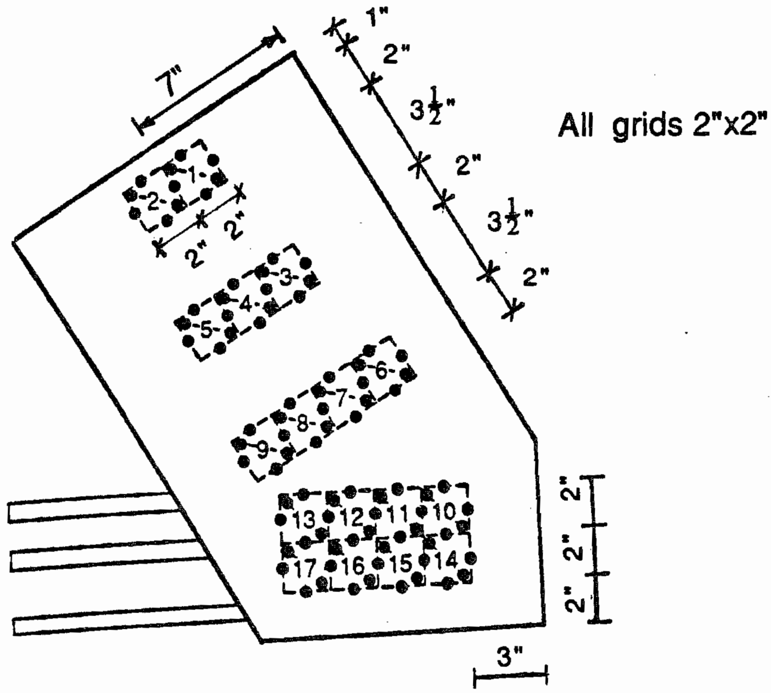

(b) All Others

Figure 5.13 Location of Points for Surface Strain Measurements.

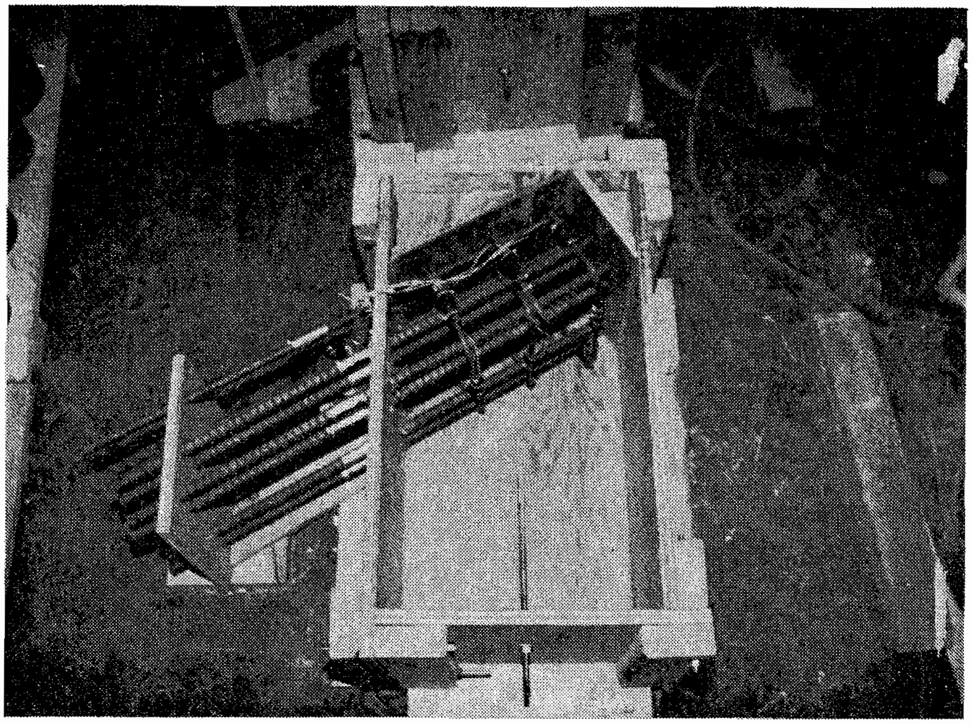

Figure 5.14 Steel Cage and Formwork.

form with reinforcement in place is shown in Fig. 5.14. The longitudinal reinforcement passed through a predrilled form. In specimens with transverse reinforcement, the hoops were placed after the longitudinal bars were positioned. After the concrete was cast, the specimens and the cylinders were covered with moist burlap to cure the concrete to reduce shrinkage effects.

5.3.5 Test Setup and Procedure. The specimen was placed in a setup shown in Fig. 5.15. Stiffeners welded to the web carried the load directly to the test machine. The top element of the setup consisted of welded steel plates (bolted to the support beam) which provided a bulkhead to anchor the protruding bars.

The specimen was placed on the support beam and bars were passed through the predrilled plate. After horizontal and vertical alignments were checked, the bars were welded to the anchor plate on the bulkhead. Hydrostone (grout) was placed between the specimen and the bottom support plate to produce a uniform bearing surface. The support plate had a thickness of 1/2 in. A sheet of teflon was placed between the bottom support plate and the inclined support to reduce frictional forces. A thin layer of hydrostone was cast on the top part of the specimen to obtain a uniform loading surface. A sheet of teflon was placed on the hydrostone layer and a supporting plate was placed on top of the teflon. A sheet of teflon also was inserted between the bearing plate and the machine head. The support beam and the specimen in the machine were centered under the machine head.

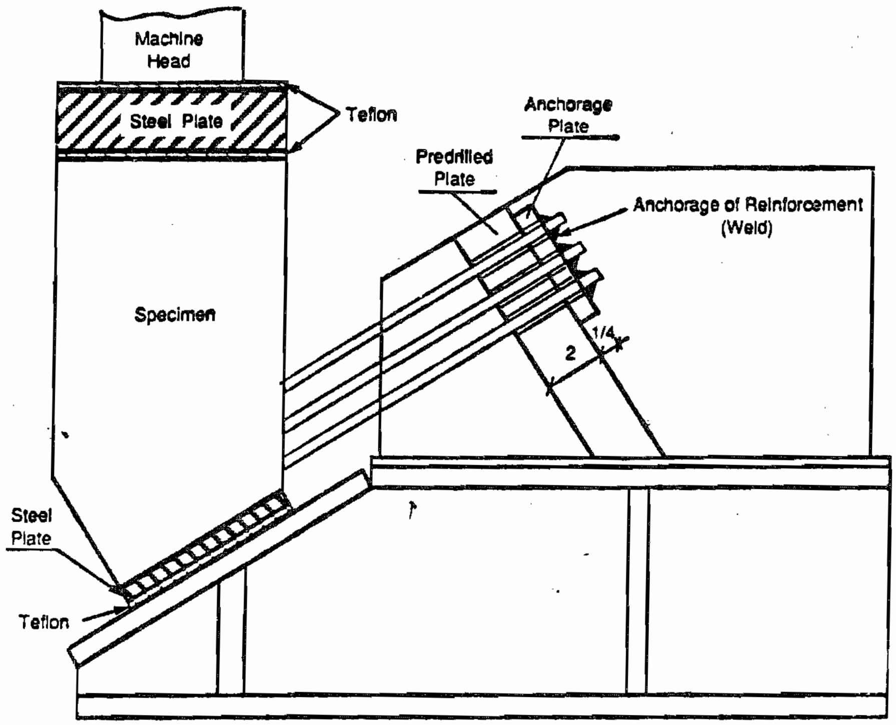

Figure 5.15 Elevation of Test Setup.

Hydrostone was used beneath the support beam to obtain uniform bearing surface between the test machine bed and the beam. The loading procedure followed for all specimens involved application of a compressive force to the top surface. Load was increased in 10 kip increments until cracking. The load increment was then reduced to 5 kips until failure.

Specimens LFO and HFO-HL did not perform well in the early stages of loading. The top layer of the reinforcing bars of LFO were in compression or had a low tensile force. When the load reached 275 kips, the specimen was unloaded. No misalignment could be found and the specimen was reloaded until failure. In HFO-HL, cracks at the top of the specimen were noted at an early stage. After unloading it was noticed that the bearing plate at the top of the specimen did not have a uniform contact surface. This was corrected by pouring a thin uniform layer of hydrostone between the plate and the specimen. The specimen was then reloaded until failure. Strain readings were recorded at every load stage. Surface strains were recorded at selected stages. Cracks were marked and maximum crack width was noted alongside the trace. Photographs of the cracks were taken at selected stages. Complete details of the tests and results are given in Ref. 25.

CHAPTER 6

TEST RESULTS - CTT NODES

6.1 Interpretation of Test Results

6.1.1 General. To aid in the interpretation of test results, crack patterns showing the development of cracks for four faces of the specimens are presented in "unfolded" views. For damage occurring at failure, photographs are used to determine crack locations. The orientation of the node specimen during testing was 90° from that of Specimen ST1. As shown in Fig. 6.1, layers of transverse reinforcement are parallel to the horizontal plane while the layers of longitudinal steel are oriented vertically. Throughout the following discussion, the layers of reinforcement located closest to the surface of the specimen are identified as the first layer of transverse or longitudinal reinforcement. Inset diagrams show the location of the strain gages and in some plots, the crack pattern on one face of the specimen is shown.

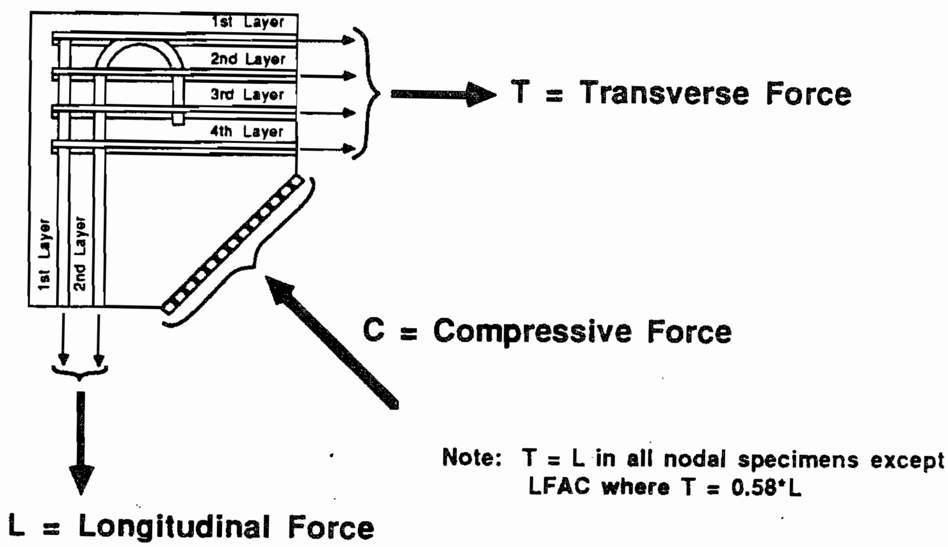

Figure 6.1 Node Specimen Force Designation.

Average external bar strains based upon the applied tensile load were plotted in lieu of the measured strain readings from the exterior gages because the latter were somewhat inconsistent. The measured external bar strains were susceptible to bending effects and were influenced by specimen cracking. This is especially true of the external longitudinal gages. In Figure 6.2, strains for the external transverse bars in HFSB are fairly well grouped. In contrast, Fig. 6.3 shows that considerably different strain rates were indicated by external longitudinal gages. The second layer of bars, closest to the interior of the specimen, displayed higher strain rates than the first layer of bars. The average of the

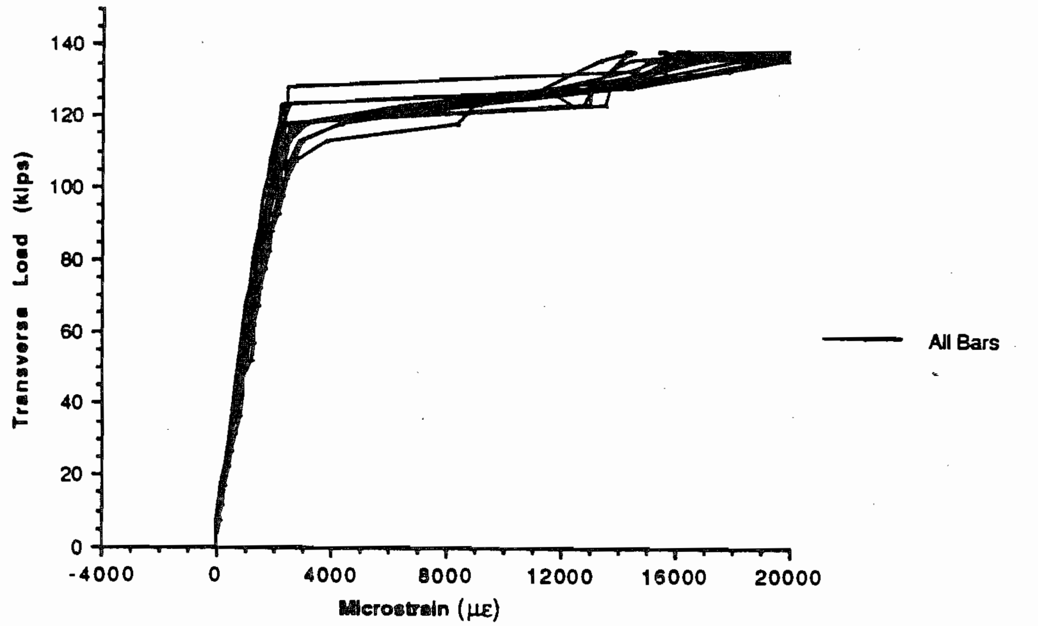

Figure 6.2 External Transverse Bar Strains for Specimen HFSB.

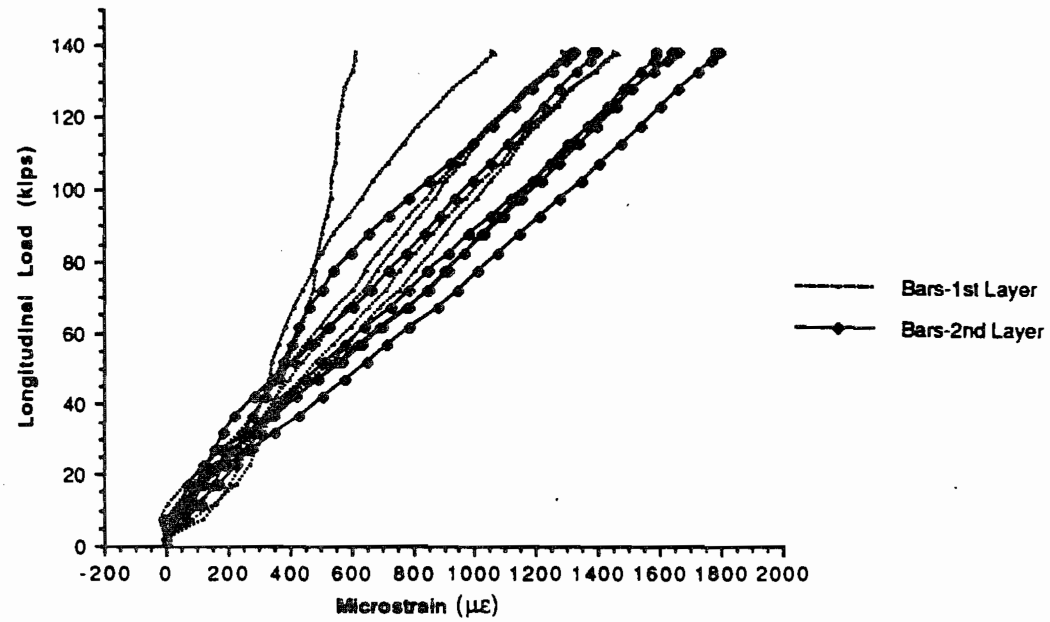

Figure 6.3 External Longitudinal Bar Strains for Specimen HFSB.

external strains for the first and second layers of longitudinal reinforcement are shown in Fig. 6.4. The average external strain produced by the applied longitudinal force is also shown in the figure. A divergence between the strain rates for the two layers of longitudinal reinforcement occurred after first cracking. The external reinforcement strain behavior exhibited by HFSB was generally typical of all the node specimens and appeared to be influenced by the location of major cracks.

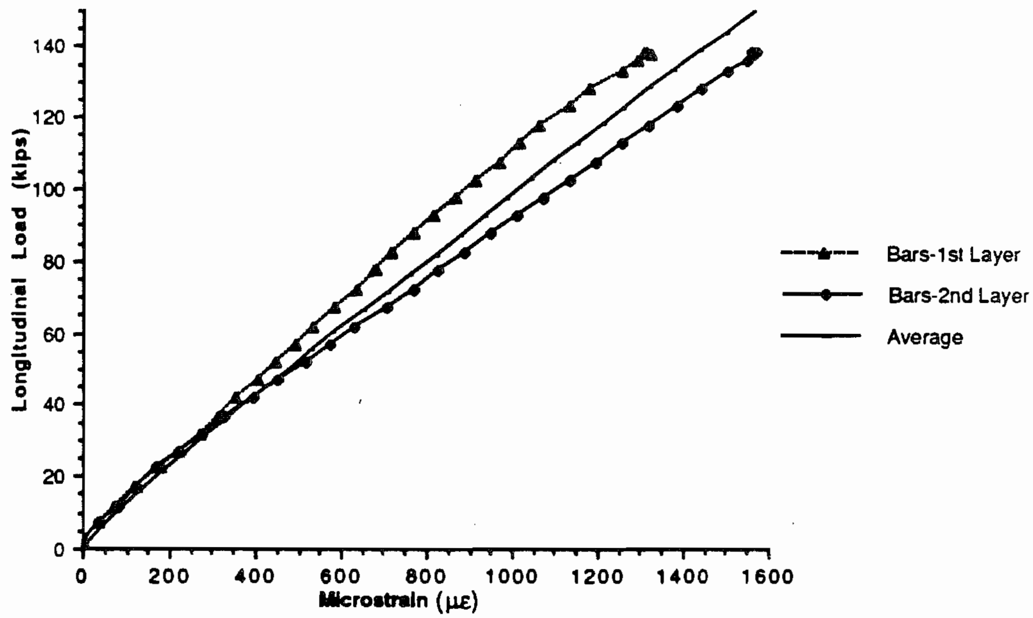

Figure 6.4 Average External Longitudinal Bar Strains for Specimen HFSB.

The percentage of applied transverse or longitudinal force carried by the bars at a particular location along the bars gives further insight regarding tie behavior. For example, with 16 transverse bars in four layers, the bars in a layer should carry 4/16's or 25% of the external applied force if no stress were transferred to the concrete along the bar. The bar forces were most helpful in assessing the role of different internal force transfer mechanisms. At early load stages, concrete tensile strength and bond forces carried most of the internal forces. With higher loads, bar stresses between nodes were nearly uniform indicating that "strut-and-tie" action had developed.

6.1.2 Comprehensive Description of Test Results for Specimen HFNC. Specimen HFNC was cast using high strength concrete, $f_c' = 5780$ psi. The transverse reinforcement provided minimal lateral confinement to the node. A 180° hook was used to anchor the second layer of longitudinal reinforcement. The specimen had a strut width of 10.6 in. and a strut angle of 45°. Equal forces were applied in the transverse and longitudinal directions during the test. The specimen was loaded in 5k increments. At 71.3 k, well-defined cracks crossed the transverse and longitudinal bars. The specimen failed with spalling of the south cover over the transverse reinforcement hooks. The peak load of 132.5k corresponds to $1.13T_y$ and $0.60L_y$, where T_y and L_y represent force at yield in the transverse and longitudinal reinforcement. The force in the compression strut was 132.5k $(\sqrt{2})$ = 187.4k since the force in both ties was equal (132.5k). The bearing area was 10.6 x 12 in. = 127.2 in^2 so that the concrete stress at the bearing surface was 1470 psi or $0.25f_c'$ when cover splitting occurred. Figure 6.5 and 6.6 show crack patterns and photographs of the specimen.

Some differences in strain for gages at similar locations in different bars are indicated in Fig. 6.7. The most significant variation was between gages TU1 and TH1. The strain at

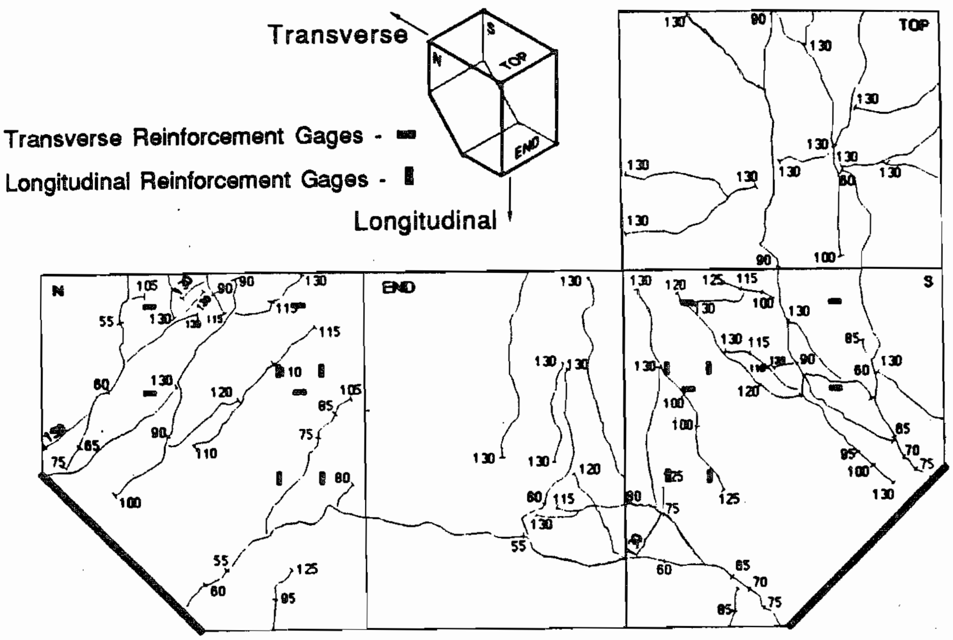

Figure 6.5 Crack Patterns for Specimen HFNC.

TU1 was much higher than at TH1 after the load exceeded 95k. This behavior was exhibited in most tests and occurred when a second crack crossed the transverse reinforcing bars. Because bearing stresses developed at the bend and the bend opened slightly as illustrated in Fig. 6.8, strain at the gage located near the inside of the bend was increased because of the bending strains.

The change in the strain in the transverse bars is shown in Fig. 6.9. At 52k, the cracking resulted in large increases in strain at locations TC and TD. At locations TA and TB, a second crack formed and led to large changes in the strains at 92k. Locations TA, TC, and TD reached yield before the specimen failed. The strain at TC is significantly higher than at TD after cracking, and similarly, strain at TA is higher than at TB. Transverse reinforcement closest to the surface of the specimen is strained more than that at the interior. Cracks developed at the edge of the specimen and crossed the outer layers of steel first.

Longitudinal bar strains are plotted in Fig. 6.10. Cracking at 56k resulted in a similar rapid increase of strains in all bars at LC. Additional cracking at higher loads caused a more gradual increase in strains at LA and LB. Diagonal tension cracks intersected the second layer (LA) of longitudinal bars at a greater distance from the free end than in the first layer of bars. The second layer (LA) was able to carry larger tensile force and could be the result of the greater efficiency of hooked anchorage. However, similar behavior was exhibited by Specimen HFSB where both layers of longitudinal reinforcement anchored with

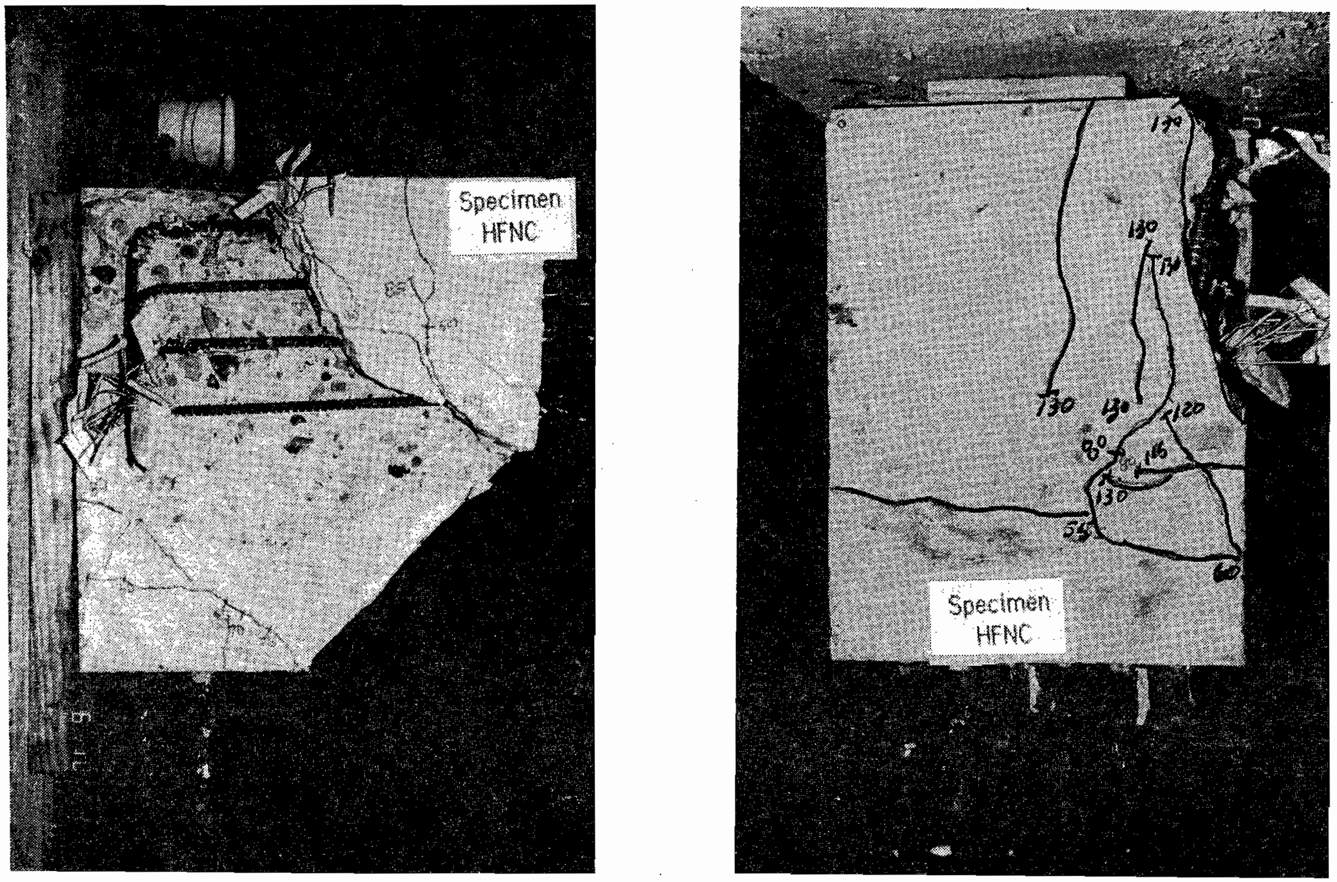

Figure 6.6 Specimen HFNC at Failure (South and End Faces)

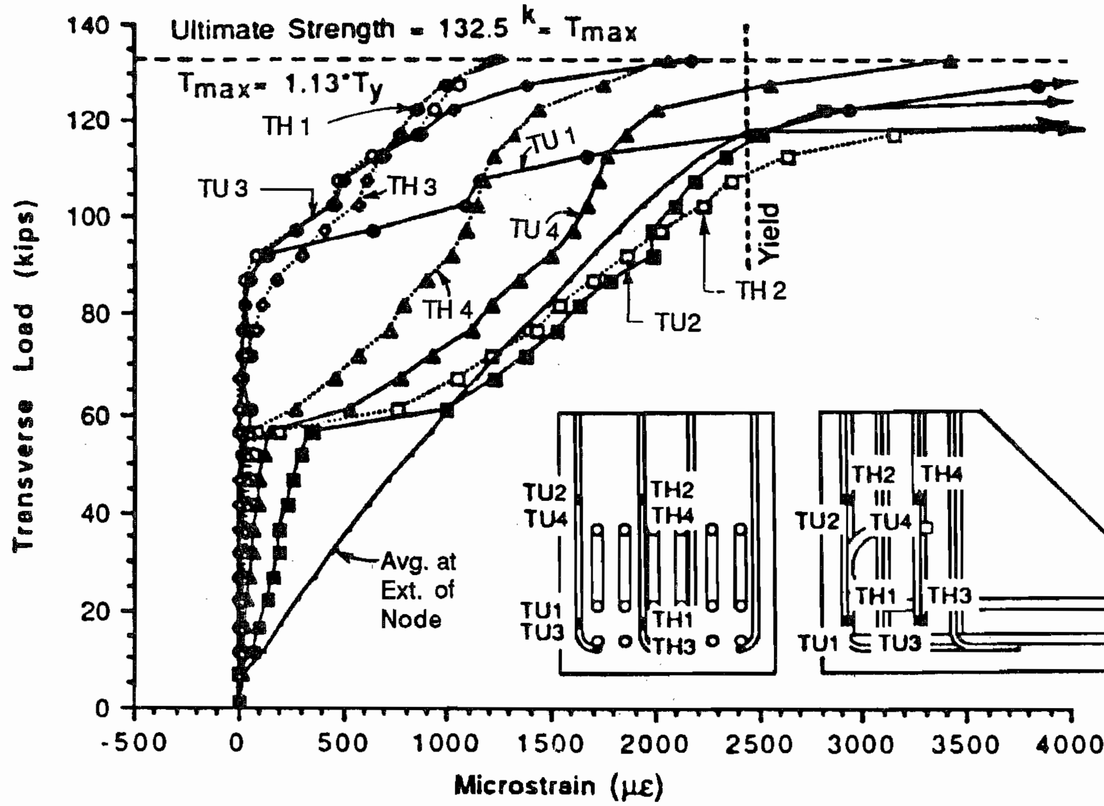

Figure 6.7 Strains in Transverse Reinforcement Bars, HFNC.

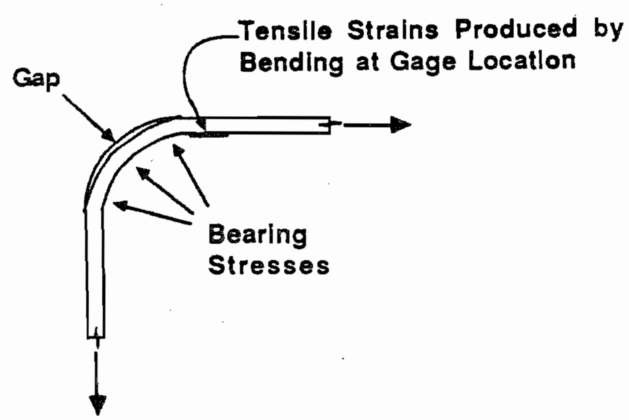

Figure 6.8 Tensile Strains Resulting from Slip at 90° Bend.

straight bars. If the strut-and-tie mechanism was fully developed, 100% of the load applied to the reinforcement in the node would be accounted for by the strain readings (measured stresses). In the transverse reinforcement, each layer should carry 1/4 of the applied load and in the longitudinal reinforcement 50%. Strut-and-tie action was well developed only when the tie reinforcement reached yield. At 50k, the concrete tensile strength was effective in carrying tension and the layers of reinforcement carried only a portion of the applied

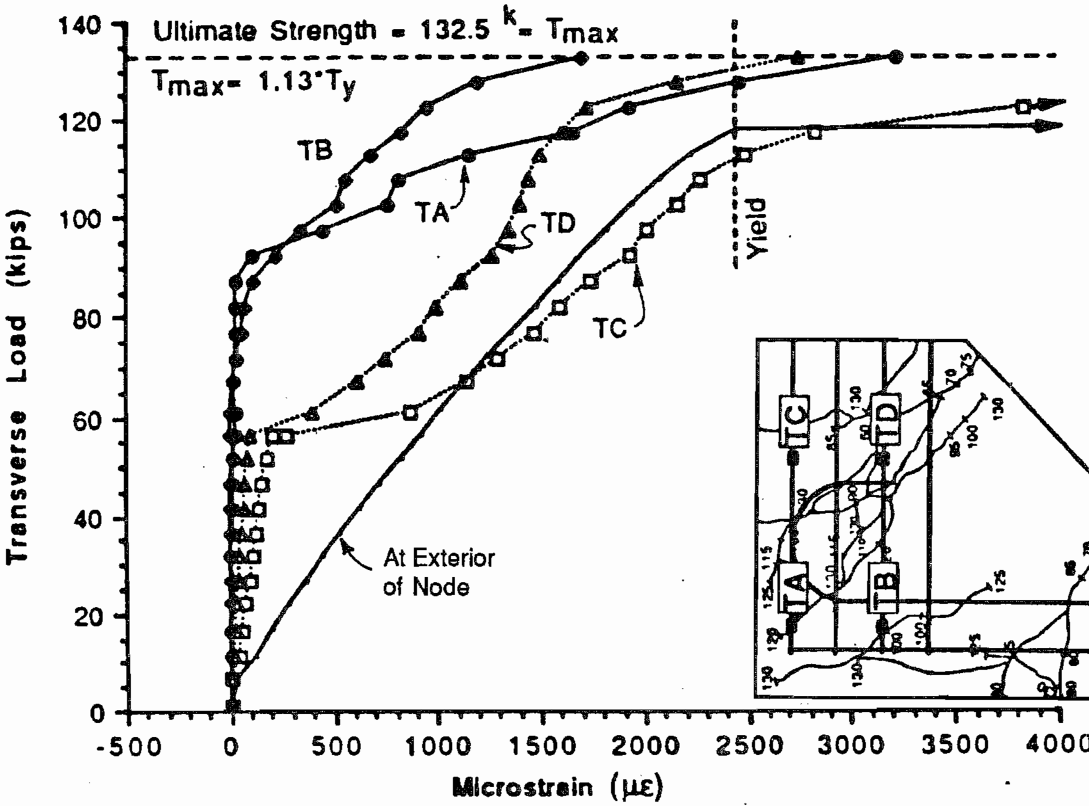

Figure 6.9 Strain in Transverse Reinforcement, HFNC.

load. An increase in the bar force at TC, TD, and LC at 75k applied load produced first cracking. For the transverse reinforcement shown in Fig. 6.11, roughly 22% of the load at 125k was carried by reinforcement layer at locations TA, TC, and TD. It was apparent that bond deterioration along the length of the bar resulted in high strain (and stresses) at those locations.

For the longitudinal reinforcement (Fig. 6.12), about 25% of the load at 125k is carried by the layer of steel with a 180° hook. Gages at LC indicate that 82% of the 125k applied load was carried at that point. The longitudinal reinforcement did not yield.

6.2 Summary of Behavior -- All Specimens

6.2.1 General. A summary of the test results at failure for all nine specimens is presented in Table 6.1. It is noted that three of the specimens were not loaded to failure because the rated capacity of the mechanical couplers used to anchor the reinforcement to the test setup was reached. Crack widths at various load stages are summarized in Table 6.2.

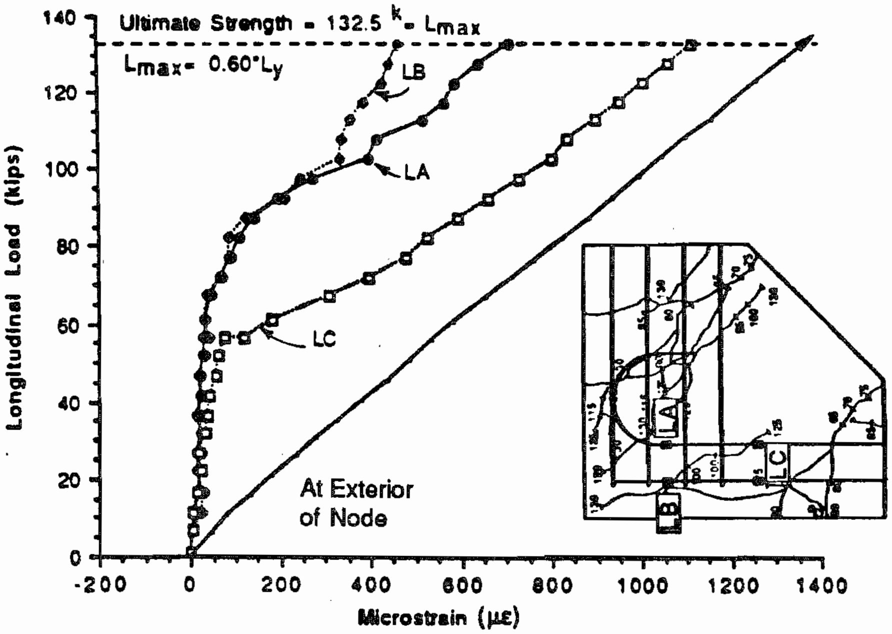

Figure 6.10 Strain in Longitudinal Reinforcement, HFNC.

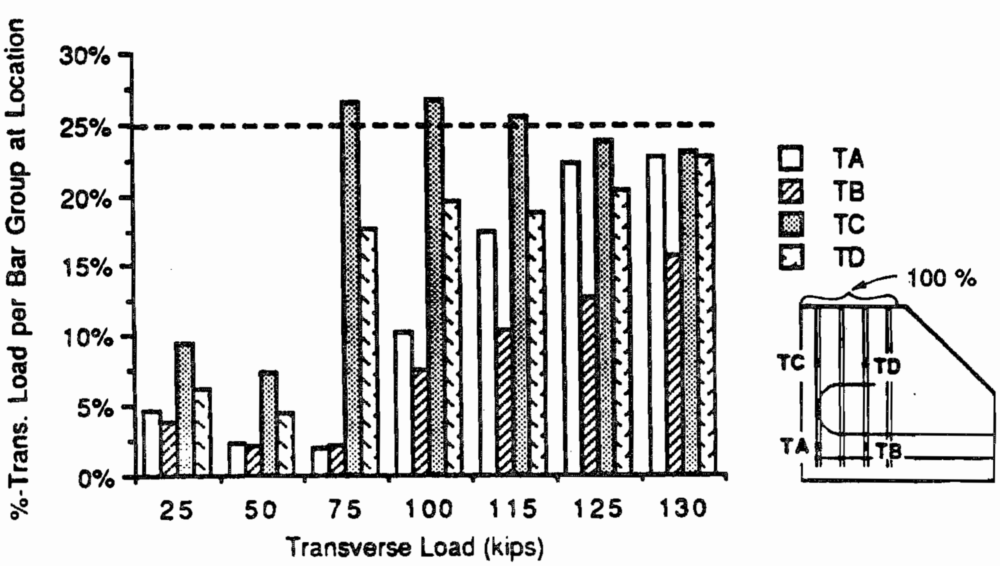

Figure 6.11 Force in Transverse Reinforcement, HFNC.

Figures and descriptions of individual tests are presented in this section as needed to make distinctions between the specimens and their behavior. Supplemental figures illustrating typical behavior patterns are presented in Ref. 21. In this section, the observed cracking and/or failure behavior of the specimens is emphasized. The specimens are grouped according to geometry and placement of steel in the following presentation of results. The results for Specimen HFNC which were described in detail in Sec. 6.1.2 will not be repeated in this section.

Table 6.1
Summary of Node Specimen Test Results

Specimen	L_{max} (kips)	Type of Failure	Bearing Stress at Peak Load (ksi)	Bearing Stress / f_c'	T_{max}/T_y	L_{max}/L_y
HFSR-A	127.4	None - Cap. of Setup	1.42	0.20	1.08	*
HFSR-B	137.5	None - Cap. of Setup	1.53	0.26	1.17	0.62
LFSR	117.4	Development - Trans.	1.31	0.35	1.00	0.53
HFNC	132.5	Cover Splitting	1.47	0.25	1.13	0.60
LFNC	117.8	Cover Splitting	1.31	0.35	1.00	0.53
HHSR	139.0	None - Cap. of Setup	4.10	0.71	1.18	0.62
LHSR	130.2	Strut Crushing	3.84	1.03	1.11	0.59
HFSB	138.1	Gross Slip - Trans.	1.54	0.27	1.17	0.62
LFAC	165.4	Development - Long.	3.19	0.81	0.82	0.74

* Reinforcement did not have definite yield point.

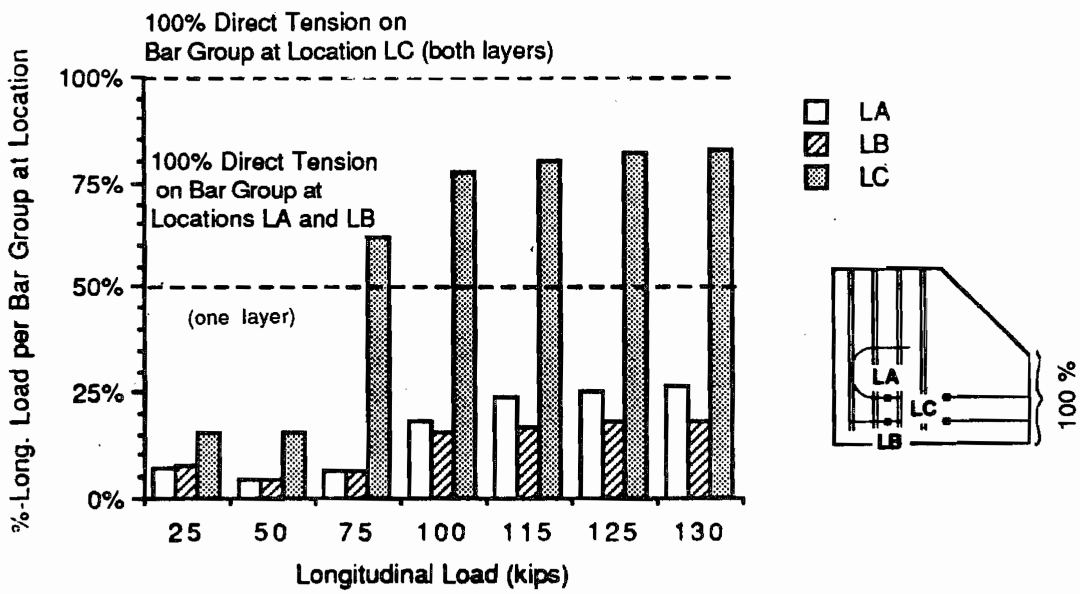

Figure 6.12 Force in Longitudinal Reinforcement, HFNC.

Table 6.2 Crack Widths

Specimen	110 kips (longitudinal)						115 kips (longitudinal)						Crack Widths at Noted Longitudinal Load						
	Transverse*		Diagonal Tension*		Longitudinal*		Transverse		Diagonal Tension		Longitudinal		Applied Load (kips)	Transverse		Diagonal Tension		Longitudinal	
	North	South	North	South	North	South	North	South	North	South	North	South		North	South	North	South	North	South
HFSR-A	0.009	NMS	DNF	DNF	0.016	NMS	0.015	NMS	DNF	DNF	0.015	NMS							
HFSR-B	0.003	0.003	0.002	0.001	0.003	0.006	0.005	0.008	0.003	0.002	0.003	0.009	135	0.040	0.050	0.005	0.005	0.007	0.013
LFSR	0.005	0.010	0.005	0.010	0.007	0.010	NMS	NMS	NMS	NMS	NMS	NMS							
HFNC	0.007	0.007	NDF	DNF	0.005	0.002	0.010	0.010	DNF	DNF	0.009	0.005	125	0.020	0.016	DNF	DNF	0.009	0.007
LFNC	0.009	0.007	0.005	0.010	0.009	0.013	NMS	NMS	NMS	NMS	NMS	NMS							
HHSR	0.005	0.009	0.005	0.007	0.002	0.002	0.007	0.010	0.006	0.003	0.003	0.009	135	0.040	0.040	0.010	0.010	0.030	0.030
LHSR	0.005	0.009	0.009	0.016	0.003	0.007	0.016	0.013	0.013	0.025	0.005	0.007							
HFSB	0.005	0.009	DNF	DNF	0.009	0.006	0.007	0.016	0.002	DNF	0.010	0.009	125	0.013	0.040	0.003	DNF	0.013	0.013
LFAC	0.003	0.003	DNF	DNF	0.010	0.013	0.010	0.009	DNF	DNF	0.020	0.016	150	0.010	0.013	DNF	DNF	0.025	0.025

NOTES:

All measurements are in inches
DNF - Crack did not form
NMS - Crack not measured

* indicates location of crack measurement; across transverse or longitudinal reinforcement, or along diagonal compression strut.

6.2.2 Specimen HFSR-A. The reinforcement in HFSR-A was identical to the CTT-node of the Specimen (ST1). The transverse steel provided lateral confinement and a 180° hook anchored the second layer of longitudinal reinforcement. Concrete strength was 7010 psi. The compression strut was 10.6 in. wide at an angle of 45° from the longitudinal tie. The geometry and placement of steel for Specimen HFSR-A were shown in Fig. 5.3. Specimen HFSR-A was subjected to a maximum tie force of 127.4k (1.08 T_y). The test was terminated to prevent overload of the mechanical connectors. Crack patterns are shown in Fig. 6.13. Strains in the transverse reinforcement are shown in Fig. 6.14.

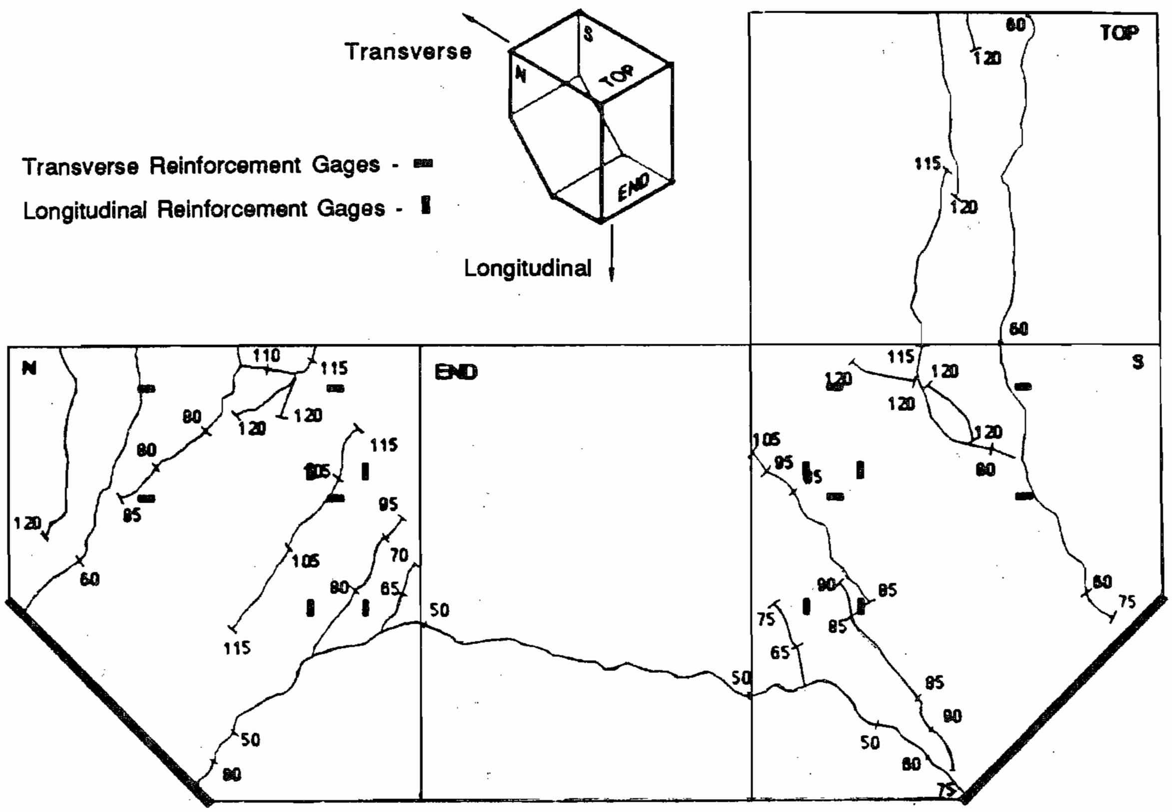

Figure 6.13 Crack Patterns, HFSR-A.

6.2.3 Specimen HFSR-B. Specimen HFSR-B (f_c' = 5780 psi) was a replicate of Specimen HFSR-A. Lateral confinement was provided by the transverse reinforcement. The second layer of longitudinal reinforcement was anchored with a 180° hook. The specimen had a strut width of 10.6 in. and strut angle of 45° from the longitudinal tie.

Specimen HFSR-B did not fail prior to conclusion of testing. The maximum force resisted by the specimen was 137.5k or 1.17 T_y and 0.62 L_y. Figure 6.15 shows that crack patterns for HFSR-B were quite similar to those of Specimen HFSR-A. The measured crack widths for HFSR-B were much smaller than for HFSR-A (Table 6.2). More cracks appeared in HFSR-B which resulted in smaller crack widths.

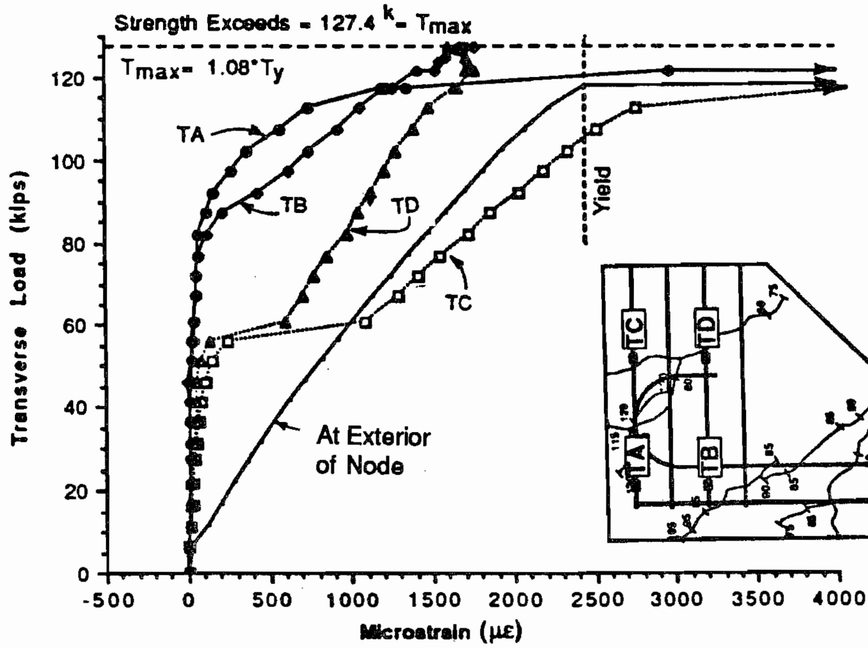

Figure 6.14 Strain in Transverse Reinforcement Layers, FHSR-A.

6.2.4 Specimen LFSR. Specimen LFSR was fabricated with low strength concrete (f_c' = 3720 psi). Reinforcement details were the same as in Specimen ST1. The strut was 10.6 in. wide and was 45° from the longitudinal tie.

The outer layer of transverse reinforcement failed in anchorage at 117.4k (1.00 T_y and 0.53 L_y). The outer transverse U-shaped stirrups split the end cover as shown in Fig. 6.16. Although the load was increased to 125k after cover splitting occurred, severe cracking and substantial redistribution of the transverse bar forces took place. Spalling was the result of radial pressure produced by bearing of the bend of the U against the concrete which split the cover. Bond cracks parallel to the transverse bars can be seen in Fig. 6.17. A failure plane developed when bond and diagonal tension cracks joined. There was a decrease in strain at gages TU2 and TH2 after the stirrup failed (Fig. 6.18).

6.2.5 Specimen LFNC. For LFNC the transverse reinforcement was detailed to provide minimal lateral confinement. The compression strut was 10.6 in. wide at an angle of 45° from the longitudinal tie (f_c' = 3720 psi). A cover splitting failure of the transverse bars occurred at 117.8k when the transverse bars split the side cover on the north and south faces (1.00 T_y and 0.53 L_y). Crack patterns are shown in Figs. 6.19 and 6.20. Bond cracks, parallel to the reinforcement, appeared when the development failure took place.

6.2.6 Specimen HHSR. The compression strut width for HHSR was 4.0 in. (f_c' = 5780 psi). Otherwise it was identical to HFSR-B. Lateral confinement was provided by the transverse reinforcement and the second layer of longitudinal reinforcement was anchored with a 180° hook. Loading of HHSR was terminated at 139.0k (1.18T_y and 0.62L_y). The

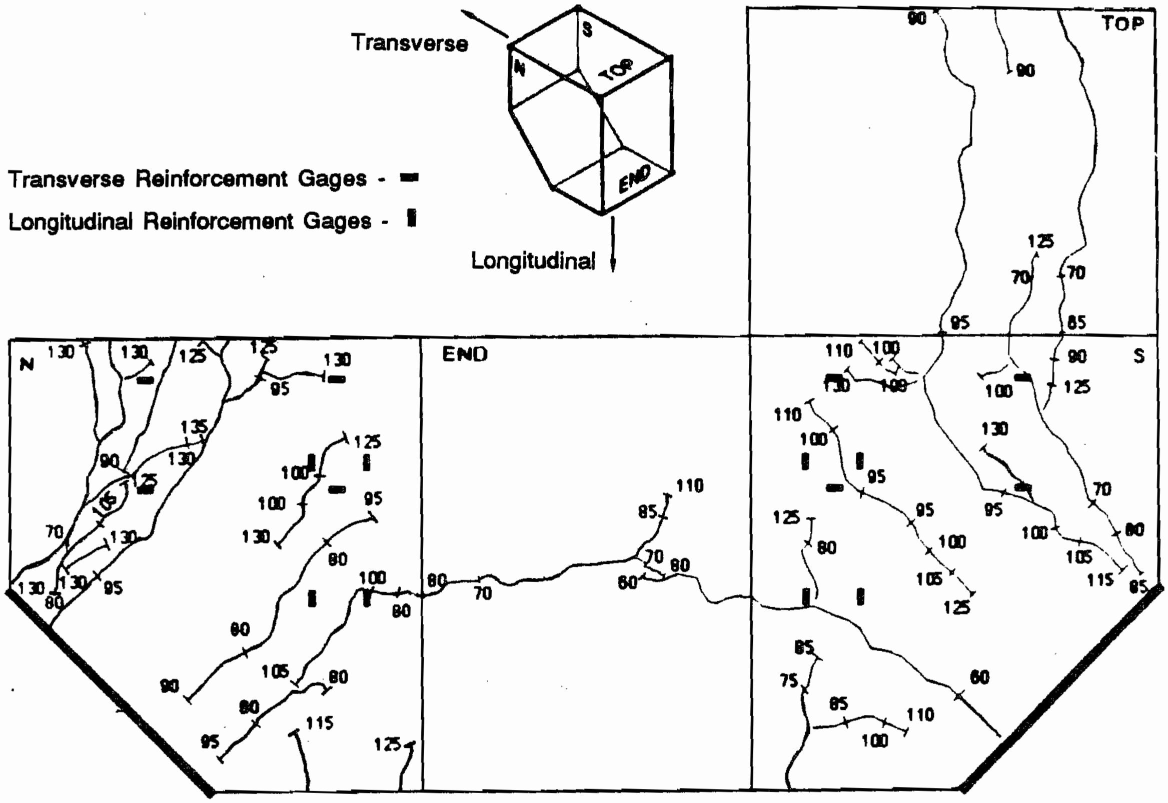

Figure 6.15 Crack Patterns, HFSR-B.

nominal concrete stress at the bearing surface was 4010 psi or 0.71 f_c'. Cracks generally were parallel to the 45° angle of the compression strut (Fig. 6.21). Strain on transverse and longitudinal ties are plotted in Figs. 6.21 and 6.22. The strains at locations TC and LA were greater than the external strains. It is likely that local bending added to direct tensile strains.

6.2.7 Specimen LHSR. In LHSR a reduced compression strut width of 4.0 in. was used (f_c' = 3720 psi). At 130.2k (1.11 T_y and 0.59 L_y), a crushing failure of the concrete strut occurred (Fig. 6.23). The nominal concrete stress at the bearing surface was 3840 psi or 1.03 f_c'. An indentation at the bearing surface can be distinguished in Fig. 6.23.

6.2.8 Specimen HFSB. In HFSB, both layers of longitudinal steel consisted of straight bars. Concrete strength was 5780 psi. At 138.1k (1.17 T_y and 0.62L_y) the specimen was no longer able to carry additional load. Cracks crossing the transverse reinforcement became quite wide. Additionally, cracks opened parallel to the transverse bars. In Fig. 6.24, strains in the longitudinal steel are shown. Diagonal cracks intersected the layers of bars at different locations along the anchored length and changed the effective development length of the reinforcement (Fig. 6.25). In other tests, the hook served to hold together the corner of the node and crossed more transverse cracks than the straight bar. For the straight bar, the cracks opened wider and resulted in a deterioration of node strength.

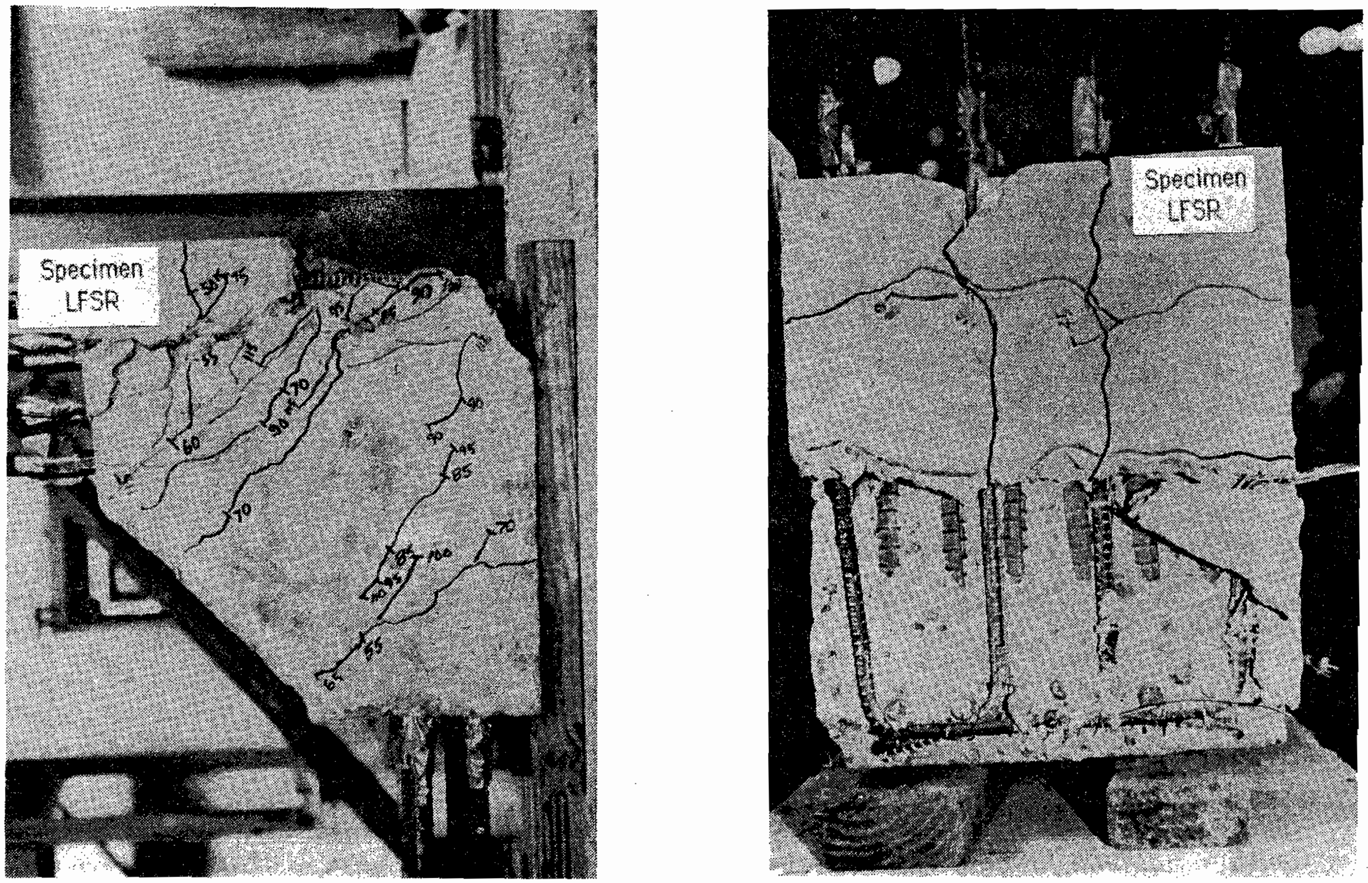

Figure 6.16 **LFSR-Development Failure of Transverse Reinforcement (North and Top Faces).**

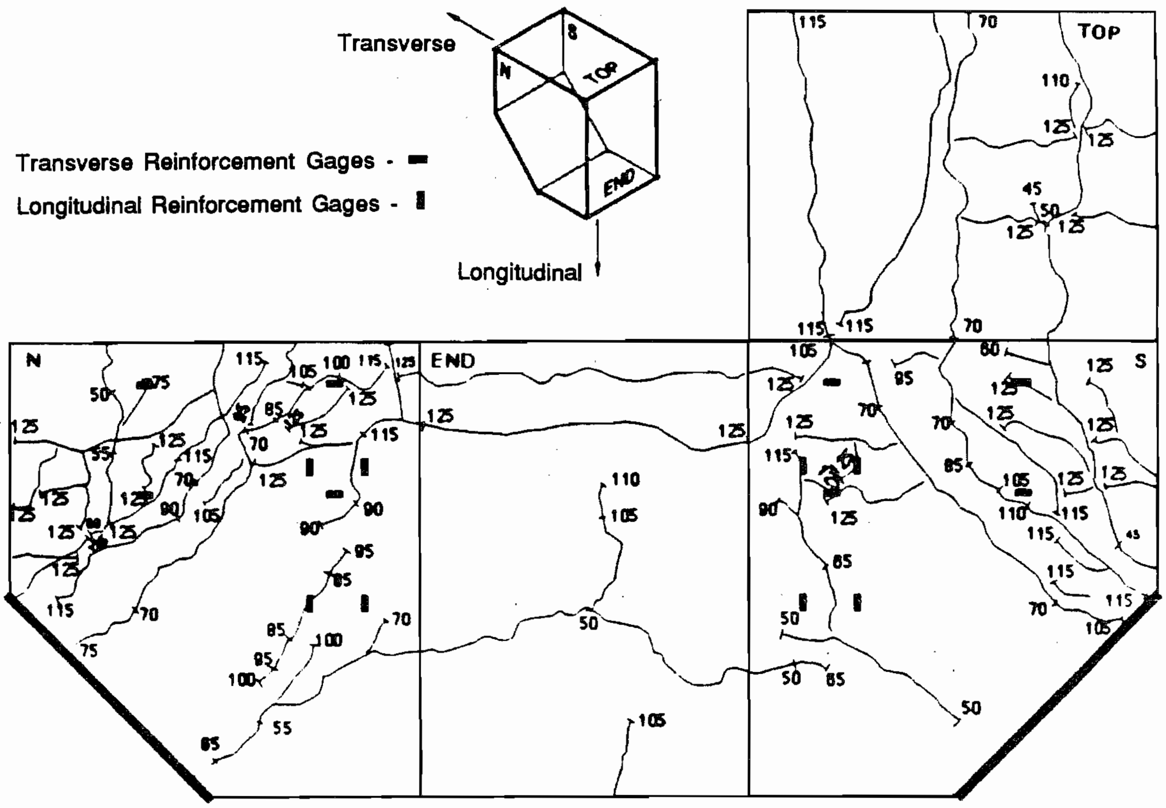

Figure 6.17 Crack Patterns, LFSR.

6.2.9 Specimen LFAC. In LFAC (f_c' = 3920 psi), lateral confinement was provided by the transverse reinforcement and a 180° hook was used to anchor the second layer of longitudinal steel. A strut angle of 30° from the longitudinal tie was induced by applying a longitudinal force (L) equal to 1.73 times the transverse force (T).

In general, cracks followed the 30° resultant of the tie forces (Fig. 6.26). At 160k, spalling occurred on the north face due to bar slip along a failure plane that originated at the lower corner of the bearing surface and extended at a ±30° angle through the centroid of the node. Neither the longitudinal or transverse ties were able to reach yield when the specimen failed at 165.4k (0.82T_y and 0.74 L_y). An anchorage failure of the longitudinal reinforcement was evidenced by slip along the failure plane and bulging of the north and south faces as the hooks caused splitting of the side faces. Cracking patterns indicated that the effective bearing surface was much less than 10.6 in. Because of the unbalanced loading in the transverse and longitudinal directions, a slight rotation of the specimen occurred. This produced a gap at the top face of the specimen and concentrated forces over the lower part of the bearing area. Through inspection of the cracks, it was estimated that the effective strut width was 5 in.

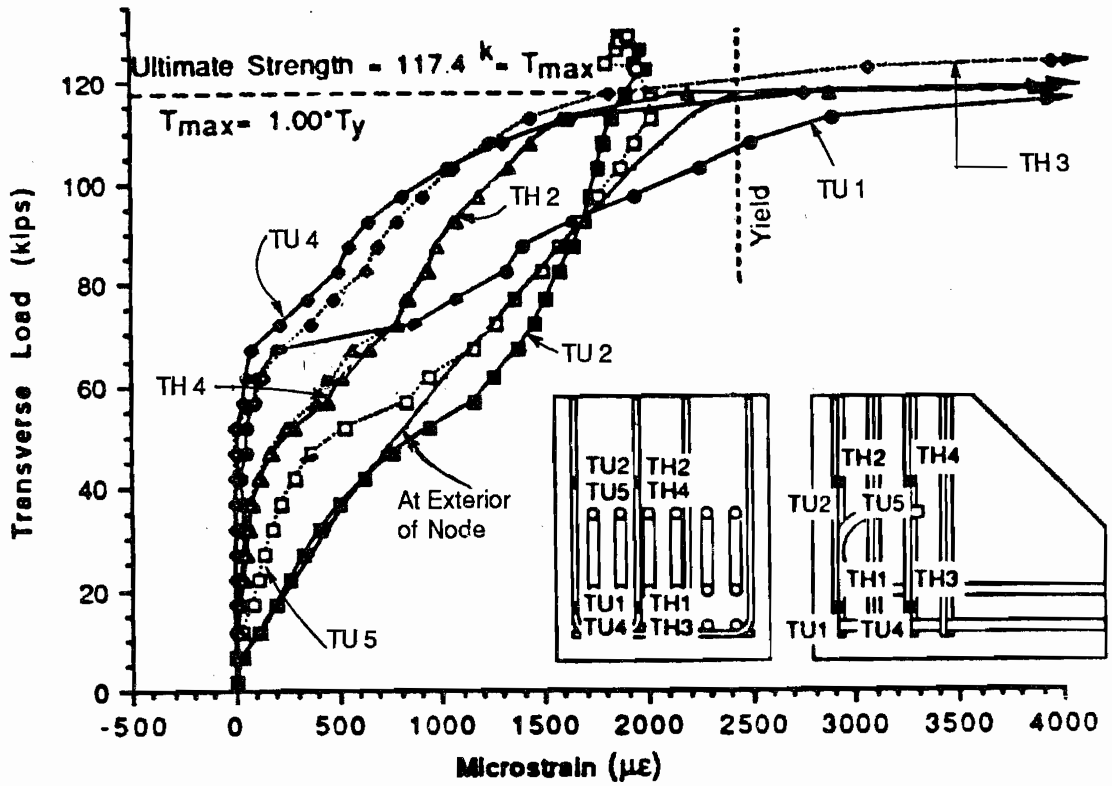

Figure 6.18 Strains in Transverse Reinforcement Bars, LFSR.

When load in the transverse tie reached 96.3k, gages at locations TA, TB and TC indicated yielding (Fig. 6.27). It is likely that the transverse gages were strained additionally because of localized bending following failure of the longitudinal hook.

Strains in the longitudinal reinforcement (Fig. 6.28) clearly indicate an anchorage failure. Gages LB3 and LB4 show a reduction in strain for loads above 140k. Force was redistributed to the second layer of hooked bars and yield was reached at LT3 and LT4. The longitudinal tie developed 0.74 L_y; hence an anchorage failure is indicated.

6.3 Comparisons of Behavioral Patterns

6.3.1 Crack Patterns. In Fig. 6.29 crack patterns for specimens of the same type have been superimposed. Three cases are considered:

1. 45° strut angle, 10.6 in. strut width - ST1, HFSR-A, HFSR-B, LFSR, HFNC, LFNC, and HFSB).

2. 45° strut angle, 4.0 in. strut width - HHSR and LHSR

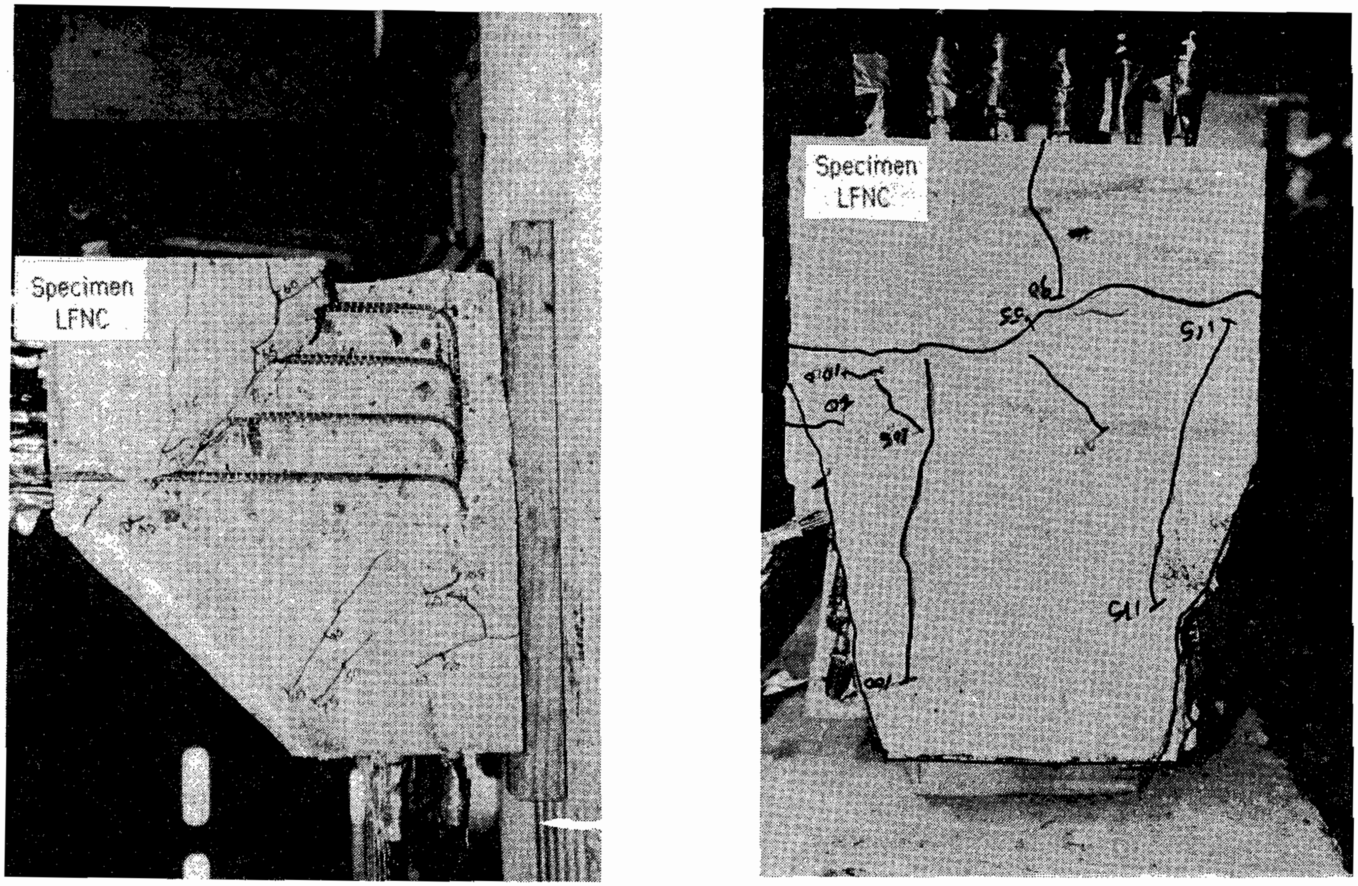

Figure 6.19 Cover Splitting Failure (North and End Faces), LFNC.

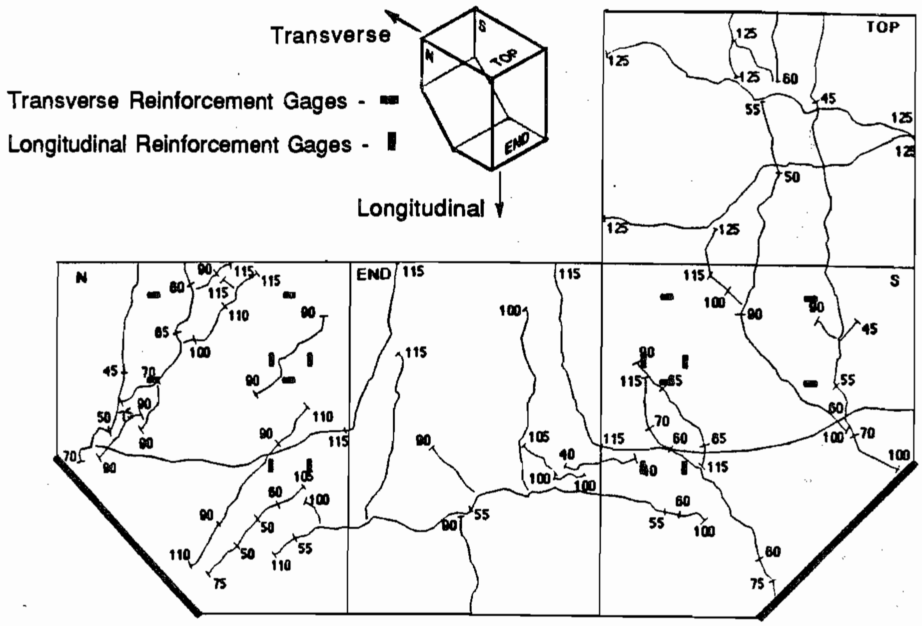

Figure 6.20 Crack Patterns. LFNC.

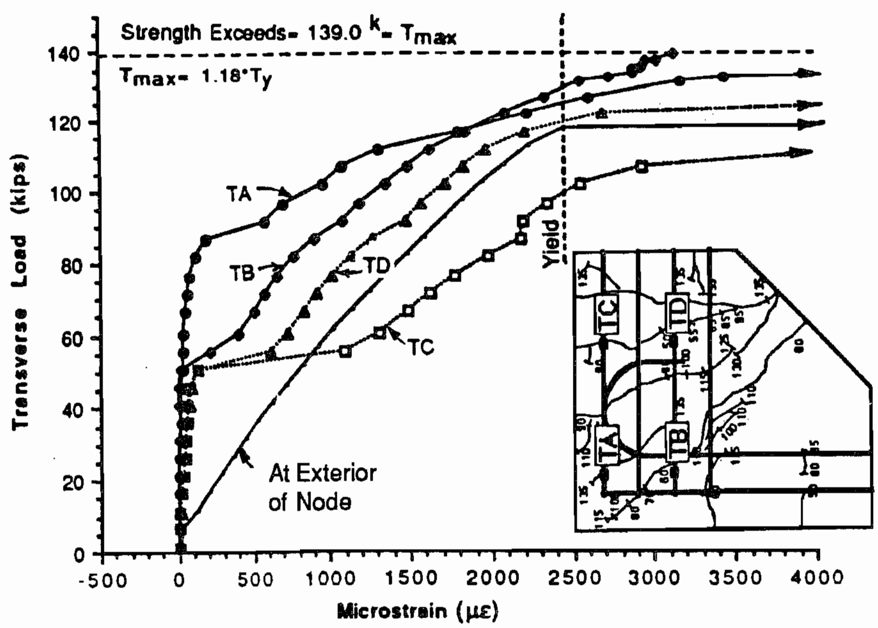

Figure 6.21 Strain in Transverse Reinforcement, HHSR.

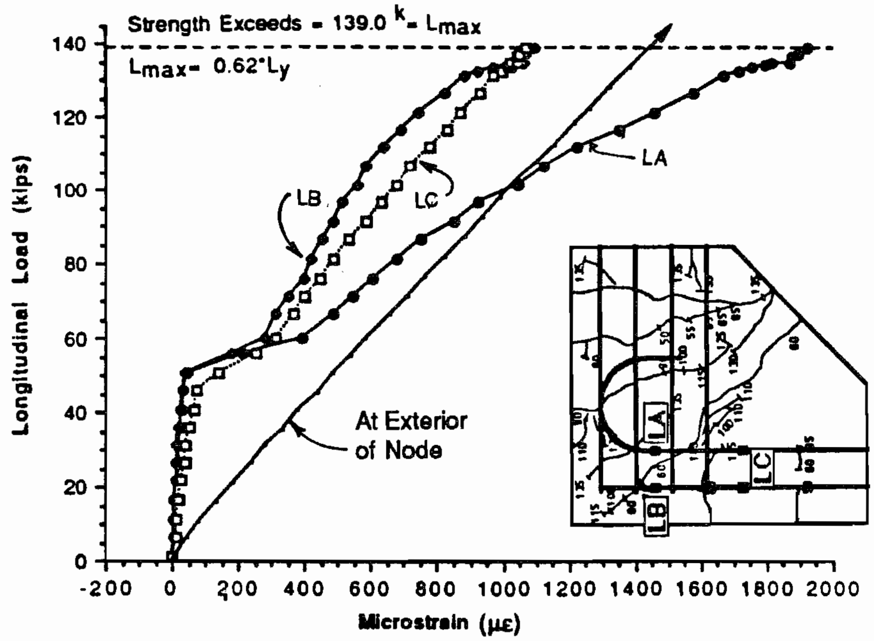

Figure 6.22 Strains in Longitudinal Reinforcement, HHSR.

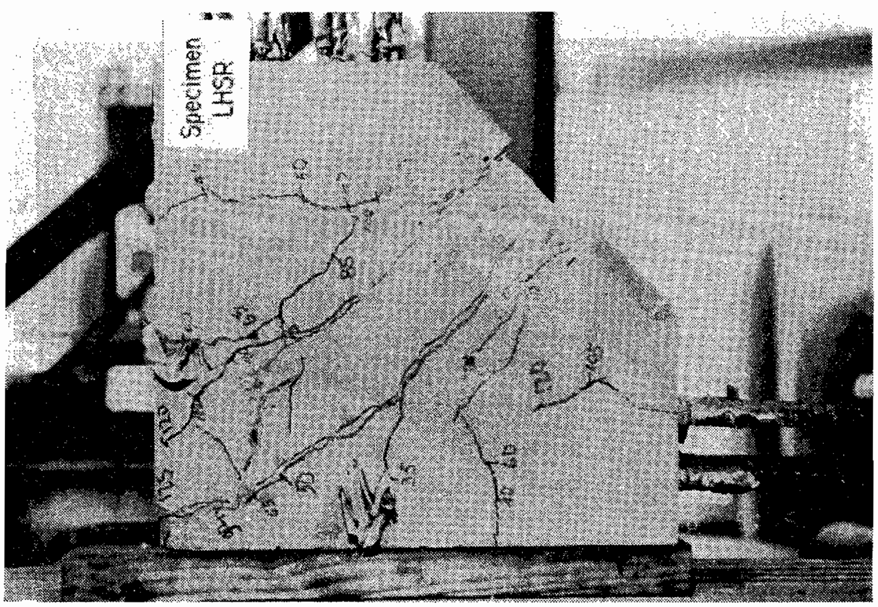

Figure 6.23 Compression Strut Crushing Failure, LHSR.

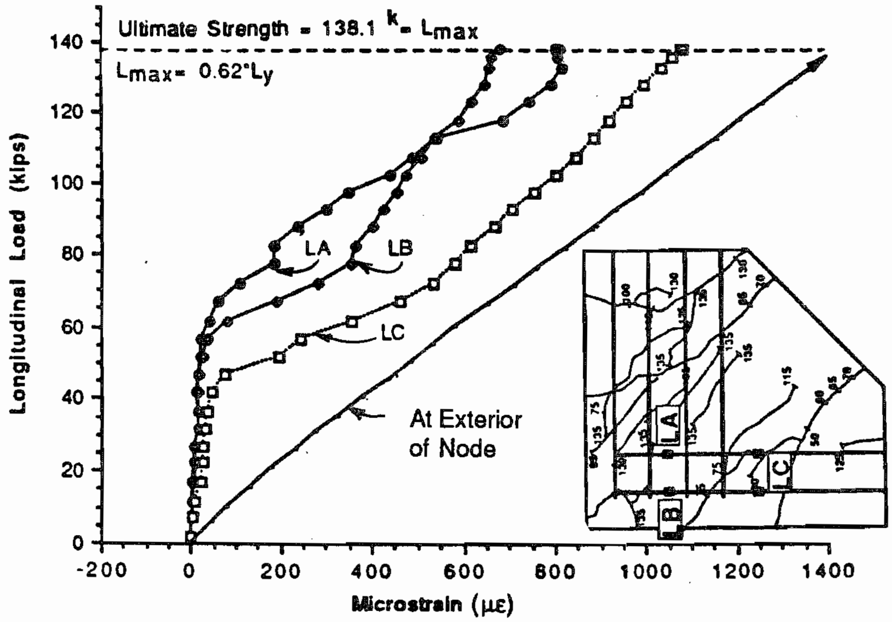

Figure 6.24 Strain in Longitudinal Reinforcement, HFSB.

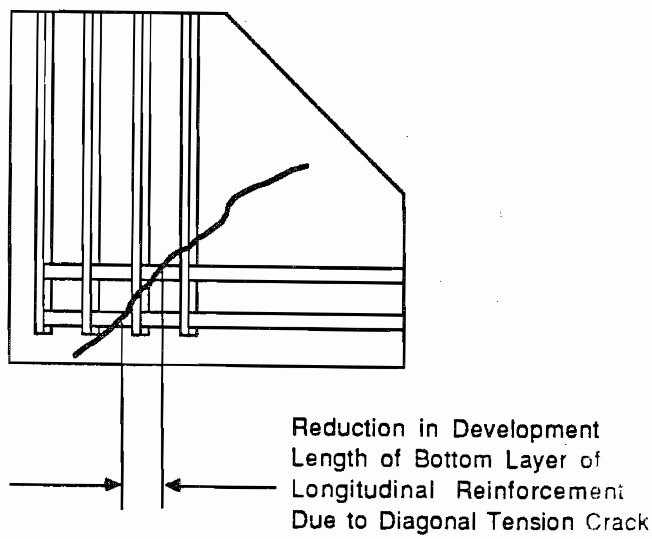

Figure 6.25 Effect of Diagonal Tension Crack Upon Reinforcement Development Length.

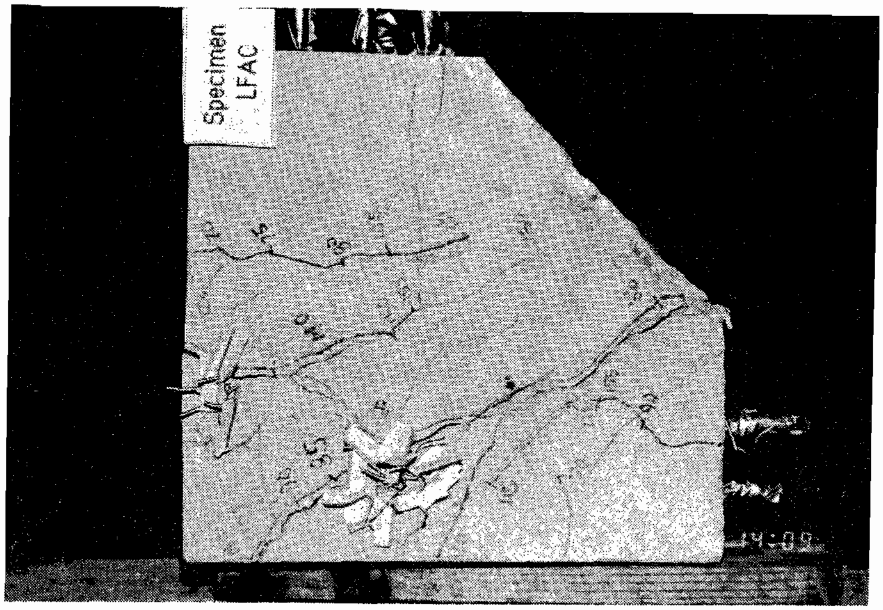

Figure 6.26 Failure of Longitudinal Reinforcement, LFAC.

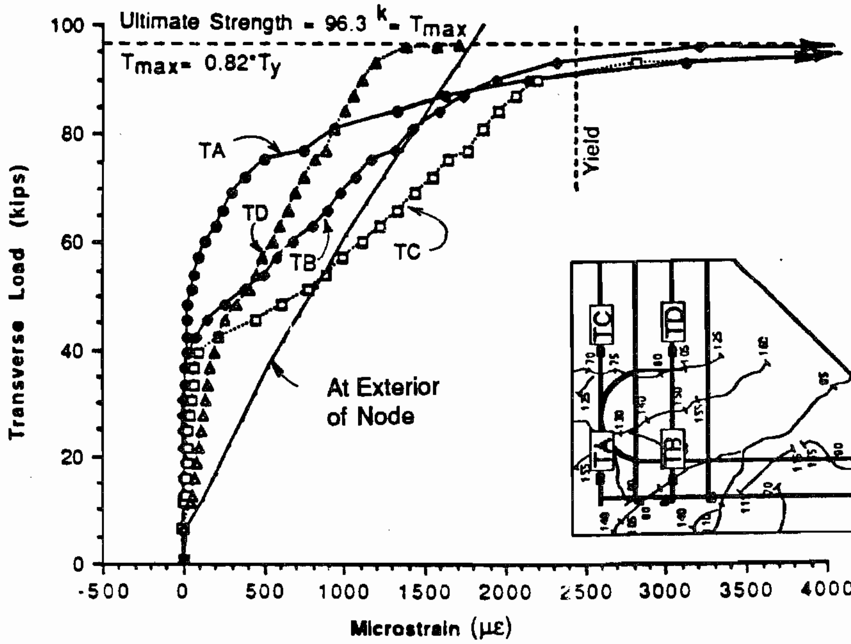

Figure 6.27 Strain in Transverse Reinforcement, LFAC.

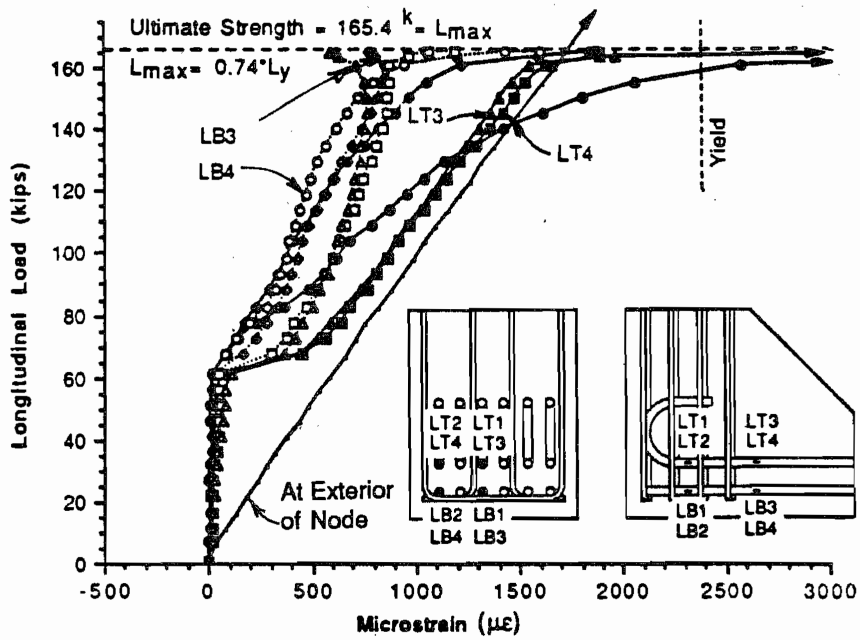

Figure 6.28 Strain in Longitudinal Reinforcement, LFAC.

3. 30° strut angle, 10.6 in. strut width - LFAC

Bold lines are drawn on the figure on the right to illustrate the general configuration of the compression fields in the different CTT-nodes. The compression fields radiate from the bearing surface at the theoretical strut angle.

6.3.2 Strains. Variations in strain measurements between specimens were generally small and could be attributed to differences in cracking loads and crack locations (Figs. 6.31 - 6.38). Significant variations in strain are identified as follows:

1. Reinforcement in Specimen LFAC reached yield well before other specimens (Figs. 6.30, 6.31, 6.32).

2. Reinforcement in Specimens HHSR and LHSR was strained more than other specimens (Figs. 6.32 - 6.34) due to the diagonal tension crack that formed when the strut width was only 4.0 in.

3. Since the node in ST1 could not be isolated, it was not possible to determine directly the applied load as was done for the isolated nodes. As a result, the strains at high loads for the dapped beam Specimen ST1 were smaller than those in the node tests (Figs. 6.30, 6.31 and 6.32).

Superimposed crack patterns Lines of compression

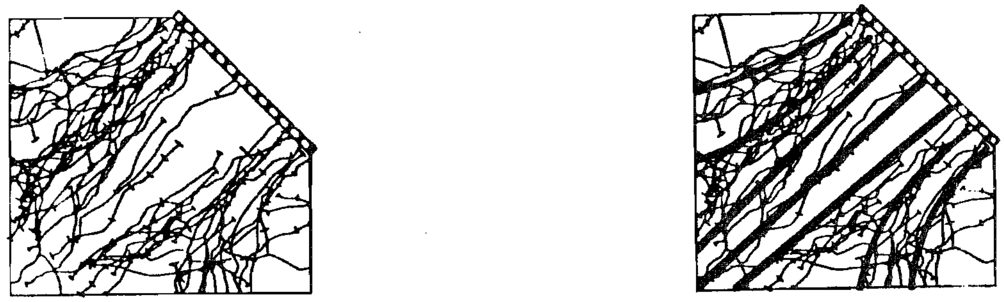

a) Recurring crack pattern and stress field for specimens with 45°-10.6 in. compression strut.

b) Recurring crack pattern and stress field for specimens with 45°-4 in. compression strut.

(c) Crack pattern and stress field for Specimen LFAC with 30°-10.6 in. compression strut.

Figure 6.29 Comparison of Crack Patterns.

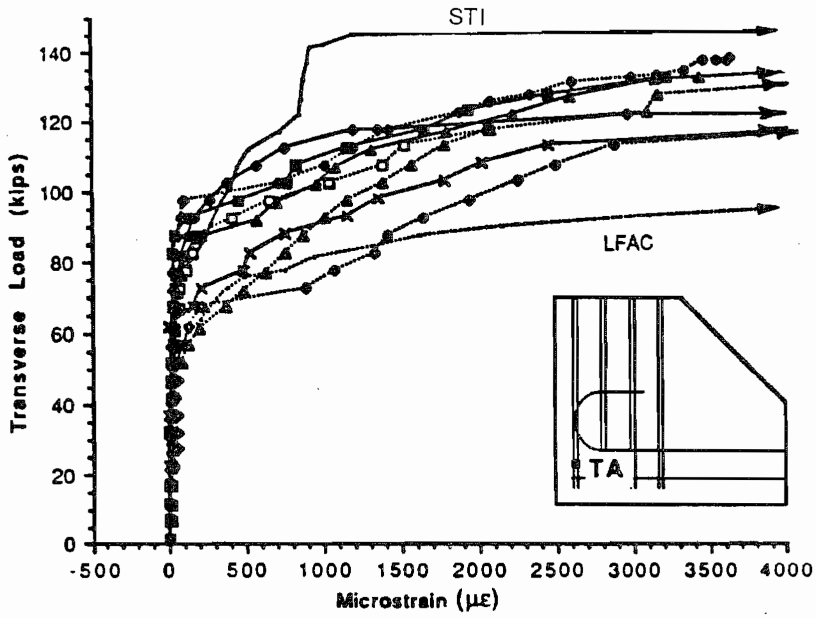

Figure 6.30 Strains at Location TA.

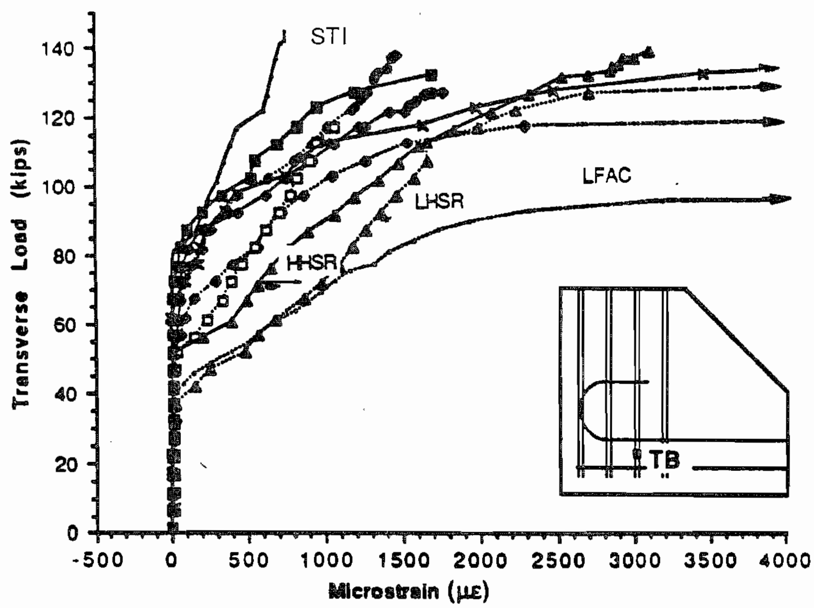

Figure 6.31 Strains at Location TB.

4. The development failure of Specimen LFSR's first group of transverse bars is evident in Fig. 6.32.

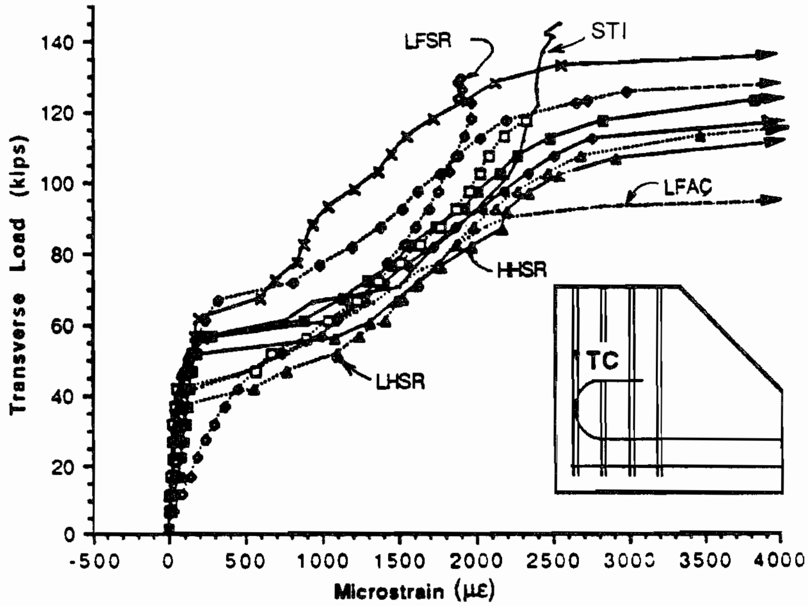

Figure 6.32 Strains at Location TC.

5. In Figs. 6.37 and 6.38, strains in the lateral reinforcement are shown. Specimens with low strength concrete exhibited much higher stress than specimens with high strength concrete where strains increased rapidly only after high load levels were imposed and concrete lateral strains were significant.

A summary of the fraction of applied forces transmitted to the ties converging at the node are given in Tables 6.3 and 6.4 for loads near failure (115k and 125k). The percentage of total applied force carried selected gage locations is given for ties in Table 6.3 and for the longitudinal layers in Table 6.4. The same data was presented in the bar graphs in Figs. 6.11 and 6.12 for Specimen HFNC. At locations TC and TD, the ratios are almost identical for all tests (0.20 to 0.25) while at TA and TB, which are further from the point where load is applied, there is a greater variation (0.13 to 0.25). For the longitudinal layers, there is considerable variation at locations LA and LB with the values in some cases exceeding 100% (influence of local bending) and others as low as 30% of the applied load. At LC, the fraction of applied load ranged from about 0.75 to 1.0.

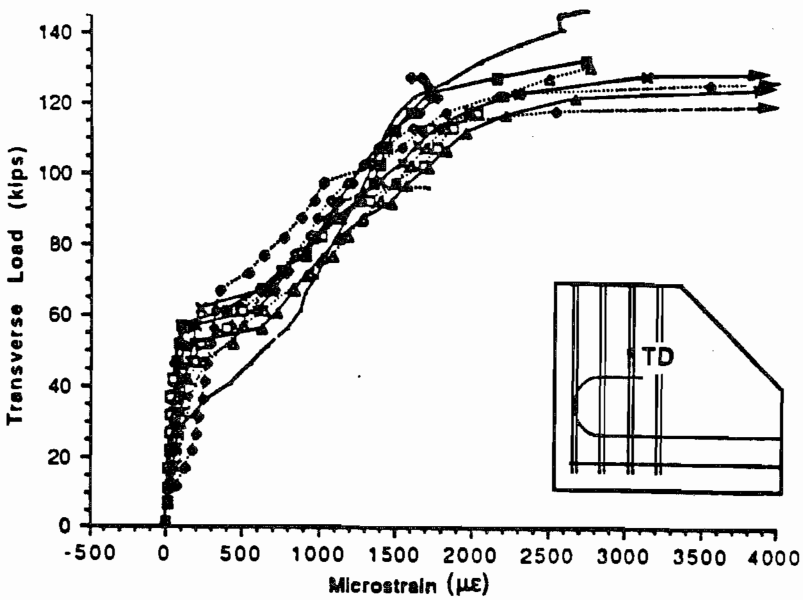

Figure 6.33 Strains at Location TD.

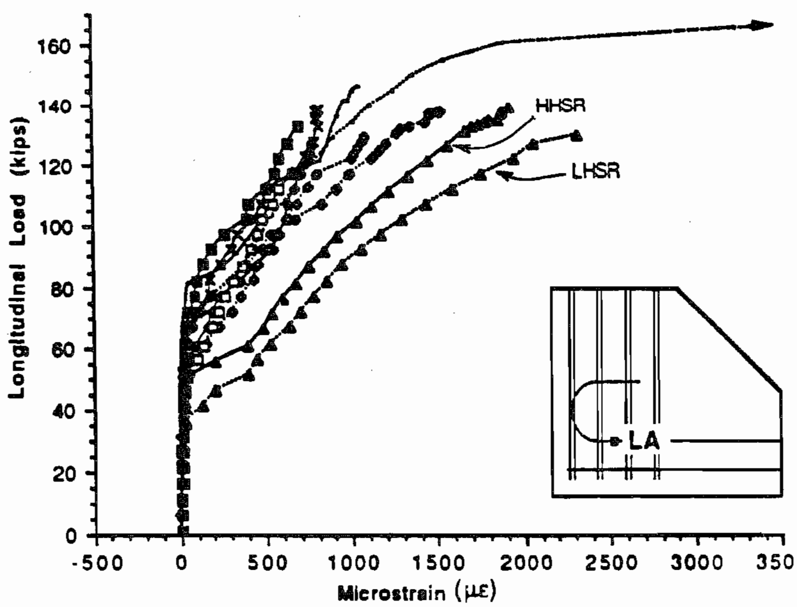

Figure 6.34 Strains at Location LA.

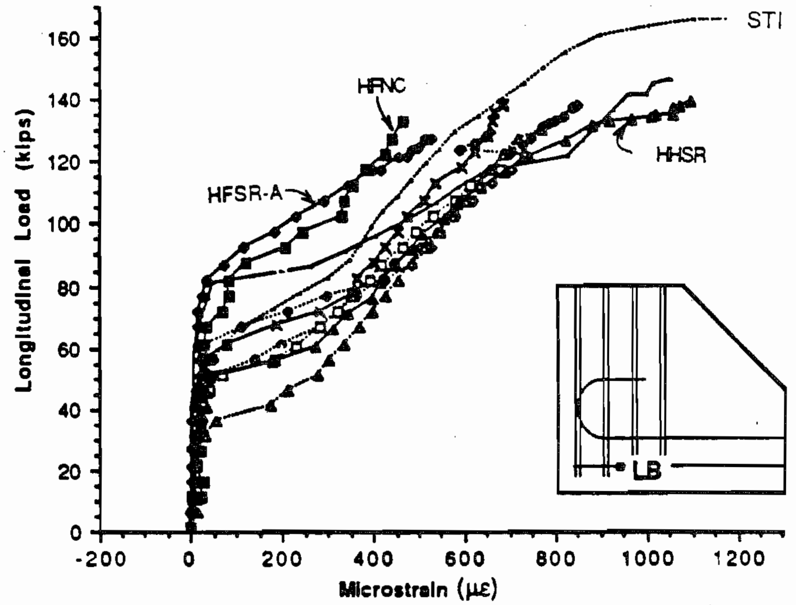

Figure 6.35 Strains at Location LB.

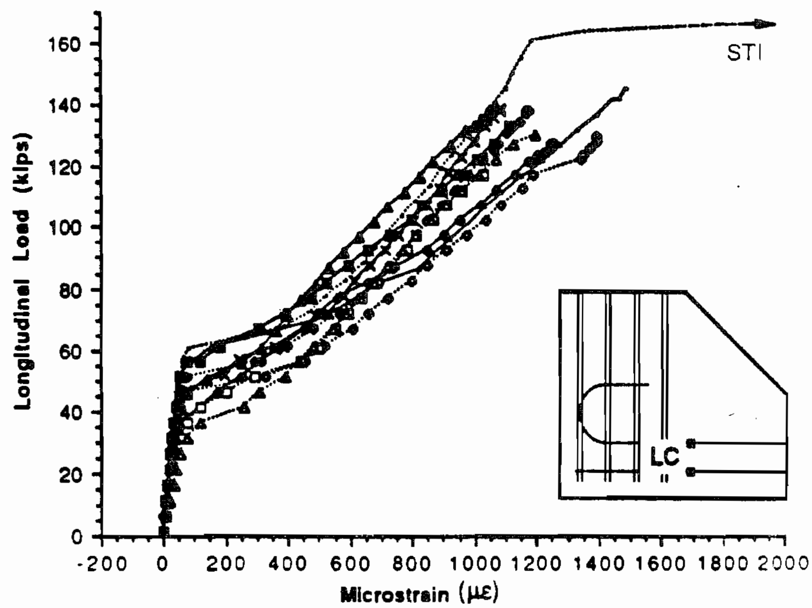

Figure 6.36 Strains at Location LC.

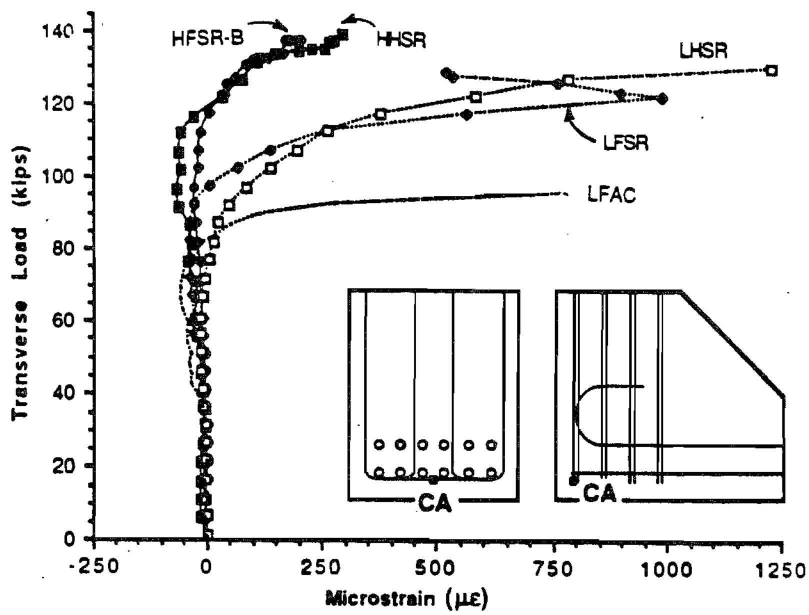

Figure 6.37 Strains in Bottom Leg of Transverse Tie at Location CA.

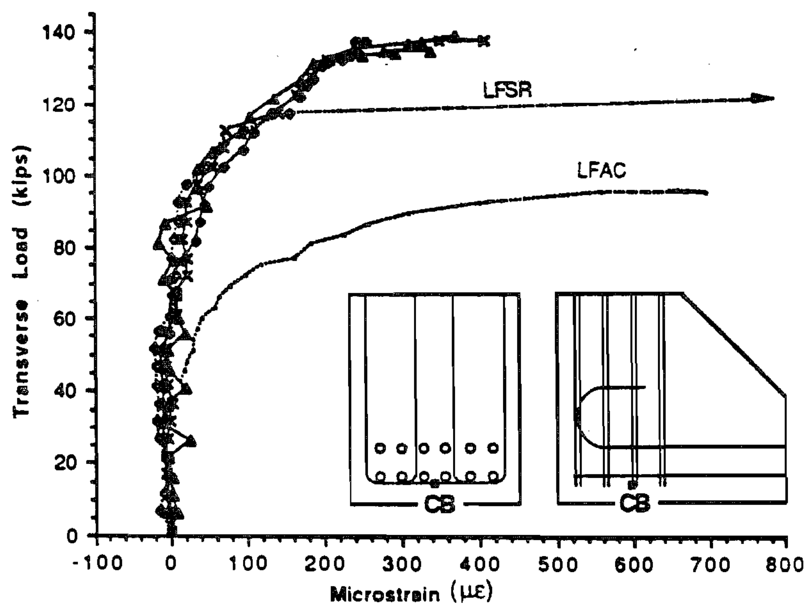

Figure 6.38 Strains in Bottom Leg of Transverse Tie at Location CB.

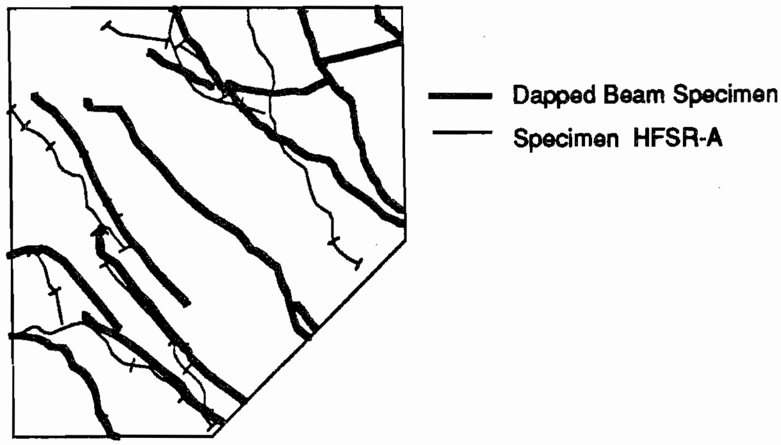

Figure 6.39 Crack Pattern Comparison of Specimen HFSR-A and Dapped Beam Specimen, ST1.

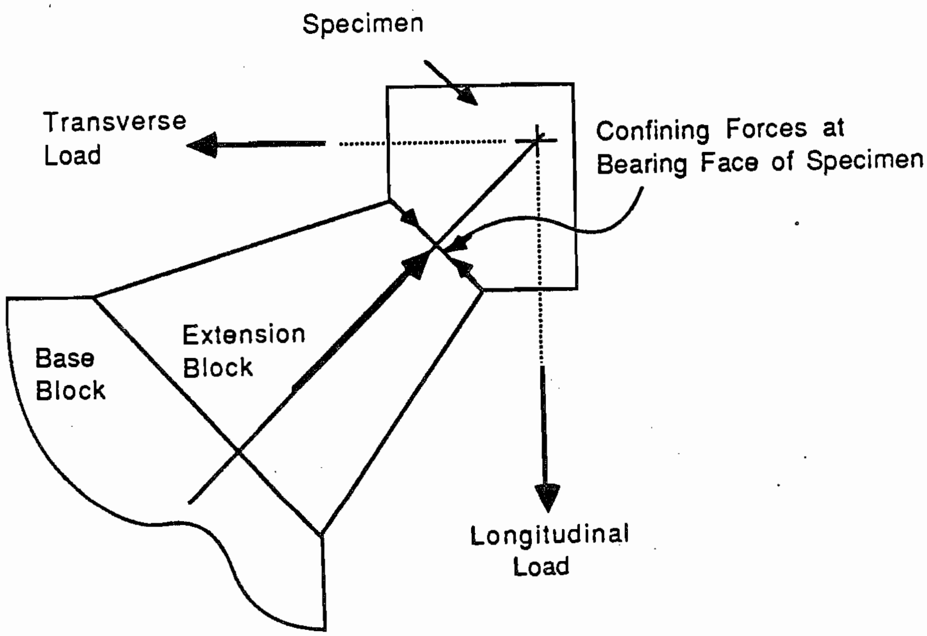

Figure 6.40 Confining Forces Produced by Test Setup.

6.4 Validity of Node Tests.

The test results from the node specimens are only meaningful if they are representative of the behavior of a CTT-node in a dapped beam. The test results for the dapped beam test ST1 and comparable node specimens provide an opportunity to assess the validity of the node tests. The cracking patterns (Fig. 6.39) for ST1 and HFSR-A were quite similar. The same cracks generally appeared in both specimens at approximately the same load. One exception was the diagonal tension crack perpendicular to the center of the bearing face in ST1. It is likely that confinement at the bearing face prevented the formation of this crack in HFSR-A (shown in Fig. 6.40).

Comparison of strains (Sec. 6.3.2) showed some differences in the transverse strains of ST1 and node specimens after the design strength was achieved. As previously mentioned, strains for the CTT-node transverse bars in ST1 did not increase after transverse steel yielded at the re-entrant corner. Since failure occurred in ST1 away from the CTT-node, additional forces were never transferred to the CTT-node at the lower corner of the dapped beam. In the node specimen, the transverse tie force could be increased through direct loading after the reinforcement yielded. Thus, transverse bar strains increased after the design strength of the specimen was achieved. While it is interesting to study the behavior of the node specimens after yielding of the transverse steel, it is unlikely that such strains would develop in an actual member. The deformation limit of the member would probably limit the amount of force that would be transferred to the CTT-node. In summary, the node specimen behavior was felt to be characteristic of behavior of the CTT-node of the full-sized, dapped beam. Correlations between the behavior of the two types of specimens were quite good, especially before yield of the transverse steel.

Table 6.3 Ratio of Measured Force to Total Applied Force - Transverse Reinforcement

Specimen	At Location TA+		At Location TB+		At Location TC+		At Location TD+	
	115 kips	125 kips	115 kips	125 kips	115 kips	125 kips	115 kips	125 kips
HFSR-A	0.13	0.24	0.15	0.18	0.26	0.24	0.19	0.19
HFSR-B	0.16	0.21	0.13	0.14	0.24	0.24	0.21	0.24
LFSR	0.26	*	0.22	*	0.22	*	0.23	*
HFNC	0.17	0.22	0.11	0.13	0.26	0.24	0.19	0.20
LFNC	0.21	*	0.13	*	0.25	*	0.22	*
HHSR	0.20	0.24	0.21	0.23	0.26	0.24	0.24	0.24
LHSR	0.22	0.24	0.21	0.24	0.26	0.24	0.22	0.23
HFSB	0.26	0.24	0.16	0.22	0.19	0.21	0.21	0.24
LFAC	*	*	*	*	*	*	*	*
Average	0.20	0.23	0.16	0.19	0.24	0.23	0.21	0.22
Ratio of Measured to Applied	0.80	0.92	0.66	0.75	0.96	0.93	0.83	0.89

+ Each set of ties (4 sets) receive 0.25 of applied load on transverse steel (See Fig. 6.11).

* Data not available

Table 6.4 Ratio of Measured to Total Applied Force - Longitudinal Reinforcement

Specimen	At Location LA+		At Location LB+		At Location LC++	
	115 kips	125 kips	115 kips	125 kips	115 kips	125 kips
HFSR-A	0.30	0.30	0.16	0.20	0.94	0.96
HFSR-B	0.41	0.46	0.28	0.29	0.83	0.84
LFSR	0.34	*	0.30	0.0	1.00	0.0
HFNC	0.24	0.25	0.17	0.18	0.80	0.82
LFNC	0.28	*	0.29	0.0	0.86	0.0
HFSB	0.27	0.31	0.25	0.26	0.78	0.78
Average	0.30	0.33	0.24	0.23	0.87	0.85
Ratio of Measured to Applied	0.61	0.66	0.48	0.47	0.87	0.85
HHSR	0.55	0.59	0.30	0.32	0.71	0.73
LHSR	0.69	0.75	0.29	0.29	0.85	0.87
Average	0.62	0.67	0.29	0.30	0.78	0.80
Ratio of Measured to Applied	1.25	1.34	0.58	0.61	0.78	0.80
LFAC	0.31	0.34	0.22	0.23	0.76	0.75
Ratio of Measured to Applied	0.63	0.68	0.44	0.46	0.76	0.75

* Data not available

+ 50% of applied load at gage location LA, LB

++ 100% of applied load at gage location LC

CHAPTER 7
TEST RESULTS - CCT NODES

7.1 General

Selected data for each specimen are presented to show trends in behavior and to help explain differences in performance. The information presented includes:

1. *Longitudinal reinforcing bar stresses*: The stresses in individual bars for each reinforcement layer are plotted against the applied load. The cumulative measured force in the bars, the computed force based on the load applied and the geometry of the specimen and the difference between measured and computed bar forces (attributed to friction in the reaction and loading surfaces) are compared. In some tests the bar strain readings were influenced by bending in the longitudinal bars caused by a mis-positioning of the bars in the forms, or by uneven bearing of the plate to which the bars were welded. Consequently, the bar stress distribution was not uniform.

2. *Concrete surface strain immediately preceding failure*: Surface tensile and compressive strains provide an indication of the strain trajectory and of the compressive strut width. The precision of the readings using the Demec gages was not always satisfactory. A slight change in the alignment of the gage can result in a different reading.

3. *Crack pattern:* Crack patterns provide an indication of the type of failure and of the effective strut width. The crack width can help in estimating the strain trajectory. The cracks on both side faces of the specimen were similar, thus only the cracks on one side will be shown.

7.2 Individual Test Results

Specimen LFT and LFT-R: The crack pattern and the appearance of LFT at failure clearly indicate that the specimen failed in compression at a load of 260 kips. The first crack appeared on the east side of the specimen at a load of 200 kips as shown in Figure 7.1. At failure the specimen separated into three segments (Fig. 7.2). The poor concrete quality was apparent because the failure plane went through the paste and did not fracture the aggregate. It appeared that the loading plate thickness (1 in.) was inadequate and there was a concentration of stress over the central portion of the bearing area. LFT-R was a replicate of LFT and was tested to examine the possible role of loading plate thickness on failure. The plate thickness for LFT-R was 2 in. The crack pattern for LFT-R is shown in Figs. 7.3 and 7.4. Although the crack patterns were quite similar for both specimens, LFT-R failed at a load of about 340k.

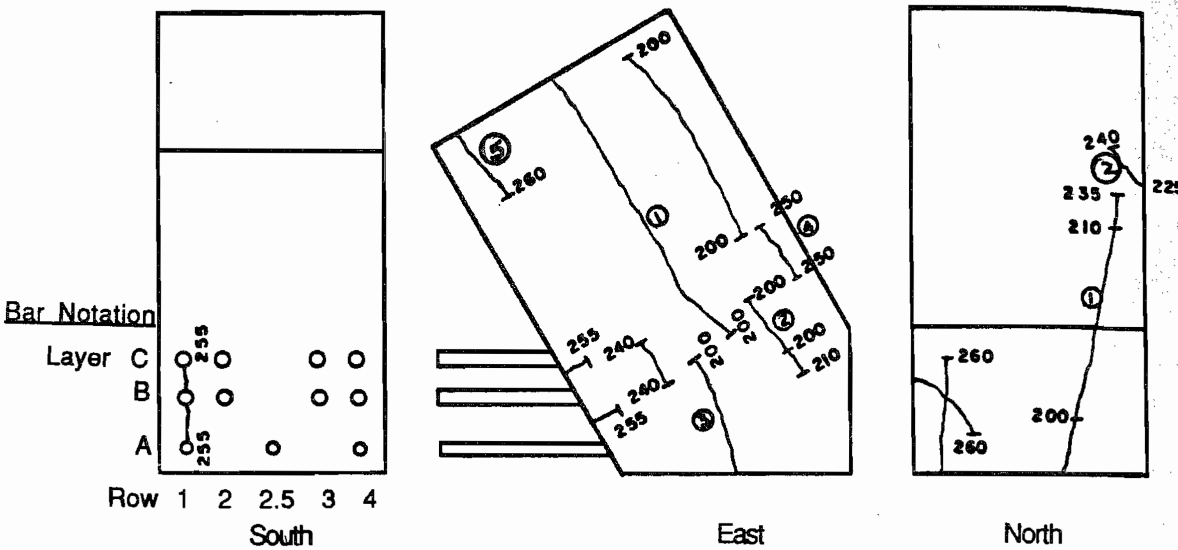

Figure 7.1 Crack Pattern Prior to Failure, LFT.

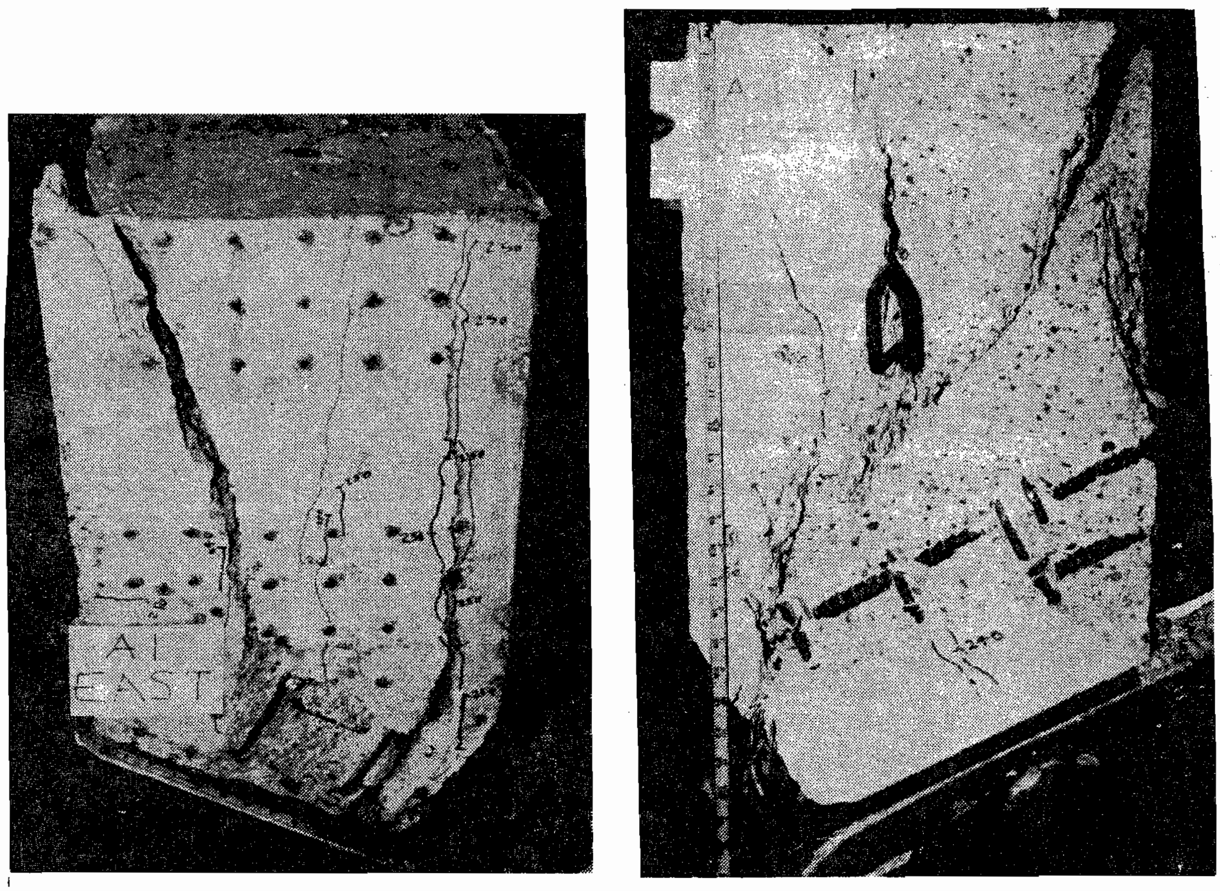

(a) East face (b) West face

Figure 7.2 Crack Patterns After Failure, LFT.

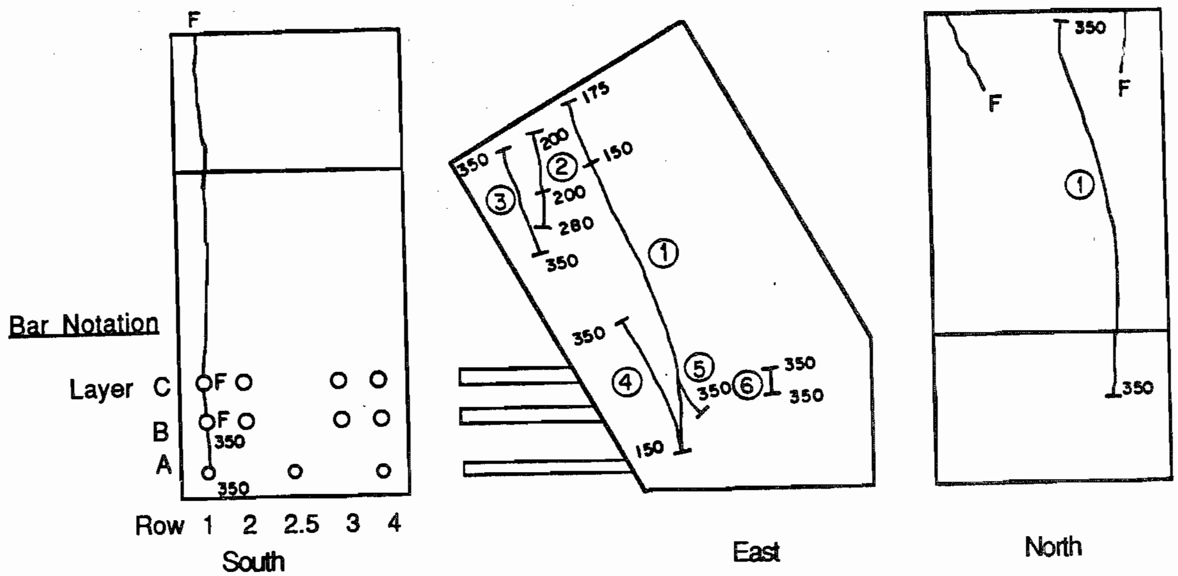

Figure 7.3 Crack Pattern Prior to Failure, LFT-R.

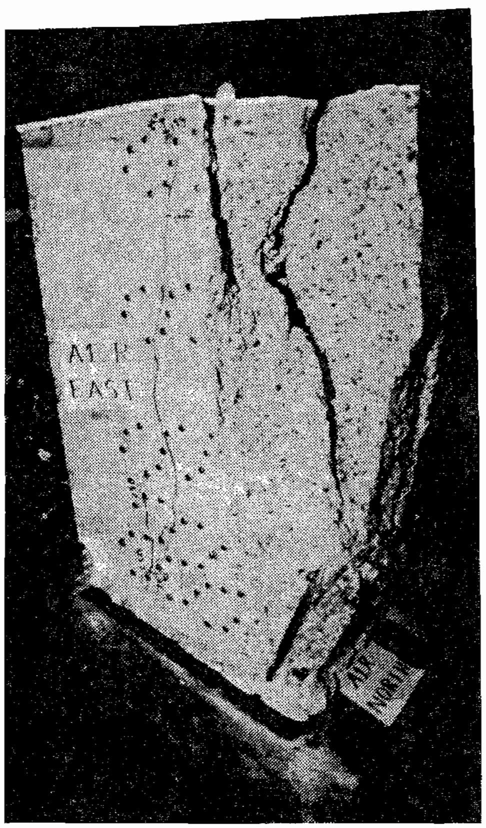

(a) Northeast corner

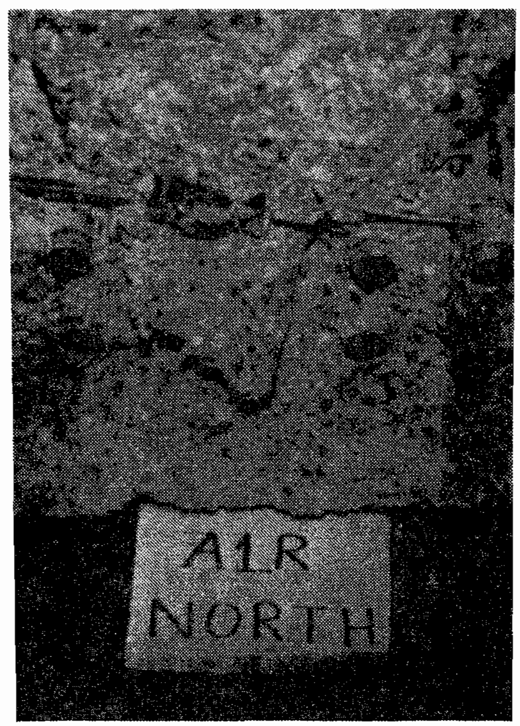

(b) North face

Figure 7.4 Crack Patterns After Failure, LFT-R.

The stress distributions for LFT (Fig. 7.5a) in the longitudinal reinforcing bars were not uniform. The lower layer (A) had the highest stresses and the highest rate of increase. The stresses in the top layer were almost bi-linear. Figure 7.5b shows the bar forces in LFT. The difference between measured and computed values is attributed to friction between the specimen and the test fixtures (Fig. 5.15). The computed value is based on the node geometry and the applied force; bar force = applied force x cos 60°. Even though teflon sheets were used, some friction was developed. Figure 7.6 shows similar curves for LFT-R.

Note: See Fig. 7.1 for bar notations

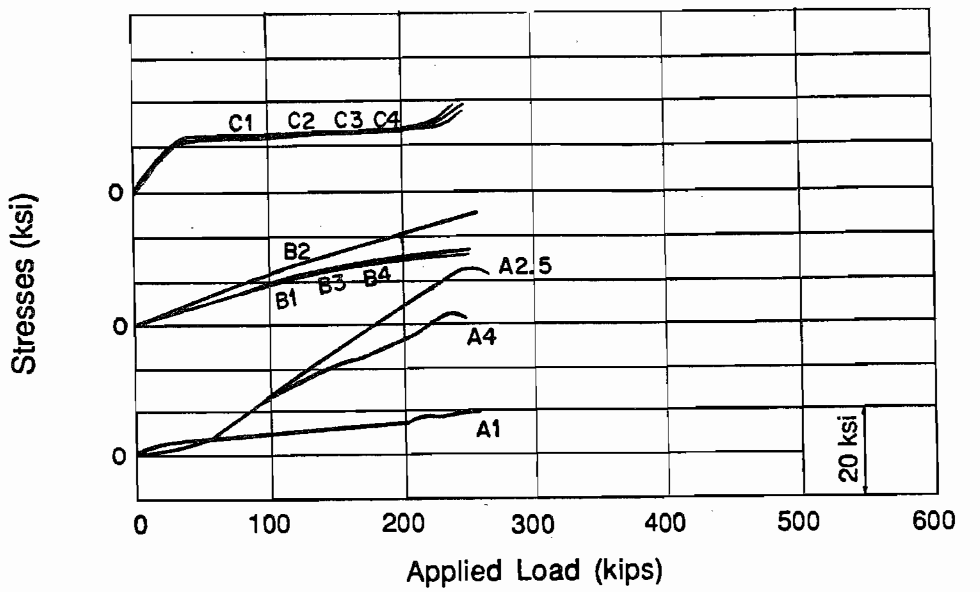

(a) Stresses in individual reinforcing bar

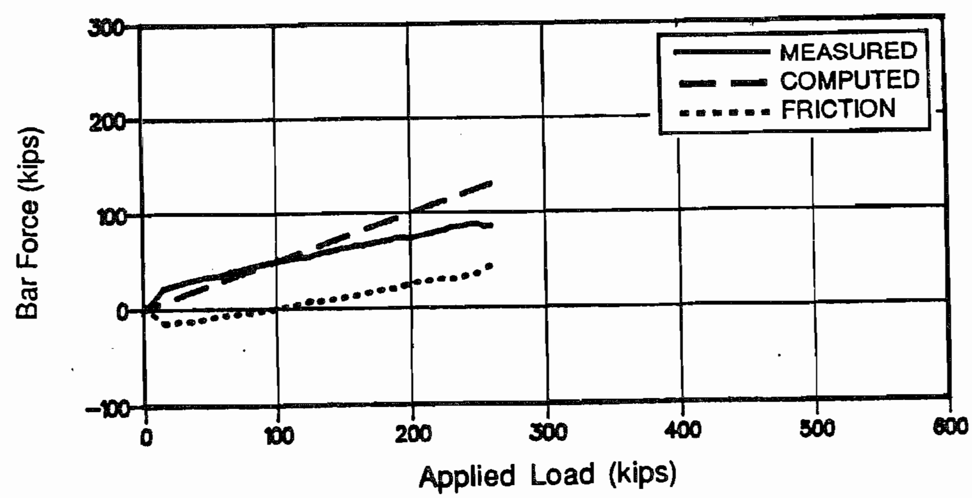

(b) Longitudinal bar total force.

Figure 7.5 Stresses and Total Force in Longitudinal Bars, LFT.

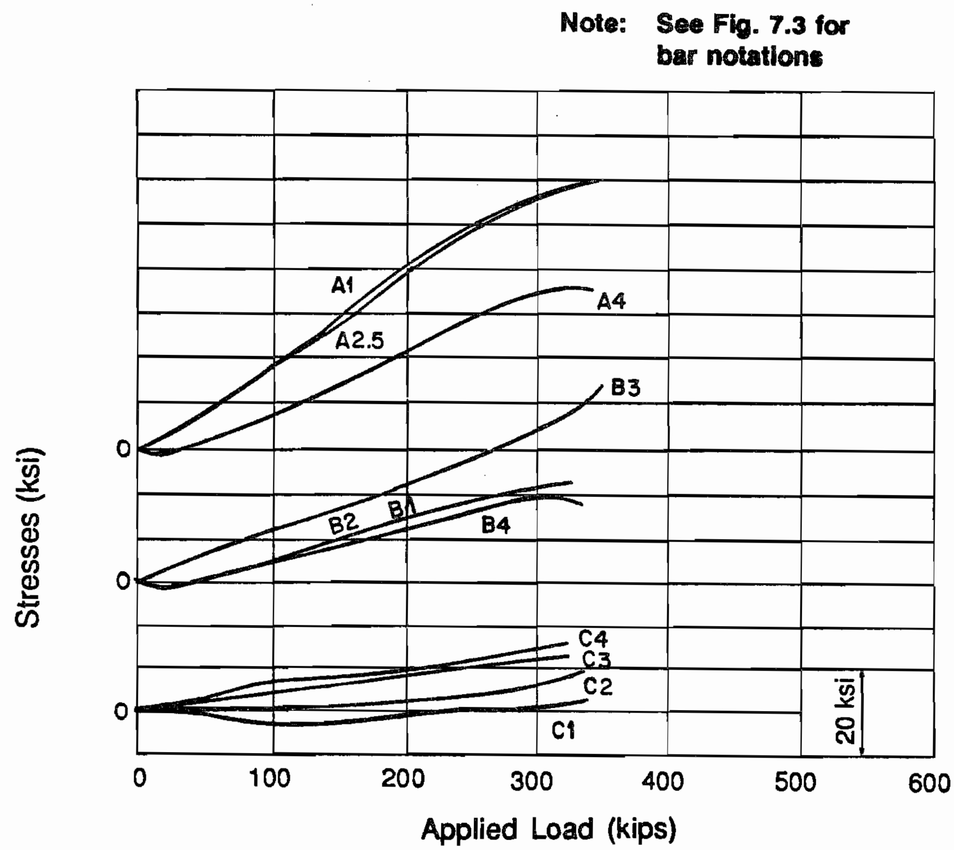

(a) Reinforcing bar stresses

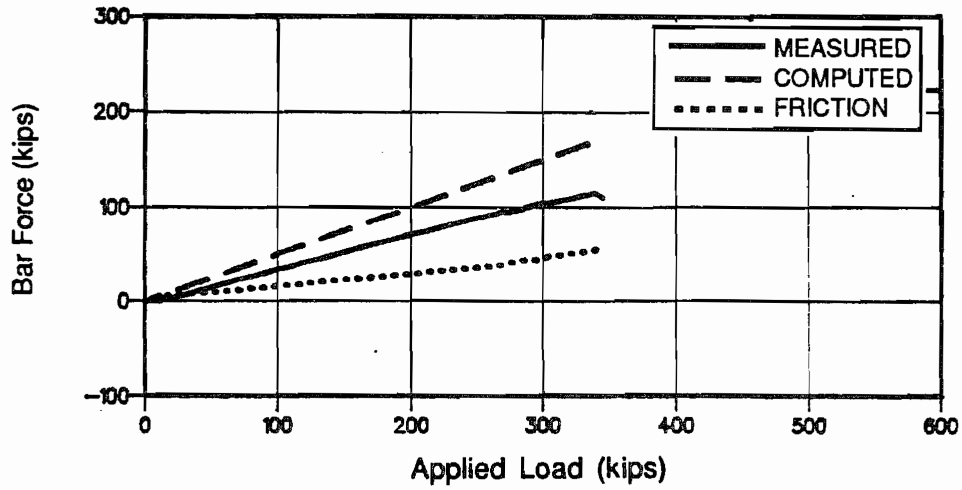

(b) Reinforcing bar total force

Figure 7.6 Stresses and Total Force in Longitudinal Bars, LFT-R.

The principal surface strains for LFT-R are shown in Fig. 7.7. The lines show the direction and magnitude of the strains. The longer the line from the midpoint (the location where measurements were taken) the greater the strain. The points between which the

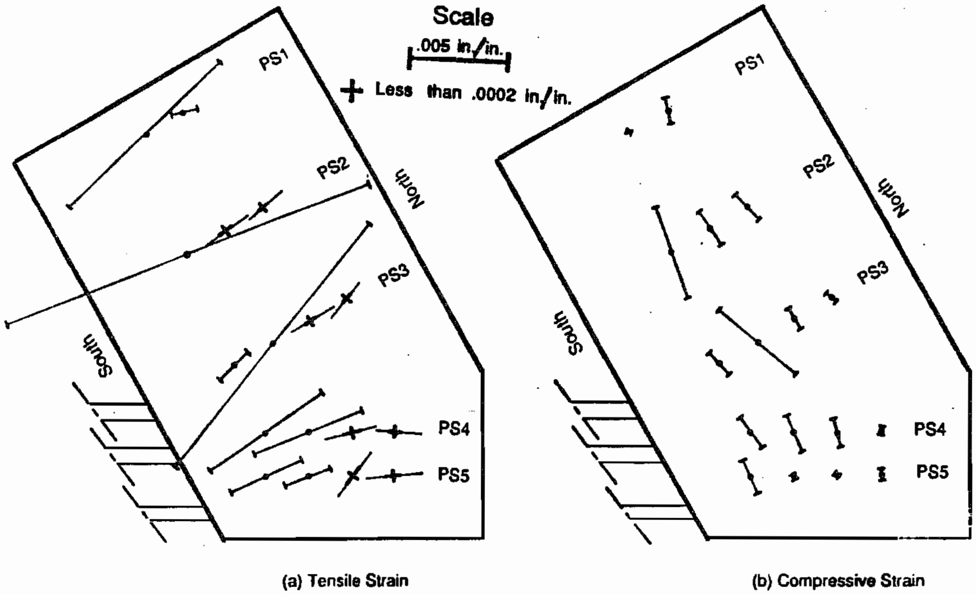

Figure 7.7 Principal Surface Strains, LFT-R.

deformation was measured were 2 in. apart, when a crack crossed between the gage points, high tensile strains were measured across the crack location and compressive strains along the crack. The strain values show that the cracks were restrained in that part of the specimen which had transverse reinforcement (the region where the longitudinal bars were anchored). Surface strains for LFT are not shown because the arrangement of reference points was found to give unreliable results.

Specimen LFO: No ties were placed in the anchorage zone for the longitudinal bars (tension tie). The first cracks that appeared on the specimen were compressive cracks that developed near the loading and reaction surface) at a load of 225 kips (Fig. 7.8). The

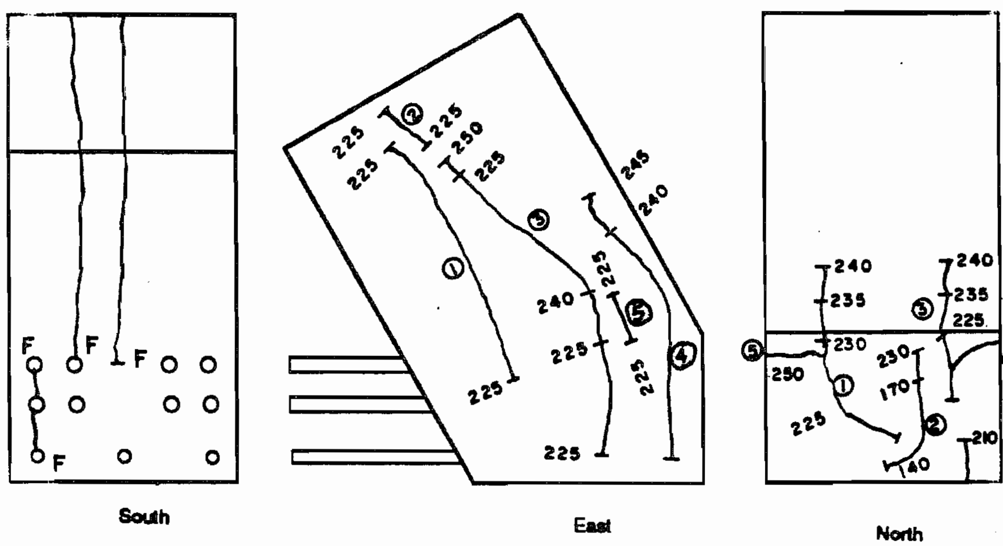

Figure 7.8 Crack Pattern Prior to Failure, LFO.

specimen failed in anchorage at a load of 260 kips. The loss of cover over the bars is apparent in Fig. 7.9.

Specimen LHT: LHT failed in compression at a load of 240 kips. The first crack appeared at a load of 140 kips at the top loading surface. Figure 7.10 shows the crack pattern just before failure.

Specimen LHO: LHO failed at a load of 240 kips. The first crack, which developed at a load of 210 kips, started from the top part of the specimen at one edge of the loading plate (Fig. 7.11). At failure the first crack opened widely and extended through the specimen as can be seen in Figure 7.12.

Specimen HFT: The reinforcement configuration was the same as in LFT but higher strength concrete was used. The specimen failed in anchorage at a load of 540 kips when splitting of the side cover occurred (Fig. 7.13). The first crack appeared at a load of 320 kips and started from the support surface.

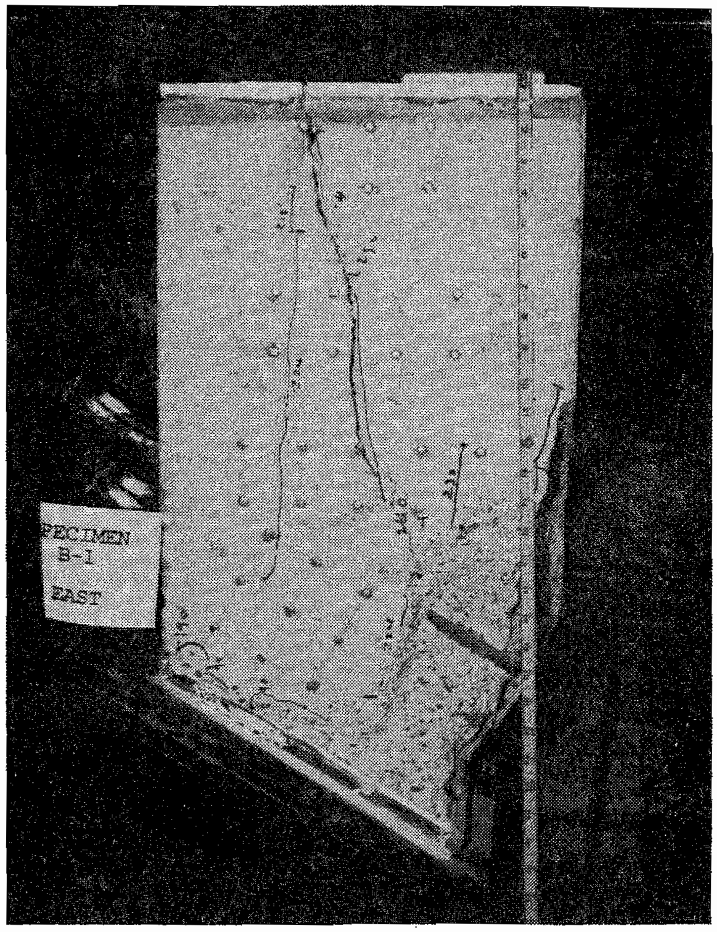

Figure 7.9 Crack Pattern After Failure, LFO.

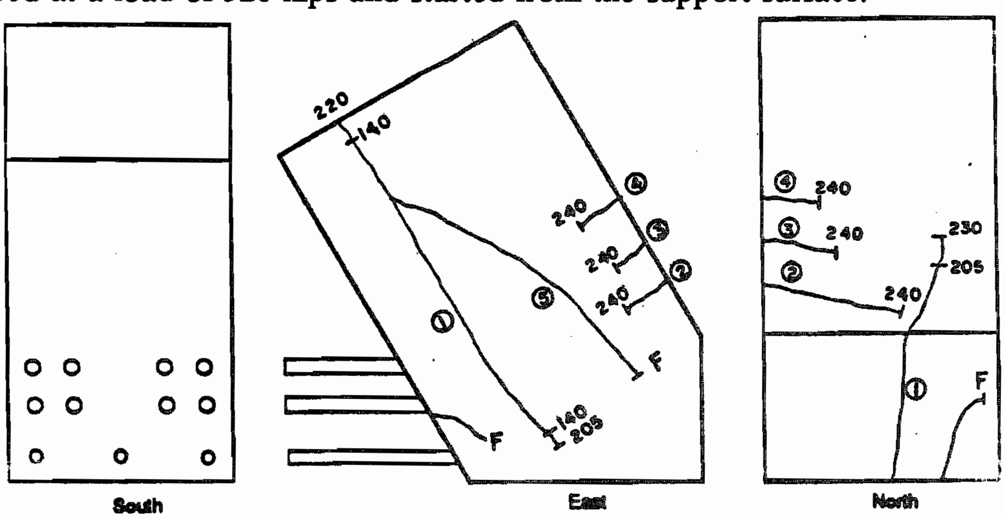

Figure 7.10 Crack Pattern Prior to Failure, LHT.

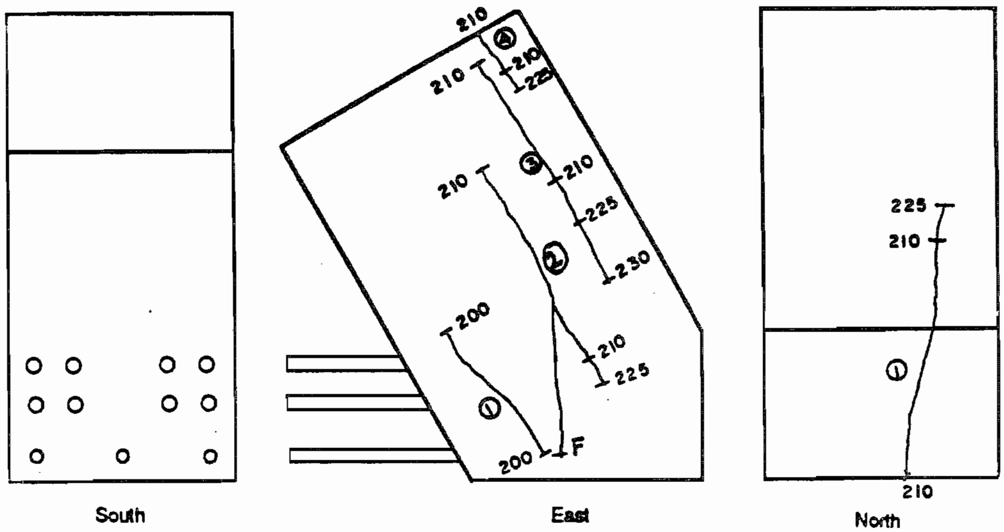

Figure 7.11 Crack Patterns Prior to Failure, LHO.

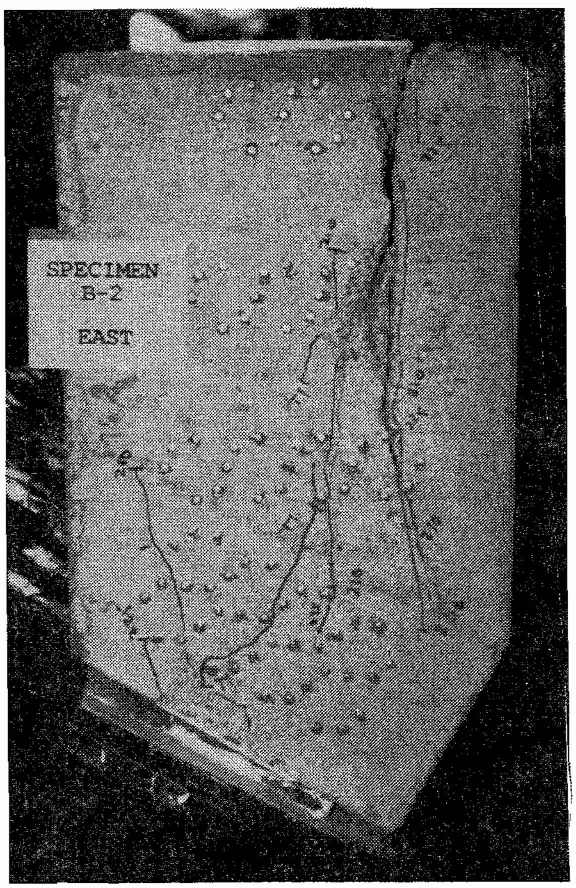

(a) East face

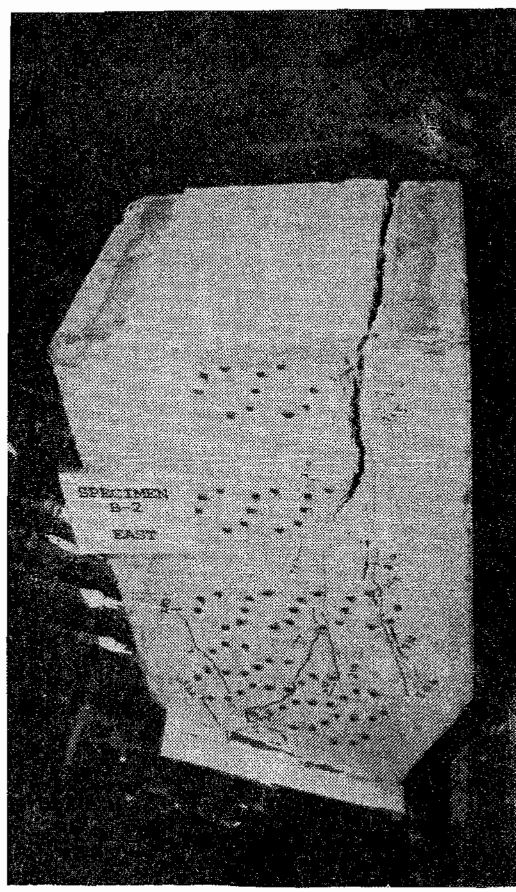

(b) Top view

Figure 7.12 Crack Patterns After Failure, LHO.

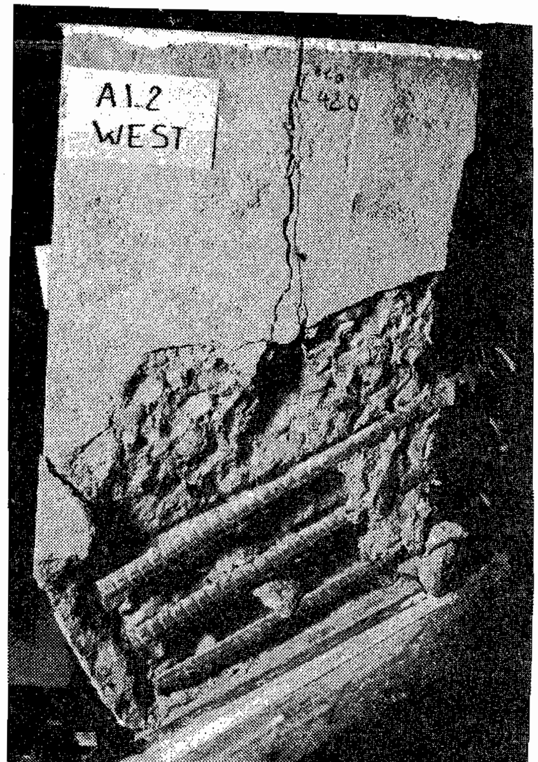

(a) West face

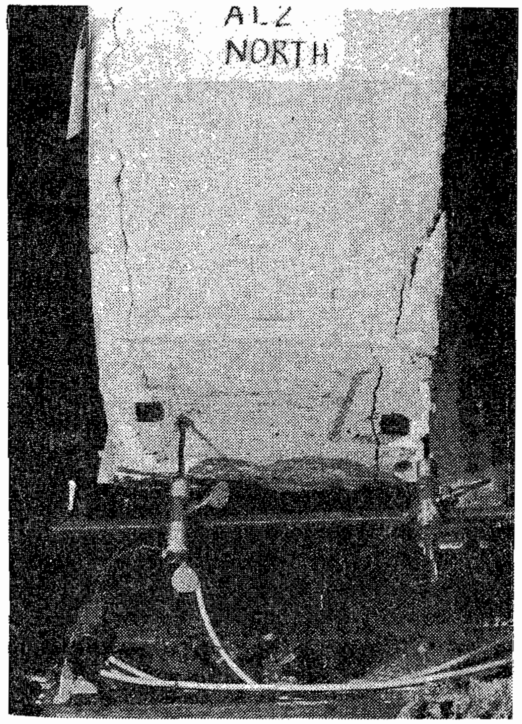

(b) North face

Figure 7.13 Appearance After Failure, HFT.

Specimen HFO-SS: The specimen failed in anchorage of the straight bars at a load of 450 kips by splitting of the side cover (Fig. 7.14). The first crack appeared at a load of 300 kips at an angle of 65° with the reinforcement. Figure 7.15 indicates that load was evenly distributed among all the bars. The friction losses were low (about 6% at applied load). The surface strain (Fig. 7.16) shows that the line of action of the compressive force in the concrete is located closer to the south face. The load converges to the center at the top surface.

Specimen HFO-HS: The bottom layer of bars terminated in hooks to improve anchorage. The first crack was located at 2.5 in. from the south face and developed at a load of 310 kips. A major crack appeared at a load of 340 kips and made an angle of 65° with the longitudinal reinforcement. Figure 7.17 shows the crack pattern. The specimen failed in anchorage at a load of 415 kips by splitting of the side cover.

Specimen HFO-SL: The concrete cover between the bottom layer and the bearing plate was increased (compared with HFO-SS) to improve anchorage. The first crack appeared at a load of 300 kips. The specimen failed at a load of 470 kips by splitting of the side cover (Fig. 7.18).

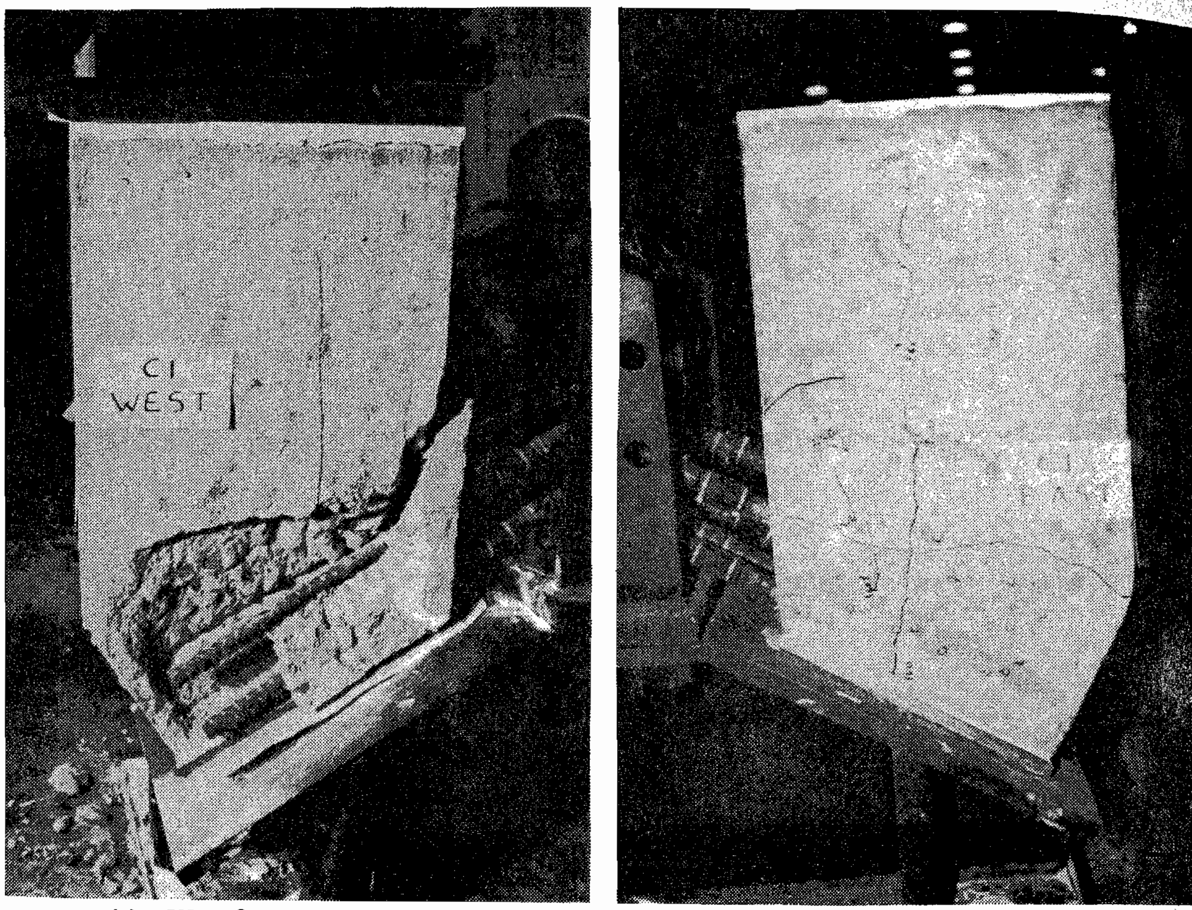

(a) West face (b) East face

Figure 7.14 Appearance After Failure, HFO-SS.

Specimen HFO-HL: Cover over the layer of hooked bars was increased (compared with HFO-HS) to improve anchorage capacity. Uneven bearing of the loading plate caused cracks to form prematurely at a load of 200 kips. The specimen was unloaded and the plate was regrouted. The specimen was reloaded without further problems. Cracks formed again at a load of 310 kips. The specimen failed at a load of 435 kips by splitting of the side cover (Fig. 7.19).

7.3 Summary of Results

Failure modes and failure loads are summarized in Table 7.1

With the exception of LFO, all the specimens cast with low strength concrete failed in compression. All specimens cast with high strength concrete and Specimen LFO failed suddenly in anchorage when cover spalled.

The load distribution in the layers of bars making up the tension tie was not uniform. With the exception of the lowest layer of bars in HFT, none of the reinforcing bars yielded prior to failure of the specimen. Table 7.1 includes values for the measured total force in

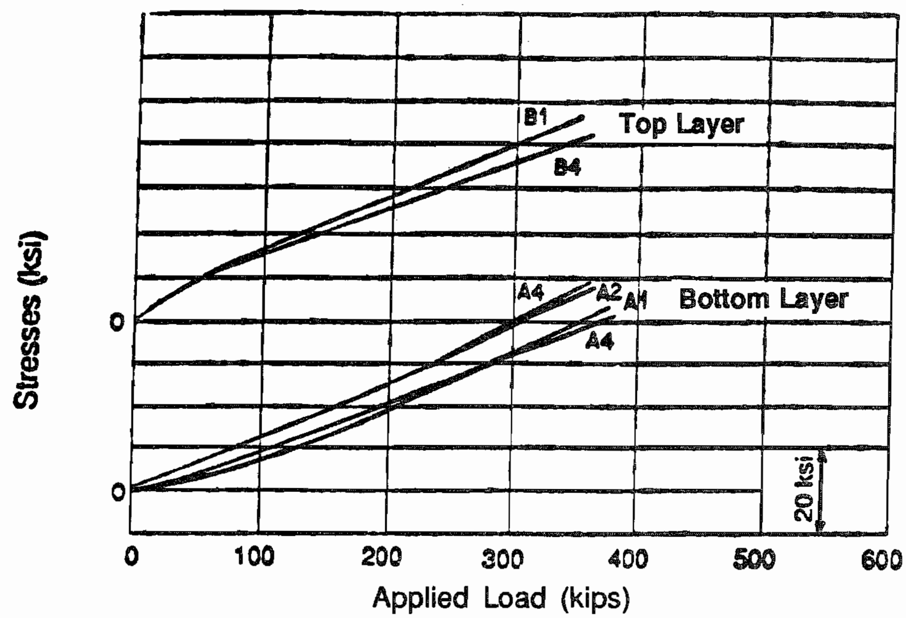

(a) Stresses in individual bars

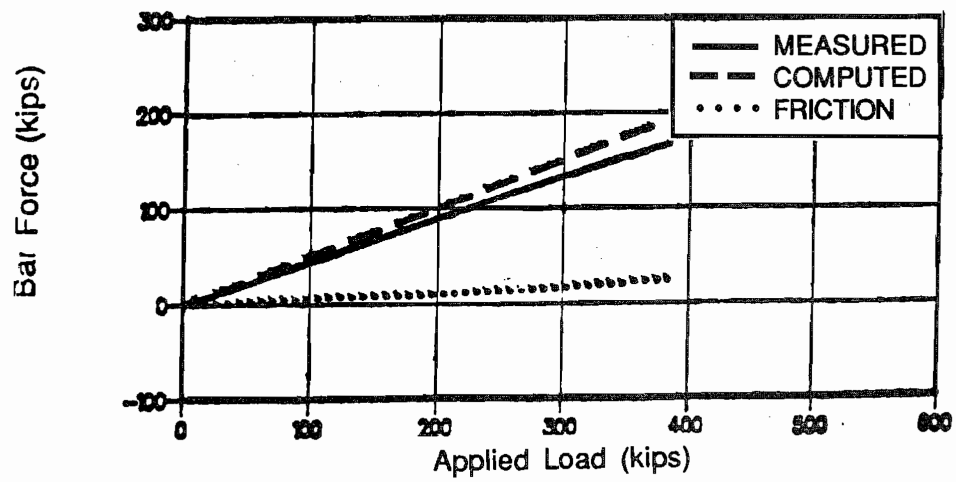

(b) Bar forces

Figure 7.15 Stresses and Force in Longitudinal Bars, HFO-SS.

the tension tie based on strain gage readings. Even though the geometry of the forces at the node was the same for all tests, friction losss (Figs. 7.5b, 7.6b and 7.15b) account for the differences between computed (failure load x cos 60°) and measured values.

In general, large surface tensile strains coincided with cracks locations, and compressive strains usually converged to the center of the bottom (reaction) surface which may indicate that even a 2-in. thick loading plate was not sufficient to ensure uniform bearing.

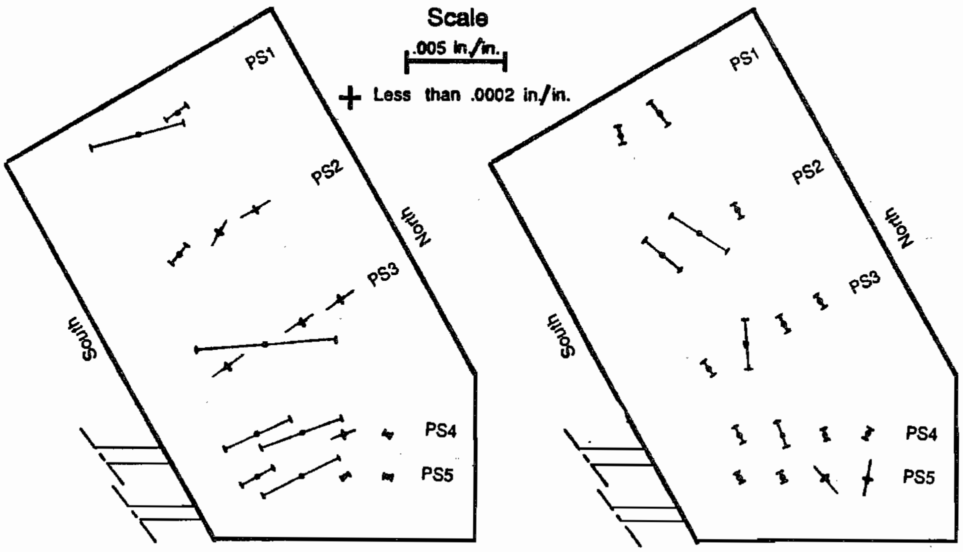

(a) Tensile strain (b) Compressive strain

Figure 7.16 Principal Surface Strains, HFO-SS.

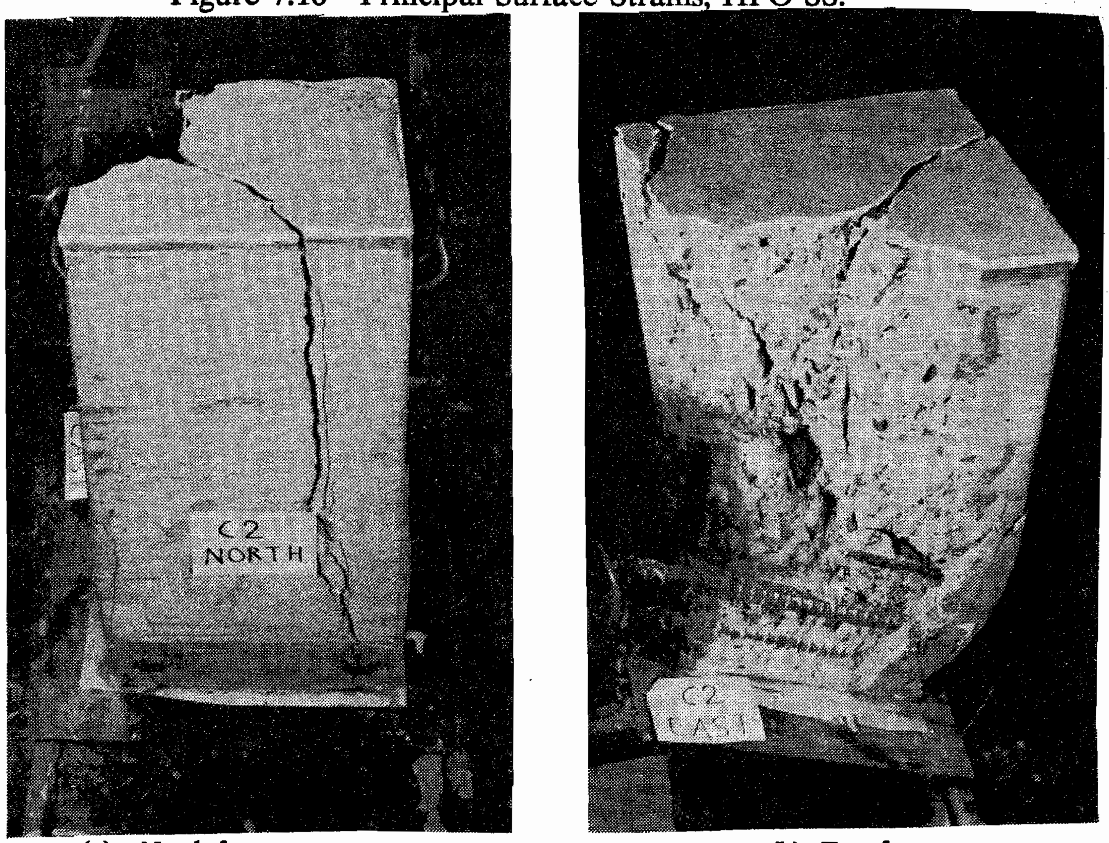

(a) North face (b) East face

Figure 7.17 Appearance After Failure, HFO-HS.

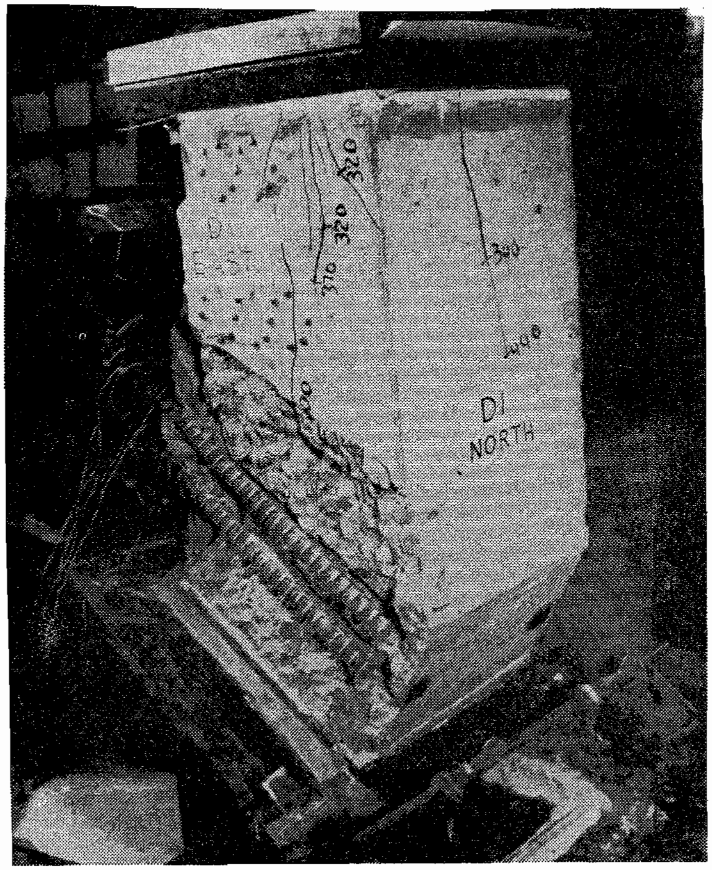

Figure 7.18 Appearance After Failure, HFO-SL.

It is difficult to compare the behavior of the CCT-nodes with the CCT node in the dapped beams. The specimens were designed to fail in either a tension or cmpression mode and similar nodes in the dapped beam tests did not reach failure. Nevertheless, it is possible to see similarities in the general crack patterns, particularly those that lie along the lines of compression in the diagonal direction.

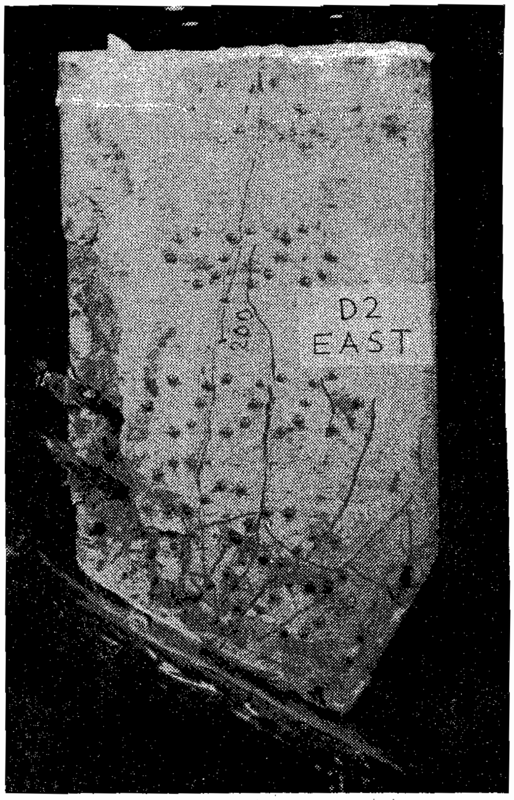

(a) East face

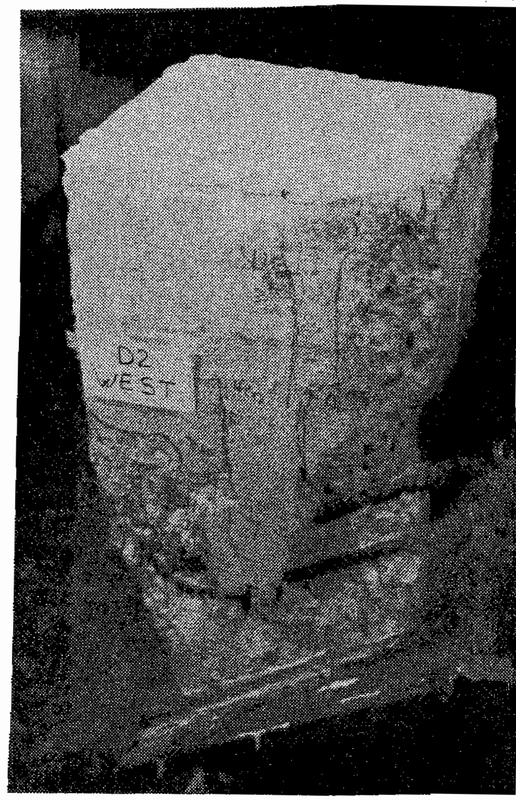

(b) West face

Figure 7.19 Appearance After Failure, HFO-HL.

Table 7.1 Failure Mode of CCT Test Specimens

Specimen	Failure Load (kips)	Measured Total Bar Force, Fm	Failure Mode	Comments
LFT	260	90	Compression	Large shear crack at failure
LFO	260	110	Anchorage	
LHT	240	110	Compression	
LHO	240	NA	Compression	
LFT-R	350	110	Compression	
HFT	540	245	Anchorage	Sudden failure
HFO-SS	450	167	Anchorage	Sudden failure
HFO-HS	415	174	Anchorage	Sudden failure
HFO-SL	470	204	Anchorage	Sudden failure
HFO-HL	435	213	Anchorage	Sudden failure

CHAPTER 8
EVALUATION OF NODE TESTS

8.1 Introduction

Nodes are critical parts of the strut-and-tie model, yet they are not fully understood. The designer is generally able to adequately develop the overall strut-and-tie model for D- and/or B-regions (Figs. 2.2 and 2.3) of a structure; however, design checks for nodes, especially those anchoring tensile ties, are unclear. Because the scope of the present study is limited to a narrow range of variables and a few tests, it is not possible to develop comprehensive design recommendations for nodes. Still, the node test results provide important information in an area where the strut-and-tie model is lacks definition. Therefore, in this chapter the test results will be used to: 1) verify proposed design guidelines where possible; 2) identify behavior patterns not considered by proposed design guidelines; and 3) provide a basis for further refinement of node design guidelines.

An assessment of the node must be made during the final design. A conceptual system (strut-and-tie model) will have already been developed to represent in a simplified form the complex state of stress within the member. The designer must make two checks of the node which are normally based on the actual reinforcement layout selected. First, the concrete stress in the node must be checked to ensure that it does not exceed the effective concrete strength limit of $f_{ce} = \upsilon f_c'$. Second, the proper anchorage of tie reinforcement must be ensured. Further design iterations are not required if these conditions are satisfied.

Figure 8.1 shows the similarities in design rationale for detailing a steel truss and for detailing a concrete member using the strut-and-tie model. After the members of the structural system are proportioned to carry the calculated forces, the nodes are detailed. Specifically, the nodes must transfer forces between elements. In the steel truss, bolts, welds, and possibly gusset plates are sized to safely transfer load between the members. In contrast, the node in a concrete member must rely on bond, anchorage, and other internal force transfer mechanisms to transfer strut and tie forces.

8.2 CTT Nodes

8.2.1 Geometry of Compressive Stress Fields. After concrete cracks, tensile stresses which were carried by the concrete must be transferred to the reinforcing steel. The size and shape of the post-cracking compressive stress fields in the concrete are affected by the placement of reinforcement. For instance, the strut width is assumed to increase if multiple layers of tie reinforcement are used[14, 15]. The strut angle of inclination must be based on the location of nodes and the width of the strut is in turn defined by the spacing and distribution of the tie reinforcement.

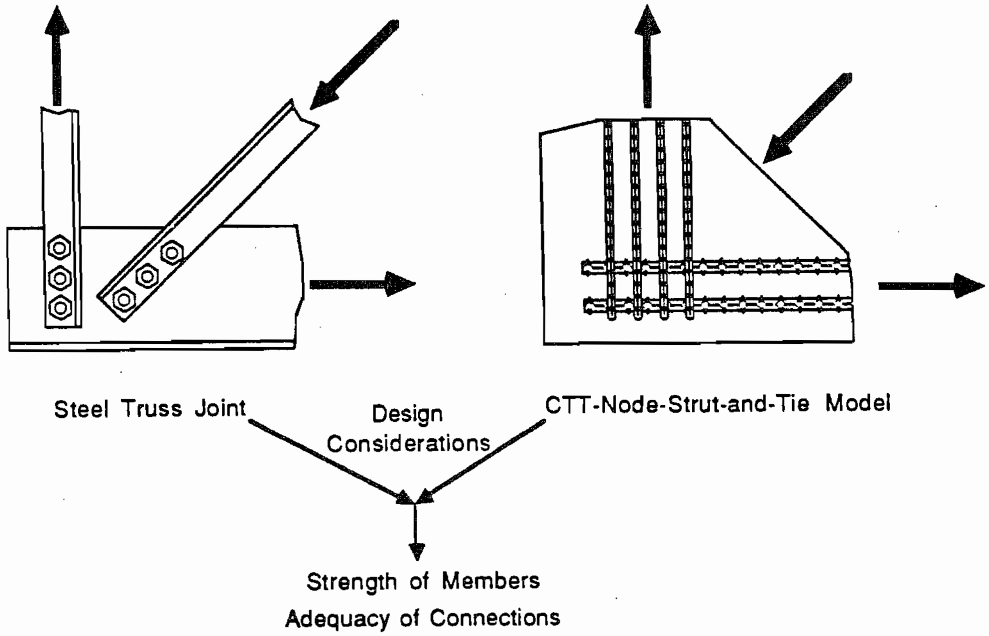

Figure 8.1 Comparisons of Design Rational Used for Nodal Region of Strut-and-Tie Model and Joint of Steel Truss.

After closely examining the reinforcement strains and the cracking patterns for the CTT specimens, estimates of the physical dimensions and configuration of the assumed stress fields for several specimen geometries are illustrated in Fig. 8.2. The compressive stress field was assumed to act at an angle α (corresponding to the effective angle of loading). The width was conservatively defined by the intersections of the outer transverse and longitudinal layers of tie reinforcement. However, when hooked bars were present, this width was increased to consider the effect of the hooks as explained later. In addition, in those cases where the bearing surface was reduced, the width of the upper face of the compression field was reduced to that limiting width.

The observed cracking patterns played an important role in estimating of strut width. The crack patterns showed that reinforcement layouts which included hooked bars tended to develop wider struts. The hooked bars developed bearing stresses at the bend. In the nodes with hooked bars, defining the width of the actual stress field by the point where the hook is tangent to the vertical bars appears to be a reasonable approach.

It is important to observe that except for HHSR, LHSR, and LFAC the estimated stress field is narrower than the effective bearing surface provided at the face of the node. It is unlikely that uniform bearing stresses were produced across the entire 10.6 in. bearing face of the CTT specimens. The estimated widths of the assumed stress fields are shown in Fig. 8.2. Both estimated widths and full widths of the bearing surface will be used when making comparisons with effective concrete stress limits.

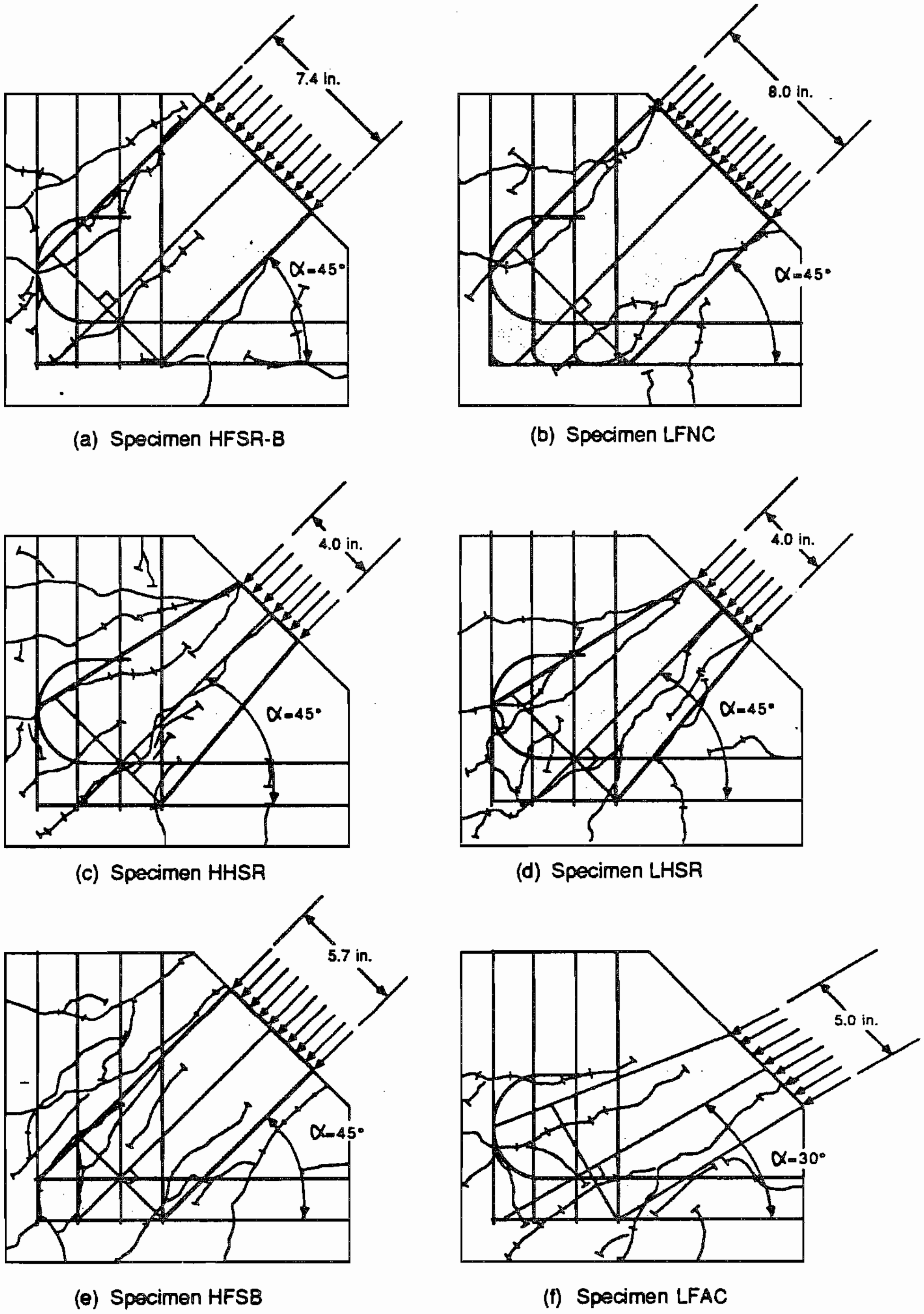

Figure 8.2 Estimated Geometries of Compressive Stress Fields in Some CTT Node Specimens.

The configuration of the compression field is also of interest in this study. Bottle-shaped struts may have lower effective concrete strength limits due to transverse tensile strains perpendicular to the axis of the strut. As illustrated in Fig. 8.2, it is estimated that the configuration of the stress field was prismatic for all specimens except HHSR, LHSR, and LFAC where fanned-shaped configurations are defined by the narrow effective width of the bearing surface.

Finally, the width of the compressive stress field may also affect development. It has been suggested that anchorage of the tie reinforcement begins where the transverse compression stress trajectories of the struts meet the bar[15].

8.2.2 Effective Concrete Strength. The effective concrete strength limit was defined as $f_{ce} = \upsilon f_c'$ where υ is an efficiency factor and f_c' is the cylinder strength. A comparison of node test results with efficiency factors (υ) recommended by several authors is made in Tables 8.1 and 8.2. When making comparison with effective concrete strength limits, the nominal widths of the bearing surface and used in Table 8.1. The estimated widths of the stress fields shown in Fig. 8.2 are used in Tables 8.2. Bearing stresses are normalized using the actual concrete strength. Since the estimated width was no different than the actual width for HHSR and LHSR, these specimens are not shown in Table 8.2. LFAC is also excluded since the adjusted bearing width was already included in Table 8.1.

Test results for most nodes are inconclusive since crushing failures were not observed. Specimen LHSR was the only specimen that exhibited a crushing failure of the compressive strut. For LHSR (in italic type), the ratios of measured (normalized) stress to the recommended efficiency are greater than one. For that case, the recommended effective concrete strength limits are conservative. HHSR and LFAC both exhibited much higher strength than the recommended values. This is particularly important for HHSR since it had a small bearing surface (as did LHSR) but did not reach a crushing failure at the low effective stresses recommended for design. It is more difficult to assess the importance of LFAC since the real bearing area is not clearly delineated.

Specimens HHSR, LHSR and LFAC showed surprisingly high effective concrete strength considering that substantial cracking parallel to the compression struts was observed. Tensile stresses and subsequent cracking orthogonal to the compression strut are normally thought to reduce the effective concrete strength[26]. The high effective concrete strength may be due to 1) the reduced bearing surface of the strut; and 2) the volume of concrete which surrounded (confined) the relatively narrow strut. Cracks occurred at roughly the same loads in the node specimens and the prototype dapped beam, and suggest that confining mechanisms in the node specimens were much the same as those in the dapped beam.

The recommended efficiency factor proposed by Schlaich et al.[15] underestimates the measured efficiency of specimen LHSR by over 50%. Effective concrete strength limits proposed by Ramirez[12] and Mitchell and Collins[11] are even more conservative. Applying

Table 8.1 Comparison of Node Test Results with Suggested Efficiency Factors

υ - Based on Nominal Bearing Area

Specimen	*Meas. Bearing Stress* / f'_c	Ramirez		Schlaich et al.		Mitchell & Collins	
		Rec.[1]	Meas.[2]/Rec.	Rec.	Meas./Rec.	Rec.	Meas./Rec.
HFSR-A	0.20	0.36	0.56	0.68	0.29	0.54	0.37
HFSR-B	0.26	0.39	0.66	0.68	0.38	0.54	0.48
LFSR	0.35	0.49	0.71	0.68	0.51	0.54	0.65
HFNC	0.25	0.39	0.63	0.68	0.37	0.54	0.46
LFNC	0.35	0.49	0.71	0.68	0.51	0.54	0.65
HHSR	0.71	0.39	*1.80*	0.68	*1.04*	0.54	*1.32*
LHSR[3]	*1.03*	*0.49*	*2.09*	*0.68*	*1.51*	*0.54*	*1.91*
HFSB	0.27	0.39	0.68	0.68	0.40	0.54	0.50
LFAC	0.81[4]	0.48	*2.07*	0.68	*1.48*	0.42	*2.34*

1 Recommended
2 Measured
3 Experienced concrete strut crushing failure
4 Based on 5-in. strut width

Table 8.2 Comparison of Node Test Results with Suggested Efficiency Factors

υ - Based on Estimated Strut Width

Specimen	*Meas. Comp. Stress* / f'_c	Ramirez		Schlaich et al.		Mitchell & Collins	
		Rec.[1]	Meas.[2]/Rec.	Rec.	Meas./Rec.	Rec.	Meas./Rec.
HFSR-A	0.29	0.36	0.81	0.68	0.43	0.54	0.54
HFSR-B	0.38	0.39	0.96	0.68	0.56	0.54	0.70
LFSR	0.50	0.49	*1.02*	0.68	0.74	0.54	.93
HFNC	0.34	0.39	0.86	0.68	0.50	0.54	0.63
LFNC	0.47	0.49	0.95	0.68	0.69	0.54	0.87
HFSB	0.49	0.39	*1.25*	0.68	0.73	0.54	0.92

1 Recommended
2 Measured

the recommendations of Ramirez and Mitchell and Collins to CTT-nodes seems to be inappropriate since they were based on tests of continuous compression fields in beams and shear panels. The state of stress in the isolated struts and nodes is quite different from that in continuous compression fields. The recommendations of Schlaich et al.[25] which differentiate between parallel and skew cracking may be more applicable. Models where the strut angle does not follow the elastic stress trajectories are penalized by lower effective concrete strength limits for the struts and nodes.

8.2.3 ACI and AASHTO Provisions for Development. The test results showed that reinforcement details affected the ultimate strength of the node. Except for Specimen LFSR, specimens without confinement (transverse reinforcement in the anchorage zone) failed before confined specimens. Specimen HFSB, which had a straight bar anchorage on the top or first layer of longitudinal reinforcement, was the only high strength specimen with confining transverse reinforcement that failed.

Proponents of the strut-and-tie model state that ties should be suitably anchored at the node. One of the vital aspects of the anchorage check is the determination of the critical section at which anchorage starts. Unfortunately, the critical sections for ties anchored in CTT-nodes are not well defined in current proposals. Schlaich et al.[15] propose that development of the reinforcement begins where the boundary of the compressive stress field intersects the axis of the bars. However, this has not been verified through physical tests.

The development length ℓ_d is the shortest length in which the maximum bar stress f_s can be developed. The development length ℓ_d is measured from the critical section to the termination point of the bar. The format of ACI and AASHTO development length equations for straight or hooked deformed bars in tension may be used to determine the capacity of an anchorage detail based upon the provided development length (ℓ_{dh} or ℓ_{dhn}).

For straight bars:

$$\ell_{dn} = \frac{0.032 \times A_b \times f_s}{\sqrt{f_c'}}$$

but not less than $\ell_{dn} = 0.00032 * d_b * f_s$ and in terms of bar stress, f_s

$$f_s = \frac{(\ell_{dn}) * \left(\sqrt{f_c'}\right)}{0.032 * A_b}$$

but not greater than $f_s = \dfrac{\ell_{dn}}{0.032 * d_b}$ where A_b is the area of an anchored bar, with diameter d_b.

The nominal development length equation for hooked bars in tension is stated in a similar form as follows

$$\ell_{dhn} = \frac{0.016 * d_b \times f_s * \psi}{\sqrt{f_c'}}$$

and rearranging in terms of bar stress,

$$f_s = \frac{(\ell_{dhn}) * \left(\sqrt{f_c'}\right)}{0.016 d_b} * \frac{1}{\psi}$$

where ψ is a modification factor of 0.8 for hooks enclosed vertically or horizontally within ties or stirrup-ties closely $(< 3d_b)$ spaced along the full development length ℓ_{dh}.

In both equations above the nominal length has been reduced from the design length by removing the factors which are included in Codes so that the bars develop yield well before an anchorage failure occurs. The ACI and AASHTO provisions are based on a 1.25 factor.

The maximum bar stress f_s may be determined by: 1) dividing the applied tie force by the area of steel in the tie; or 2) the external strain gage readings. Comparison between the calculated nominal development length and the observed behavior of the anchored bars in the CTT nodes is difficult. Several of the specimens did not fail through mechanisms involving anchorage. Secondly, development length requirements are not directly applicable to anchored U-stirrups. The U-stirrup is generally considered to be fully anchored when it is enclosed around a longitudinal bar. For these reasons, comparisons are not made between the test results and development provision for specimens where the transverse ties fully confined the longitudinal bars.

In the unconfined specimens, LFNC and HFNC, code provisions would require hooked bars with less than 2-1/2 inches of side or bottom cover to be enclosed within ties or stirrup ties along their full development length to prevent splitting failure. In Specimens LFNC and HFNC, the ties were not enclosed and splitting failures occurred at 117.8 kips and 132.5 kips, respectively. Nonetheless, comparisons between the observed and predicted behavior in the unconfined specimens are interesting. Comparisons between the calculated nominal development length (based on measured f_s), cracking patterns, and the compressive stress field are shown in Fig. 8.3. The critical section is defined by the boundary of the assumed stress field following the proposal of Schlaich et. al.[15].

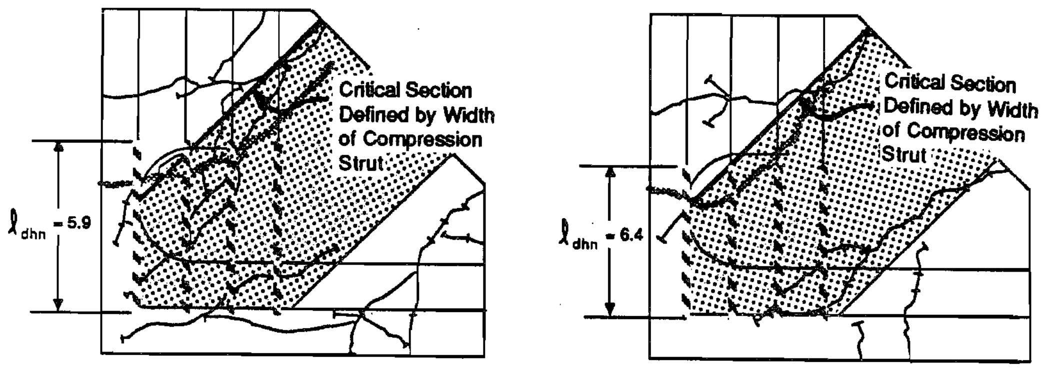

HFNC, f_s = 73.5 ksi **LFNC, f_s = 66.9 ksi**

(a) Transverse reinforcement

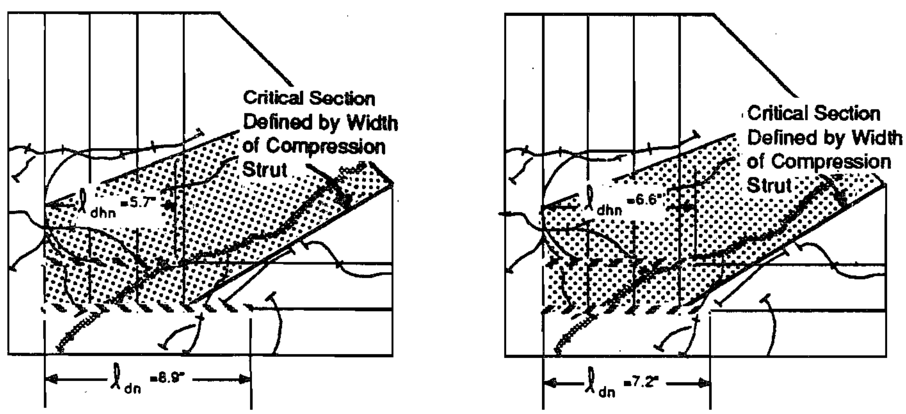

Hooked and straight longitudinal bars equally stressed at 44.5 ksi (average stress)

Unequal longitudinal bar stresses 52 ksi = hook and 36 ksi = straight bar (measured in individual bars)

(b) Longitudinal reinforcement in LFAC

Figure 8.3 Evaluation of Anchorage Conditions.

In both HFNC and LFNC the critical section for the transverse reinforcement defined by the compressive strut intersects the first layer of transverse bars just before the nominal development length. The calculated nominal development length for HFNC is

$$\ell_{dhn} = \frac{0.016 * 0.375 * 75300}{\sqrt{5780}} = 5.9 \ in.$$

The measured stress in this specimen was greater than yield indicating that the bars reached strain hardening. For the second layer of bars, the boundary of the actual stress field and starting point of development nearly coincide. The calculated nominal development length for the third and fourth layers of transverse bars lie within the stress field boundary. It would be expected that transverse bars in the unconfined specimens would experience a progressive failure. The first layer of bars would be most critical for development and would fail first. Unless the force could be redistributed to the remaining transverse reinforcement, the other layer of bars would fail sequentially. The major observed cracks are shown boldly in Fig. 8.3a. The major transverse crack occurred near the critical section as defined by the compressive field in both HFNC and LFNC. The cracks provide an indication that the assumed compression field is reasonable.

Specimen LFAC was the only specimen in which a loss of anchorage for the longitudinal reinforcement produced a side splitting failure. Anchorage deteriorated along the first layer of straight bars and the forces were gradually redistributed to the second layer of hooked bars until an anchorage failure of both layers of reinforcement occurred. At ultimate, the average stress of the longitudinal reinforcement was 0.74 * f_y (44.5 ksi); however, external strain gage readings showed the hooked bars were stressed more than the straight bars. Average measured stresses from the external gages were 52 ksi for the hooked bars and 36 ksi for the straight bars. While the measured stresses are more likely to be correct, both values are shown in Fig. 8.3(b). Major cracks and slip occurred along the failure plane which is shown boldly. The nominal development lengths for the hooked bars in LFAC is

$$\ell_{dhn} = \frac{0.016 * 0.625 * 52000 * 0.8}{\sqrt{3920}} = 6.6 \ in.$$

A factor of 0.8 is applied because the hooked bar is confined by the hoops which make up the tie in the orthogonal direction. For the straight bars, the nominal development length is

$$\ell_{dn} = \frac{0.032 * 0.31 * 36000}{\sqrt{3920}} = 5.7 \ in.$$

but $\ell_{dn} \geq 0.00032 * 0.625 * 36000 = 7.2\ in.$ (controls)

The computed nominal development length for the layer of straight longitudinal bars extends past both the failure plane and the critical section defined by the compressive stress field and indicate a potential anchorage failure. For the hooked bars the computed development length and the failure plane nearly coincide but are well inside the boundary of the stress field indicating sufficient anchorage length.

An assessment of the capacity based on development length available using the boundary of the compression stress field is made in Table 8.3. The distance from the critical section defined by the boundary of the compression field to the termination point of the tie reinforcement is used to calculate the capacity of each tie. The stress in layers of reinforcement with measured development lengths greater than necessary to develop f_y are based on the yield strength. The computed tie capacities for LFNC, HFNC, and LFAC are compared with measured loads at failure and show good agreement. In the other specimens, anchorage was not considered to be critical and values are not calculated in Table 8.3. Comprehensive design recommendations for development cannot be based on the test results from three node tests but it appears that, for these three tests, it is reasonable to define the critical section for development by the boundary of the compression field.

8.2.4 Design Guidance for CTT-Nodes.

<u>Tie Anchorage Details.</u> The tie anchorage detail is generally idealized as an end plate which distributes the tie force over the depth of the node. The end plate must be wide enough so that the stresses at the node face do not exceed the effective compressive stress.

In a real element, the tie force may be anchored with a continuous reinforcement detail, such as the U loops shown in Fig. 8.4. The U's must also be distributed over a minimum area of concrete so the stress in the node does not exceed the effective concrete strength. Cook and Mitchell[27] suggest that the effective width be taken as the distance between the end layers of the tie's reinforcement (Fig. 8.5). The definition of the effective width of the U loop in the plane perpendicular to the U is also important. Cook and Mitchell assume that the concrete cover spalls to the centerline of the tie legs at the node. While such assumptions may be based on observed test results, adequate definition is lacking. If the tie reinforcement is placed unevenly, as shown in Fig. 8.6, or if only one layer is used, the effective concrete area cannot be clearly defined. Another consideration is the transverse reinforcement detail in wide members as shown in Fig. 8.7. Strut action will tend to concentrate forces at the bend; however, a portion of the force may deform the horizontal leg of the tie and cause splitting cracks if the center portion of the tie leg is unsupported by a cross tie. Based on test results, Leonhardt and Walther[28, 29] suggest that where large shear stresses exist in the member, the lateral spacing of stirrup legs parallel to the web width "b_w" should not exceed 7.5 in. Where the nominal shear stress is small,

Table 8.3 Specimen Exhibiting Anchorage Problems: Computed Strength Based on Available Development Lengths

Specimen	Available Dev. Length	Calculated Capacity (kips)
LFNC - #3 ties (transverse)		
1st Layer	4.5	20.1
2nd Layer	6.5[1]	28.5[2]
3rd Layer	8.5[1]	28.5[2]
4th Layer	10.5[1]	28.5[2]
	Total Calc. Cap.	105.5
	Meas. Capacity	117.8
	Meas./Calc.	1.12
HFNC - #3 ties (transverse)		
1st Layer	4.5	25.1
2nd Layer	6.5[1]	28.5[2]
3rd Layer	8.5[1]	28.5[2]
4th Layer	10.5[1]	28.5[2]
	Total Calc. Cap.	110.5
	Meas. Capacity	132.5
	Meas./Calc.	1.20
LFAC - #5 bars (longitudinal)		
Straight Bars	6.0	55.8
Hooked Bars	9.5[1]	111.2[2]
	Total Calc. Cap.	167.0
	Meas. Capacity	164.5
	Meas./Calc.	0.98

[1] Length needed to develop f_y is less than available length.
[2] Based upon f_y.

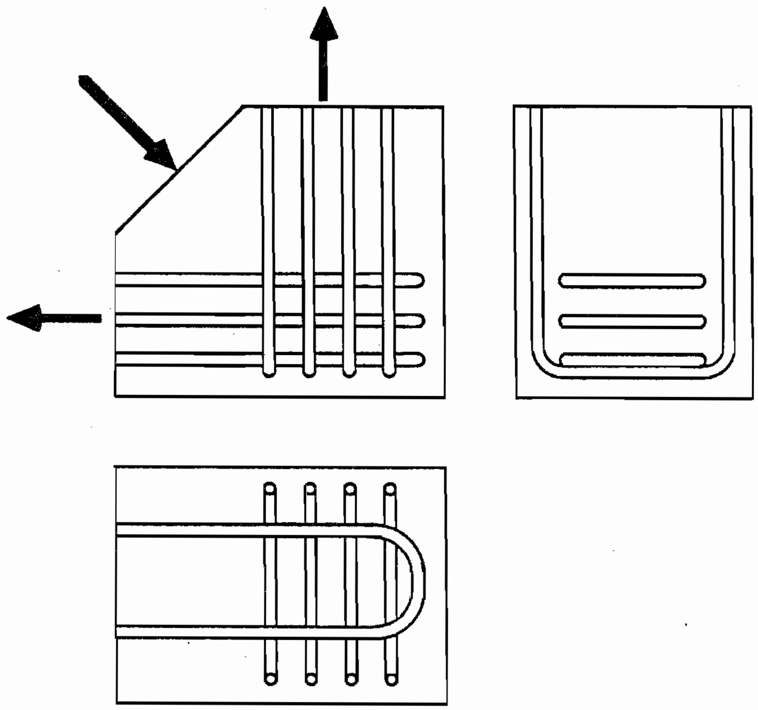

Figure 8.4 Continuous Reinforcement Details for Anchoring Tensile Ties in CTT-Node.

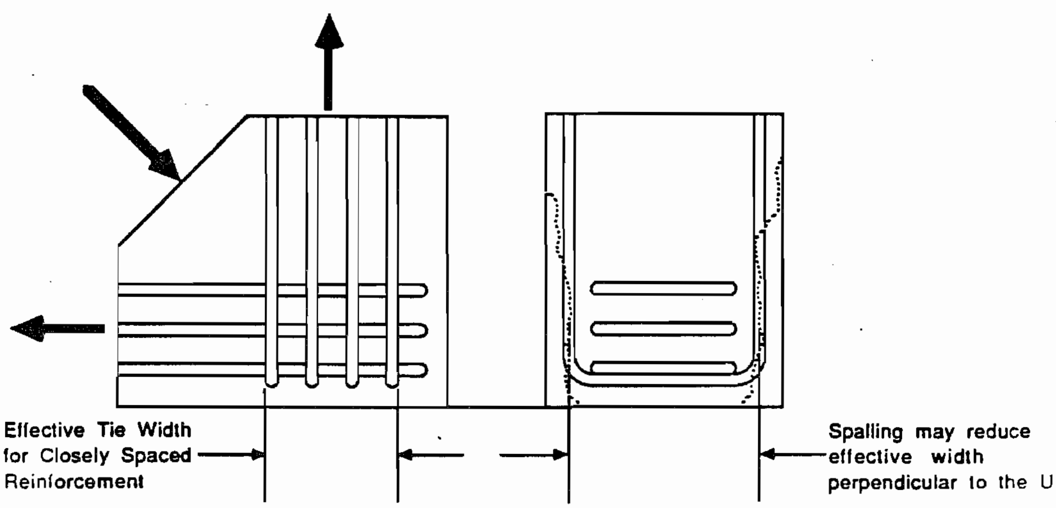

Figure 8.5 Defining the Effective Width of Continuous Reinforcement Tie Anchors.

the distance may be increased to 15 in. or more but should not exceed the effective depth "d" of the member.

With end plates and continuous (hoop) reinforcement details, the tie force is transferred to the node through bearing. However, bearing is not developed in the same way for ties anchored with straight bars as in Fig. 8.8 where single layers of straight bars

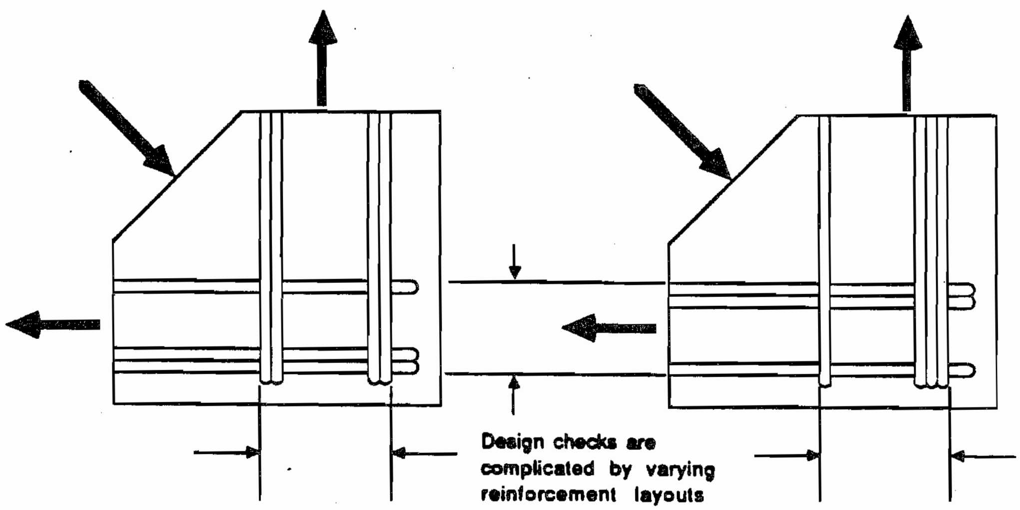

Figure 8.6 Design Complications Resulting from Uneven Placement of Reinforcement.

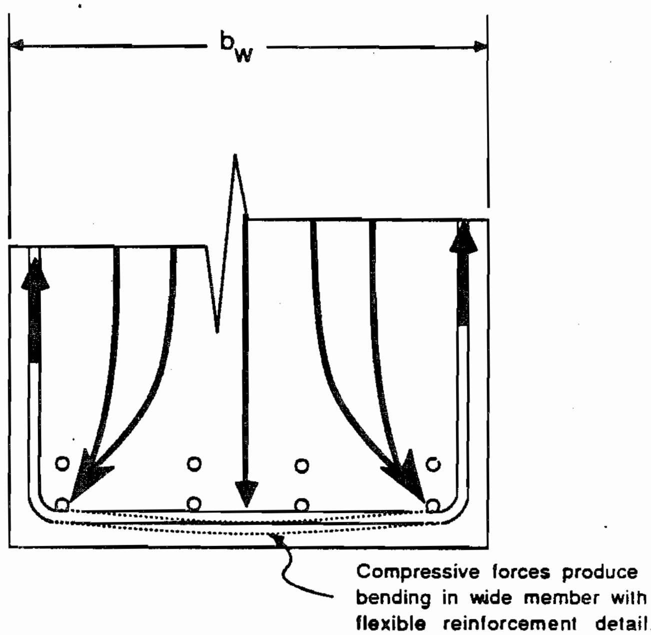

Figure 8.7 Undesirable Effects Resulting from the Use of Continuous Reinforcement Details in Wide Members.

anchor ties T_1 and T_2. The tie forces must be developed entirely through bond stresses which develop along the length of the straight bar. The development length for each layer of tie reinforcement is assumed to begin at the intersection point of the two ties. If insufficient development length is provided, the bar may pull out or a cover splitting failure may occur. If adequate development length is provided, the CTT-node will not fail until: 1) the effective concrete strength is exceeded; or 2) tensile capacity of the anchorage detail is achieved. There has been little attention to the straight bar anchorage problem in the literature. Positive anchorage details (Fig. 8.9) must be designed so the tie force is

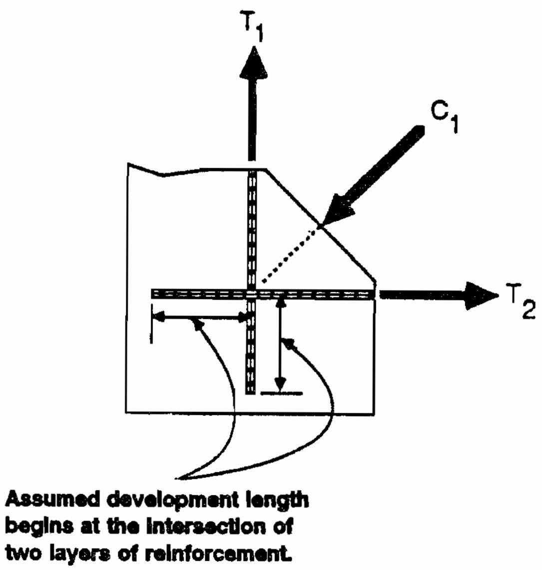

Figure 8.8 Force Transfer in CTT-Node with Simple Reinforcement Layout.

distributed over a sufficient area to prevent the node from being overstressed. Straight bar anchorages without any transverse or confining reinforcement may not perform well once cracking or splitting along the bar starts. More research is needed to clarify development of bars in CTT nodes.

<u>Design Development Length at Nodes.</u> End plates and continuous reinforcement details are fairly easy to evaluate. However such details are not always required nor are they always desirable because they create congestion during fabrication. End plates or continuous reinforcement details should be provided only if the transfer of strut-and-tie forces is so abrupt that sufficient bond and anchorage forces cannot be developed.

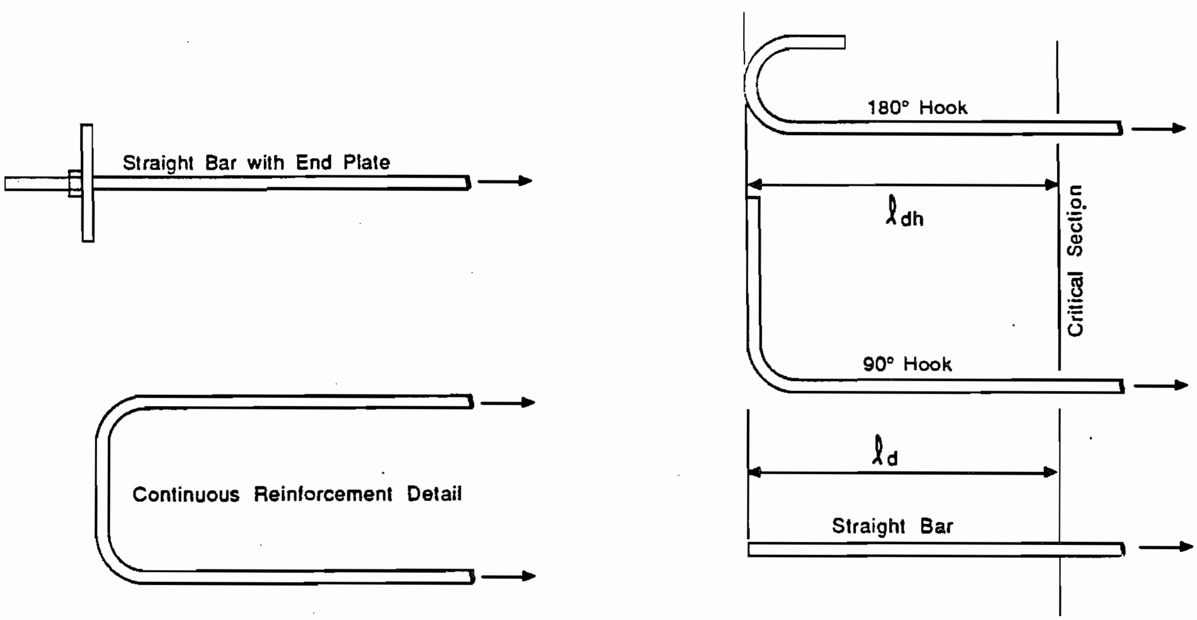

(a) Positive anchorage details

(b) Development length anchorage details

Figure 8.9 Positive and Development Length Anchorage Details

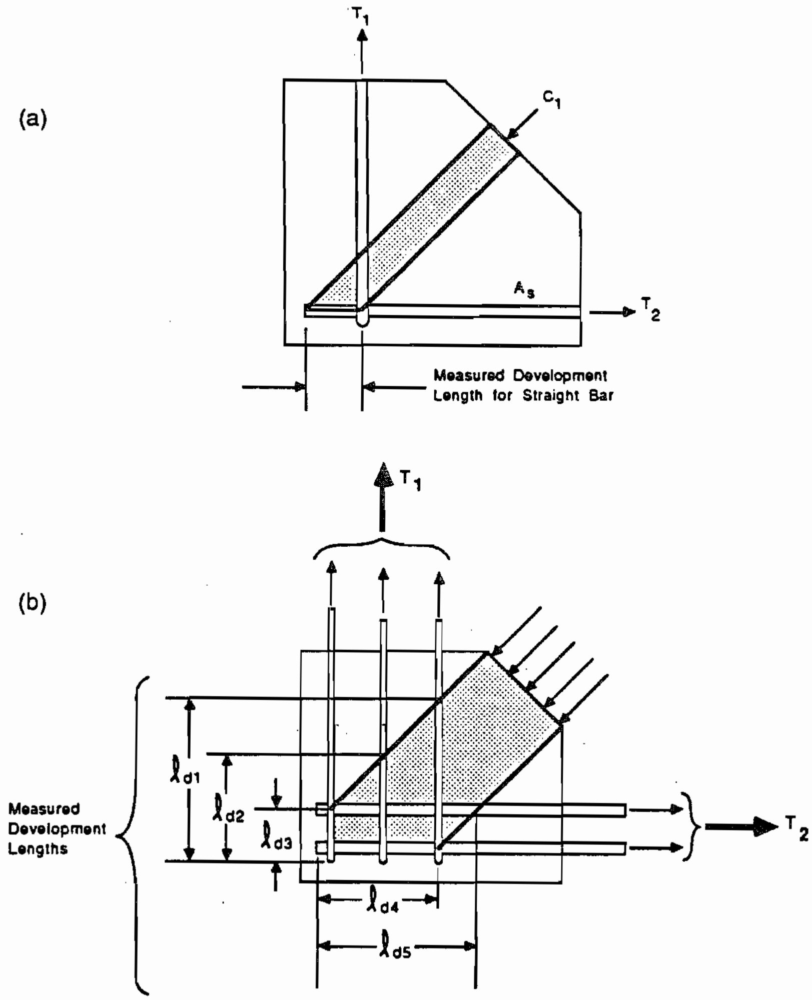

(c)

	Design Checks	
Strut Stress	Calculated Strut Stress Based Upon Reinforcement Layout	$\leq \upsilon f_c'$ (Effective Concrete Strength Limit)
Anchorage	Calculated Tie Capacity Based Upon Measured Development Length	$\geq$ Applied Tie Forces T_1 or T_2

Figure 8.10 Design Checks for Ties Anchored with Single and Multiple Layers of Reinforcement.

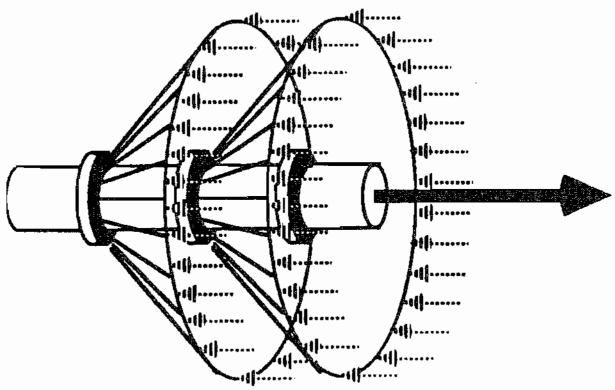

Figure 8.11 Bond Force Transfer Mechanism (From Ref. 30).

A simple design situation is illustrated in Fig. 8.10 for a CTT-node with two intersecting layers of reinforcement. One set of ties (T_1) is continuous while the other (T_2) is made up of straight bars. The centroid of the CTT-node is located at the intersection point of the two ties. The node implies an abrupt change in the direction of the forces. However, in the concrete member the transfer of force between strut and tie members would occur more gradually by the mechanical locking of the lugs into the surrounding concrete (Fig. 8.11).

To evaluate the anchorage requirements for a CTT-Node where each tie is made up of multiple layers of reinforcement, the critical section is defined by the compression field. The geometry of a typical design situation is illustrated in Fig. 8.10(b). Anchorage would be considered adequate if the capacity of a layer in the tie based on the available development length exceeds the anticipated force in the layer. Generally the outermost layer will have the shortest available development length and may fail first.

Generally, increasing the spacing of the transverse reinforcement will lessen the development requirements of the longitudinal tie; however, it may create problems with the strut-and-tie design model. For the dapped beam, increasing the spacing of the transverse reinforcement too much will lead to an inefficient design model that does not agree well with the elastic flow of forces. The tests of dapped beams discussed in Chapters 3 and 4 indicated that strains for tie reinforcement are less uniform if the bars are more widely spaced. Figure 8.12 shows how the spacing of transverse reinforcement affects the overall design model. Increasing the width of the tie results in flat strut angles α_1 and α_2. It is seen that the forces in the vertical tension ties, T_1 and T_2, are not affected by the change in the strut angle. In contrast, the forces in the horizontal ties, T_3 and T_4 are largely dependent on the strut angle. The most efficient model is one with steep strut angles to reduce the horizontal tie forces and the amount of tie reinforcement. It is apparent that the angle α_1 is constrained by the geometry of the dapped beam. The distance "x" must be large enough to accommodate the placement of steel required for the tie T_1. If the transverse reinforcement of tie T_1 is anchored with a continuous reinforcement detail, the reinforcement must be spread over a sufficient area to prevent crushing of the struts C_1 and C_2. The anchorage requirements of the longitudinal reinforcement for tie T_3 also must be assessed.

Practical solutions for improving three dimensional confinement for the CTT-node in this study are shown in Fig. 8.13. The first and simplest detail to control splitting cracks of the end cover involves extending the longitudinal bars a short distance past the transverse

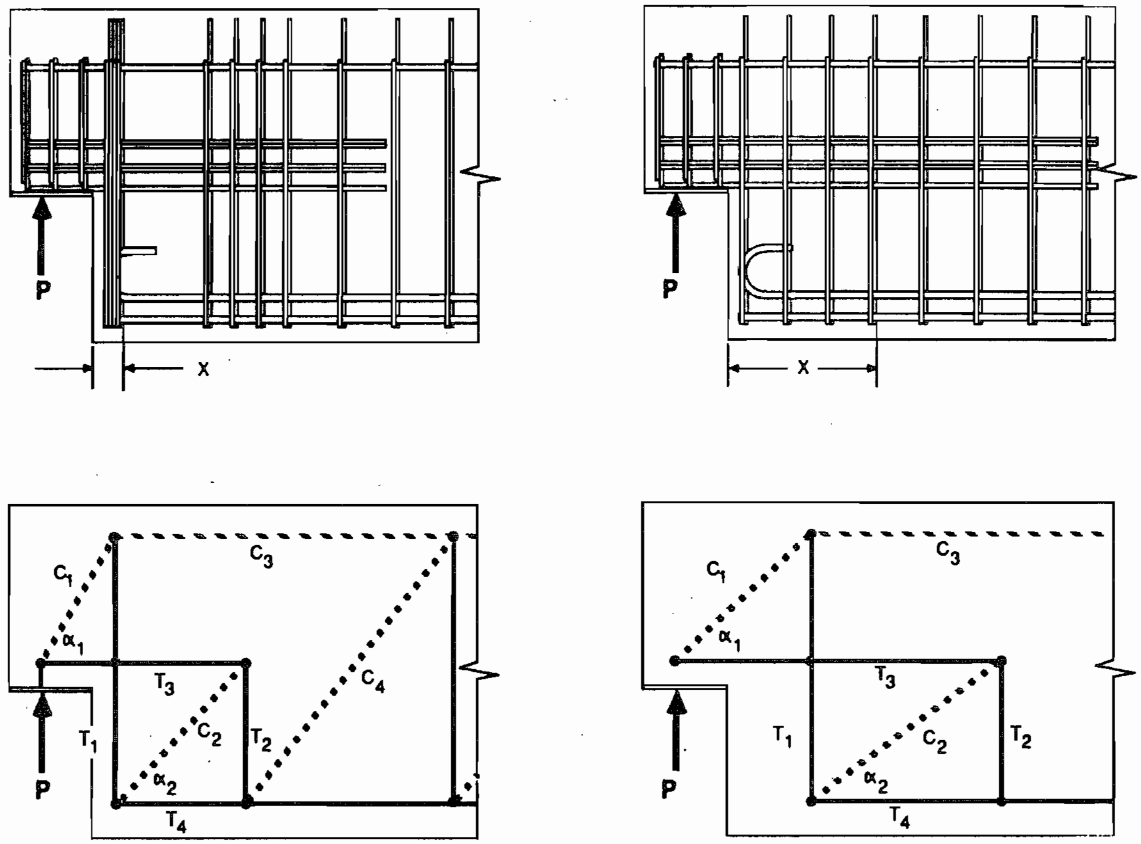

(a) Efficient Design Model Uses Closely Spaced Reinforcement for Tie T_1

(b) Widely Spaced Transverse Reinforcement Reduces the Efficiency of the Design Model

Figure 8.12 Consequence of Reinforcement Spacing in Dapped Beam.

hooks as shown in Fig. 8.13(a). A less economical detail involves the placement of extra hoop reinforcement as shown in Figs. 8.13(b) and 8.13(c). Confinement provided by hoops is beneficial to the performance of both the transverse and longitudinal steel.

Cover is also needed to prevent splitting failures. The steel layout and corresponding isolated strut-and-tie model at the termination point of the straight longitudinal bars in the node specimens is presented in Fig. 8.14. The strut-and-tie model shows forces redirected at a point; however, sufficient bond stresses cannot develop at the free end of the horizontal bar to deviate the strut force. It is also noted that concrete cover may be somewhat effective in maintaining equilibrium of the system. Indeed, the actual force flow is much more complex and relies on bond stresses distributed over some distance and on the tensile strength of the concrete. The concrete cover acts as a tie and resists a portion of the horizontal strut force. Much more testing is needed to develop design recommendations for such complex force transfer mechanisms.

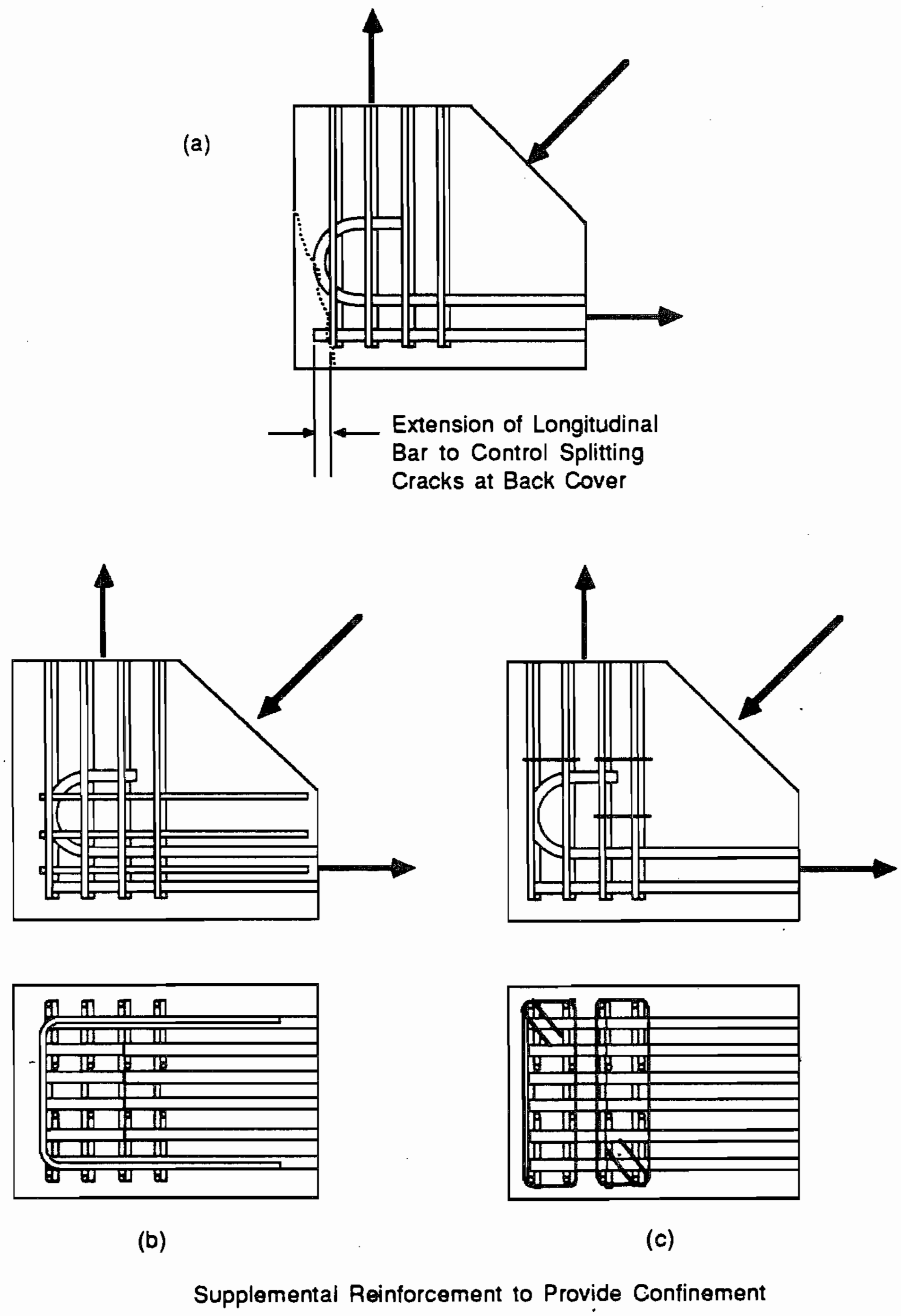

Figure 8.13 Detailing the CTT-Node to Provide Three-Dimensional Confinement.

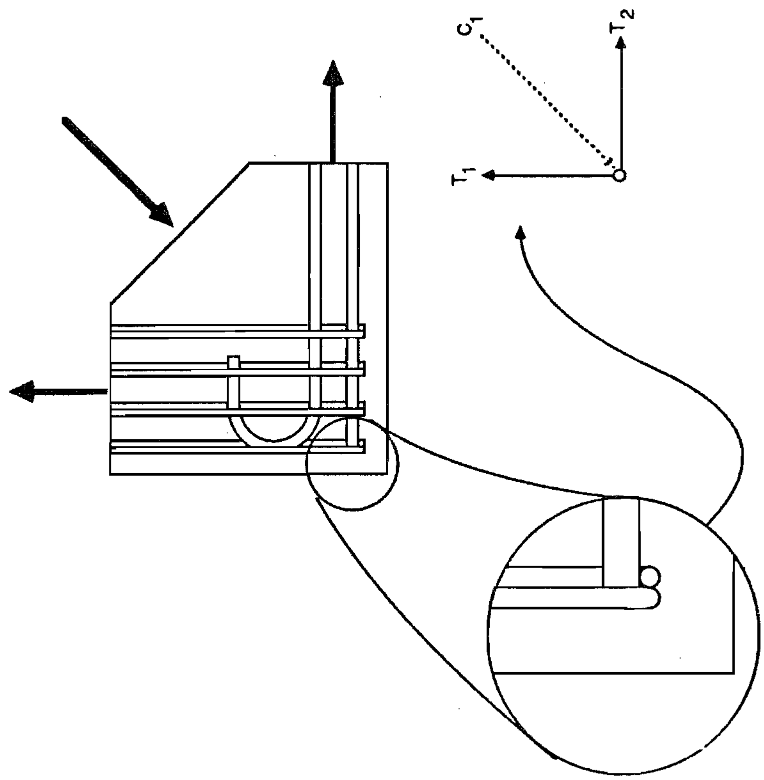

(a) Reinforcement at termination point of straight bars

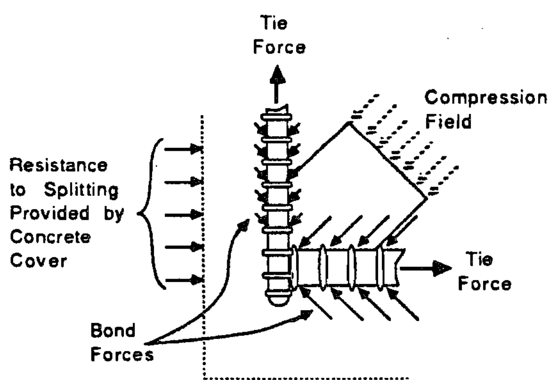

(b) Detail of local force transfer

Figure 8.14 Force Transfer Mechanisms at Interaction of Straight Bars with Hoop Reinforcement.

8.3 CCT Nodes

8.3.1 Geometry of Compressive Stress Fields. The function of the CCT node is to provide for a transfer of forces between a tension tie and two compressive forces. For the tests in this program, the CCT node is at the point where the compressive forces from a reaction and an internal strut meet. The compressive stresses of the internal strut and the reaction bearing plate must remain below a safe level and the tie must be properly anchored. In designing or checking the node for these two parameters, the geometry of the node must be determined. Node geometry as suggested by Schlaich(15) based on the strut angle (β), the edge of the bearing plate, and reinforcement configuration (which determines w_3 is shown in Fig. 8.15(a). As a result of the other constraints, w_1 may not be the entire width of the bearing plate and the center of the effective bearing width (line of action of the load C_1) does not necessarily correspond to the center of the real support width. Such a condition may not satisfy equilibrium requirements. The use of a roller with a well-defined line of action is a prime example of such a case. The geometry defined in Figure 8.15b avoids the problem and gives approximately the same results. In this case, w_3, β and the location of C_1 determine the node geometry. Based on the geometry shown in Fig. 8.15(b), effective dimensions of the specimens are given in Table 8.4 as a function of the location assumed for C_1.

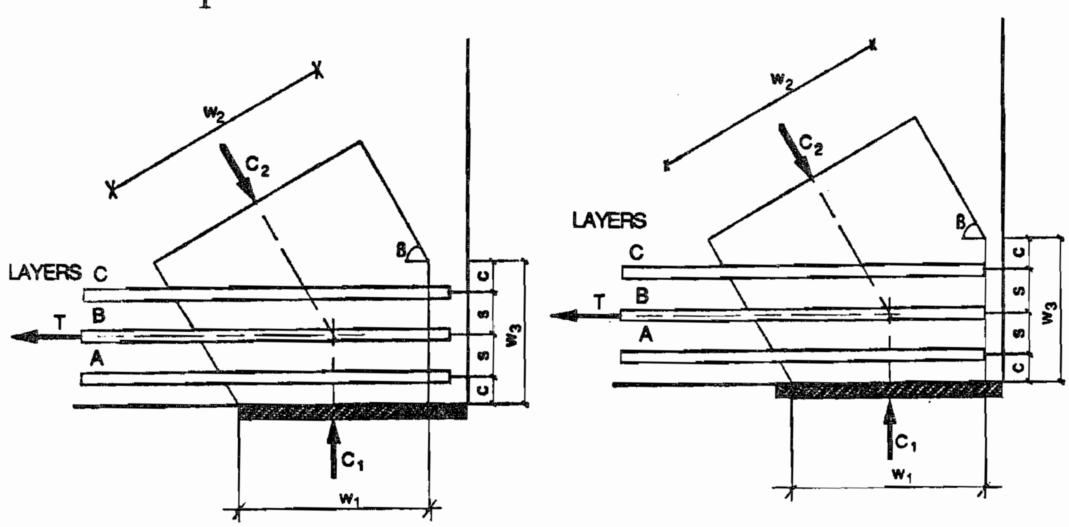

Figure 8.15 Node Effective Dimensions.

8.3.2 Effective Concrete Stress. Four specimens (LFT, LHT, LHO, LFT-R) failed in compression. The applied load on the strut was measured, and the reaction force was calculated from equilibrium of forces at the node using the geometry defined in Figure 8.15(b). The stresses and efficiency factors are summarized in Table 8.5 and were computed using the effective compressive width of the strut (w_2) and reaction zone (w_1). Although Specimen LFT had the same geometry and reinforcement layout as LFT-R, it failed at a lower load level because of the thickness of the loading plate (1 in. instead of 2 in.) that

Table 8.4 Node Dimensions						
Specimen	w_1 in.	w_2 in.	w_3 in.	Bar* Layer	Anchorage Length	Hook
LFT	8	10.6	7.4	A	10.7	No
				B	12.1	No
				C	13.5	No
LHT, LHO	6	8.9	7.4	A	6.7	No
				B	8.2	No
				C	9.5	No
LFO, LFT-R, HFT	10	12.4	7.4	A	10.7	No
				B	12.2	No
				C	13.5	No
HFO-SS	10	11.2	5.1	A	10.72	No
				B	12.20	No
HFO-HS	10	11.2	5.1	A	10.72	No
				B	12.20	Yes
HFO-SL	10	12.2	7.1	B	12.20	No
				C	13.46	No
HFO-HL	10	12.2	7.1	B	12.20	Yes
				C	13.46	No

* Layers defined in Fig. 8.15.

caused a stress concentration in the center of the plate and reduced the effective strut width. Therefore, the effective widths w_1 and w_2 were reduced to 8 in. and 10.6 in. for calculating bearing stresses.

It is interesting to compare the measured efficiency factors with those proposed by others. Based on tests of beam webs, Thürlimann[16] proposed the following equation for the strut compressive strength:

$$f_{ce} = 0.36 f_c' + 700\ psi \qquad \text{for} \qquad f_c' \leq 4800\ psi \qquad \text{(limit of test data)}$$

Collins and Mitchell[31] based their estimation of the efficiency factor υ for a compression strut on an experimental study made on shear panels. They related the efficiency factor to the principal tension strain:

$$f_{ce} = \upsilon f_c'$$

where

$$\upsilon = \frac{1}{0.8 + 170 e_1}$$

and

$$e_1 = e_x + \frac{e_x + 0002}{\tan^2\beta}$$

The principal compressive strain is assumed equal to 0.002. The bar strain (e_x) is conservatively taken as the yield strain.

Based on an experimental study of web concrete strength Nielsen et al.[9] proposed the following equation for the efficiency factor:

$$\upsilon = 0.7 - \frac{f_c'\ [\text{psi}]}{29000}$$

Schlaich et al.[15] proposed an efficiency factor based on the state of strain. In the case of a CCT node, the efficiency factor is:

$$\upsilon = 0.68$$

Table 8.5 Measured and Proposed Efficiency Factors for Concrete Stress				
	LFT	LHT	LHO	LFT-R
Concrete Strength, f_c', ksi	2.34	2.49	2.60	2.61
Measured Stress:				
f_L Loading surface, ksi	2.03	2.24	2.24	2.32
f_L / f_c'	0.86	0.90	0.86	0.89
f_b, bearing (reaction) surface, ksi	2.34	2.90	2.90	2.49
f_b / f_c'	1.00	1.16	1.12	0.95
Proposed Efficiency Factors for Struts:				
Thurlimann (16)	0.65	0.65	0.65	0.65
Mitchell and Collins (32)	0.72	0.72	0.72	0.72
Nielsen (9)	0.72	0.72	0.72	0.72
Schlaich et al. (15)	0.68	0.68	0.68	0.68

From the results shown in Table 8.5, the values were consistently higher than the efficiency factors proposed by different researchers. (It should be noted that efficiency factors based on other conditions (thin web, shear panel) may not be applicable to a CCT node at a beam support.) Specimen LFO was similar to Specimen LFT and LFT-R but did not have any transverse reinforcement around the tension tie. It failed in anchorage and illustrates the critical role of transverse reinforcement in increasing the bond anchorage capacity of the tie and permitting compressive fields to develop fully. The tests suggest that with a decrease in the loaded (and reaction) area, the efficiency factor increased.

8.3.3 Anchorage of Tension Tie. Six specimens, (LFO, HFT, HFO-SS) experienced anchorage failures. All of the specimens failed before the bars yielded with the exception of Specimen HFT. The effective anchorage lengths of all bars were measured from the boundary of the effective node and were summarized in Table 8.4. The effective lengths were checked against AASHTO and ACI 318 requirements. Using nominal value for f_y (60 ksi), the required bar lengths are summarized in Table 8.6. The lengths which may govern tie capacity in tension are shown with an asterisk. Table 8.7 gives the measured (from Table 7.1) versus computed failure load ratios. To illustrate the procedure used in developing the values in Tables 8.6 and 8.7, detailed computations for specimen HFTare described. The anchorage lengths (denoted ℓ_a) of layers A, B, and C of specimen HFT are 10.7, 12.2, and

Table 8.6 Specimens Failing in Anchorage: Available and Computed Anchorage Lengths

Specimen	Bar Layer	Available ℓ_a	ℓ_{dn} or ℓ_{dhn}	ℓ_a / ℓ_n
LFO	A	10.7	12.3	0.87
	B*	12.2	17.5	0.75*
	C	13.5	17.5	0.77
HFT	A	10.7	12.0	0.89
	B*	12.2	17.0	0.71*
	C	13.5	17.0	0.79
HFO-SS	A*	10.7	16.3	0.65*
	B	12.2	16.3	0.75
HFO-HS	A	10.7	11.9	0.90
	B*	12.2	16.3	0.73*
HFO-SL	B*	12.2	16.3	0.73*
	C	13.5	16.3	0.83
HFO-HL	B	12.2	11.9	1.03
	C*	13.5	16.3	0.83*

* Layer controlling anchorage

13.5 in., respectively. The nominal lengths (ℓ_n, Sec. 8.2.3) required by AASHTO or ACI 318 to develop yield (f_y = 60 ksi) are 12.0, 17.0, and 17.0 in. The ratios of available length (ℓ_a) to nominal required length (ℓ_n) to develop yield are then computed and are 0.89, 0.7 and 0.79 for layer A, B, and C, respectively. Assuming that the bond strength is constant along the bar length, the bars of layer B will trigger an anchorage failure when the level of the stresses on the bars reach $0.71 f_y$ which is indicated by an asterisk in Table 8.6. The force in the tension tie corresponding to anchorage failure using AASHTO or ACI 318 for layer B is 0.71 (60 ksi) (3 x 0.31 in.^{2} + 8 x 0.44 in.^{2}) = 189k as shown in Table 8.7 and F_{Code}/F_m = 189/245 = 0.77.

The force to yield the tie in specimen HFT was computed assuming yield stresses in all bars. Since the specimen was reinforced with 8 #6 and 3 #5 bars, the bar force needed to develop yield is:

$$F_y = [8(.44) + 3(.31)] * 60 = 267 \ kips$$

The measured total bar force (F_m) is expressed as a fraction of F_y and is reported in Table 8.7. For HFT, $F_m/F_y = 0.92$

Table 8.7 Comparison of Computed and Measured Force in Tension Tie					
Specimen	Measured F_m (kips)	F_y	F_m / F_y	AASHTO or ACI 318 F_{Code} (kips)	F_{Code} / F_m
LFO	Not reliable	267	----	200	----
HFT	245	267	0.92	189	0.77
HFO-SS	167	216	0.77	140	0.84
HFO-HS	174	216	.80	157	0.90
HFO-SL	204	216	0.94	157	0.76
HFO-HL	213	216	0.99	128	0.84

From the values given in Table 8.7, changes in cover and bar geometry (hooked or straight bars) produced the following differences in performance:

1) An increase in clear cover from 7/8-in. (HFO-SS and HFO-HS) to 3 in. (HFO-SL and HFO-HL) increased the anchorage capacity by 22% in both cases.

2) The addition of hooks to the lower layer of bars (HFO-HS and HFO-HL) resulted in a very small (4%) change in the capacity over that of the straight bars (HFO-SS and HFO-SL).

The use of nominal development lengths in the AASHTO or ACI 318 format (Sec. 8.2.3) gave strengths that were about 80% of measured values.

CHAPTER 9
SUMMARY AND CONCLUSIONS

9.1 Summary

The objective of the research described herein was to examine methods of detailing structural concrete. Most detailing practices are based on past experiences and judgement. Empirical design procedures have been developed for specific "problem" details. The ever increasing complexity of concrete structures creates numerous new and unusual details. It has become difficult to adapt old details to new situations. Research cannot be carried out to develop empirical design procedures to cover every detailing situation. A recently proposed method, the strut-and-tie model is the subject of this study. The model involves a few basic principles to cover a large range of design problems. While the literature contains considerable general information, there is a lack of test data to corroborate assumptions of the strut-and-tie model. To help verify strut-and-tie procedures, a dapped-end beam detail was selected for testing. In addition, a series of tests was conducted on isolated nodes representing portions of the beam where strut and tie elements meet.

<u>Dapped Beam Tests.</u> Three different procedures for the design of dapped beams were used. The strut-and-tie models and two empirically based methods, the PCI design procedure and the Menon/Furlong design procedure were studied. Four different dapped end details were tested. Two of the details were based on strut-and-tie models. The design model was varied to examine the ability of the strut-and-tie model to adapt to different reinforcement patterns. As a basis for comparison, two details were designed using empirical methods.

<u>Compression-Tension-Tension (CTT) Nodes.</u> Portions of the strut and tie model dealing with nodes, especially those anchoring tensile ties, are not well defined, nor have they been subjected to comprehensive evaluation through tests. To develop an understanding of an isolated CTT-node, a laboratory investigation was implemented to verify current proposals, identify significant behavioral patterns of the CTT-node, and develop design guidelines. The dapped beam tests served as the prototype for the node tests. The nine isolated node specimens were designed and tested to duplicate, as closely as possible, boundary conditions that exist at a critical CTT-node in the dapped beams. Variables included concrete strength, lateral confinement provided by transverse reinforcement, anchorage details, and node geometry.

<u>Compression-Compression-Tension (CCT) Nodes.</u> The CCT node was also isolated from the end reaction region of the prototype dapped beam. Ten specimens were tested in which concrete strength, size of bearing area, amount of transverse reinforcement, and longitudinal reinforcement configuration were varied.

9.2 Conclusions

Based on the results of the tests on the dapped end details and on the isolated nodes, conclusions are presented with regard to overall behavior complex details, correlation of strut-and-tie models to observed behavior, general guidance for anchorage placement of reinforcement, and limits for concrete stress.

9.2.1 Dapped Beam Tests.

Overall Behavior. The overall behavior of specimens designed using strut-and-tie models was found to be comparable with details designed using current design standards. The ultimate capacity of details designed using the strut-and-tie models, as well as those designed using other approaches, exceeded the computed capacity substantially. A ductile failure mode in which the steel yielded before the concrete failed was exhibited by each of the specimens. The strut-and-tie design procedure required slightly more shear reinforcement compared to the other design procedures. The test results indicated that in some cases the ties provided were not needed and could have been reduced or omitted. However, this discrepancy is due to the fact that concrete carries tension (which is neglected in the strut-and-tie model). Unless some tension is assigned to the concrete, it is necessary to develop tension through the placement of ties. For design, it is not advisable to rely on concrete in tension in detailing of members. In the first strut-and-tie model detail (ST1), cracking was controlled at service loads as effectively as details designed using other design methods (PCI and Menon-Furlong). Slightly more cracking was exhibited by strut-and-tie model ST2. The additional cracking in ST2 was due to placement of vertical reinforcement farther away from the dap.

Comparison of Strut-and-Tie Models to Observed Behavior. Internal force measurements at the design load (100 k) compared well to forces predicted by the design strut-and-tie models. The only major discrepancy between the design models and observed behavior is the means through which the horizontal force from the dap is transferred into the full depth section.

As load was increased beyond the design load of 100 k, the distribution of internal forces changed. Strut-and-tie model representations of the upper portion of the daps based on measured forces at ultimate resulted in varying degrees of error. The source of this error is believed to be partly the result of the method of testing (large reaction on top surface of beam) and partly due to the presence of force transfer mechanisms (concrete in tension) not considered by the strut-and-tie model.

Placement of Reinforcement. A comparison of the behavior of the dapped ends indicates that placing the main vertical reinforcement close (as in the PCI detail) to the change in section was most efficient. In addition, grouping the reinforcement with as small a spacing as possible appeared to offer the best performance.

Anchorage of Reinforcement. Anchorage requirements based on the strut-and-tie model were found to be conservative and resulted in applied loads well beyond design values. Proper anchorage of the horizontal reinforcement within the dap (bars welded to a bearing plate) and of the beam flexural reinforcement (use of hooks) was found to be particularly important.

Selection of Compression Strut Inclination. An increase in the angle of the compression strut reduced the amount of horizontal reinforcement at the node. In the dapped beam tests, the strut angles developed ranged between 45 and 55° and tended to increase as load increased. Strut angles up to 60° seem reasonable from the test results but higher angles are probably not reasonable because reinforcement areas for the tension tie at the node become quite small. It should also be noted that in the dapped beams the upper end of the compression strut in the dap ends in a node which is near the top of the beam. The steeper the strut angle, the higher is the node in the beam. Based on the test results it appeared that better performance (especially under large overloads) was obtained if the node lower in the beam. This can be done in design by reducing the strut angle and adding horizontal reinforcement at the bottom of the dap.

The strut-and-tie models did lead to the provision of one strut and a node which was not observed in the tests. The model indicates a node is needed along the horizontal dap reinforcement at some distance from the restraint corner. There was no indication that the node actually developed to the extent that additional tie reinforcement was needed. It is likely that the tension in this area was carried by the concrete.

9.2.2 CTT Nodes. While data was collected from a relatively small number of CTT tests, the unique nature of the isolated node specimens provides interesting insight into node behavior and design.

1) Specimens were generally able to reach the design strength which was governed by yielding of tie reinforcement. The ultimate strength of the CTT nodes was affected by concrete strength; however, internal force transfer mechanisms were more affected by the specimen geometry and placement of steel.

2) In all the specimens, different layers of tie reinforcement were observed to strain at different rates. In the strut and tie model the reinforcement making up a single tie is normally assumed to be similarly strained. The reinforcement strains were affected by the location of major cracks. The longitudinal ties in some of the layers of reinforcement closest to the external surface were strained less. In these cases, the major cracks appeared to reduce the available development length enough to cause a deterioration in the tensile capacity of the tie.

3) Correlations between the behavior of the node specimens and the prototype dapped beam specimen were quite good. This was evidenced by similar crack patterns and comparable reinforcement strains.

4) Evaluation of the strut-and-tie model in the light of the test results indicate that

   a) Cracks were generally parallel with the angle of the compression strut,

   b) The geometry of the strut is best defined by the strut angle and the point of intersection of the layers of tie reinforcement in both directions.

   c) Recommended effective concrete strength limits proposed by other authors were found to be conservative.

   d) Defining the critical section of the reinforcement by the boundaries of the compression fields appeared to produce reasonable estimates of the capacity of ties anchored through development of hooks or straight bars.

5) The splitting failures that occurred in several specimens underscored the importance of detailing the CTT-node as a three-dimensional element. Reinforcement should be provided across all planes of weakness to control cracking. Confining reinforcement normal to planes of hooks and bends is especially important.

9.2.3 CCT Nodes. The primary conclusions to be made on the basis of the CCT isolated node tests are:

1) Two failure modes were observed for the CCT node specimens: anchorage failure and compressive failure. Anchorage failure was due to inadequate bar development length. The appearance of the specimen at failure and the crack pattern clearly indicated which mode controlled in each case.

2) The primary element in designing a CCT node is the determination of inclination of compression struts. Tests of dapped beams designed using the strut and tie model approach indicated that the strut developed in the beam was oriented as assumed in the design calculations. For these tests an angle of 60° was selected. This is at the upper end of the range considered acceptable for design.

3) Effective bearing areas based on theoretical models proposed by other researchers were generally satisfactory for evaluating tie anchorage characteristics and effective compressive strength of the strut.

4) The measured efficiency factor (the ratio of average compressive stresses on the strut to the concrete strength) for specimens which failed compression failure was found to be about 1.0. Efficiency factors proposed in the literature were found to be conservative for the specimens in this study.

5) Transverse reinforcement restrained the cracks and prevented an anchorage failure. The capacity increased sufficiently in some tests to change the mode of failure from one involving anchorage to one in which the compression strut failed.

6) The anchorage lengths for straight and hooked bars given in current Codes were found to be very conservative. The use of hooks did not substantially increase the capacity of the specimens. An increase in cover was found to improve anchorage capacity.

9.3 Additional Comments

The results of research described herein show that the strut-and-tie model is an acceptable design procedure for detailing structural concrete. The use of strut-and-tie models along with a knowledge of behavior derived from experimental research seems a good basis for developing efficient design procedures. The strut-and-tie model represents a rational approach which can be extended to detailing situations not covered by existing procedures.

The results of this research alone cannot justify the use of strut-and-tie models. Further experimental verification on other types of details is necessary. In addition, guidelines on analysis and design of nodes, serviceability criteria, and tie layout need development. In order to develop comprehensive design criteria for nodes, future studies should include specimens with a number of different bar spacings and amounts of tie reinforcement. Test specimens with high percentages of reinforcement and narrow web widths are also suggested so that effective concrete strength limits could be evaluated more closely. The behavior of specimens with anchor plates and straight or hooked bars needs to be examined. In addition, the effect of strut orientation should be studied more closely, particularly the effects of skew cracks on the effective concrete strength of the compressive strut should be determined. The isolated node specimens used in this study provide much useful data but it is never possible to remove a portion of a structural element and isolate it in a manner that does not produce some change in boundary conditions. In spite of that, the node specimens offer a means of acquiring a large amount of data on detailing at a minimal cost.

REFERENCES

1. American Concrete Institute, *Building Code Requirements for Reinforced Concrete* (ACI 318-83), Detroit, 1983.

2. American Association of State Highway and Transportation Officials, *Standard Specification for Highway Bridges*, Washington, 1981.

3. *PCI Design Handbook* (Third Edition), Prestressed Concrete Institute, Chicago, Illinois, 1985, pp. 6.28-6.32.

4. *Post - Tensioning Manual, 4th Ed.*, Post - Tensioning Institute, Phoenix, AZ, 1987, 406 pp.

5. *Reinforcing Bar Detailing, 5th Ed.*, Concrete Reinforcing Steel Institute, Chicago, Illinois, 1986, 280 pp.

6. Ritter, W., "Die Bauweise Hennebique", (The Hennebique Design Method) Schweizerische Bauzeitung, Vol. 33, No. 7, Zurich, 1899.

7. Morsch, E., *Der Eisenbetonbau, seine Theorie und Anwendung* (Reinforced Concrete Theory and Application), Verlag Konrad Wittwer, Stuttgart, 1912.

8. Leonhardt, F., "Über die Kunst des Bewehrens von Stahlbetontragwerken (About the Art of Reinforcing Detailing for Reinforced Concrete Girders)", *Beton-und-Stahlbetonbau*, Vol. 60, No. 8, 1965, pp. 181-192; No. 9, pp. 212-220.

9. Neilsen, M.P., Braestrup, M.W., Jensen, B.C., and Bach, F., "Concrete Plasticity, Beam Shear - Shear in Joints - Punching Shear", Special Publication, Danish Society for Structural Science and Engineering, Technical University of Denmark, Lyngby, 1978.

10. Lampert, P., and Thürlimann, B., "Ultimate Strength and Design of Reinforced Concrete Beams in Torsion and Bending," *Publications No. 31-1*, International Association for Bridge and Structural Engineering, Zurich, 1971, pp. 107-131,

11. Collins, M.P. and Mitchell D., "Shear and Torsion Design of Prestressed and Non-Prestressed Concrete Beams," *PCI Journal*, Vol. 25, No. 5, Sept.-Oct. 1980, pp. 32-100.

12. Ramirez, J., "Re-evaluation of AASHTO Design Procedures for Shear and Torsion in Reinforced Concrete Beams," Ph.D. Dissertation, The University of Texas at Austin, December 1983.

13. MacGregor, J.G., *Reinforced Concrete -- Mechanics and Design*, Prentice-Hall, Englewoods Cliffs, N.J., 1988.

14. Marti, Peter, "Basic Tools of Reinforced Concrete Beam Design," *ACI Journal*, January 1985, pp. 46-56.

15. Schlaich J., Schafer, K., and Jennewein, M., "Towards a Consistent Design of Structural Concrete," PCI Journal, May-June 1987, pp. 75-150.

16. Grob, J., and Thurlimann, Bruno, "Ultimate Strength and Design of Reinforced Concrete Beams under Bending and Shear", *Memoires*, International Association for Bridge and Structural Engineering, 1976, pp. 105-120.

17. C.E.B. Ad Hoc Commission IV/VI, "Contribution to the Revision of the C.E.B. - M.C. 1990, June 1986.

18. Schlaich, J., Schafer, K., "Towards a Consistent Design of Reinforced Concrete", *Final Report*, 12th Congress of the International Association for Bridge and Structural Engineering, September 1984, pp. 8-15.

19. Schlaich, J., and Weischede, D., "Detailing of Concrete Structures, First Draft of a Design Manual" (In German), *Bulletin D'Information*, No. 150, Paris, 1982, pp. 141-143.

20. Mattock, A.H., and Chan, T.C., "Design and Behavior of Dapped-End Beams," *PCI Journal*, Vol. 24, No. 6, Nov.-Dec. 1979, pp. 28-44.

21. Anderson, R.B., "Behavior of CTT-Nodes in Reinforced Concrete Strut-and-Tie Models", MS Thesis, University of Texas at Austin, Dec. 1988.

22. Mattock, A.H. and Theryo T., "Strength of Members with Dapped Ends," PCI Research Project No. 6 Report, University of Washington, Seattle, 1986.

23. Menon, G., and Furlong, R.W., "Design of Reinforcement for Notched Ends of Prestressed Concrete Girders," Research Report 196-1F, Center for Transportation Research, Bureau of engineering Research, University of Texas at Austin, 1977.

24. Barton, D.L., "Detailing of Structural Concrete Dapped End Beams," MS Thesis, The University of Texas at Austin, December, 1988.

25. Bouadi, A., "Behavior of CCT Nodes in Structural Concrete Strut-and-Tie Models", MS Thesis, University of Texas at Austin, December 1989.

26. Collins, M.P., and Vecchio, F., "The Response of Reinforced Concrete to In-Plane Shear and Normal Stresses," Publication No. 82-03, University of Toronto, March, 1982.

27. Cook, W., and Mitchell, D., "Studies of Disturbed Regions near Discontinuities in Reinforced Concrete Members," *ACI Structural Journal*, Vol. 85, No. 2, Mar.-Apr., 1988, pp. 206-216.

28. Leonhardt, F., and Walther, R., "Tests on T-Beams Under Severe Shear Load Conditions," Bulletin 152, Deutscher Ausschuss fur Stahlbeton, 1962, Berlin.

29. Leonhardt, F., and Walter, R., "Shear Tests on T-Beam with Varying Shear Reinforcement," Bulletin 156, Deutscher Ausschuss fur Stahlbeton, 1962, Berlin.

30. Goto, Y., "Cracks Formed in Concrete Around Deformed Tension Bars," *ACI Journal*, Vol. 68, No. 2, Mar.-Apr. 1971, pp. 31-36.

31. Collins, M.P., and Mitchell, D., "A Rational Approach to Shear Design - The 1984 Canadian Provisions", *ACI Journal*, Nov.-Dec. 1986, pp. 925-933.

32. Orangun, C.O., Jirsa, J.O., and Breen, J.E., "A Re-evaluation of Test Data on Development Length and Splices", *ACI Journal*, Vol. 74, No. 3, March 1977, pp. 114-122.